Faculty of Health and Life Sciences

Oxford Brookes University

Oxford

Understanding the composition and function of the flagellar groove in bloodstream form *Trypanosoma brucei*

Laura Smithson

Supervisors: Professor Sue Vaughan and Dr Jack Sunter

Date: 14 October 2021

Word count: 41,688

A thesis submitted in partial fulfilment of the requirements of the award of Doctor of Philosophy

Declaration

I declare that the material contained in this thesis has not been used in any other submission for an academic award. I confirm that all the research and findings presented in this thesis are my own work unless otherwise indicated through the use of a clear referencing system.

Abstract

African Trypanosomiasis is a neglected tropical disease caused by the *Trypanosoma brucei* parasite and is transmitted by the bite of an infected tsetse fly. A characteristic feature of the bloodstream from of *T. brucei* is the flagellum, which is laterally attached to the side of the cell body and is not disassembled during the cell cycle. Instead, a new flagellum is formed alongside the old flagellum, with the distal tip of the new flagellum embedded within a cell body membrane invagination, called the groove. The groove is a highly mobile transmembrane junction and requires continuous remodelling of the subpellicular microtubule array as the new flagellum grows. To date, no molecular components of the groove are known, with the function of this structure undetermined. Moreover, in order to complete the cell cycle, the groove must resolve and release the new flagellum tip to initiate cytokinesis, with details of this process being unclear.

We identified 13 proteins that localise to the flagellar groove using endogenous tagging of putative groove proteins identified through TrypTag. Five distinct patterns of localisation were observed. A deletion screen using CRISPR/Cas9 of the groove proteins releveled a selection of proteins involved in cytokinesis, such as CIF4, FAZ15 and FAZ16, as well as proteins involved in flagellum tip attachment, such as FCP4, Tb427.01.2710 and Tb427tmp.01.3030. These results have provided a knowledge base of the composition and function of the flagellar groove.

Moreover, 3D electron microscopy techniques were used to understand the timing of groove resolution. We have demonstrated that the groove resolves post mitosis, when the new flagellum surpasses the old flagellum in length. We have also determined that two evolutionarily related trypanosomatids to *T. brucei, Trypanosoma vivax* and *Trypanosoma congolense*, do not fully embed their new flagellum distal tip in a canonical groove.

Acknowledgements

I am extremely grateful to my supervisors, Prof Sue Vaughan and Dr Jack Sunter for their invaluable advice, continuous support, and patience during my PhD. Their knowledge and experience have encouraged and inspired me every day during the last three years, and for that I am tremendously thankful.

I would also like to thank Dr Flavia Moreira-Leite for the many hours of electron microscopy mentorship, I couldn't have done this without her support or patience. I would also like to thank the members of my lab, particularly my fellow PhD students, for their support and the many tea and biscuit breaks. My gratitude extends to the Global Challenges Research Fund and Oxford Brookes University for the funding opportunity and support during my PhD.

Finally, I would like to thank my family for their encouragement and support over the course of my academic career, I could not have done any of this without you. "Thank you" doesn't come close to expressing how grateful I am to you.

Thank you to the person who sent me this excerpt from The Correspondence of Charles Darwin (1861) during my final month of writing. It helped to know that even Darwin had tough science days.

"But I am very poorly today & very stupid & I hate everybody & everything. One lives only to make blunders."

Table of Content

Declaration 3

Abstract 4

Acknowledgements 5

List of Figures 10

List of Tables 13

Abbreviations 14

1 Introduction and literature review 17

1.1 The African trypanosomiasis burden 17

1.2 Trypanosome life cycle 17

1.3 Biology of the trypanosome parasite 19

1.3.1 *T. brucei* cell shape 19

1.3.2 *T. brucei* flagellum 20

1.4 Cell cycle of *T. brucei* 22

1.4.1 Cell division in the procyclic form 22

1.4.2 Cell division in the bloodstream form 24

1.4.3 Cytokinesis 25

1.5 Eukaryotic intercellular junctions 28

1.6 Intracellular junctions in *T. brucei* 30

1.6.1 The flagellum attachment zone (FAZ) 31

1.6.2 The flagella connector 36

1.6.3 The flagellar groove 39

2 Project aims 46

2.1 Aim 46

2.2 Objectives 46

3 Methodology 47

3.1 Protein candidate selection and cell culture 47

3.1.1 Genomic database mining 47

3.1.2 Proteome analysis 47

3.1.3 Orthologue identification in other kinetoplastid species 47

3.1.4 *Trypanosoma brucei* bloodstream cell culture 48

3.1.5 *Trypanosoma congolense* bloodstream cell culture 48

3.1.6 Collection of *Trypanosoma vivax* bloodstream form cells from infected mice 48

3.2 Gene editing techniques 49
3.2.1 Generation of cell lines expressing fluorescently tagged proteins 49
3.2.2 Generation of gene deletion cell lines using CRISPR/Cas-9 50
3.2.3 Confirmation of the deletion cell lines 51
3.2.4 Inducible RNAi cell line generation 52
3.3 Preparation of solutions for microscopy 52
3.3.1 Preparation of 0.2 M phosphate buffer stock solution 52
3.3.2 Preparation of 10% paraformaldehyde solution 52
3.3.3 Preparation of buffered fixative solution for electron microscopy 52
3.4 Sample processing and image capture 53
3.4.1 Fluorescent microscopy of live cells 53
3.4.2 Scanning electron microscopy (SEM) 53
3.4.3 Single osmium processing for TEM 54
3.4.4 Double osmium processing for serial block-face scanning electron microscopy 54
3.5 Section production for electron microscopy 55
3.5.1 Glass knife preparation 55
3.5.2 Thin sectioning for TEM 56
3.5.3 Serial section ultramicrotomy for Array tomography 56
3.6 Data processing and model rendering 56
3.7 Statistical analysis 57

4 Characterisation of the groove using electron microscopy 58

4.1 The resolution of array tomography is sufficient to visualise key cytoskeletal structures surrounding the groove but is limited for 3D reconstruction of multiple cells 58
4.2 The groove resolves prior to the cleavage furrow ingresses 60
4.3 The groove resolves post-mitosis and prior to cytokinesis 62
4.4 Groove resolves when the new flagellum surpasses the old flagellum in length 68

5 Identification of 13 proteins that localise to the bloodstream form flagellar groove 71

5.1 Preface 71
5.2 A cell line expressing a flagellum tip protein was chosen as a marker 71
5.3 45 putative groove proteins were identified using TrypTag 76
5.4 13 proteins localised to the BSF flagellar groove 76
5.4.1 FAZ10 and FAZ2 localised to the full length of the FAZ and to the groove 77
5.4.2 FPRC and CIF4 localised to the distal FAZ of the old flagellum and to the groove 80
5.4.3 Five proteins localised specifically to the groove 83
5.4.4 Two proteins localised to a portion of the new FAZ and to the groove 89
5.4.5 FCP5 and FLAM3 localised to several areas in the cell and to the groove 92

5.5 Presence and absence of the proteins as the groove resolves 96
5.6 Identifying protein domains using online databases..... 100
5.7 Protein conservation among the kinetoplastids..... 102
5.7.1 Identifying orthologues of the groove proteins via reciprocal best blast 102
5.7.2 Is the groove present in *Trypanosoma vivax* and *Trypanosoma congolense*?..... 104
6 The groove is composed of proteins involved in new flagellum tip attachment to the groove and cytokinesis initiation..... 109
6.1 Preface..... 109
6.2 Confirmation of the deletion of CIF4 and FAZ15 in the provided cell lines..... 110
6.3 The deletion/depletion of CIF4, Tb427.01.2710, FCP4 and Tb427tmp.01.3030 caused groove resolution defects 111
6.3.1 Deletion of CIF4 resulted in a cytokinesis defect and premature new flagellum tip release from the groove..... 111
6.3.1.1 Deletion of CIF4 caused a severe growth defect and a cytokinesis delay..... 111
6.3.1.2 Deletion of CIF4 caused premature new flagellum tip release from the groove 113
6.3.2 Deletion of Tb427.01.2710 causes premature new flagellum distal tip release..... 117
6.3.3 Depletion of FCP4 using RNAi resulted in premature new flagellum tip release..... 121
6.3.4 Deletion of Tb427tmp.01.3030 caused delayed new flagellum tip release..... 127
6.4 The deletion of FAZ15, FAZ16, FAZ10 and FCP5 caused either a cytokinesis defect or a minor delay to the cell cycle 132
6.4.1 Deletion of FAZ15 caused a cytokinesis defect due to an accumulation of pre-cytokinetic cells and delayed new flagellum tip release 132
6.4.2 Deletion of FAZ16 caused a cytokinesis delay through the accumulation of >2K>2N and pre-cytokinetic 2F cells..... 137
6.4.3 Deletion of FAZ10 caused a minor delay to the cell cycle and new flagellum detachment from the cell body..... 142
6.4.4 Deletion of FCP5 caused a minor delay to the cell cycle but did not impact the groove 147
7 Discussion..... 153
7.1 Preface..... 153
7.2 Groove resolves as the new flagellum length exceeds the old flagellum length 154
7.3 FCP4 and Tb427.01.2710 tether the new flagellum distal tip to the groove..... 160
7.4 The groove is an elaboration of the FAZ..... 160
7.5 The full embedding of the new flagellum distal tip in a groove appears to be unique to *T. brucei* 162
7.6 Concluding remarks and future perspectives..... 165

8 References ..... Error! Bookmark not defined.

9 Appendix A: Tagging primers and relevant information regarding the gene of interest... 181

10 Appendix B: Localisation of the 45 candidate proteins 185

11 Appendix C: Non-groove proteins..... 190

12 Appendix D: Conservation of the candidate groove proteins 193

13 Appendix E: Primers for CRISPR/Cas9 and deletion confirmation 195

List of Figures

Figure 1: Morphology of kinetoplastid parasites and the life cycle of *Trypanosoma brucei* in the tsetse fly and mammalian bloodstream.....18
Figure 2: *Trypanosoma brucei* procyclic trypomastigote cell (insect host).....20
Figure 3: Biology of the *T. brucei* flagellum.....21
Figure 4: Schematic of the differences during cell division between the *T. brucei* procyclic and bloodstream form parasite.....24
Figure 5: Schematic of the cytokinesis initiation cascade in *T. brucei*.....27
Figure 6: Schematic of cell division of *T. brucei* PCF cells.....28
Figure 7: Schematic of the organisation of cell junctions in two different epithelial cells.....30
Figure 8: Organisation of the FAZ in *T. brucei*.....32
Figure 9: Alternating models of FAZ assembly.....33
Figure 10: Comparative organisation of desmosomes and the FAZ.....35
Figure 11: The FC in the PCF of *T. brucei*. 37
Figure 12: Protein composition in the FC.....38
Figure 13: Distal tip of the new flagellum in the BSF.....40
Figure 14: Association between the subpellicular microtubule cytoskeleton and the new flagellum in the groove.....41
Figure 15: Ultrastructural organisation of the cytoplasmic face of the groove.....42
Figure 16: Movement of the groove by SBFSEM.....44
Figure 17: Strategy for CRISPR/Cas9 employing a modular system for PCR-amplification or fragments targeting the gene of interest.....51
Figure 18: Array tomography image series showing sequential cross sections through the new flagellum distal tip.....58
Figure 19: Array tomography image series showing sequential longitudinal sections through the new flagellum distal tip.....59
Figure 20: Schematic representation of the groove.....60
Figure 21: SEM series of the *T. brucei* bloodstream form cell cycle.....61
Figure 22: 3D surface rendering of representative cells during stages 1-3.....63
Figure 23: Enlarged regions of the new flagellum distal tip in stage 2 and 3.....64
Figure 24: 3D surface rendering of representative cells during stages 4-7.....65
Figure 25: Enlarged region of the distal tip of the new flagellum in stage 4 and 5.....66
Figure 26: Nucleus and nucleolus volume across stages 1-7.....67
Figure 27: 3D surface rendering of representative cells during stages 3-6.....68
Figure 28: Mean length of the old and new flagellum during stages 1-7.....69
Figure 29: Growth curve of the mSc::Tb427.02.5860 marker cell line vs the 427 parental cell line.....72

Figure 30: Cell cycle of the *T. brucei* cell line expressing a flagellum tip marker Tb427.02.5860 fused to the mScarlet fluorescence protein.....73
Figure 31: Marker cell line characterisation.....75
Figure 32: Cell line expressing mSc::Tb427.02.5860 and mNG::Tb427.07.3330 (FAZ10).....78
Figure 33: Cell line expressing mSc::Tb427.02.5860 and mNG::Tb427.01.4310 (FAZ2).....79
Figure 34: Schematic of the fluorescence signal of the "Full length FAZ + groove" category.....80
Figure 35: Cell line expressing mSc::Tb427.02.5860 and mNG::Tb427.10.8240 (CIF4).....81
Figure 36: Cell line expressing mSc::Tb427.02.5860 and mNG::Tb427.10.6360 (FPRC).....82
Figure 37: Schematic of the fluorescence signal of the "Distal FAZ + groove" category.....83
Figure 38: Cell line expressing mSc::Tb427.02.5860 and mNG::Tb427tmp.01.3030.....84
Figure 39: Cell line expressing mSc::Tb427.02.5860 and mNG::CIF3.....85
Figure 40: Cell line expressing mSc::Tb427.02.5860 and CIF1::mNG. 86
Figure 41: Cell line expressing mSc::Tb427.02.5860 and mNG::FAZ16. 87
Figure 42: Cell line expressing mSc::Tb427.02.5860 and mNG::FCP4. 88
Figure 43: Schematic of fluorescence signal of the "Groove only" category. 89
Figure 44: Cell line expressing mSc::Tb427.02.5860 and mNG::FAZ15. 90
Figure 45: Cell line expressing mSc::Tb427.02.5860 and Tb427.01.2710::mNG.....91
Figure 46: Schematic of fluorescence signal of the "Comet-tail" category.....92
Figure 47: Cell line expressing mSc::Tb427.02.5860 and mNG::FCP5.....93
Figure 48: Schematic of fluorescence signal of the "Complex" category containing the expressed fusion protein, mNG::FCP5.....93
Figure 49: Cell line expressing mSc::Tb427.02.5860 and mNG::FLAM3.....95
Figure 50: Schematic of fluorescence signal of the "Complex" category containing the expressed fusion protein, mNG::FLAM3.....96
Figure 51: Map of redefined positions in the cell.....97
Figure 52: Presence and absence of the groove proteins.....98
Figure 53: CIF1, CIF3 and CIF4 localised to the cleavage furrow during cytokinesis.....99
Figure 54: Domain analysis of the 13 groove proteins identified in the localisation screen.....101
Figure 55: Protein conservation of the 13 groove proteins across selected kinetoplastids according to reciprocal best blast.....103
Figure 56: 3D surface rendering of representative cells with short new flagella in *T. brucei*, *T. congolense* and *T. vivax*.....106
Figure 57: 3D surface rendering of representative cells with long new flagella in *T. brucei*, *T. congolense* and *T. vivax*.....108
Figure 58: CIF4 and FAZ15 were successfully deleted.....110
Figure 59: The deletion of CIF4 caused a growth defect.....111
Figure 60: Deletion of CIF4 caused an accumulation of 2K2N and >2K>2N cells.....112

Figure 61: Example images of the “Other” and “>2K>2N” categories used for cell cycle analysis of the deletion cell lines……112
Figure 62: Deletion of CIF4 caused an accumulation of multinucleic cells……113
Figure 63: Deletion of CIF4 caused cytokinesis defects, premature flagellum tip detachment……..114
Figure 64: Example images of the defined zones used to analyse the position of the new flagellum distal tip……115
Figure 65: Deletion of CIF4 caused an accumulation of cells with a free new flagellum distal tip…..116
Figure 66: Deletion of Tb427.01.2710 was successful and did not cause a growth defect……..117
Figure 67: The Tb427.01.2710 deletion cell line was comparable to the control……118
Figure 68: Deletion of Tb427.01.2710 caused a slight reduction in the number of 1K1N cells…….118
Figure 69: Deletion of Tb427.01.2710 caused premature new flagellum tip release……..119
Figure 70: Deletion of Tb427.01.2710 caused premature new flagellum tip detachment……120
Figure 71: The depletion of FCP4 did not cause a growth defect……121
Figure 72: Depletion of a FCP4 caused a reduction in green signal after induction……..122
Figure 73: The depletion of FCP4 did not appear to affect cell cycle progression……..123
Figure 74: The depletion of FCP4 caused an accumulation of cells with a free new flagellum tip…..124
Figure 75: Depletion of FCP4 caused premature new flagellum tip release from the groove……125
Figure 76: Depletion of FCP4 caused premature new flagellum tip detachment……..126
Figure 77: Deletion of Tb427tmp.01.3030 was successful and did not cause a growth defect…….127
Figure 78: Deletion of Tb427tmp.01.3030 caused a minor delay to the cell cycle……..128
Figure 79: Deletion of Tb427tmp.01.3030 caused a delay in new flagellum tip release from the groove……129
Figure 80: Deletion of Tb427tmp.01.3030 caused delayed new flagellum tip……..131
Figure 81: Deletion of FAZ15 resulted in a severe growth defect……..132
Figure 82: Deletion of FAZ15 resulted in an accumulation of 2K2N cells……..133
Figure 83: Deletion of FAZ15 caused an increase in >2K>2N and zoid cells……..133
Figure 84: Deletion of FAZ15 caused an accumulation of multiflagellated cells……..134
Figure 85: Deletion of FAZ15 caused an increase in pre-cytokinetic cells and delayed new flagellum tip release……135
Figure 86: FAZ16 was successfully deleted……137
Figure 87: Deletion of FAZ16 caused growth defect and an accumulation of 2K2N cells……..138
Figure 88: Deletion of FAZ16 caused an accumulation of multinucleic cells……..139
Figure 89: Deletion of FAZ16 caused an increase in pre-cytokinetic 2F cells……140
Figure 90: Deletion of FAZ16 caused an accumulation of multiflagellated cells……..141
Figure 91: Deletion of FAZ10 was successful and caused a slight delay in the growth rate……142
Figure 92: Deletion of FAZ10 caused an accumulation of 2K2N cells and free flagella……143
Figure 93: Deletion of FAZ10 caused accumulation of cells with an attached new flagellum tip…….144

Figure 94: Deletion of FAZ10 caused an accumulation of multiflagellated cells joined at the posterior and cells with a detached new flagellum……146
Figure 95: Deletion of FCP5 clone 2 was successful……147
Figure 96: Deletion of FCP5 caused a growth defect……148
Figure 97: Deletion of FCP5 caused an accumulation of 2K2N and >2K>2N cells……149
Figure 98: Deletion of FCP5 caused an accumulation of pre-cytokinetic cells……150
Figure 99: Deletion of FCP5 caused a minor accumulation of multiflagellated cells but no other observable defects……151
Figure 100: Proposed models for groove resolution and new anterior cell tip formation……156
Figure 101: Subpellicular microtubule array repair in the "Release" model……157
Figure 102: Subpellicular microtubule array repair in the "Release-and-slide" model……158
Figure 103: Subpellicular microtubule array repair in the "Run-off" model……159
Figure 104: The *T. brucei* FC versus the *T. vivax* BSF new flagellum distal tip……164
Figure 105: Comparative models of the composition of the groove in the BSF and flagella connector in the PCF of *T. brucei*……166

List of Tables

Table 1: Cell cycle categories used to determine the changes to the volume of the nucleus and nucleolus……63
Table 2: Mean volume of the nucleus and nucleolus in each cell cycle stage……67
Table 3: The mean length of the old and new flagellum in stages 1-7……69
Table 4: Summary of the proteins that localised to the groove in bloodstream form *T. brucei*……77
Table 5: Summary of the CRISPR/Cas9 screen……109

Abbreviations

2F – two flagella

1K1N – One kinetoplast, one nucleus

2K1N – Two kinetoplasts, one nucleus

2K2N – Two kinetoplasts, two nuclei

aa – amino acids

BB – basal body

BSF – bloodstream Form

BLAST – Basic local alignment search tool

bp – base pairs

Cas9 - CRISPR-associated gene 9

CRISPR – Clustered regularly interspaced short palindromic repeats

DAPI – 4', 6'-diamidino-2-phenylindole

DMSO – dimethyl sulphoxide

FAZ – flagellum attachment zone

FC – flagella connector

FCS – Foetal calf serum

FP – flagellar pocket

gDNA – Genomic DNA

GFP – green fluorescent protein

HAT – human African trypanosomiasis

IFT – intraflagellar transport chain

kDa – Kilodalton

LB – Luria-Bertani broth

mNG – mNeonGreen

mSc – mScarlett

ORF – open reading frame

PBS – Phosphate buffered saline

PCF – procyclic form

PCR- polymerase chain reaction

PFR – Paraflagellar rod

PLK – polo-like kinase

RNAi - RNA interference

SBF-SEM – serial-block face scanning electron microscopy

SEM – scanning electron microscopy

sgRNA – Single guide nucleic acid

TEM – transmission electron microscopy

Tet – tetracycline

UTR - untranslated region

VSG - variant surface glycoprotein

1 Introduction and literature review

1.1 The African trypanosomiasis burden

African trypanosomiasis, or sleeping sickness, is a vector-borne neglected tropical disease caused by parasites of the *Trypanosoma* genus and is transmitted by the bite of an infected tsetse fly (*Glossina* genus). Two forms of the disease are endemic to sub-Saharan Africa: Human African Trypanosomiasis (HAT) and the zoonotic Animal African Trypanosomiasis (AAT), also known as *Nagana* (Aksoy, 2014). *Nagana*, caused by *Trypanosoma brucei brucei*, *Trypanosoma vivax* and *Trypanosoma congolense*, is considered to be the main disease that limits the trade of livestock in sub-Saharan Africa and kills approximately 3 million cattle annually, with an estimated loss of US $4.5 billion (Schofield and Kabayo, 2008; Hamil *et al*., 2013).

Despite the advances in controlling HAT transmission, with less than 1000 cases of human infection in 2019 (WHO, 2021), *Nagana* remains a major threat to livestock and food production across sub-Saharan Africa (Holt *et al*., 2016) and despite trypanosomiasis being extensively studied for more than a century, successful disease control strategies targeting the parasite itself are limited. There are presently no vaccines or drugs that meet all the criteria of safe, effective and affordable, making continued research into the biology of the parasite of paramount importance (Aksoy, 2014).

1.2 Trypanosome life cycle

T. brucei is a unicellular protozoan parasite from the Kinetoplastida class of excavate eukaryotes. A defining feature of kinetoplastids is the presence of the kinetoplast, an oval-shaped structure containing the mitochondrial DNA (Hammarton, 2019) (Fig. 1A). The kinetoplastid group consists of free-living biflagellates, such as *Bodo saltans*, monoxenous uniflagellates, such as *Paratrypanosoma confusum*, and dixenous parasitic flagellates such as trypanosomatids*, Leishmania* spp., and *Leptomonas* spp. (Flegontov *et al*., 2013; Skalický *et al*., 2017). *T. brucei* has a complex life cycle with several proliferative and non-proliferative stages present in both the mammalian and the insect host, each exhibiting specific adaptions to their chosen ecological niche (Wheeler *et al*., 2013). Additionally, kinetoplastid parasites display different cell shapes throughout their life cycle, including the trypomastigote,

epimastigote and promastigote forms (Sunter and Gull, 2016) (Fig. 1A). In the trypomastigote form, the life cycle form forming the basis of this PhD, the kinetoplast is posterior to the nucleus and the parasite has a long, attached flagellum (Fig. 1A).

Tsetse flies ingest the short stumpy bloodstream trypomastigote form when feeding from an infected mammalian host (Fig. 1B). Inside the fly midgut, the parasite transforms into the insect-adapted procyclic trypomastigote form (Sunter and Gull, 2016) before the parasites leave the midgut and invade the proventriculus where they differentiate into dividing epimastigotes (Langousis and Hill, 2014) (Fig. 1B). In this form, the parasites migrate to the salivary glands and establish as an epimastigote infection, before transforming into metacyclic trypomastigotes, which are infectious to mammalian hosts during the bite of the tsetse fly (Langousis and Hill, 2014) (Fig. 1B).

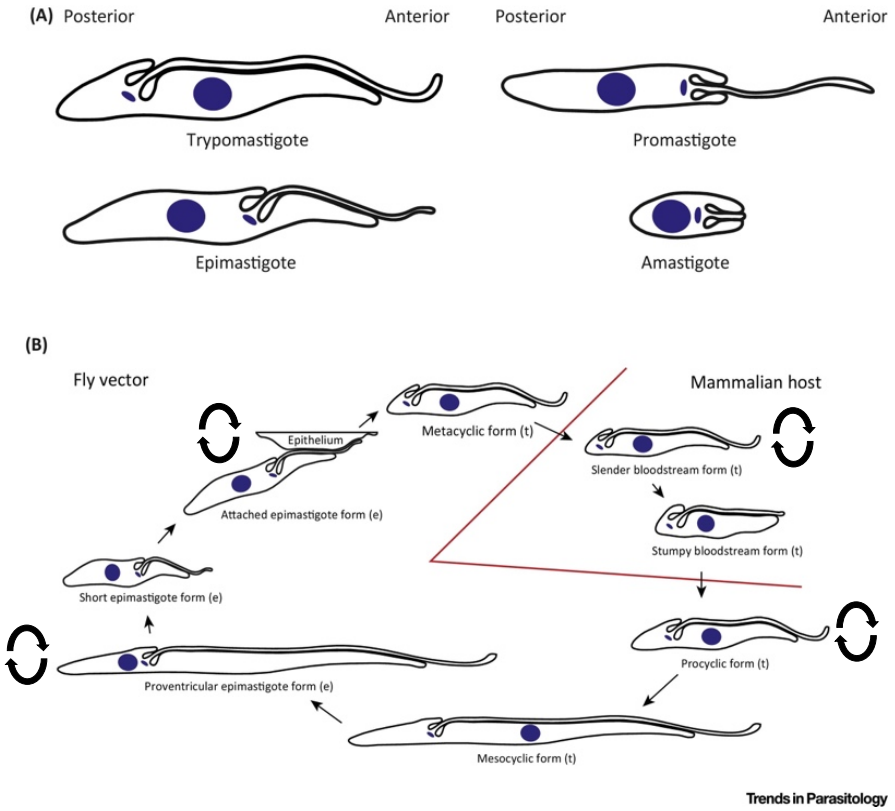

Figure 1: Morphology of kinetoplastid parasites and the life cycle of *Trypanosoma brucei* in the tsetse fly and mammalian bloodstream. A) Schematic of the morphologies of kinetoplastid parasites, each with a nucleus (large circle) and kinetoplast, containing the mitochondrial DNA (small oval at the base of the flagellum). B) Schematic of the dixenous life cycle of *T. brucei* through the tsetse fly vector and mammalian bloodstream. Circular arrows indicate proliferative life cycle forms (Sunter and Gull, 2016).

1.3 Biology of the trypanosome parasite

1.3.1 *T. brucei* cell shape

T. brucei has a slender cell shape defined by a highly structured array of subpellicular microtubules cross-linked to one another and to the cell body plasma membrane, helping to coordinate cell shape through the cell cycle (Vickerman, 1969; Sherwin and Gull, 1989; Robinson *et al*., 1995; Gull, 1999) (Fig. 2). The subpellicular microtubules are spaced every 18-22 nm and are arranged according to their intrinsic polarity with the microtubule plus ends accumulating at the posterior end of the cell body (Robinson *et al*., 1995). Unlike many other protists, *T. brucei* is able to complete cell division with a cytoskeleton dominated by microtubules, including the subpellicular microtubule array (Wheeler *et al*., 2013). The microtubule-based cytoskeleton remains almost completely intact during the cell cycle, forcing the parasite to undergo significant spatial and temporal remodelling in order to produce two daughter cells in the confines of the subpellicular microtubule array (Sherwin and Gull, 1989). Furthermore, during cell division, new microtubules are added to the existing array, with both daughter cells inheriting a mix of old and newly assembled microtubules (Sherwin *et al*., 1987; Sherwin and Gull, 1989).

The shape and form of *T. brucei* is defined by certain single copy organelles, such as the mitochondrion, kinetoplast, basal body and flagellum, and with the microtubule cytoskeleton, regulate organelle positioning, mitosis and cytokinesis (Sherwin and Gull, 1989; Robinson *et al*., 1995; Gull, 1999). A G1 cell has a single flagellum attached along the cell body via the flagellum attachment zone (FAZ) and contains a nucleus, kinetoplast, basal body pair, and flagellar pocket (Fig. 2) (Sherwin and Gull, 1989; Bastin *et al*, 2000). Cell division in *T. brucei* involves both a semi-conservative (subpellicular microtubule array) and conservative (flagellum, FAZ, basal body) inheritance pattern (Gull, 1999). During the cell cycle, a new flagellum grows alongside the old flagellum, with each new daughter cell inheriting one flagellum upon cytokinesis completion, supporting the theory of structural inheritance of shape and form in eukaryotic cells (Sonneborn, 1964; Vaughan, 2010).

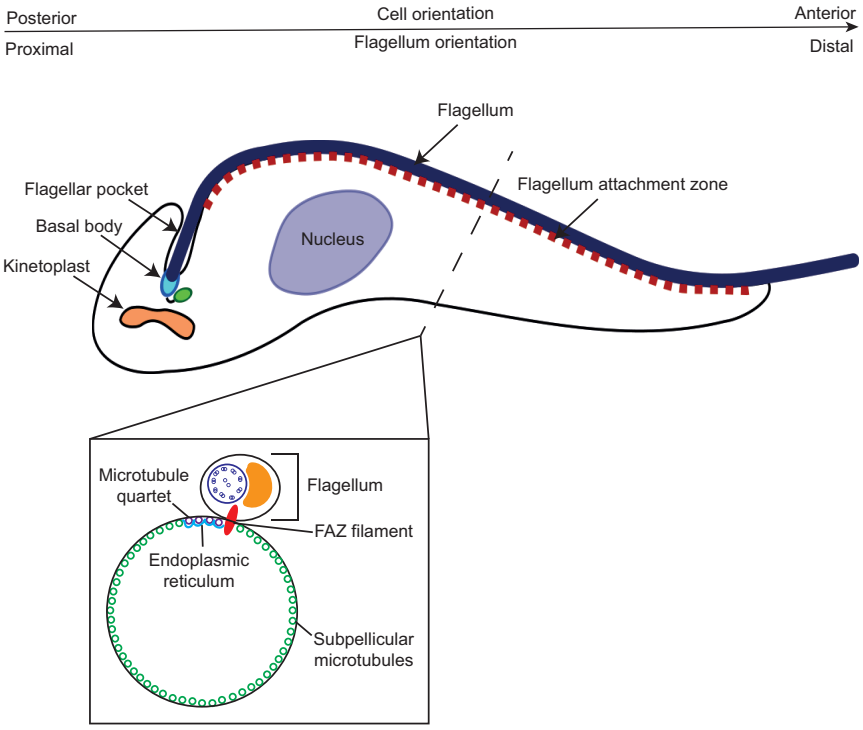

Figure 2: ***Trypanosoma brucei*** **procyclic trypomastigote cell (insect host).** Schematic of a procyclic trypomastigote with a single flagellum emerging from the flagellar pocket, attached to the cell body by the FAZ. Enlarged area shows cross section through the cell body, with subpellicular microtubules underlying the surface of the cell body plasma membrane.

1.3.2 *T. brucei* flagellum

Flagella are highly conserved biological structures found in many eukaryotes, with distinct roles in motility, cell division and cell signalling (Vincensini *et al.*, 2011; Khan and Scholey, 2018). In humans, defects in flagellum assembly and function have been linked to a number of diseases (ciliopathies), supporting their importance in human development (Waters and Beales, 2011; Maric *et al.*, 2010). In *T. brucei*, the flagellum is essential for cell morphogenesis, motility, pathogenicity and cell division and can be related to survival mechanisms through the evasion of the host's innate and adaptive immune system (Vickerman, 1985; Bastin *et al.*, 1998; Griffiths *et al.*, 2007; Vaughan and Gull, 2008). Since motility is essential for parasite survival within the mammalian bloodstream, examining how flagellum growth affects pathogenicity is very relevant to understanding infection in both animal and human hosts.

The flagellum is nucleated by the basal body, which is attached to the mitochondrial DNA containing kinetoplast, located at the proximal end of the flagellum (Fig. 2) (Sherwin and

Gull, 1989; Woodward and Gull, 1990; Gluenz *et al*., 2011). At the posterior end of the cell body, the flagellum extends out of the flagellar pocket (FP) (Fig. 2). The FP is a highly differentiated invagination of the plasma membrane that enhances the pathogenicity of the parasite in the mammalian vasculature by being the only site of endocytosis and exocytosis in the cell (Field and Carrington, 2009; Gadelha *et al*., 2009), with RNAi of BILBO1, a key cytoskeletal protein in the flagellar pocket collar leading to cell death in the BSF (Bonhivers *et al*., 2007). All life cycle stages of *T. brucei* have a flagellum, attached along the cell body length by the FAZ and is composed of the highly conserved 9+2 microtubule axoneme structure (Sherwin and Gull, 1989) (Fig. 3A). A para-crystalline structure, the paraflagellar rod (PFR), becomes associated with the axoneme at the flagellar pocket neck region and runs along most of the axoneme length, tapering out before the distal tip of the flagellum (Sherwin and Gull, 1989; Gull, 1999; Portman and Gull, 2010; Vaughan, 2010) (Fig. 3B).

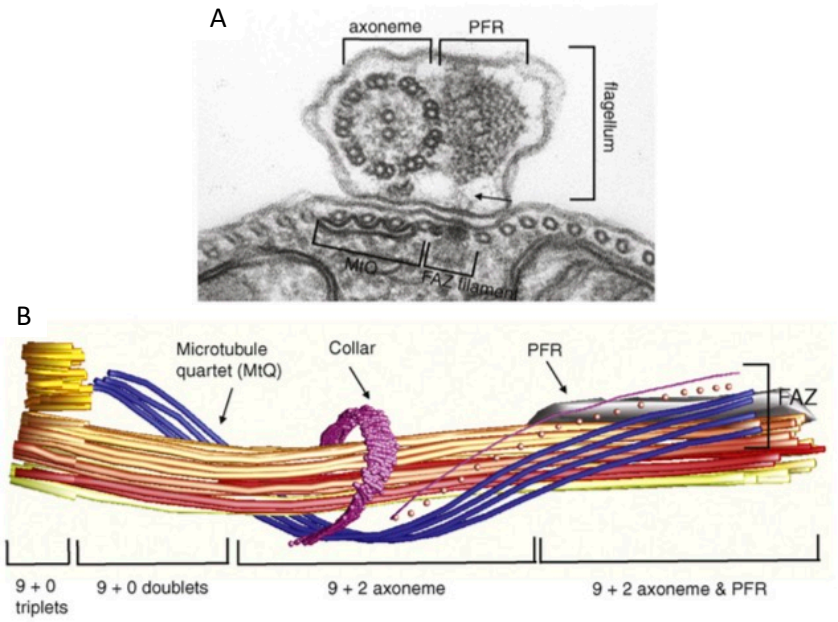

Figure 3: Biology of the *T. brucei* flagellum. A) Transmission electron micrograph (TEM) cross section through the trypanosome flagellum. The 9+2 microtubule axoneme, PFR, microtubule quartet and associated FAZ filament are indicated. B) 3D reconstruction of a tomogram of the FP, with membranes removed (E). Key: BB = basal body; PBB = pro-basal body; FP = flagellar pocket; PFR = paraflagellar rod; MtQ = microtubule quartet; FAZ = flagellum attachment zone = ER, endoplasmic reticulum. (Reproduced with copyright permission from Elsevier, taken from Vaughan, 2010).

Additionally, a set of four microtubules, the microtubule quartet (MtQ), is associated with the FAZ filament and flagellum in *T. brucei* (Gull, 1999) (Fig. 3A). The MtQ is nucleated near

the pro-basal body and wraps around the FP before extending along the FAZ for the entire length of the cell (Lacomble *et al*., 2009; Sunter *et al*., 2015a) (Fig. 3B).

1.4 Cell cycle of *T. brucei*

In *T. brucei*, the regulation and coordination of the cell cycle is necessary for cell morphogenesis and persistence in both the insect vector and mammalian host. *T. brucei* has three distinct sub-cycles which control the duplication and segregation of three vital cellular components: the nucleus, the kinetoplast and the cytoskeleton (Wheeler *et al*., 2019). The sub-cycles are able to work independently from each other, for example, the inhibition of nuclear S-phase or mitosis has little impact on the ability of the cytoskeletal structures like basal body and flagellum to duplicate and segregate, however, the resulting daughter cells post-cytokinesis are often abnormal (Ploubidou *et al*., 1999; Hammarton, 2007). Two proliferative forms of *T. brucei*, the procyclic and bloodstream forms, have been the basis for much of the research into *T. brucei* cell shape, morphogenesis, pathogenicity and cell biology due to the successes of axenic cell culture. However, several differences in organelle structure and biochemical adaptations exist between the two life cycle forms (Vickerman, 1962; Vickerman, 1969).

1.4.1 Cell division in the procyclic form

At the beginning of each cell cycle (G1), procyclic form (PCF) *T. brucei* cells have a long, slender cell shape with a single flagellum that exits the FP at the posterior end of the cell body. The flagellum is laterally attached along the length of the cell body and the cell possesses a set of single-copy organelles including one kinetoplast and one nucleus (Wheeler *et al*., 2013) (Fig. 4A). During cell division, a PCF cell nucleates a new flagellum from the pro-basal body, which exits the existing FP to grow alongside the old flagellum (Fig. 4A). The new flagellum distal tip is physically attached to the old flagellum by the flagella connector (FC), a mobile transmembrane junction that connects the two flagella external to the cell body (Moreira-Leite *et al*., 2001; Briggs *et al*., 2004; Davidge *et al*., 2006) (Fig. 4B). The FC migrates along the old flagellum as the new flagellum elongates, and the flagellar pockets segregate, with the FP of the new flagellum always positioned more posterior than the FP of the old flagellum (Fig. 4C). Furthermore, the new flagellum is positioned to the left of the old

flagellum when viewing the parasite from the posterior end (Sherwin and Gull, 1989) (Fig. 4C).

As the new flagellum grows, the two flagella begin to move progressively further apart at the posterior end as the FC migrates towards the cell's anterior tip, indicative of the insertion of new microtubules into the subpellicular array (Wheeler *et al*., 2013) (Fig. 4C). Once the new flagellum is approximately 0.6 of the length of the old flagellum, the FC reaches a "stop point" before cytokinesis occurs (Davidge *et al*., 2006; Varga *et al*., 2017) (Fig. 4C). Once the FC has halted its migration, the division fold forms between the two flagella, representing an invagination in the plasma membrane delineating the two daughter cells (Fig. 4D). The division fold defines two nascent posterior ends of the daughter cells, representing the asymmetry of PCF cell division, with the daughter cell associated with the new flagellum (new daughter cell) more posterior to the daughter cell associated with the old flagellum (old daughter cell) (Fig. 4D-E). The posterior end of the old daughter cell is positioned along the ventral surface of the new daughter cell (Fig. 4D-E) (Campbell and De Graffenried, 2020). The FC maintains the connection between the new flagellum distal tip and the old flagellum when a cleavage furrow begins to ingress along the division fold from the anterior end of the cell towards the posterior, separating the two daughter cells (Briggs *et al*., 2004; Davidge *et al*., 2006) (Fig. 4E). The FC releases the new flagellum distal tip and abscission of the membrane joining the two posterior ends separates the two daughter cells (Moreira-Leite *et al*., 2001) (Fig. 4G).

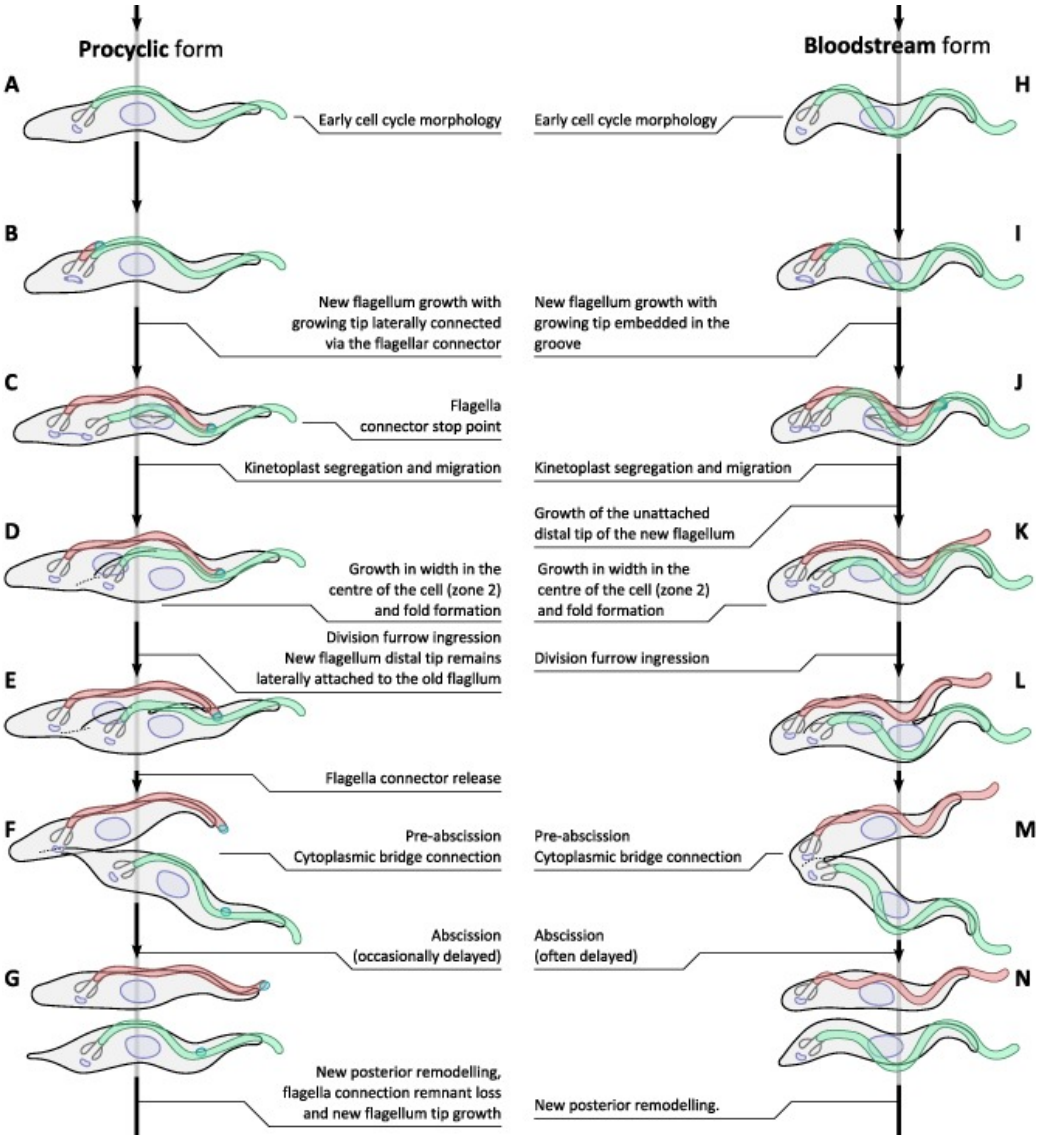

<u>Figure 4:</u> Schematic of the differences during cell division between the *T. brucei* procyclic (A-G) and bloodstream form parasite (H-N). Key: old flagellum in green, new flagellum in red (Wheeler *et al*., 2013).

1.4.2 Cell division in the bloodstream form

The bloodstream form (BSF) of *T. brucei* also has a single attached flagellum at the beginning of the cell cycle (G1) that extends out from the FP at the posterior end of the cell body and is attached to the length of the cell body via the FAZ (Fig. 4H). The first morphogenetic difference between the BSF and PCF is that in the BSF, the FP is positioned closer to the posterior cell tip than in the PCF (Fig. 4H). The new flagellum exits the FP and is positioned posterior to the old flagellum (Fig. 4I); however, during new flagellum growth, the BSF does not have a FC tethering the distal tip of the new flagellum to the side of the old flagellum,

instead the new flagellum distal tip is embedded in a discrete invagination of the cell body plasma membrane, termed the groove (Hughes *et al*., 2013) (Fig. 4I-J). The groove is a mobile transmembrane junction that migrates beside the old flagellum as the new flagellum elongates (Fig. 4I-J), initiating significant remodelling of the subpellicular microtubule array during its migration (Hughes *et al*., 2013). As the new flagellum continues to elongate, the flagellar pocket associated with the new flagellum moves further posterior to the flagellar pocket associated with the old flagellum, and the new flagellum is positioned to the left of the old flagellum when viewing the cell from the posterior end (Fig. 4J-K). Once the groove approaches the anterior cell tip, the groove resolves and releases the distal tip of the new flagellum prior to cleavage furrow ingression (Fig. 4K). This highlights a further morphogenetic difference between the PCF and BSF, with the new flagellum remaining attached to the FC as the cleavage furrow ingresses in the PCF (Wheeler *et al*., 2013). Once the groove has resolved, the division fold is formed between the two flagella, delineating the two daughter cells through an invagination in the cell body plasma membrane (Fig. 4K-L). The cleavage furrow ingresses along the division fold from anterior to posterior, separating the two daughter cells; however, the BSF is unlike the PCF in that the two posterior ends of the daughter cells are much closer together and remain tethered at the posterior cell tip through until abscission of the connecting membrane to produce two daughter cells, each inheriting a set of single-copy organelles and a flagellum (Fig. 8L-N).

1.4.3 Cytokinesis

Cytokinesis is the final stage of cell division where the cytoplasm and organelles are divided (Hammarton, 2019). Eukaryotes such as yeasts, mammals and nematodes make use of a highly regulated mechanism for cytokinesis that relies upon an actomyosin contractile ring (Hartwell *et al*., 1970; Schroeder, 1972). However, this mechanism of cytokinesis is not a one-size-fits-all model outside of the eukaryotic groups Opisthokonta and Amoebozoa (Burki *et al*., 2020), with non-muscle myosin II, the most constrictive force during Opisthokonta cytokinesis, not conserved in other evolutionary supergroups (Richards and Cavalier-Smith, 2005; Foth *et al*., 2006). In some eukaryotes, cell division is both myosin II-independent and actin-independent, suggesting that cytokinesis in eukaryotes may be more mechanistically diverse than originally thought (Richards and Cavalier-Smith, 2005). Land plants and some green algae species use vesicles to deliver the machinery to assemble the phragmoplast to undergo cytokinesis, which is composed of actin, microtubules, membranes and proteins

(Livanos and Muller, 2019), while other green algae species, such as *Chlamydomonas*, make use of a microtubule-based phycoplast (Cross and Umen, 2015). The protozoan *Entamoeba* possess myosin II but lack the actomyosin ring, making use of the primitive method of cytofission, whereas *Theileria* and some *Eimeria* spp. make use of apicomplexan budding and hijacking of host mitotic machinery in order to undergo cytokinesis (Hammarton, 2019). Interestingly, the parasitic *Naegleria* spp. appear to divide using the actomyosin ring despite the majority of the Excavata parasites, including *T. brucei*, *Giardia* and *Trichomonas*, lacking myosin II (Richards and Cavalier-Smith, 2005; Odronitz and Kollmar, 2007; Sebe-Pedros *et al*., 2014). Parasitic protozoa that lack myosin II appear to divide along the longitudinal axis of the cell body, relying on flagellar motility, cytoskeletal rearrangements and complex signalling pathways to complete cell division (Hammarton, 2019). Given that cytokinesis is a highly divergent mechanism amongst eukaryotes, identifying key cytokinesis proteins and understanding the nuances of cytokinesis mechanisms in parasitic protozoa represents potential for developing novel drugs targeting cytokinesis.

Cytokinesis in *T. brucei* is synchronised by a complex cascade of evolutionarily conserved and trypanosomatid-specific regulatory proteins and a microtubule-based mechanism for cell morphogenesis. *T. brucei* utilises a progressive recruitment of proteins to the cytokinetic complex at the distal tip of the new FAZ and to the cleavage furrow in order to initiate cytokinesis. A collection of proteins in the PCF, such as CIF1, CIF2, CIF3, CIF4 and FPRC, form a hierarchy during cytokinesis initiation and the depletion of each individual protein results in a severe cytokinesis defect through the accumulation of multiflagellated and multinucleic cells and a disruption in cleavage furrow ingression (McAllaster *et al*., 2015; Zhou *et al*., 2016a; Sinclair-Davis *et al*., 2017; Hilton *et al*., 2018; Kurasawa *et al*., 2018; Zhou *et al*., 2018; Hu *et al*., 2019) (Fig. 5).

In summary, TOEFAZ1 (Tip of the extending FAZ protein 1), also known as CIF1 (Cytokinesis initiation factor 1) recruits a homologue of the well-characterised Polo-like kinase protein, TbPLK, to the new FAZ tip, which in turn recruits key cytokinesis regulating proteins to the new FAZ tip (Kumar and Wang, 2006; Hammarton *et al*., 2007; De Graffenried *et al*., 2013). In PCFs, CIF1 is likely to function as a scaffold protein by recruiting other cytokinesis regulating proteins to the new FAZ to initiate cytokinesis (Sinclair-Davis *et al*., 2017; Hilton *et al*., 2018; Kurasawa *et al*., 2018; Zhou *et al*., 2018; Hu *et al*., 2019). Furthermore, some kinetoplastid-specific proteins form complexes with each other at the new FAZ tip in PCFs,

such as the CIF1-CIF2, the CIF1-CIF3 and the CIF4-FPRC-CIF1 complexes (Zhou *et al*., 2016a; Zhou *et al*., 2016b; Zhou *et al*., 2018; Kurasawa *et al*., 2018). More recently, the interaction between CIF1, CIF2 and CIF3 have been outlined in BSFs, with comparable phenotypes resulting from RNAi depletion, suggesting that the hierarchy of these proteins is similar between the BSF and PCF (Zhang *et al*., 2019). A schematic of potential interactions and hierarchy of the proteins involved in the cytokinesis initiation cascade in PCFs has been proposed, and with it, a hypothesis that cytokinesis initiation in the BSF displays a similar cascade of protein recruitment and interaction (Fig. 5). However, there may be functional differences between conserved proteins across the two life cycle forms, with the parasite repurposing specific proteins in order to persist in their chose ecological niche.

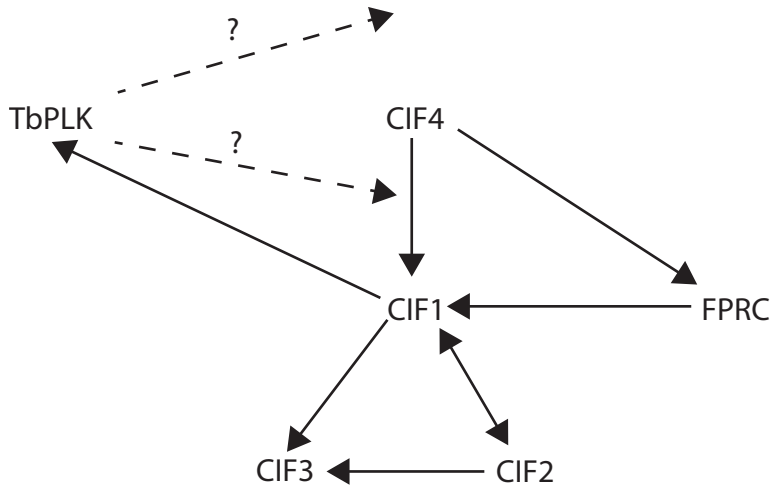

Figure 5: Schematic of the cytokinesis initiation cascade in *T. brucei*. Solid arrows indicate the direction of interaction between each protein, supported by experimental evidence. Dashed arrows indicate proposed direction of interaction in the cascade; however, no experimental evidence is present to date.

The location and movement of the cleavage furrow in *T. brucei* is likely distinct from other well-studied eukaryotic organisms, due to the lack of non-muscle myosin II and the actomyosin ring in *T. brucei* (García-Salcedo *et al*., 2004). In *T. brucei*, cleavage furrow ingression likely occurs due to the reorganisation, severing and reforming of the highly polarised microtubule cytoskeleton and the complex sequential recruitment of cytokinetic proteins to the new FAZ tip (Campbell and De Graffenried, 2020). The developing new MtQ may provide the blueprint for the cleavage furrow to ingress along in order to divide the subpellicular microtubule array between the nascent daughter cells, as the new MtQ is associated with the new FAZ of the new flagellum and is said to transport TbPLK during its migration to the new FAZ tip (Lacomble *et al*., 2010; Ikeda and De Graffenried. 2012;

Campbell and De Graffenried, 2020) (Fig. 6). Furthermore, as the MtQ microtubules are opposite in polarity to the subpellicular microtubules, they may aid in recruiting and transporting proteins to the cytokinetic complex during cell division (Robinson *et al*., 1995; Campbell and De Graffenried, 2020) (Fig. 6).

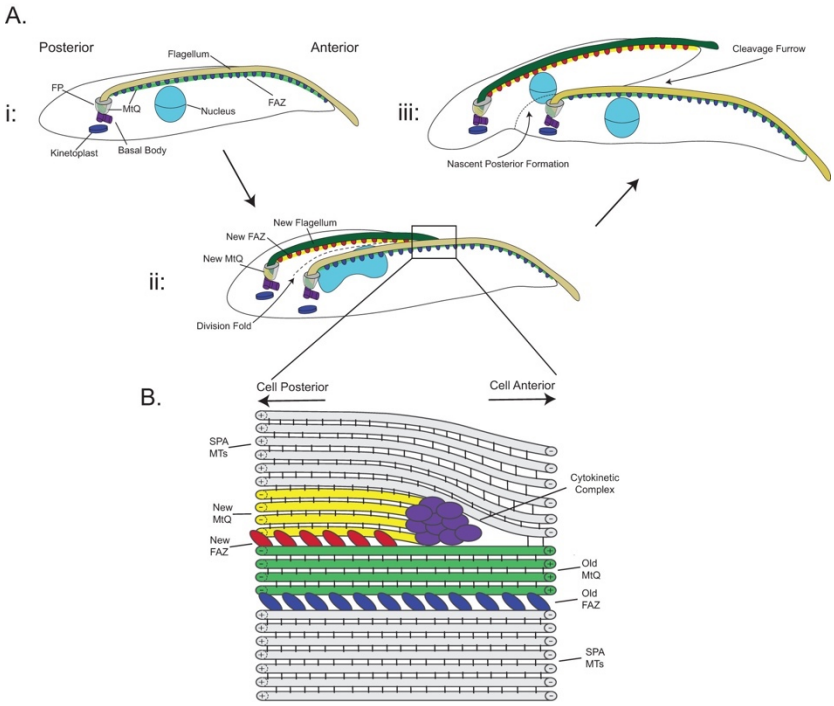

Figure 6: Schematic of cell division in *T. brucei* PCF cells. A) Schematic of cell division in the PCF of *T. brucei*. Dashed line bisecting the cell in (ii) indicates division fold formation. Dashed line (iii) indicates the formation of the nascent posterior end of the daughter cell. B) Schematic of the organisation of the new FAZ filament and new MtQ in relation to the old FAZ and MtQ and the subpellicular microtubule array. The cytokinetic complex at the distal end of the extending new MtQ is likely severing the crosslinks between the old MtQ and the adjacent subpellicular microtubules (Campbell and De Graffenried, 2020).

As the majority of proteins involved in cytokinesis localise to the new FAZ to initiate cytokinesis, the new MtQ may, by association with the new FAZ, direct the formation of the cleavage furrow along the division fold to bisect the two nascent daughter cells.

1.5 Eukaryotic intercellular junctions

Cell junctions connect cells to each other and other tissues and are crucial for the formation of multicellular organisms by anchoring cells to each other or supporting tissues, whilst enabling cell-cell communication (Garcia *et al*., 2017). Epithelial tissues show a range of cell-

cell junctions, including tight junctions, adherens junctions and desmosomes, which all form connections between two adjacent cells (Garcia *et al*., 2017). Plant cells, on the other hand, have plasmodesmata that span the plant cell walls to connect protoplasts of adjacent cells (Han *et al*., 2019). Cell-cell junctions maintain homeostasis across the plasma membrane of cells through ion exchange, regulating structural integrity, aiding in cell division and cell migration (Garcia *et al*., 2017). Each junction serves a specific purpose within epithelial tissues, thereby utilising a unique composition of proteins to achieve these functions (Abedin and King, 2010). Taken together, these proteins provide sufficient adhesive and structural support that allow the junction to resist mechanical stress, block particles from entering or leaving the cell and to communicate with the adjacent cell via the passage of signalling molecules (Abedin and King, 2010).

Tight junctions are associated with apical end of the lateral plasma membrane and provide a physical barrier between adjacent cells (Zihni *et al*., 2016). The dominant proteins in tight junctions are the transmembrane proteins claudin and occludin (Van Itallie and Anderson, 2014) which can form complexes that tether cells to each other (Fig. 7). Claudin and occludin bind directly to cytoplasmic adaptor proteins that in turn bind to the actin cytoskeleton, with actin turnover and actomyosin contraction regulating the tight junction barrier function (Umeda *et al*., 2004; Shen *et al*., 2006; Van Itallie *et al*., 2009; Fanning *et al*., 2012) (Fig. 7). Adherens junctions are responsible for initiating and maintaining the adhesion between two adjacent cells, as well as actively regulating the organisation of the actin cytoskeleton and establishing a signalling hub along the cell junction (Takeichi, 2014). Adherens junctions are composed mainly of transmembrane cadherins, E-cadherin in particular, which forms a ternary complex with Beta- and alpha-catenin, members of the Armadillo family of proteins (Shapiro and Weis, 2009; Buckley *et al*., 2014) (Fig. 7). Desmosomes, on the other hand, are composed of transmembrane cadherin proteins, such as desmoglein and desmocollin which establish a direct link to neighbouring cells to prevent damage due to mechanical stress by interacting with two members of the Armadillo family of proteins called plakoglobin and plakophilin (Broussard *et al*., 2017) (Fig. 7).

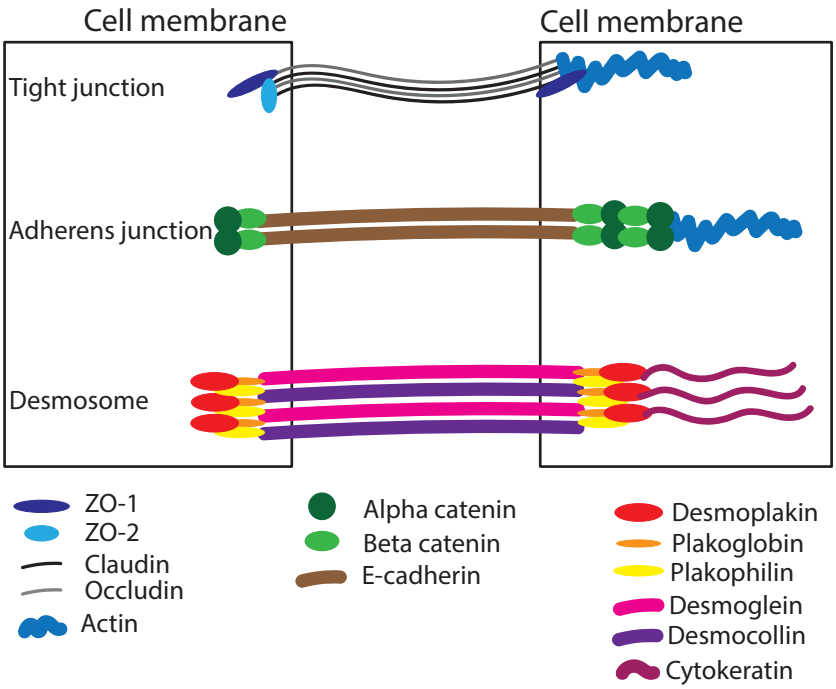

Figure 7: Organisation of cell junctions in two adjacent epithelial cells. Schematic representation of the protein composition and spatial arrangement of adhesive cell junctions in epithelial cells including the tight junction (top), adherens junction (middle) and desmosome (bottom).

1.6 Intracellular junctions in *T. brucei*

Cell junctions can also occur within the same cell, representing intracellular junctions, with cytoskeletal connections securing these frameworks to provide a distinct membrane-to-membrane junction (Sunter *et al*., 2015a; Höög *et al*., 2016). *T. brucei* is able to form several types of cell junctions to enhance pathogenicity in both the insect and mammalian host, with four distinct junctions present during the *T. brucei* lifecycle: 1) the junction between the *T. brucei* flagellum and the host epithelial cells; 2) the FAZ; 3) the flagella connector in the procyclic form; 4) the groove in the bloodstream form.

During its life cycle, *T. brucei* forms an asymmetric intercellular junction between the flagellum and the epithelia in the tsetse fly salivary glands in order to divide while attached to the host cells (Tetley and Vickerman, 1985). Certain lifecycle stages of other kinetoplastid parasites, such as *Trypanosoma congolense*, *Trypanosoma vivax* and *Leishmania mexicana*, also attach to host epithelia through intercellular junctions extending from the parasite flagellum across the host plasma membrane (Vickerman, 1973; Beattie and Gull, 1997; Gluenz *et al*., 2010).

1.6.1 The flagellum attachment zone (FAZ)

The FAZ is a defining feature of *T. brucei* cell shape and acts as a determinant of cell morphology by aiding the regulation of cell length and organelle positioning, making it structurally important for cell division (Sunter and Gull, 2016). The FAZ represents one of the most complex plasma-membrane-to-plasma-membrane intracellular junctions described in eukaryotic cells given that the FAZ embodies a filamentous connection between two distinct plasma membranes within the same cell (Sunter *et al*., 2015a).

Initially, the FAZ was defined as an arrangement of macular densities (approximately 70 nm apart) on the cytoplasmic side of the junction between the flagellum and cell body, with fibres extending from the PFR to the attachment plaques of the FAZ (Vickerman, 1969; Hogan and Patton, 1976; Höög *et al*., 2012). Flagellum attachment is maintained by structures within the FAZ that encompass three major zones: (i) the flagella and cell body membranes; (ii) the fibres that extend from the axoneme and PFR to the flagellar membrane; (iii) the FAZ filament and MtQ within the cell body and their connections to the cell body membrane (Robinson *et al*., 1995; Vaughan *et al*., 2008; Höög *et al*., 2012; Hayes *et al*., 2014) (Fig. 8B-C).

Once emerged from the FP at the posterior end of the cell, the new flagellum is elongated whilst remaining attached to the cell body, with the assembly of the flagellum and the FAZ occurring at similar rates (Kohl *et al*., 1999). The axoneme and PFR are assembled from the distal tip of the flagellum, with proteins being transported to along the flagellum via the intraflagellar transport (IFT) system (Bastin *et al*., 1999; Kohl *et al*., 2003; Farr and Gull, 2009); however, it was determined that the FAZ is assembled at the proximal end of the flagellum, with two proposed models of how the elongation of the FAZ coordinates with new flagellum elongation (Sunter and Gull, 2016). The FAZ assembly 'push' model suggests that as a FAZ protein is added to the proximal end of the FAZ, this addition will effectively 'push' the assembled FAZ along as the new flagellum elongates (Sunter and Gull, 2016) (Fig. 9B). The second model, the FAZ assembly 'pull' model, suggests that the there is a putative protein complex present at the distal end of the flagellum that 'pulls' the assembled FAZ along as the new flagellum elongates, with new FAZ proteins filling in the available space at the proximal end (Sunter and Gull, 2016) (Fig. 9C).

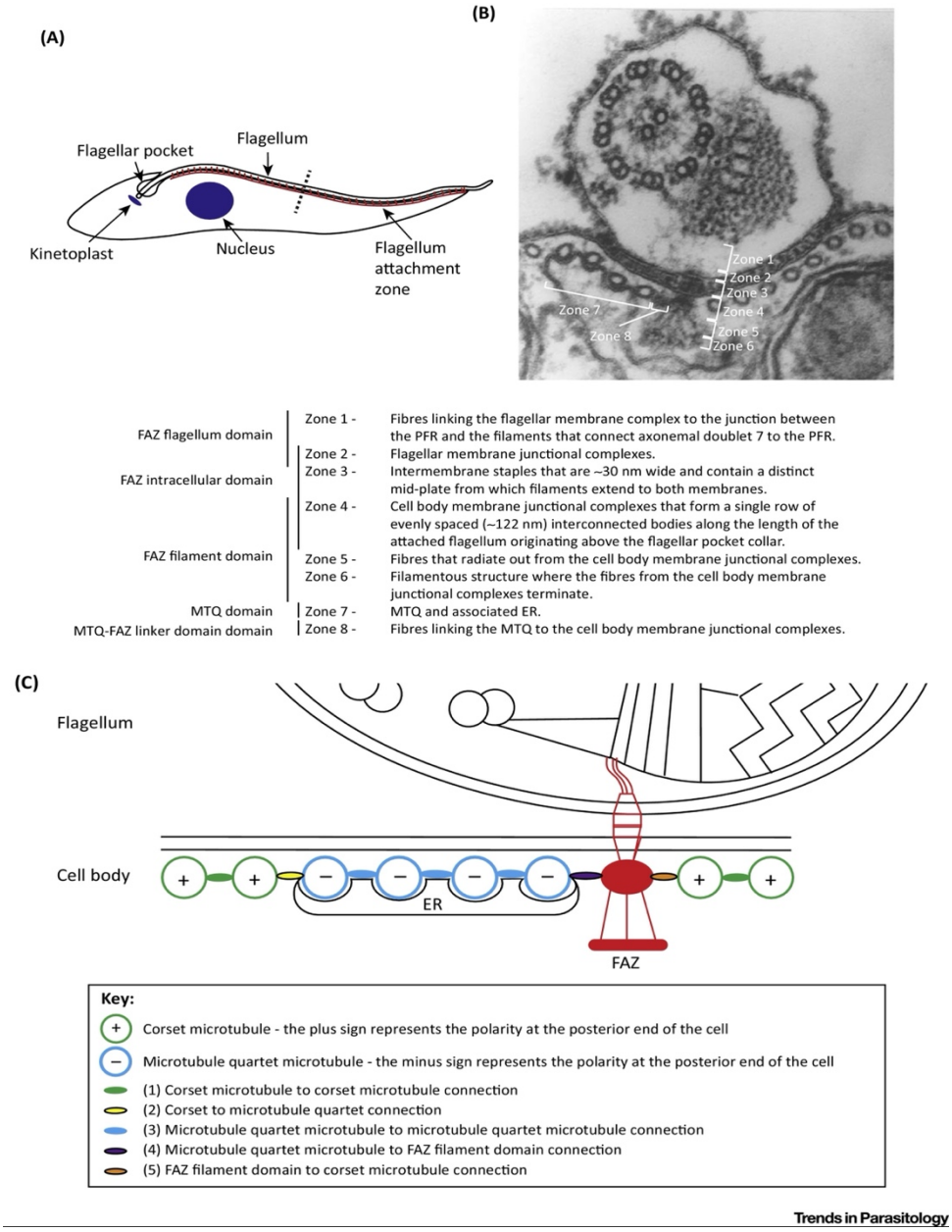

<u>Figure 8:</u> Organisation of the FAZ in *T. brucei*. A) Schematic of a trypomastigote *T. brucei* cell. B) TEM cross section through a flagellum showing eight zones of the FAZ. C) Schematic of the FAZ in cross section showing five distinct filament connections. Opposite polarity of the MtQ (blue, - polarity) and the subpellicular microtubules (green, + polarity) indicated. Key: MtQ = microtubule quartet; FAZ = flagellum attachment zone = ER, endoplasmic reticulum; + = plus-end of the microtubule; - = minus-end of the microtubule. (Sunter and Gull, 2016).

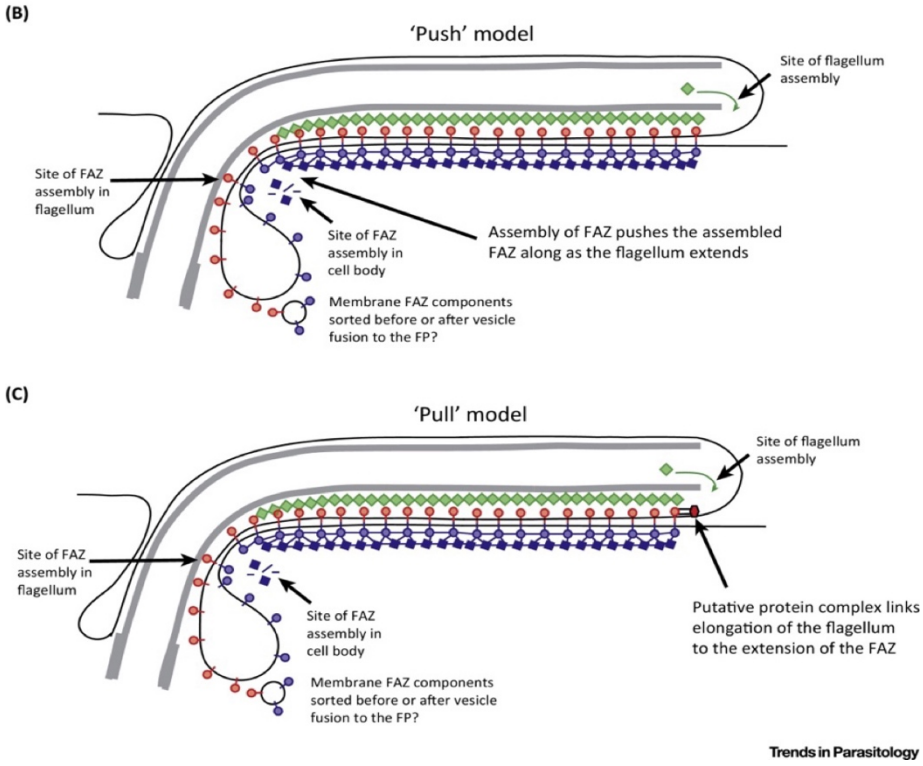

Figure 9: Alternating models of FAZ assembly. B) The FAZ assembly 'push' model. The FAZ is assembled from the proximal end of the flagellum and the FAZ is pushed out with the extending flagellum, like a conveyor belt. C) The FAZ assembly 'pull' model. A putative protein complex at the distal end of the FAZ pulls the assembling FAZ out with the elongating flagellum. (Adapted from Sunter and Gull, 2016).

The ability to define in which FAZ domain proteins are present may predict resulting phenotypes from the depletion of a given protein (Sunter and Gull, 2016). Depletion of proteins present in the FAZ flagellum domain, such as Calpain-like protein GM6 (ClpGM6) and FLAM3, results in the repositioning of the kinetoplast, basal body, Golgi and the FP as well as FAZ shortening (Hayes *et al*., 2014; Sunter *et al*., 2015b) (Fig. 10B). Whereas the depletion of proteins present in the FAZ filament domain on the cell body side of the junction, such as FAZ1, CCD2 and FAZ2, cause flagellar detachment defects (Vaughan *et al*., 2008; Zhou *et al*., 2011; Zhou *et al*., 2015) (Fig. 10B). The FAZ intracellular domain lies between the FAZ flagellum and FAZ filament domains and is composed of a small number of transmembrane proteins with an intracellular domain and a glycosylated extracellular region involved in protein interaction (Moreira *et al*., 2017) (Fig. 10B). FLA1, FLA1BP and FAZ10 are three proteins present in the FAZ intracellular domain (Nozaki *et al*., 1996; LaCount *et al*., 2002; Sun *et al*., 2013; Sunter and Gull, 2016; Moreira *et al*., 2017) (Fig. 10B). FLA1 and FLA1-binding protein (FLA1BP) interact with each other in a zipper-like manner, and bind to

opposite membranes in the FAZ, thereby ensuring flagellum attachment to the cell body (Sun *et al*., 2013) (Fig. 10B). FAZ10, on the other hand, localises to the intermembrane staples in the FAZ intracellular domain, with its depletion resulting in defects in cell morphogenesis, flagellum attachment and kinetoplast/nucleus positioning (Moreira *et al*., 2017). Furthermore, FAZ10 is also involved in the correct orientation of the cleavage furrow, suggesting that FAZ10 plays a role in cytokinesis as a major FAZ component (Moreira *et al*., 2017).

The arrangement of fibrillary links in the FAZ is reminiscent a cell-cell adhesive desmosome-like structure found in other multicellular organisms (Vickerman, 1969; Hemphill and Ross, 1995), thereby connecting the flagellum to the trypanosome cell body through interconnected fibres, filaments and junctional complexes (Sunter and Gull, 2016) (Fig. 10A). Desmosomes consists of an intercellular adhesive core, consisting of cadherins such as desmoglein and desmocollin, connecting two plasma membranes (Nekrasova *et al*., 2011) (Fig. 10A). Underlying each plasma membrane, is the cytoplasmic plaque that connects the internal intermediate filaments to the cadherins of the intercellular junction and consists of proteins from the Armadillo protein family, including plakoglobin and plakophilin, as well as desmoplakin, a cytoskeletal adaptor protein (Garrod and Chidgey, 2008) (Fig. 10A). Protein conservation between the FAZ and desmosome was explored by interrogating the *T. brucei* genome for known desmosomal proteins and despite the lack of proteins containing cadherin repeats, three *T. brucei* proteins containing armadillo repeats were identified (Branche *et al*., 2006; DeGrasse *et al*., 2009). One of these proteins (Tb927.10.14320 or FAZ9) was recently localised to the proximal end of the FAZ in the FAZ filament domain, reminiscent of the position of plakoglobin, plakophilin and desmoplakin (Branche *et al*., 2006; DeGrasse *et al*., 2009). Furthermore, the interaction between FLA1 and FLA1BP between the flagellum and cell body plasma membrane and their association with cytoskeletal components is similar to transmembrane cadherins in desmosomes that interact with the actin cytoskeleton in adjacent cells (Sun *et al*., 2013) (Fig. 10A).

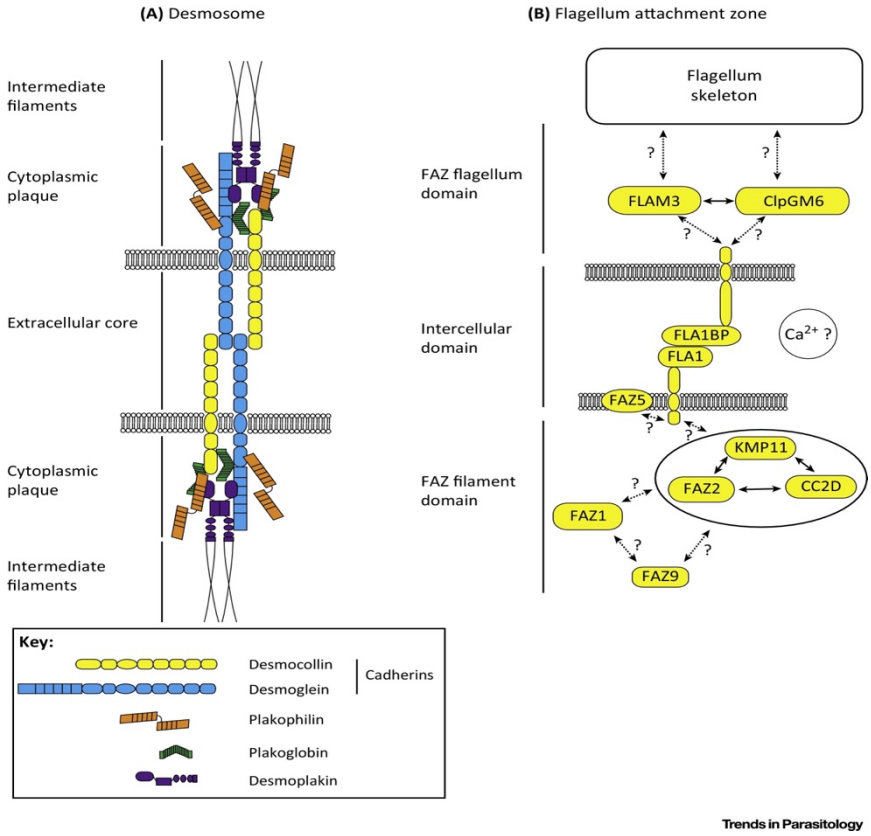

Figure 10: Comparative organisation of desmosomes and the FAZ. A) Schematic of a desmosome junction, showing the transmembrane organisation of the filament extensions. B) Predicted model of the protein composition of the FAZ junction, showing analogous organisation to desmosomes. Interactions with experimental evidence represented with a solid black arrow, whereas predicted interactions are represented by a dotted black arrow (Sunter and Gull, 2016).

Despite the lack of protein conservation between desmosomes and the FAZ, it is evident that the structure of the FAZ is reminiscent of desmosomes with the FAZ also composed of three distinct domains: 1) The cytoplasmic filament; 2) The transmembrane junctional complexes; 3) The flagellum filament (Sunter *et al*., 2015a). With this in mind, the FAZ may merely represent an intracellular modification of the desmosome, repurposing structural components that are able to resist mechanical stress during parasite motility through the insect and mammalian hosts.

Structures resembling the desmosome and FAZ are seen in other eukaryotic organisms, suggesting that this parallel is more frequent than originally thought. One of the four flagella in *Trichomonas vaginalis* is positioned along the body of the organism in close proximity to the undulating membrane, joined by a costa, which is "a thick filamentous rod composed of large, striated fibres that oppose the undulating membrane on the cytosolic side"

(Ovčinnikov *et al*., 1974). Furthermore, two species of *Hydra* (*Pelmatohydra oligactis* and *Chlorohydra viridissima)* possess structures termed "intercellular attachment lamellae" which join two adjacent epithelial cells in a desmosome-like manner (Wood, 1959). These were coined *septate desmosomes*, and similar transverse connections were observed as desmosome-like connections in the lamellar sheath of earthworm nerve fibres (Hama, 1959), in the sea anemone (Grimston *et al*., 1958) and in sea urchin embryos (Balinsky *et al*., 1959). Septate desmosomes in *Hydra* possess an accumulation of fine fibrils underlying the plasma membrane of adjacent cells, showing some similarity to vertebrae desmosomes but also unique modifications of the structure itself (Wood, 1959). Furthermore, at the region where the flagellum exits the flagellum pocket in *Crithidia fasciculata*, the flagellar membrane is tightly opposed to the cell membrane through what the authors call a "desmosome," a fine fibrous material approximately 18 nm thick on the cytoplasmic side of the junction reminiscent of the FAZ in *Leishmania* (Brooker, 1971).

Undoubtedly, the FAZ, represents one of the most complex plasma membrane structures found in eukaryotic cells, with this connection being maintained within the same cell and not between two different cells like other known cell junctional complexes.

1.6.2 The flagella connector

The flagella connector (FC) represents a specifically adapted flagellum-to-flagellum connection during the *T. brucei* life cycle (Moreira-Leite *et al*., 2001). As the FC physically connects the distal tip of the growing new flagellum to the lateral aspect of the old flagellum in the PCF, it represents a highly complex mobile transmembrane junction (Briggs *et al*., 2004) (Fig. 11A-B). The FC is a trilaminar cytoskeletal structure with an overall width of ~90 nm (Briggs *et al*., 2004) comprised of three distinct electron dense layers found across the new flagellum membrane, the old flagellum membrane and the intermediate space between the membranes (Höög *et al*., 2016). The central layer (2) is ~18 nm in width, with zone 3 at ~16 nm and zone 1 at ~13 nm in width (Briggs *et al*., 2004) (Fig. 11C). The layer closest to the new flagellum (1) is connected to the distal tip of the new flagellum axoneme microtubules through a set of filaments (Briggs *et al*., 2004) (Fig. 11C).

The FC is an asymmetrical structure able to link the growing axonemal microtubules at the distal tip of the new flagellum to the old flagellum axonemal microtubules through five

distinct zones (Varga *et al*., 2017) (Fig. 11D). Zone 1 of the FC represents a filamentous network linking the microtubule tips of the new flagellum axoneme to the electron-dense layer (zone 2) underlying the new flagellum membrane at the FC junction, whereas zone 3 represents the connecting layer between the new flagellum membrane and the old flagellum membrane, also known as the interstitial layer (Varga *et al*., 2017) (Fig. 11D). Zone 4 represents a discrete electron-dense layer underlying the membrane of the old flagellum, linked to zone 5 which is a filamentous network tethering zone 4 to the lateral aspect of the microtubules of the old axoneme (Varga *et al*., 2017) (Fig. 11D).

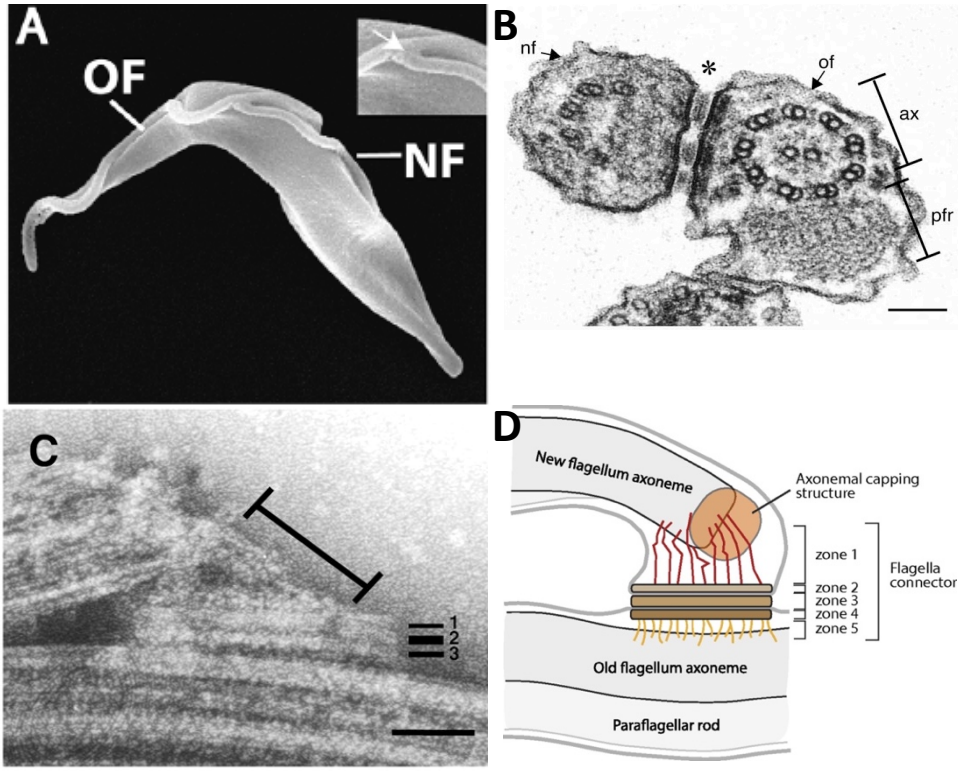

Figure 11: The FC in the *T. brucei* PCF. A) SEM of the PCF with the new flagellum laterally attached to the old flagellum via the FC (arrow). B) TEM of the FC connecting the new flagellum to the old flagellum, with axoneme (ax) and paraflagellar rod (pfr) indicated. C) Negatively stained whole-mount cytoskeleton of a PCF showing that the FC consists of a trilaminar core structure with distinct layers of electron dense material representing zones 1, 2 and 3. Filamentous connections between the FC and the axoneme microtubules (bracket). Scale = 100 nm. D) Schematic of the FC indicating distinct zones and domains (Adapted from Hughes *et al*., 2013 and Varga *et al*., 2017. B and C reproduced with copyright permission from The Company of Biologists, taken from Briggs *et al*., 2004).

From the initial stages of new flagellum development within the FP, the FC is present and remains so, providing continuous attachment between the two flagella during the growth of the new flagellum (Moreira-Leite *et al*., 2001; Briggs *et al*., 2004). The FC is present until the

new flagellum is between 40-60% of the old flagellum length, whereupon the FC reaches a "stop -point" before severing during cytokinesis to release the new flagellum distal tip (Davidge *et al*., 2006).

The FC is a highly complex structure composed of both evolutionarily conserved and kinetoplastid-specific proteins constituting its new and old flagellum zones (Briggs *et al*., 2004; Höög *et al*., 2016; Varga *et al*., 2017). Seven proteins have been identified that localised to specific zones in the FC, with two specific kinesins connecting to cytoskeletal components in two separate flagella (Varga *et al*., 2017) (Fig. 12). One component of interest, flagella connector protein 4 (FCP4, also known as TbKin15), is a member of the ubiquitous kinesin-15 family of microtubule plus-end-directed motors and is responsible for linking the plus ends of the extending new flagellum axonemal microtubules to the FC junction (zone 1) (Fig. 12).

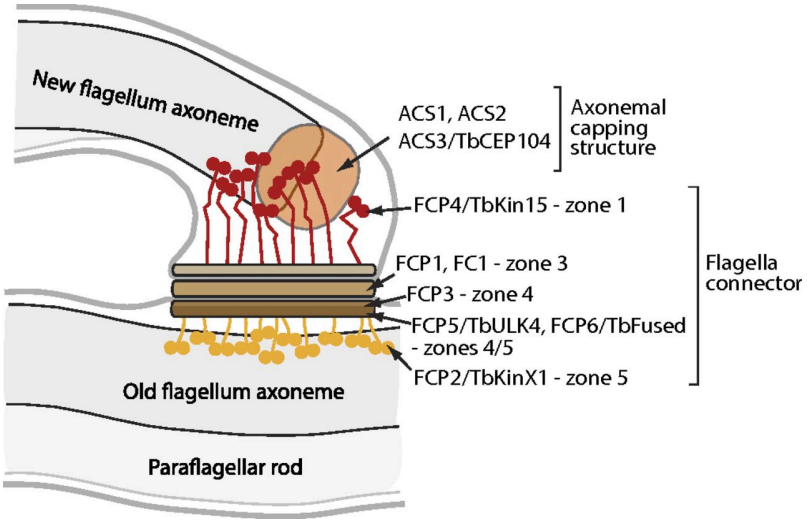

Figure 12: Protein composition of the FC. Defined zones of the flagella connector indicated. (Varga *et al*., 2017).

Three other proteins, FCP1, FCP3 and flagellar connector 1 (FC1) localised to the tri-laminar core of zones 3-4 of the FC (Varga *et al*., 2017) (Fig. 12). Furthermore, zones 4 and 5 also contain two evolutionarily conserved kinases from the ULK family of proteins (FCP5/TbULK4 and FCP6/TbFused) previously implicated in flagellum-related functions in animals, such as the construction of motile cilia (Wilson *et al*., 2009; Liu *et al*., 2016) (Fig. 12). Orthologues of FCP5 and FCP6, have previously been associated with phragmoplast organisation in plants, with ULK4 in plants possessing microtubule-binding activity (Oh *et al*., 2005; Krupnova *et al*., 2009). FCP2, on the other hand, is a kinetoplastid-specific kinesin present in zone 5 of the FC

and is responsible for attaching the FC to the old axoneme through fibrous connections (Varga *et al*., 2017) (Fig. 12). FCP2 may also be responsible for the movement of the FC junction along the old flagellum axoneme as this protein appears to be ATP-hydrolysis-competent (Sack *et al*., 1997; Varga *et al*., 2017). Clearly, the FC is a complex intracellular junction and despite the abundance of cell-cell junctional complexes in eukaryotic cells, the mobility of the FC is a rare occurrence, especially as this membrane connection occurs within the same cell and not between two individual cells.

1.6.3 The flagellar groove

One of the key morphogenetic differences between the PCF and BSF is that instead of the FC, the BSF trypomastigote cells possess a novel transmembrane structure, called the groove (Hughes *et al*., 2013). The groove represents a discrete invagination in the cell body plasma membrane in which the distal tip of the new flagellum is situated (Hughes *et al*., 2013) (Fig. 13B), making the groove a uniquely differentiated area of the plasma membrane which connects the flagellar membrane to the cell body plasma membrane, two membranes of different compositions (Maric *et al*., 2010). The distal tip of the new flagellum is fully enclosed by the cell body plasma membrane and is positioned within a defined gap in the subpellicular microtubule array, with this indentation representing the groove (Hughes *et al*., 2013) (Fig. 13D). Furthermore, the groove is closely associated with the new MtQ and the assembling new FAZ during new flagellum growth (Hughes *et al*., 2013) (Fig. 13C-F).

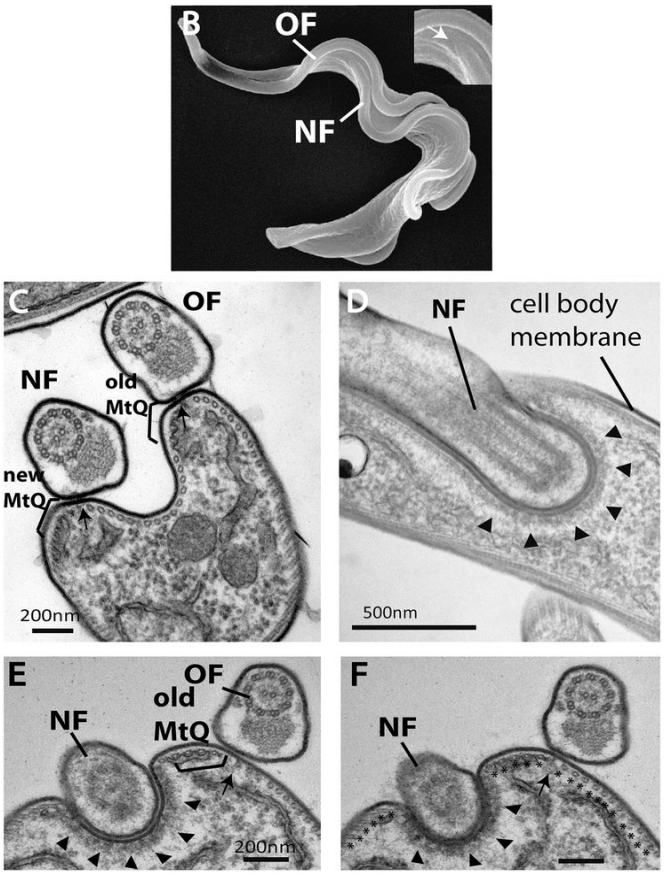

Figure 13: Distal tip of the new flagellum in the BSF. B) SEM image of the BSF with the new flagellum tip embedded in an invagination of the cell body plasma membrane (arrow). C) Transverse TEM section through an old and new flagellum indicating the attachment of the flagella to the cell body through the FAZ filament (arrow) and the association with the new and old MtQ. D) Longitudinal TEM through the distal tip of the new flagellum within the groove (arrowheads). E-F) Adjacent serial cross sections (100 nm thickness) through and old and new flagellum showing that the distal tip of the new flagellum is positioned within an indentation in the cell body plasma membrane (arrowheads). Subpellicular microtubules indicated (asterisk) (Adapted from Hughes *et al*., 2013).

The groove represents a modified intracellular structure that is able to significantly remodel the subpellicular microtubule array as the groove migrates from the posterior end of the cell towards the anterior during new flagellum growth (Hughes *et al*., 2013). The subpellicular microtubules terminate immediately anterior to the groove, in the direction of new flagellum growth (Fig. 14A), and posterior to the groove, where the tip of the new flagellum becomes embedded in the plasma membrane (Fig. 14B).

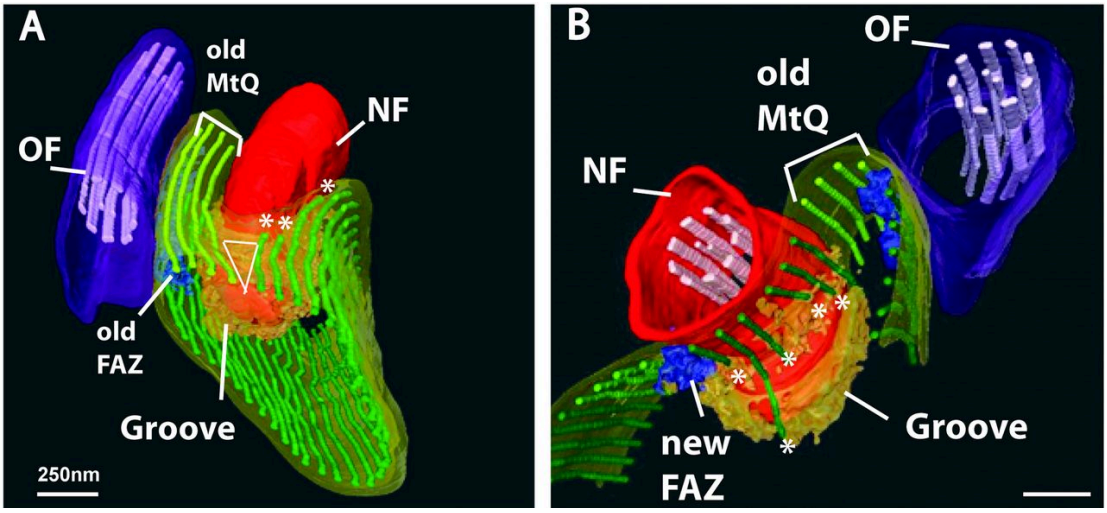

Figure 14: Association between the subpellicular microtubule cytoskeleton and the new flagellum in the groove. A) 3D surface rendering of a tomogram dataset. The new flagellum distal tip is positioned within a gap in the subpellicular microtubule array (green), in the groove. The groove is positioned adjacent to the old MtQ and the old FAZ. B) Posterior view of the groove showing that the new FAZ does not extend into the groove and that the subpellicular microtubules terminate (asterisk) before the new flagellum distal tip embeds in the groove. Scale = 250 nm. (Hughes *et al*., 2013).

Furthermore, the cytoplasmic face of the groove is characterised by a network of electron densities with radiating filaments from each density that connect with each other and to the cell body plasma membrane (Hughes *et al*., 2013) (Fig. 15H, orange and blue boxes). Similarities in this structure are seen with that of the spectrin-based cytoskeleton found in erythrocytes (Bennett, 1985; Li *et al*., 2007; Zhang *et al*., 2013) and a similar structural arrangement of analogous proteins to the erythrocyte network might be involved in providing a dynamic complex that allows microtubule cytoskeletal connections to be repeatedly broken and remade during the groove's migration along the cell body (Hughes *et al*., 2013). Furthermore, these filamentous extensions are reminiscent of the electron dense filaments connecting the flagellar membrane to the cell body plasma membrane in the phagotrophic *Peranema trichophorum*, with the indentation in the cell body referred to as a groove in the plasma membrane (Roth, 1959). The ridges of the pellicle, a thin layer of proteinaceous material underlying the plasma membrane to offer support, are modified to form a groove in which the trailing flagellum lies, with tubular elements extending across the membrane and penetrating the outer zone of the flagellum (Roth, 1959; Hilenski and Walne, 1985). Furthermore, underlying the low points of the ridges of the groove are a subpellicular filament arrangement (Roth, 1959), which, in cross section, are reminiscent of the *T. brucei*

subpellicular microtubules and the microtubules underlying the periplast in *Leptomonas pessoai* promastigotes (De Souza *et al*., 1976). Potentially, the *T. brucei* flagellar groove may share some structural similarities to other eukaryotic intracellular junctions.

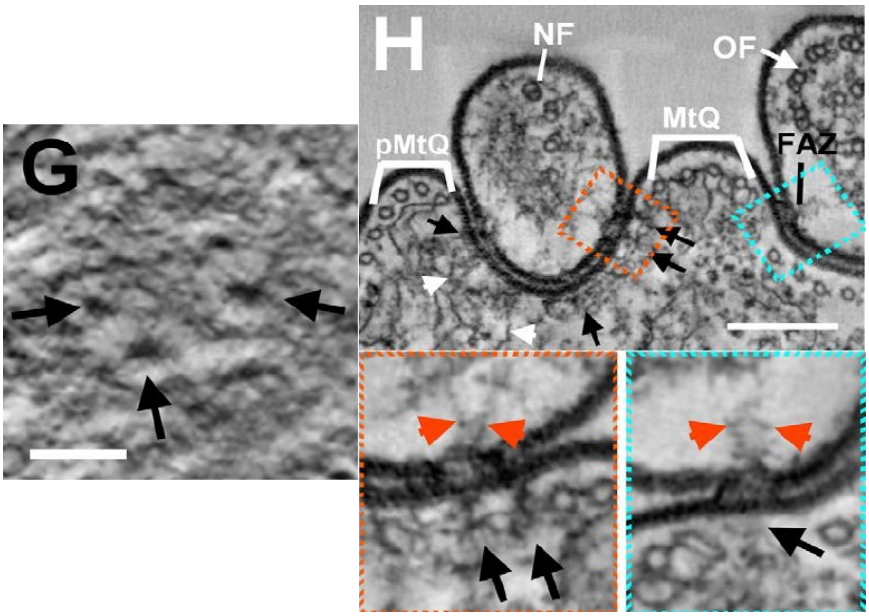

Figure 15: Ultrastructural organisation of the cytoplasmic face of the groove. G) Tomogram slice showing the electron densities, or punctate *maculae*, underlying the cytoplasmic face of the groove (arrows). H) Transverse section through an old and new flagellum indicating the FAZ filament associated with the old flagellum (blue box) connecting across the flagellar and cytoplasmic membranes. The new flagellum has filamentous structures crossing both membranes (orange box), like with the old FAZ, suggesting a filamentous connection present for the new flagellum. Scale = 250 nm. (Adapted from Hughes *et al*., 2013).

Furthermore, the groove is a region where the cell body plasma membrane is able to provide an attachment point for the new flagellum tip, potentially resembling a modified version of the FAZ or flagella connector structure. Hughes *et al*., (2013) highlighted the presence of punctate and filamentous electron-dense material underlying the cytoplasmic face of the cell body plasma membrane of the groove structure (Fig. 15G, arrows), suggesting a method of flagellum tip attachment in the groove. Furthermore, filament connections across both the flagellum and cell body plasma membranes in the groove were seen by conventional thin-section TEM, supporting the observations of a mechanism of flagellum attachment within the groove (Fig. 15H, orange box). These filamentous connections resembled the FAZ filament connection seen attaching the old flagellum (OF) to the cell body (Fig. 15H, blue box).

Despite the presence of the new FAZ associated with the growing new flagellum, and the appearance of a similar FAZ-like structure connecting the new flagellum to the cell body within the groove, the groove lacks a canonical FAZ filament within the groove structure itself (Hughes *et al*., 2013). This poses an interesting question as to how the new flagellum distal tip is tethered to the cell body plasma membrane within the groove. An anti-FAZ filament antibody, DOT1, which labels the punctate *maculae* of the FAZ (Woods *et al*., 1989), and an anti-FAZ1 protein, L3B2 (Kohl *et al*., 1999; Vaughan *et al*., 2008), were used to determine if the filaments seen in the groove were indeed FAZ filaments (Hughes *et al*., 2013). DOT1 localised to the flagellar groove as an elaboration at the distal end of the new flagellum, however, FAZ1 did not localise to the groove in the BSF (Hughes *et al*., 2013). Furthermore, the filaments located on the flagellum side of the attachment area within the groove were unlike those previously defined by Vickerman, (1969), where the FAZ usually connects to the paraflagellar rod (Hughes *et al*., 2013). This would support evidence that the groove filament network, despite sharing some biochemical similarities with the FAZ, is not wholly just an extension of the FAZ but an elaboration of this structure. However, research into the protein composition of the groove has been limited, with the DOT1 antibody localisation in the groove being the only experimental evidence of a FAZ-like connection present in the groove.

As the new flagellum emerges from the flagellar pocket at the posterior end of the cell, the distal tip is embedded in the groove and is maintained there until the groove approaches the anterior cell tip (Hughes *et al*., 2013) (Fig. 16A-B). In cells where the new flagellum tip was beyond the anterior tip of the cell, or had begun cytokinesis, the groove was not observed (Hughes *et al*., 2013) (Fig. 16C), suggesting that the groove had resolved to release the new flagellum distal tip. It is unknown, however, how and exactly when in the cell cycle the groove resolves.

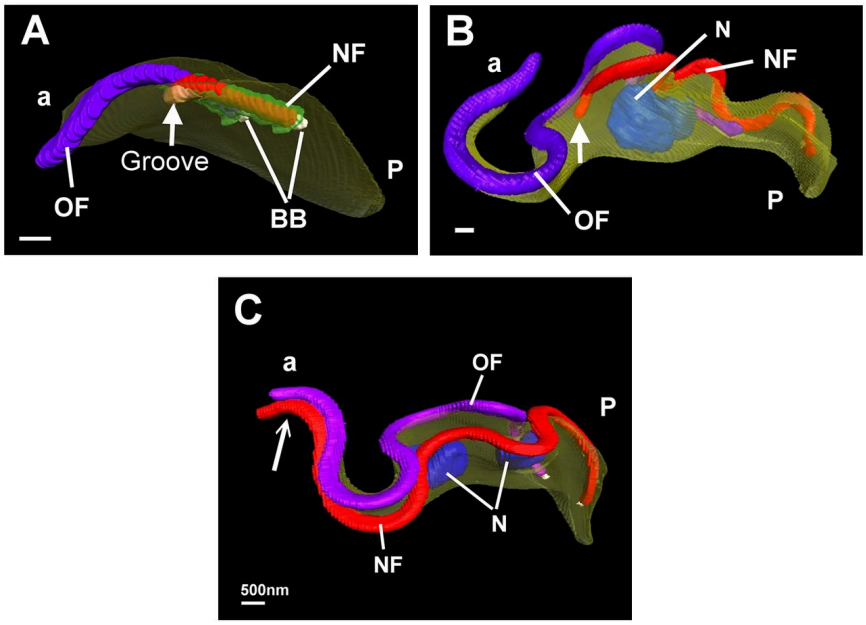

Figure 16: Movement of the groove by SBFSEM. A) 3D surface reconstruction of an SBFSEM dataset. The new flagellum (red) emerges from the flagellar pocket (green), with its distal tip embedded in the groove (arrow). B) The new flagellum distal tip is fully embedded in the groove (arrow). C) The new flagellum has extended beyond the anterior cell tip, with the distal tip free from the cell body (arrow). The groove does not appear to be present at this point. Key: P = posterior; A = anterior; BB = basal body; OF = old flagellum; NF = new flagellum; N = nucleus. Scale = 500 nm. (Adapted from Hughes *et al*., 2013).

The precise structural and molecular components contributing to the formation, migration and resolution of the groove are mostly unknown. It is speculated that the groove is specifically adapted to reduce the exposure of transmembrane junctions to the mammalian immune system (Hughes *et al*., 2013). Thus, the use of a groove in bloodstream proliferating trypomastigotes might represent a modification of the trypanosome division process for enhanced pathogenicity in the mammalian bloodstream. In the BSF, a discrete FC structure may potentially be exposed to mammalian antibody recognition when the FC is resolved at the end of the cell cycle by leaving an exposed face on the FC when the two cells split (Davidge *et al*., 2006; Hughes *et al*., 2013). This exposure of potentially invariant antigenic structures might activate the mammalian immune system and provide consistent antigen recognition sites (Hughes *et al*., 2013). Therefore, the groove may act as a safe pocket where the new flagellum distal tip is protected from these immune components, thereby shielding any invariant proteins from the host's immune system. It is, however, intriguing that two trypomastigote lifecycle forms of *T. brucei* have evolved discrete mechanisms for new flagellum distal tip attachment during the growth of the new flagellum. This poses the

question of whether other kinetoplastid parasites, particularly closely related trypanosomatid parasites, possess a similar structure at the distal tip during new flagellum growth, or whether the groove evolved with the parasitic lifestyle of the bloodstream trypomastigote form.

My project seeks to determine the molecular composition and function of the flagellar groove. By identifying proteins that localise to the groove, the role that the groove plays in flagellum attachment, cell morphogenesis and cell division may be further understood. Understanding the importance of the groove in cell morphogenesis in the mammalian bloodstream may provide information on possible weaknesses in the trypanosome's life cycle that could be examined for exploitation in the future with novel targets for vaccine research and disease control schemes.

2 Project aims

2.1 Aim

The aim of this PhD project is to understand the structural and functional role of the flagellar groove in the bloodstream form of *Trypanosoma brucei*. We also aimed to examine how and when the groove resolves in order for the cell to complete cell division.

2.2 Objectives

- Identify putative flagellar groove proteins using bioinformatics and online genomic resources.
- Localise candidate flagellar proteins using PCR-based endogenous tagging and fluorescence microscopy.
- Characterise the candidates using knockdown and/or gene deletion cell lines.
- Analyse the resolution of the groove using 3D electron microscopy.
- Use 3D electron microscopy to determine if *Trypanosoma vivax* and *Trypanosoma congolense* possess a groove.

3 Methodology

3.1 Protein candidate selection and cell culture

3.1.1 Genomic database mining

Putative *Trypanosoma brucei* groove proteins were chosen using TrypTag (http://tryptag.org/) (Dean, Sunter and Wheeler, 2016), which contains the localisation of every protein encoded in the *T. brucei* procyclic parasite genome. The database was mined for proteins localising to the (i) distal FAZ; (ii) anterior cell tip; (iii) flagella connector. 45 proteins were chosen for a localisation screen.

3.1.2 Proteome analysis

An online resource, TriTrypDB (https://tritrypdb.org), was used to collect the protein sequences of the screen candidates, as well as other relative information such as molecular weight and isoelectric point. Protein sequences were mined for protein domains using Interpro (https://www.ebi.ac.uk/interpro/), Pfam (https://pfam.xfam.org) and SMART (http://smart.embl-heidelberg.de) with an e-value cut-off of e^{-10}.

3.1.3 Orthologue identification in other kinetoplastid species

The protein sequences of the 45 putative groove proteins were examined by TriTrypDB (https://tritrypdb.org/tritrypdb/), and by reciprocal best BLAST (RBB) using the protein BLAST tool on NCBI (https://blast.ncbi.nlm.nih.gov/Blast.cgi) to determine if other kinetoplastid organisms possessed orthologues of the candidate proteins. Full list of orthologues is in **Appendix D.** We interrogated the non-redundant database with an e-value cut-off of e^{-10} and examined the proteomes of *Trypanosoma vivax* (Y486), *Trypanosoma congolense* (IL3000), *Trypanosoma cruzi* (Dmc28 2018), *Leishmania major* (Friedlin), *Blechomonas ayalai* (B08-376), *Leptomonas pyrrhocoris* (H10), *Paratrypanosoma confusum* (CUL13) and *Bodo saltans* (Lake Konstanz) for orthologous proteins.

3.1.4 *Trypanosoma brucei* bloodstream cell culture

Lister-427 bloodstream *T. brucei* cells were grown in HMI9 (Gibco, UK; 2007538) medium (pH 7.4) supplemented with heat-inactivated 15% foetal calf serum (FCS) (Gibco, UK; 08G9275K), at 37°C in a 5% CO_2 incubator. Medium was warmed to 37°C before use and cells were harvested during log phase ($6x10^5$ - $1x10^6$ cells/ml). Cell3. lines were stored in liquid nitrogen in medium supplemented with 10% glycerol. For growth curves, cells were counted every 24 hours using an automated cell counter and split to approximately 1 x 10^5 cells/mL.

3.1.5 *Trypanosoma congolense* bloodstream cell culture

IL3000 bloodstream *T. congolense* cells were grown and maintained at 37°C in a 5% CO_2 incubator in basal medium supplemented with complete Tc-BSF3 medium. Basal medium consists of Minimal Essential Medium Eagle (MEM) (Sigma, UK; M0643) in ddH_2O supplemented with 50 mM acid HEPES (Sigma, UK; H3375), 52 mM $NaHCO_3$ (Sigma, UK; 1063290500), 11 mM D-Glucose (Sigma, UK; G8270); 2 mM Sodium Pyruvate (Sigma, UK; P3662), 0.08 mM Adenosine (Sigma, UK; A4036), 0.2 mM Hypoxanthine (Sigma, UK; H9636), 0.03 mM Thymidine (Sigma, UK; T1895) and 0.05 mM Bathocuprine sulfate acid (Sigma, UK; B1125). Basal medium pH was adjusted to 7.3 and filtered through a 0.22 μm filter under sterile conditions. To complete the medium, 375 mL basal medium was supplemented with 15% heat-inactivated goat serum (FCS) (Gibco, UK; 16210064), 5% Serum Plus™ II Medium Supplement (Sigma, UK; 14009C), 1.4% β-mercaptoethanol and 200 mM glutamine and stored at 4°C. Complete medium was warmed to 37°C before use and cells were harvested during log phase ($5x10^5$ - $6x10^6$ cells/ml). Cell line stocks were stored in liquid nitrogen in medium supplemented with 10% glycerol.

3.1.6 Collection of *Trypanosoma vivax* bloodstream form cells from infected mice

Strain (IL1392) of bloodstream form *T. vivax* was derived from the Y486 strain and was kindly provided by Dr Delphine Autherman and Professor Gavin Wright from the University of York. The parasites were administered to wild-type female BALB/c mice by intraperitoneal administration and maintained by weekly serial passage according to Autherman *et al*., (2021). In summary, 15 mice were infected and harvested 6 days post-infection to acquire parasites in the exponential phase of growth. The parasites were collected from the blood

via intracardiac puncture using heparin before diluting the blood with 20 mM of PBS-glucose solution. The blood was centrifuged (5 min at 3000 rpm) to separate parasites and red blood cells. The supernatant containing the parasites was removed and centrifuged (30 min at 3000 rpm). The parasite solution was resuspended in 20 mM PBS-glucose. The *T. vivax* sample was sent to Oxford Brookes University in 2.5% EM-grade glutaraldehyde in 0.1M phosphate buffer solution (pH 7.4) and stored at 4°C.

3.2 Gene editing techniques

3.2.1 Generation of cell lines expressing fluorescently tagged proteins

A *T. brucei* bloodstream marker cell line containing a blasticidin resistance plasmid was provided by Dr Jack Sunter. This cell line contains an integrated construct that encodes the T7 RNA polymerase, TetR and Cas9 nuclease with a flagellum tip protein (Tb427.02.5860) endogenously tagged with the mScarlet (red) fluorescent protein. The marker cell line was cultured *in vitro* (Section 3.1.4) and maintained with 0.1 µg/ml puromycin and 5 µg/ml blasticidin.

Primers for PCR were developed using the known *T. brucei* bloodstream form (strain Lister 427) genome sequence derived from https://tritrypdb.org/tritrypdb/ and using the primer design tool in http://www.leishgedit.net/Home.html. Primers are listed in **Appendix A**. Constructs for endogenous tagging with mNeonGreen (mNG) in *T. brucei* was generated by long-primer PCR and transfection of cells, as described by Dean *et al*., (2015). In summary, pPOT PCR involves a plasmid (pPOT version 6) encoding a fluorescent protein and a resistance gene, in this case mNG and neomycin (G418) respectively. Each template reaction was made up to 50 µl and each guide reaction was made up to 20 µl using the Expand High Fidelity PCR System (Roche, Germany; 19012324). The reaction conditions were as follows: initial denaturation period (94°C, 5 min), followed by 35 cycles of 94°C for 30s, 60°C for 30s and 72°C for 2 min, before a final elongation step (72°C, 7 min). The PCR products were visualised using a 1X TAE 0.8% Agarose Gel, supplemented with 1X Sybr® Safe DNA stain and the products precipitated with ethanol prior to electroporation. The PCR products were combined with $3x10^7$ cells/mL and transfected using the Amaxa Nucleofactor II system into the Tb427.02.5860 marker cell line. Transfectants were selected with 5 µg/ml blasticidin, 2.5 µg/ml G418 (neomycin) and 0.1 µg/mL puromycin.

3.2.2 Generation of gene deletion cell lines using CRISPR/Cas-9

T. brucei BSF cells derived from the marker cell line (Section 3.2.1), containing the 1339 Cas9 nuclease, were cultured *in vitro* and maintained with 0.1 µg/ml puromycin and 5 µg/ml blasticidin. Primers for PCR were designed against the known *T. brucei* BSF (Lister-427) genome sequences derived from https://tritrypdb.org/tritrypdb/ and using the CRISPR/Cas-9 primer design tool in http://www.leishgedit.net/Home.html. Primers are listed in **Appendix E**. Deletion constructs were generated using plasmids containing neomycin and hygromycin drug resistance markers for PCR amplification of the deletion cassettes (Beneke *et al*., 2017). PCR amplification involved the Expand High Fidelity PCR System (Roche, Germany; 19012324) and each 50 µl reaction contained 5 µl 10x Expand High Fidelity buffer, 3 mM $MgCl_2$, 2% DMSO, 0.2 mM dNTPSs, 20 ng of plasmid (containing either Neo or Hyg), 1 µM of each primer (upstream froward or downstream reverse) and 0.5 µl of polymerase.

Reaction conditions were as follows: initial denaturation period (94°C, 5 min), followed by 35 cycles of 94°C for 30s, 60°C for 30s and 72°C for 2 min, before a final elongation step (72°C, 7 min). To successfully delete both alleles of a gene, sgRNAs targeting the 5' and 3' UTR were introduced to generate double-stranded breaks around the gene ORF (Fig. 17). sgRNAs were amplified by PCR using a common sgRNA primer sequence (G00). Each 20µl reaction contained 2 µl 10x buffer, 1.5 mM $MgCl_2$, 0.2 mM dNTPs, 1 µM guide primer, 1 µM G00 and 0.5 µl polymerase. Thermocycling conditions were 30s at 98°C, followed by 35 cycles of 10s at 98°C, 30s of annealing at 60°C and 15s at 72°C. PCR products were visualised, precipitated and transfected as outlined previously (Section 3.2.1) and were selected for with 5 µg/ml blasticidin, 0.1 µg/ml puromycin, 2.5 µg/ml G418 (neomycin) and 5 µg/ml hygromycin.

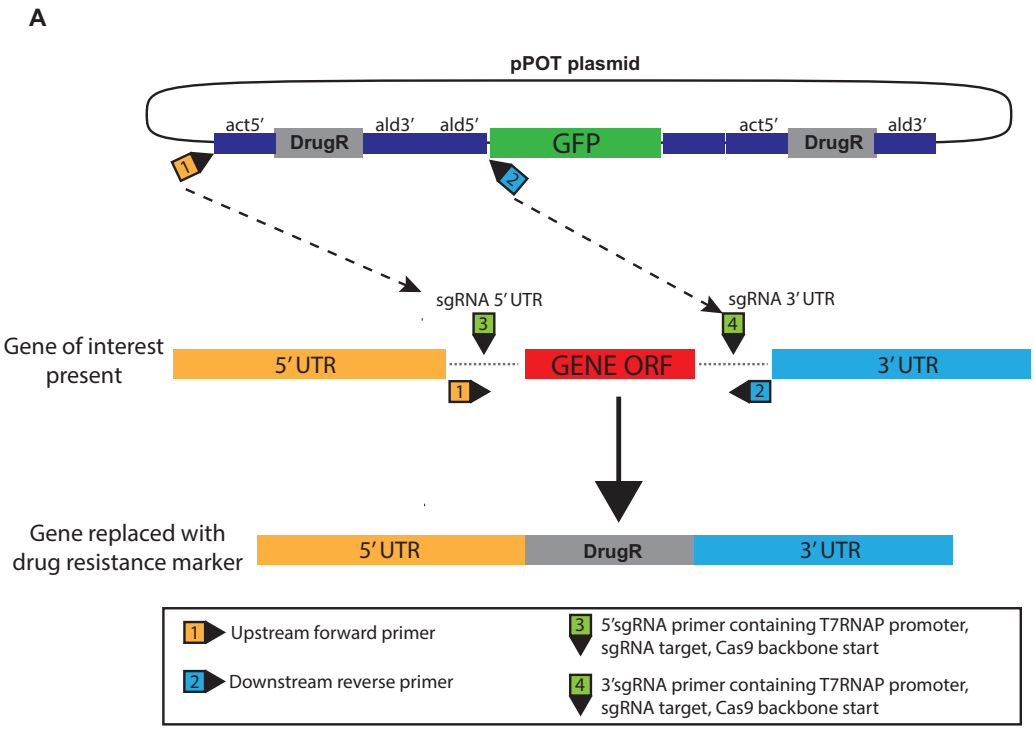

Figure 17: Strategy for CRISPR/Cas9 employing a modular system for PCR-amplification or fragments targeting the gene of interest. Schematic of the pPOT plasmid used to generate donor DNA for repairing double-stranded breaks in the DNA around the gene of interest. Two sgRNAs (3-4) cut the upstream (5') and downstream (3') of the gene ORF. Repair cassettes with drug selectable marker genes (DrugR) and nucleotide sequences specific to the target locus (1-2) replace the gene ORF and delete the gene (Adapted from Beneke *et al*., 2017).

3.2.3 Confirmation of the deletion cell lines

To confirm the successful deletion of the gene of interest, genomic DNA was extracted using the DNEASY Blood and Tissue kit (Qiagenl 69506) according to the manufacturer's instructions. gDNA was quantified using a Nanodrop spectrophotometer (Lab Tech; ND-100). Primers were designed to amplify the ORF of the gene of interest and listed in **Appendix E**. PCR amplification using the Expand High Fidelity PCR System (Roche, Germany; 19012324) was used to confirm the deletion. Each 50 µl reaction consisted of 5 µl Expand High Fidelity Buffer, 1.5 mM $MgCl_2$, 2% DMSO, 0.2 mM dNTPs, 200-300 ng gDNA, 0.1 µM of each primer (forward and reverse) and 0.5 µl polymerase. Thermocycling conditions were as described previously (Section 3.2.1). PCR amplification was checked using gel electrophoresis using parental gDNA and ddH_2O as positive and negative controls.

3.2.4 Inducible RNAi cell line generation

An RNAi plasmid against FCP4 (Hairpin pDEX777 #9) was kindly provided by Dr Vladimir Varga at the Institute of Molecular Genetics of the Czech Academy of Sciences, Prague. The plasmid was linearised with Not1 digestion overnight before heat inactivation at 65°C for 20 min prior to transfection. The plasmid was transfected into the FCP4 cell line endogenously tagged with mNG as outlined previously (Section 3.2.1) and was selected for with 5 µg/ml blasticidin, 0.1 µg/ml puromycin and 5 µg/ml phleomycin. Doxycycline (1 µg/mL) was used to induce knockdown of FCP4.

3.3 Preparation of solutions for microscopy

3.3.1 Preparation of 0.2 M phosphate buffer stock solution

Sodium dihydrogen phosphate (solution A) was prepared by dissolving 69 g NaH_2PO_4 in 500 ml ddH_2O. Disodium hydrogen phosphate (solution B) was prepared by dissolving 8.9 g Na_2HPO_4 in 250 mL ddH_2O. Approximately 23.4 mL of solution A was mixed with 91.5 mL of solution B, and 10 M NaOH was added until the solution reached a pH of 7.4.

3.3.2 Preparation of 10% paraformaldehyde solution

Ten percent paraformaldehyde solution was prepared by adding 2 g of 95% paraformaldehyde (Sigma, UK; 14009C) to 20 mL of ddH_2O and placed on a 60^{o}C stirring hot plate. Once at 60^{o}C, drops of 1 M NaOH were added until the solution became transparent. The solution was filtered using a 0.22 µm pore filter (Millex, Millipore).

3.3.3 Preparation of buffered fixative solution for electron microscopy

Primary fixative was made fresh before each use and consisted of 10% paraformaldehyde solution (final concentration 2%), 25% EM-grade Glutaraldehyde (final concentration 2.5%) (TAAB) and 0.2 M phosphate buffer solution (final concentration 0.1 M).

3.4 Sample processing and image capture

3.4.1 Fluorescent microscopy of live cells

To image live cells expressing the fluorescent fusion proteins, *T. brucei* cells were harvested from culture in log phase ($6x10^5$ – $1x10^6$ cells/mL) and centrifuged (8 min, 800g). The cells were resuspended in 1 mL 1X Dulbecco's Modified Eagle Medium (DMEM) (Gibco, UK; 2091322) supplemented with 0.001% Hoechst 33342 and centrifuged again, before being washed in 1 mL DMEM only. The cells were resuspended in 20 µl DMEM. 20 µl of 0.04% methanol-free Formaldehyde (16% stock; TAAB; 22810) was added before settling 2.4 µl of cells onto glass slides with 0 mm coverslips. The cells were imaged on a Zeiss Imager-Z2 fluorescence microscope using the Zen Blue software and a 63X oil-immersion objective. Images were processed using ImageJ with an automated script (Fiji; https://imagej.net/Welcome).

Cell counts for the cell cycle analysis was performed by counting the number of kinetoplasts (K) and nuclei (N) per cell in a total population of 500 cells. The nucleus and kinetoplast were stained with Hoechst 33342. The cells were classed into 1K1N, 2K1N, 2K2K, >2K>2N and "Other" (see Chapter 6).

3.4.2 Scanning electron microscopy (SEM)

T. brucei BSF cells were harvested in log phase and 2.5% EM-grade Glutaraldehyde (TAAB, 22970) was added directly to the culture flask. Cells were centrifuged (8 min, 800 g) before being resuspended in buffered fixative containing 2.5% Glutaraldehyde and 0.1 M phosphate buffer solution. The cells were washed again in buffered fixative, resuspending thoroughly before incubation (1 hour at RT). The cells were settled onto 13 mm round glass coverslips (Scientific Laboratory Supplies, UK; MIC3276) coated in 0.1% Poly-L-lysine (Sigma, UK; P8920) in a 24-well cell culture plate, washed with ddH_2O, and taken through an ethanol dehydration series, each step lasting 5 minutes: 30%, 50%, 70% and 90% in ddH_2O followed by three incubations in 100% absolute ethanol. The coverslips were dried using an Autosamdri-931.GL critical point dryer (Tousimis, Canada) before being coated in 11-13nm thickness of gold using an Automatic Gold Sputter Coater (Agar Scientific, UK; AGB7341). The cells were

imaged using a Hitachi S-3400N Scanning Electron Microscope (conditions: 5 Kv, 5-7 mm working distance, 20-50 µA, 260s image capture).

Cell counts for SEM analysis of the control and deletion cell lines was done by imaging a field of view at a magnification of x500-1000. The proportion of 2F and multiflagellated cells was determined from the total number of cells counted.

3.4.3 Single osmium processing for TEM

T. brucei BSF cells were harvested in log phase and directly fixed in culture with 2.5% Glutaraldehyde. The fixed culture was centrifuged (8 min, 800 g) and resuspended in fresh buffered fixative and incubated (1 hour at RT). Fixed cells were washed five times (3 min per wash) in 0.1 M phosphate buffer, pelleting by centrifugation (1 min, 14,000 rpm). Cells were incubated in 1% osmium tetroxide for 1 hour at 4^{o}C in the dark. The cells were washed five times (3 min per wash) in ddH_2O, pelleting as before between washes. Cells were incubated in filtered 0.5-1% uranyl acetate overnight at 4^{o}C in the dark. Cells were washed three times in ddH_2O (5 min per wash) then dehydrated by a series of 10 min incubations in 30%, 50%, 70%, 90% ethanol and three changes of 100% absolute ethanol. Cells were incubated in a series of ratios of ethanol to 25% epoxy resin (TAAB 812 hard resin kit) as follows: 3:1 ethanol/resin (1 hour), 1:1 ethanol/resin (2 hours), 1:3 ethanol/resin (1 hour), then 2-3 changes of 100% resin (6 hours each incubation), on rotation. Resin-infiltrated pellets were embedded in Beem capsules™ with fresh 100% resin and polymerised at 60^{o}C for 24 hours. Samples were sectioned (Section 3.5.2) and viewed on a Jeol JEM-1400 series 120kV transmission electron microscope using a OneView 16 Megapixel camera (Jeol, USA).

3.4.4 Double osmium processing for serial block-face scanning electron microscopy

T. brucei and *T. congolense* BSF cells were harvested in log phase and fixed directly in culture with 2.5% Glutaraldehyde. Cells were centrifuged (8 min, 800 g) and resuspended in fresh buffered fixative and left to incubate for an hour at room temperature. *T. vivax* cells suspended in buffered, as well as the *T. brucei* and *T. congolense* cells, were washed five times (3 min per wash) in 0.1 M phosphate buffer pelleting by centrifugation (1 min, 14,000 rpm) between each wash. Cells were incubated in 1% osmium tetroxide and 1.5% filtered potassium ferricyanide for 1 hour at 4^{o}C in the dark. The *T. vivax* cells were washed five times

in ddH_2O whereas the *T. brucei* and *T. congolense* cells were washed in 0.1 M phosphate buffer five times (3 min per wash), pelleting via centrifugation between washes (1 min, 14,000 rpm). The *T. vivax* cells were incubated separately in freshly-made 1% filtered thiocarbohydrazide (TCH) for 20 min at RT in the dark. The *T. congolense* and *T. brucei* cells were incubated in 1% filtered Tannic Acid for 30 min at RT. Cells were washed three times (5 min per wash) in ddH_2O before incubating in 2% osmium tetroxide for 30 min at 4^{o}C in the dark. Cells were washed as before and incubated in filtered 0.5-1% uranyl acetate overnight at 4^{o}C in the dark. Cells were washed three times in ddH_2O (5 min per wash) then dehydrated by a series of 10 min incubations in 30%, 50%, 70%, 90% ethanol and three changes of 100% absolute ethanol. Cells were incubated in a series of ratios of ethanol to 25% epoxy resin (TAAB 812 hard resin kit) as follows: 3:1 ethanol/resin (1 hour), 1:1 ethanol/resin (2 hours), 1:3 ethanol/resin (1 hour), then 2-3 changes of 100% resin (6 hours each incubation). Resin-infiltrated pellets were embedded in Beem capsules™ with fresh 100% resin and polymerised at 60^{o}C for 24 hours. Samples were sectioned (Section 3.5.2) and viewed on a Jeol JEM-1400 series 120kV transmission electron microscope using a OneView 16 Megapixel camera (Jeol, USA) to check the quality of the fix and embedding. Using a razor blade, the sample was trimmed to 0.5 mm^2 and mounted on an aluminium pin specifically for 3View SBFSEM. Using epoxy conductive resin from Circuitworks™. The resin was polymerised at 60^{o}C for 24 hours. Silver DAG was added to the sample before being coated in 10-12 nm of gold using an Automatic Gold Sputter Coater (Agar Scientific, UK; AGB7341). The sample was inserted into a Zeiss™ Merlin scanning electron microscope with Gatan™ 3View™ automated sectioning and image capture system. The samples were sectioned using a 3 mm intra-microscope diamond knife, with a slice thickness of 100 nm. The block-face was scanned by an electron beam at an accelerating voltage of 1.8Kv with nitrogen gas administered using a Focal Charge Compensation (FCC) device. Other conditions include: pixel size between 3-5 nm; pixel stime of 3-4 µs; 20 µm aperture. Datasets ranged from 300-500 sections.

3.5 Section production for electron microscopy

3.5.1 Glass knife preparation

Glass knives were made from glass rods (6 mm x 25.4 mm x 406 mm). Glass rods were split to form triangular knives with a glass knife maker (Boeckeler™ by RMC™) used according to the manufacturer's instructions.

3.5.2 Thin sectioning for TEM

Following polymerisation, the resin-embedded samples were removed from the Beem capsules™ with a razor blade and roughly trimmed with a glass knife. The samples were finely trimmed using a PowerTome™ PT-PC ultramicrotome (Boeckeler™ by RMC™), with a glass knife angle of 6˚. A trapezium-shaped block face (longest side ~1 mm) was made using the glass knife and subsequently sectioned by ultramicrotomy using a diamond knife (3 mm, cutting-edge 35˚, wet ultra-Diatome™ diamond knife). Microtome advance was set at 70 nm. A copper grid (TAAB G200) was used to pick up the sections.

3.5.3 Serial section ultramicrotomy for Array tomography

A *T. brucei* 427 BSF sample was grown in culture (see 3.1.4) and was processed by using the single osmium sample preparation for TEM (see 3.4.4). Ultrathin serial sections (70 nm) were prepared using using a PowerTome™ PT-PC ultramicrotome (Boeckeler™ by RMC™), with a wet ultra-Diatome™ diamond knife. The sections were collected in ribbons onto Kapton Tape using an ATUMtome (Boeckeler™ by RMC™) and settled onto double coated carbon tape on an aluminium wafer coated with Silver DAG to reduce electron charging. The images were collected using a Zeiss Merlin VP Compact electron microscope using a GeminiSEM stage and the ATLAS 5™ programme (Zeiss, Germany).

3.6 Data processing and model rendering

SBF-SEM data was processed using Cygwin™ terminal (a command line interface software tool) and 3Dmod (IMOD™, University of Colorado; https://bio3d.colorado.edu/imod/). Separate image files were converted from .dm4 format and combined into a single .mrc file before adjusting the voxel size in Z using the ‘altheader’ command in IMOD™. The data was binned once (reducing file size by combining adjacent pixels), the data stack flipped and smoothed (averaging of pixels with their neighbours) by using the ‘clip’ command in IMOD™. The data stack was automatically aligned and trimmed using the ‘trimvol’ command in IMOD™. Regions of interest were identified, highlighted and combined into a single model file before polishing the model in IMOD™.

3.7 Statistical analysis

Statistical analysis was performed using GraphPad Prism version 9.0 for Mac (GraphPad Software, USA; www.graphpad.com). The Fisher's Exact Test was used to assess the statistical significance between two categorical variables and a Student's t test was used to assess the significance in flagellum growth through the cell cycle.

4 Characterisation of the groove using electron microscopy

4.1 Resolution of array tomography is sufficient to visualise key cytoskeletal structures surrounding the groove but is limited for 3D reconstruction of multiple cells

As the structure of the groove has previously been examined using high resolution electron microscopy (Hughes *et al*., 2013), we used the groove as a reference to develop a protocol for using array tomography on trypanosomes at the Oxford Brookes Bioimaging Unit. This technique is able to process large datasets containing many cells at nanometre resolution. We successfully imaged serial sections at a pixel count of 8K by 8K, pixel size of 3 µm and a pixel time of 5 µs. The image series progressed from the distal tip of the new flagellum being fully embedded in a groove in the cell body plasma membrane (Fig. 18A) to the new flagellum extending out of the groove (Fig. 18E-F). The groove appeared to be associated with the endoplasmic reticulum (ER) with the ER surrounding the cytoplasmic face of the groove on all sides (Fig. 18-19). We have hypothesised that the ER is able to modify its shape to outline the groove on all faces and remodel rapidly as the groove migrates along the cell body during new flagellum growth (Fig. 18-19).

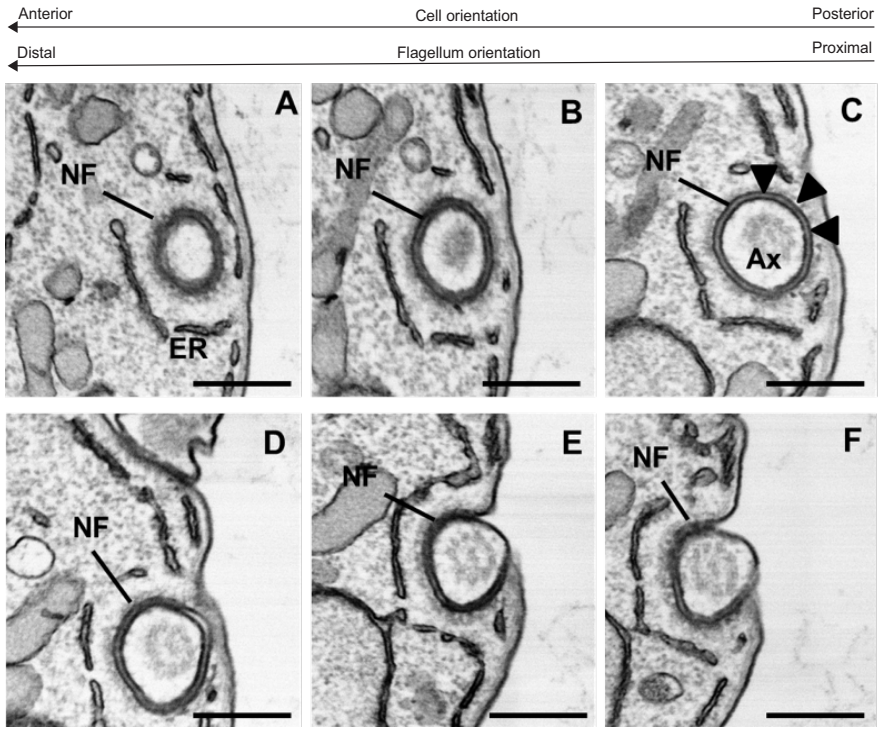

Figure 18: Array tomography image series showing sequential cross sections through the new flagellum distal tip, from distal (A) to proximal (F). Distinct double membrane (arrowheads) and

endoplasmic reticulum (ER) indicated. Key: NF = new flagellum; Ax = axoneme; ER = endoplasmic reticulum. Scale = 500 nm.

Additionally, a group of highly ordered electron densities were observed on all sides of the cytoplasmic face of the cell body plasma membrane in the groove, which have been characterised previously as punctate *maculae* (Hughes *et al*., 2013) (Fig. 19A-B, arrowheads). A schematic representation of the groove ultrastructure displays the characteristic features of the groove identified by array tomography (Fig. 20).

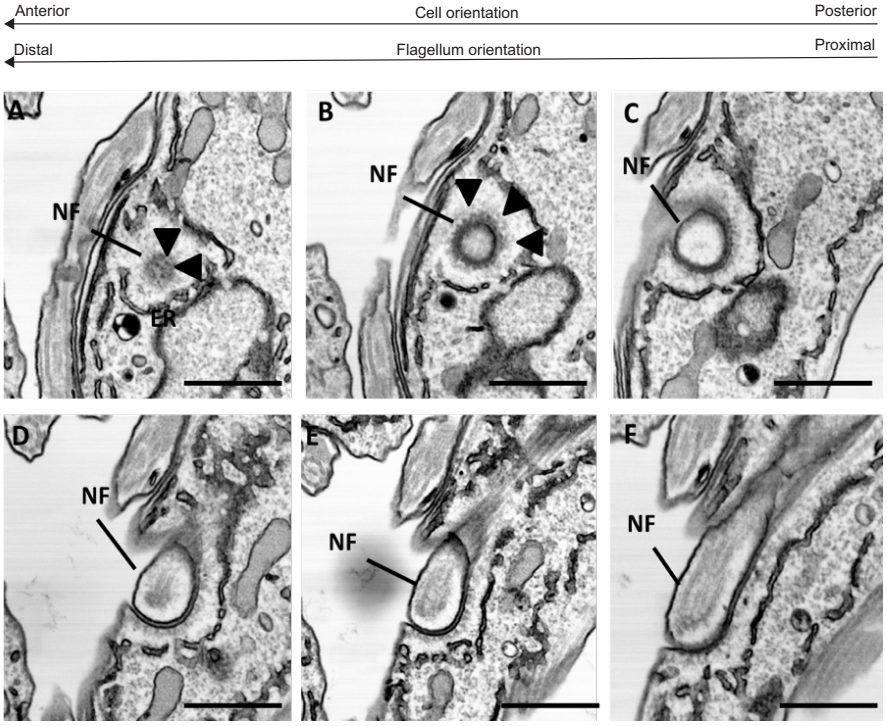

Figure 19: Array tomography image series showing sequential longitudinal sections through the new flagellum distal tip, moving from distal (A) to proximal (F). Electron densities (punctate maculae) underlying the cytoplasmic face of the groove (arrowheads) and ER indicated. Key: NF = new flagellum; ER = endoplasmic reticulum. Scale = 500 nm.

Array tomography is very time consuming and requires extensive data manipulation to reconstruct cells in 3D, making this method acceptable for high resolution ultrastructure of a small number of cells but not for 3D reconstructions of an entire dataset of cells. It is also limited in that we are unable to determine whole cell phenotypes by observing cells externally. Other methods such as SEM and SBFSEM are more appropriate for observing the parasite surface; however, their resolution is more limited than array tomography or TEM.

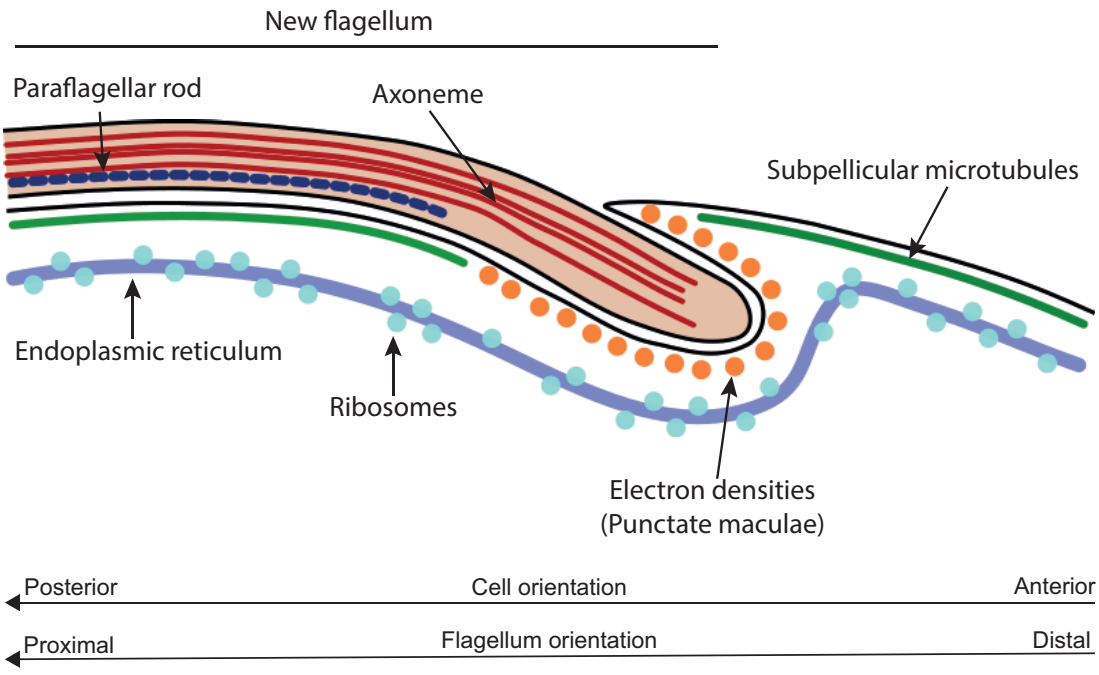

Figure 20: Schematic representation of the groove (Adapted from Hughes *et al*., 2013 and this work).

4.2 The groove resolves prior to the development of the cleavage fold and cleavage furrow.

SEM was performed to understand the cell cycle in bloodstream form *T. brucei* in an attempt to visualise the resolution of the groove. Before analysing the resulting phenotypes in null mutant and RNAi cell lines, groove movement along the cell body was outlined in *T. brucei* 427 parental cells (Fig. 21). In G1 cells, a single flagellum extended out of the flagellar pocket at the posterior end of the cell (Fig. 21A). As a new flagellum began to grow, the new flagellum extended from the new flagellar pocket at the posterior end of the cell (Fig. 21B). At this new flagellum length, the distal tip was only partially embedded in a shallow groove in the cell body plasma membrane (Fig. 21B, inset); however, as the new flagellum elongated, the distal tip became fully embedded in a deep groove in the cell body plasma membrane as the groove migrated to the anterior cell tip (Fig. 21C-D, inset). Once the groove reached the anterior cell tip, the new flagellum distal tip began to emerge from the groove (Fig. 21E, inset), before becoming releasing fully from the cell body (Fig. 21F, inset). As the new

flagellum distal tip released from the cell body groove, the cell formed a division fold and cleavage furrow before undergoing cytokinesis (Fig. 21F-H).

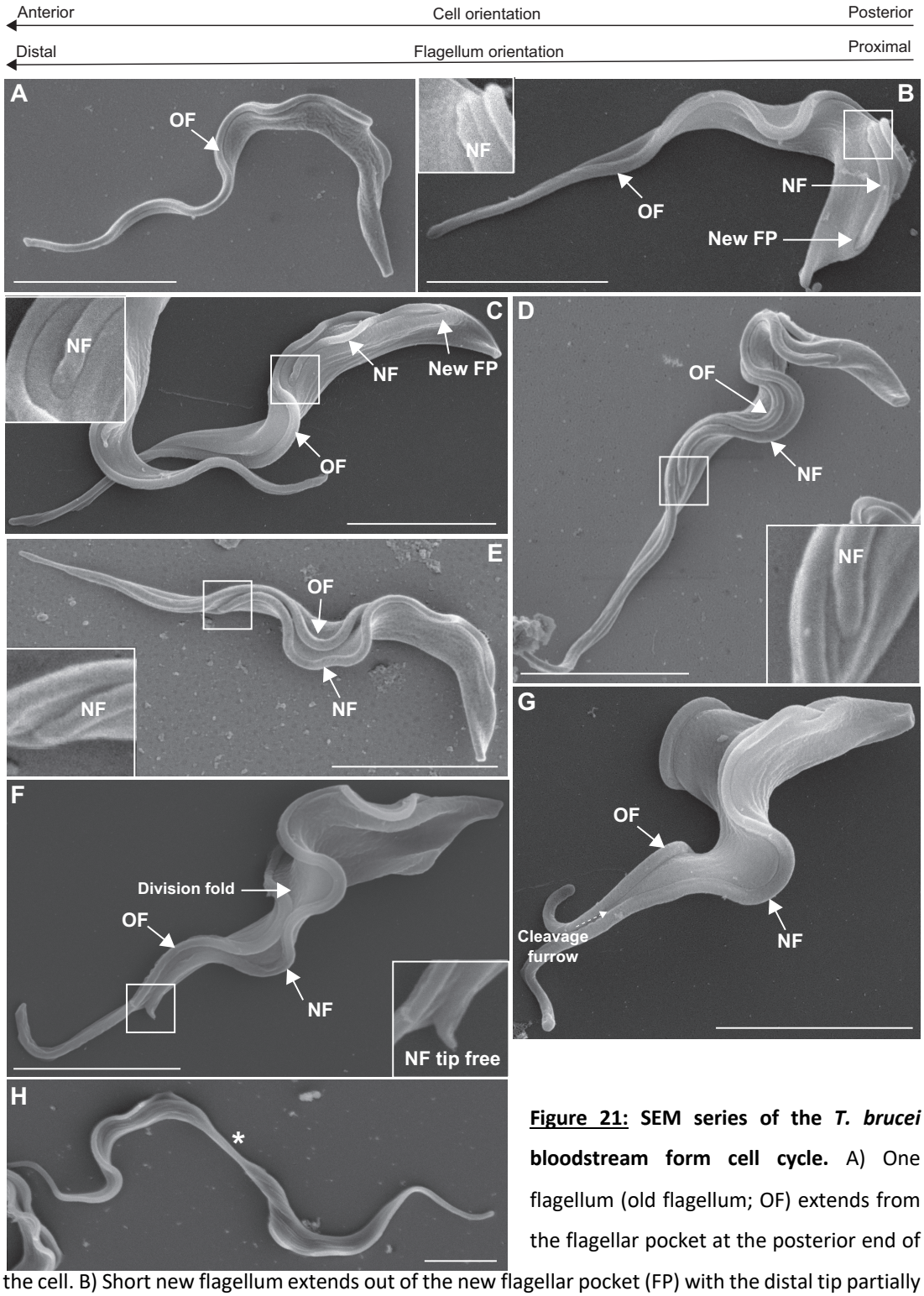

Figure 21: SEM series of the *T. brucei* bloodstream form cell cycle. A) One flagellum (old flagellum; OF) extends from the flagellar pocket at the posterior end of the cell. B) Short new flagellum extends out of the new flagellar pocket (FP) with the distal tip partially embedded in a shallow groove (inset). C-D) Long new flagellum with distal tip fully embedded in the groove (inset box). E) As the groove approaches the anterior cell tip, the distal tip begins to emerge from the groove (inset). F) New flagellum distal tip fully emerged from the groove (inset). Division fold

present. G) New flagellum elongates past the anterior cell tip. Cleavage furrow beings to ingress between the OF and NF (dashed arrow). H) Cytokinesis occurring with two cells joined at their posterior ends (asterisk). Key: OF = old flagellum; NF = new flagellum; FP = flagellar pocket. Scale = 5 μm.

The new flagellum continued to extend free from the cell body, and the cleavage furrow was initiated between the old and new flagellum as the cell entered cytokinesis (Fig. 21G, dashed arrow). The cleavage furrow ingressed from the anterior towards the posterior end of the cell, where the cells remained joined by their posterior ends before abscission (Fig. 21H, asterisk).

SEM is an invaluable tool to study cell morphogenesis in *T. brucei*; however, it is limited in certain aspects, one of which being that SEM can only examine the parasite externally as it does not have the capacity to penetrate the cell surface and visualise internal structures. It was also unclear using SEM at which cell cycle stage the groove resolves and releases the new flagellum distal tip. To identify when the groove resolves, serial block-face scanning electron microscopy (SBFSEM) was used to model the internal and external structures of whole cells.

4.3 The groove resolves post-mitosis and prior to cytokinesis

To complete the cell cycle, the groove must resolve to release the distal tip of the new flagellum and enter cytokinesis to successfully divide. These events have not been studied in detail; therefore, to investigate the timing of groove resolution during the cell cycle, we used SBF-SEM to reconstruct whole trypanosomes in three dimensions using IMOD (https://bio3d.colorado.edu/imod/) (Kremer *et al.*, 1996).

We used the data generated from the SBFSEM, containing sequential serial sections (orthoslices), to segment and model 45 individual cells across the cell cycle. The cells were grouped into seven distinct cell cycle stages according to the changes in nucleus and nucleolus volume (Table 1).

Table 1: Cell cycle categories used to determine the changes to the volume of the nucleus and nucleolus.

Cell cycle stage	Key features
1	Short new flagellum, groove, nucleus and small nucleolus
2	Growing new flagellum, groove, nucleus increasing in volume, small nucleolus
3	Growing new flagellum, groove, nucleus and nucleolus increasing in volume
4	Long new flagellum, groove, large nucleus and dividing nucleolus
5	Long new flagellum, groove, nucleus dividing
6	Free new flagellum tip, two nuclei and nucleoli
7	Cells undergoing cytokinesis

The cell cycle started with a G1 cell containing one kinetoplast (K), one nucleus and nucleolus, with a single flagellum (OF) (Fig. 22; stage 1). At this stage of the cell cycle, the average nucleus volume was $2.77x10^9$ μm^3 and the average volume of the nucleolus was $1.74x10^8$ μm^3 (Table 2). Once a new flagellum emerged from the flagellar pocket, the nucleus and nucleolus increased in volume ($3.28x10^9$ μm^3 and $2.75x10^8$ μm^3 respectively) (Fig. 22; stage 2) (Table 2). At this stage, the new flagellum distal tip was partially embedded in a shallow groove in the cell body plasma membrane (Fig. 23A-C). After kinetoplast division (Fig. 22; stage 3), the new flagellum distal tip is fully embedded in a deep groove in the cell body plasma membrane as the groove migrates towards the anterior cell tip (Fig. 23D-F). At this stage, the nucleus ($5.07x10^9$ µm3) and nucleolus ($3.46 x10^8$ μm^3) increased further in volume (Table 2).

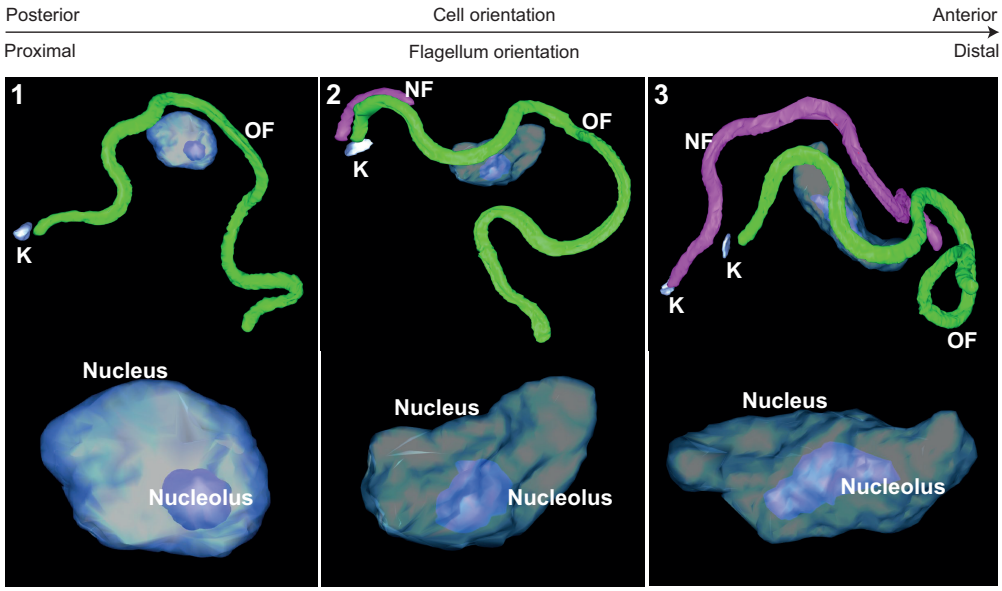

Figure 22: 3D surface rendering of representative cells during stages 1-3. 1) G1 cell with one kinetoplast, one nucleus and a single flagellum. 2) Cell with a short new flagellum alongside the old flagellum, with the nucleus is increasing in volume and the new flagellum distal tip embedded in a shallow groove. 3) Cell with two kinetoplasts and one large nucleus and nucleolus and a long new

flagellum with the distal tip fully embedded in the groove. Number of cells modelled per cell cycle stage as follows: Stage 1 = 3; Stage 2 = 4; Stage 3 = 4. Three independent SBFSEM datasets were used to model cells in the defined cell cycle stages. Key: K = kinetoplast; NF = new flagellum; OF = old flagellum.

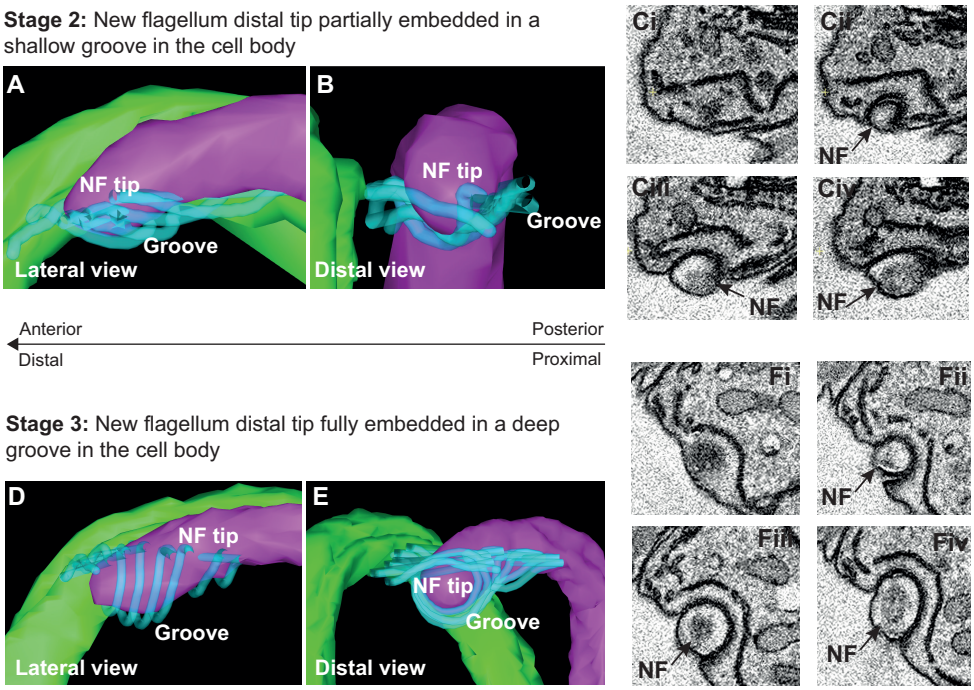

Figure 23: Enlarged region of the new flagellum distal tip in stage 2 and 3. A-C) Surface rendering of the new flagellum tip in stage 2. Lateral (A) and distal (B) view of the new flagellum tip partially embedded in a shallow groove in the cell body (blue lines represent the depth of indentation of the plasma membrane). SBFSEM raw data images (C) of the modelled area in (A) and (B), confirming that the distal tip is not fully embedded in the cell body. D-E) Surface rendering of the distal tip in stage 3. Lateral (D) and distal (E) view of the new flagellum tip fully embedded in a deep groove in the cell body (blue lines represent the depth of indentation of the plasma membrane). SBFSEM raw data images (F) of the modelled area in (D) and (E), confirming that the distal tip is fully embedded in the cell body.

During mitosis, the nucleolus began to divide, with an average volume of $4.94x10^8$ μm^3, inside an elongated nucleus ($5.73x10^9$ μm^3) (Fig. 24; stage 4) (Table 2). At this stage, the new flagellum distal tip remained fully embedded in the groove (Fig. 25A-B). As the nucleus began to divide, the two nuclei remained connected by what we have termed a nuclear bridge ($8.8x10^9$ μm^3), each containing a discrete nucleolus with an average volume of $2.59x10^8$ μm^3 (Fig. 24; stage 5). During this stage, the new flagellum remained fully embedded in a deep groove (Fig. 25C-D).

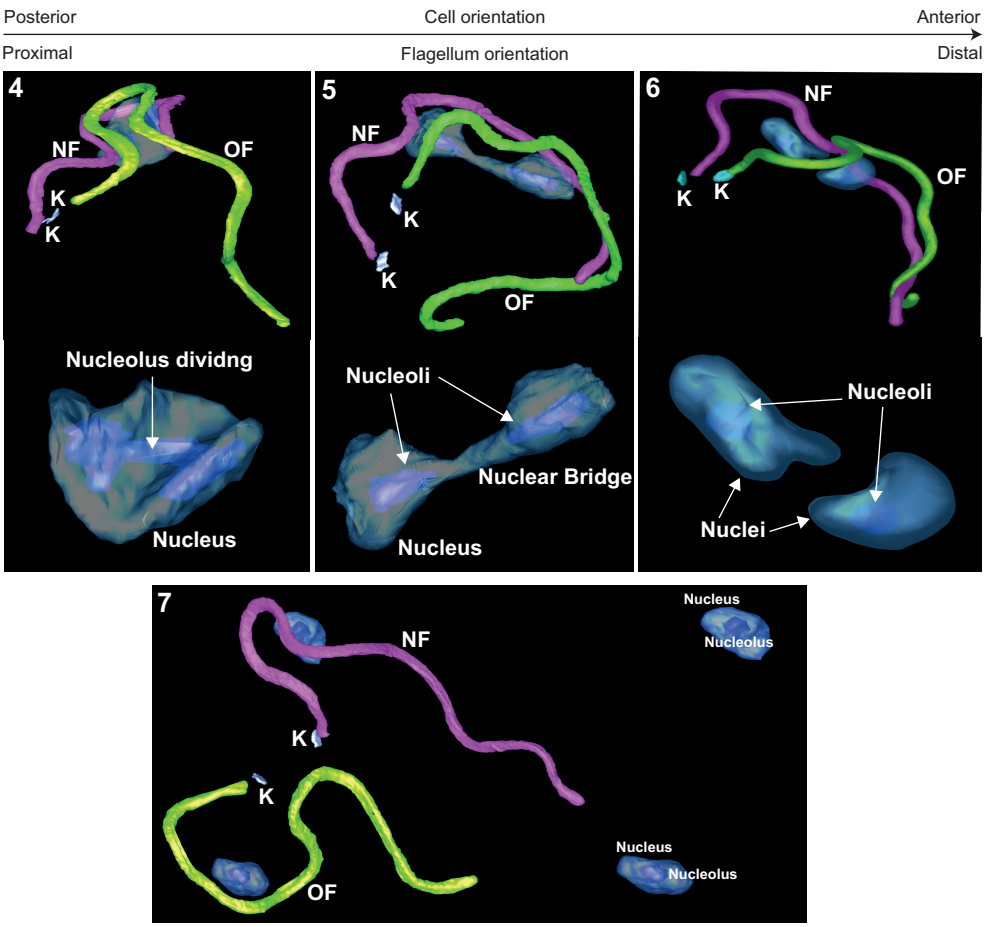

Figure 24: 3D surface rendering of representative cells during stages 4-7. 4) Cell with two kinetoplasts and one large nucleus (containing a dividing nucleolus), with a long new flagellum. 5) Cell containing two kinetoplasts and a dividing nucleus connected by a nuclear bridge, with a long new flagellum and groove present. 6) Cell containing two kinetoplasts and two nuclei, each containing a small nucleolus. At this stage, the groove has resolved and released the new flagellum distal tip from the cell body. 7) Cells undergoing cell division. Number of cells modelled per cell cycle stage as follows: Stage 4 = 3; Stage 5 = 4; Stage 6 = 22; Stage 7 = 5. Three independent SBFSEM datasets were used to model cells in the defined cell cycle stages. Key: K = kinetoplast; NF = new flagellum; OF = old flagellum.

In post-mitotic cells (Fig. 24; stage 6), there are two discrete nuclei (approximately $3.06x10^9$ μm^3), with each nucleus containing a small nucleolus ($1.74x10^8$ μm^3) (Table 2). The new flagellum distal tip was free from association with the cell body, suggesting that the groove had resolved post-mitosis (Fig. 24; stage 6). Cytokinesis was initiated to produce two daughter cells with each containing one kinetoplast, one nucleus ($2.98x10^9$ μm^3) and nucleolus ($2.16x10^8$ μm^3) and a single flagellum (Fig. 24; stage 7).

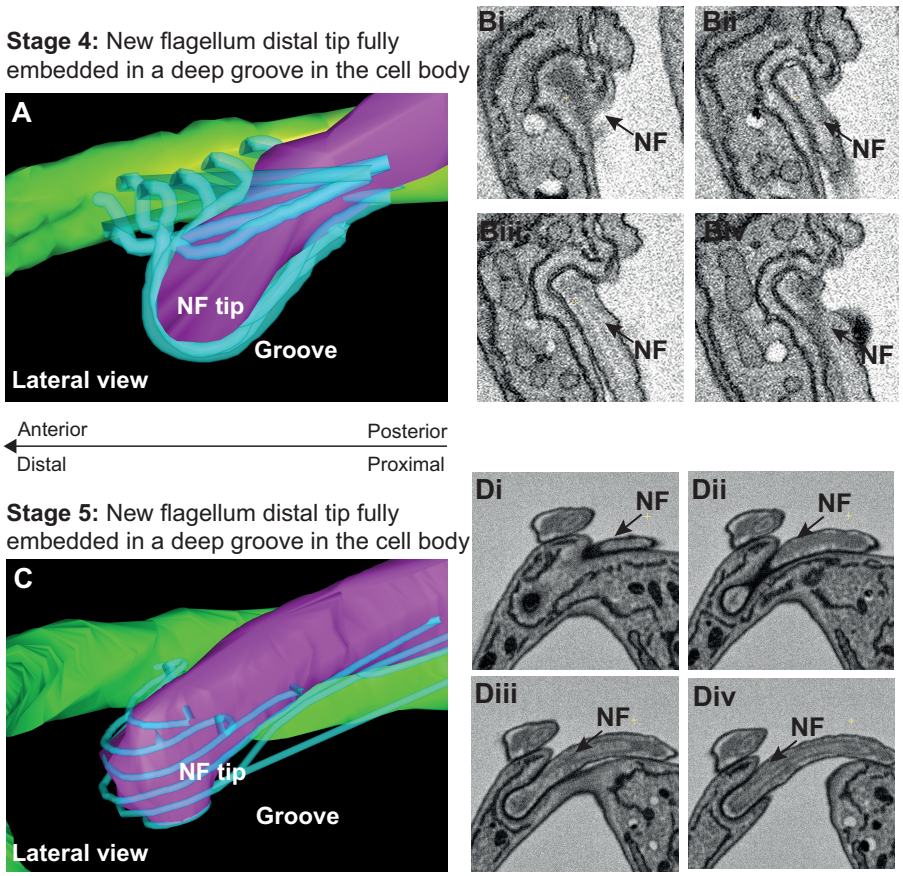

Figure 25: Enlarged region of the distal tip of the new flagellum in stage 4 and 5. A-B) Surface rendering of the new flagellum distal tip in stage 4. Lateral (A) view of the new flagellum tip fully embedded in a deep groove in the cell body (blue lines represent the depth of indentation of the plasma membrane). SBFSEM raw data images (B) of the modelled area in (A), confirming that the distal tip is fully embedded in the cell body. C-D) Surface rendering of the new flagellum distal tip in stage 5. Lateral (C) view of the new flagellum tip fully embedded in a deep groove in the cell body (blue lines represent the depth of indentation of the plasma membrane). SBFSEM raw data images (D) of the modelled area in (C), confirming that the distal tip is fully embedded in the groove.

We measured the volume of the nucleus and nucleolus of the 40 individual cells through the cell cycle to better understand the changes to these organelles across the cell cycle, and to determine when the groove resolved in relation the nucleus and nucleolus volume. The average volume of the nucleus and nucleolus during each stage was calculated and represented graphically (Table 2; Fig. 26).

Table 2: Mean volume of the nucleus and nucleolus in each cell cycle stage.

Cell cycle stage	Mean nucleus volume (μm^3)	SD of the mean	Mean nucleolus volume (μm^3)	SD of the mean
1	2.77E+09	2.83E+07	1.74E+08	4.24E+06
2	3.28E+09	1.52E+08	2.75E+08	5.80E+07
3	5.07E+09	1.98E+08	3.46E+08	6.67E+07
4	5.73E+09	4.71E+08	4.94E+08	3.89E+07
5	8.80E+09	2.96E+09	2.59E+08	5.44E+07
6	3.06E+09	4.00E+07	1.74E+08	2.50E+07
7	2.98E+09	5.57E+07	2.16E+08	3.38E+07

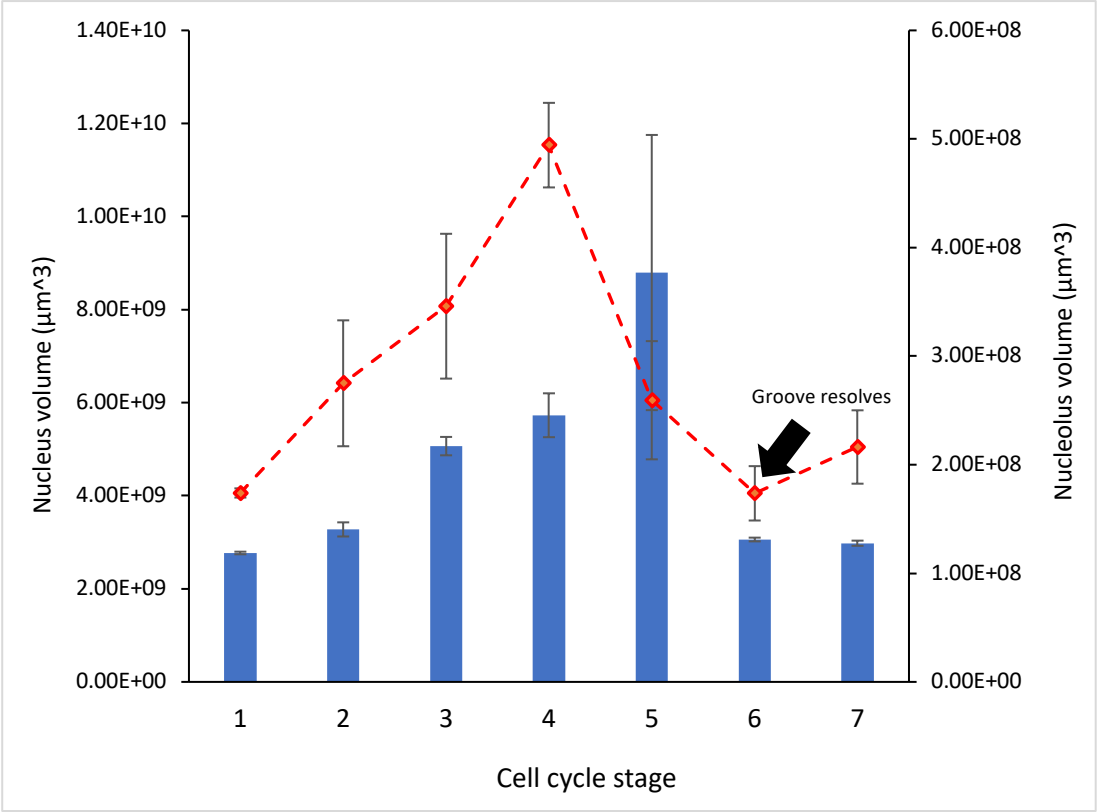

Figure 26: Nucleus (blue bars) and nucleolus (red line) volume across stages 1-7. The mean nucleus and nucleolus volume during each stage. Left axis represents the mean volume of the nucleus, and right axis represents the mean volume of the nucleolus. Number of cells modelled per cell cycle stage as follows: Stage 1 = 3; Stage 2 = 4; Stage 3 = 4; Stage 4 = 3; Stage 5 = 4; Stage 6 = 22; Stage 7 = 5. Three independent SBFSEM datasets were used to model cells in the defined cell cycle stages. Error bars show the standard deviation of the mean volume of the nucleus and nucleolus according to Table 2 (±SD).

32 mitotic and post-mitotic cells were examined to determine when the groove resolves in relation to the division of the nucleus and nucleolus, and it has been determined that the groove resolves post-mitosis and prior to cytokinesis. In 100% of mitotic cells, the new

flagellum distal tip was fully embedded in a deep groove in the cell body (Fig. 27A-B). However, once the nuclei divided, only 30% of 2K2N cells possess a groove (N = 20) (Fig. 27C), suggesting that the groove resolves post-mitosis with the majority of 2K2N cells possessing a free new flagellum distal tip (Fig. 27D).

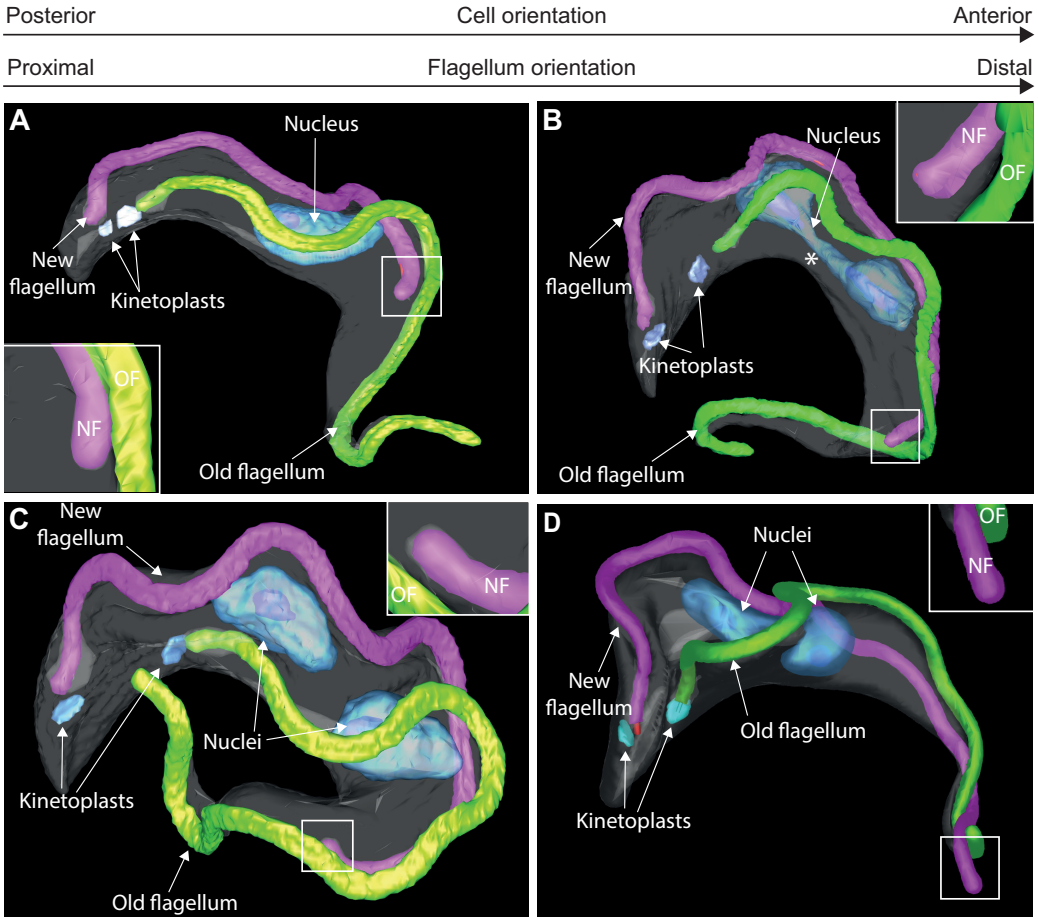

Figure 27: 3D surface rendering of representative cells during stages 3-6. A) Cell containing two kinetoplasts and one large nucleus, with the new flagellum distal tip embedded in the groove (inset). B) Mitotic cell containing a dividing nucleus connected by a nuclear bridge (asterisk), with a long new flagellum whose distal tip is embedded in the groove (inset). C) Post-mitotic cell containing two kinetoplasts and two nuclei, each containing a small nucleolus. The groove is still present (inset). D) Post-mitotic cell containing two kinetoplasts and two nuclei, each containing a small nucleolus. At this stage, the groove has resolved and released the new flagellum distal tip from the cell body (inset). Key: NF = new flagellum; OF = old flagellum.

4.4 Groove resolves when the new flagellum surpasses the old flagellum in length

We determined that the groove resolves post-mitosis but prior to cytokinesis; however, it was hypothesised that the ratio of the length of the new flagellum to the old flagellum may also correlate with groove resolution. I discovered that for most of the cell cycle (stages 1-

5), the new flagellum was shorter than the old flagellum (Table 3; Fig. 28), and in these stages, the new flagellum distal tip was embedded in the groove. However, in the 2K2N cells where the groove had resolved (as in Fig. 27D), the average length of the new flagellum (27.5 µm) was longer than the average length of the old flagellum (25.9 µm) (Table 3; Fig. 28). Therefore, we suggest that groove resolution correlates with the new flagellum surpassing the old flagellum in length and that this extension of the new flagellum may be the trigger for the groove to resolve and release the new flagellum distal tip.

Table 3: The mean length of the old and new flagellum in stages 1-7.

Cell cycle stage	Mean length of the old flagellum (µm)	SD of the mean	Mean length of the new flagellum (µm)	SD of the mean
1	27.16	1.07	1.65	1.54
2	28.44	2.91	10.28	5.87
3	27.07	1.26	18.46	1.18
4	28.23	1.31	21.63	0.70
5	30.30	0.44	28.26	0.05
6	25.97	2.46	27.50	3.11
7	25.67	0.75	25.97	1.80

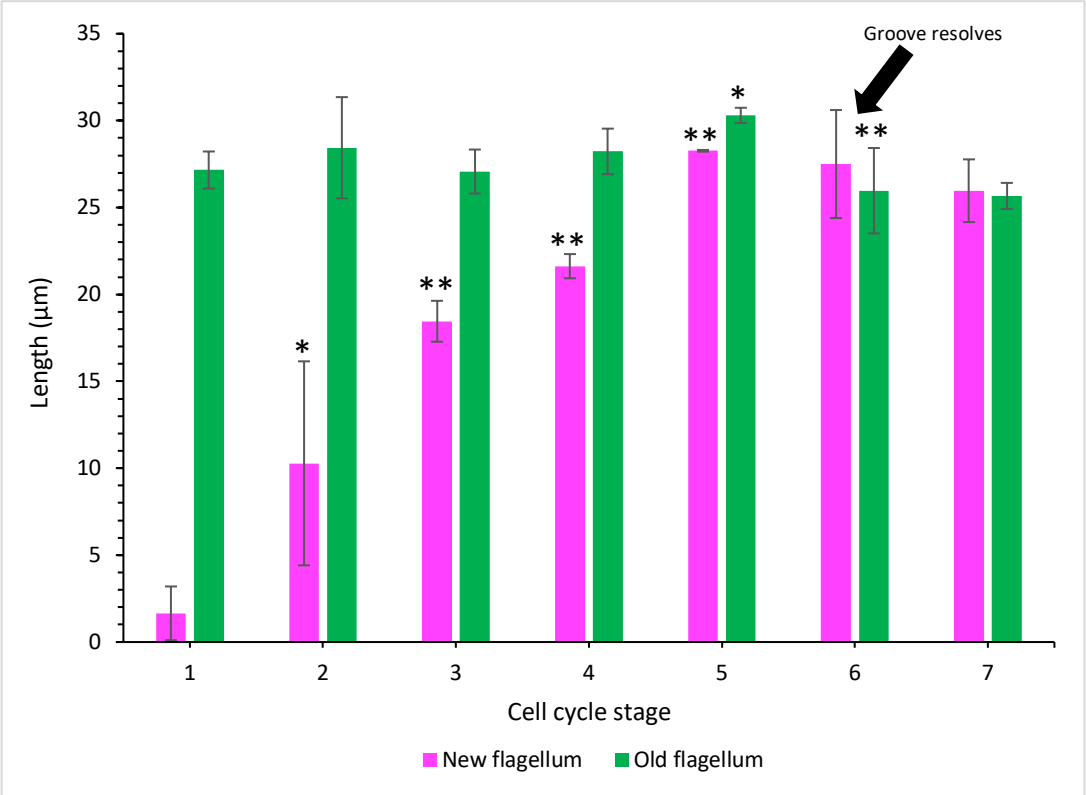

Figure 28: Mean length of the old and new flagellum during stages 1-7. Number of cells modelled per cell cycle stage as follows: Stage 1 = 3; Stage 2 = 4; Stage 3 = 4; Stage 4 = 3; Stage 5 = 4; Stage 6 = 22; Stage 7 = 5. Three independent SBFSEM datasets were used to model cells in the defined cell cycle

stages. Error bars show the standard deviation of the mean length of the new and old flagella per cell cycle stage (±SD). * P<0.05; ** P<0.01 by Student's t test.

It has been determined that the groove resolves and releases the new flagellum distal tip post-mitosis and prior to cytokinesis, when the new flagellum surpasses the old flagellum in length.

5 Identification of 13 proteins that localise to the bloodstream form flagellar groove

5.1 Preface

To understand the molecular function of the groove, putative groove proteins had to be identified and localised in the BSF using PCR-based endogenous tagging to generate individual cell lines with the candidate groove protein fused to the mNeonGreen fluorescent protein (Dean *et al*., 2015).

5.2 A cell line expressing a flagellum tip protein was chosen as a marker for the localisation screen due to the lack of groove-specific marker cell lines

Owing to the relatively recent identification of the groove (Hughes *et al*., 2013), there is a lack of known groove proteins to be used as a marker to colocalise with putative groove proteins. FAZ10 (Tb927.7.3330) was confirmed as a groove protein through monoclonal antibody detection with DOT1 (Hughes *et al*., 2013); however, FAZ10 was not used as a marker in our screen due to the possibility of the fluorescent signal of FAZ10 obscuring the signal of the candidate groove proteins if colocalised. Therefore, a marker cell line expressing a flagellum tip protein (Tb427.02.5860) fused to the mScarlet fluorescent protein was used to clarify putative flagellar groove proteins instead. According to TrypTag, Tb427.02.5860 localised to both the old and new flagella tips throughout the cell cycle, making this protein a good marker for identifying the groove, which should co-localise around the marker signal on the new flagellum distal tip. The marker cell line grew at a similar rate to the *T. brucei* 427 parental cell line, suggesting that the incorporation of a red fluorescent tag was not detrimental to cell growth (Fig. 29). Due to these features, this protein was chosen as a suitable marker in lieu of a groove-specific marker.

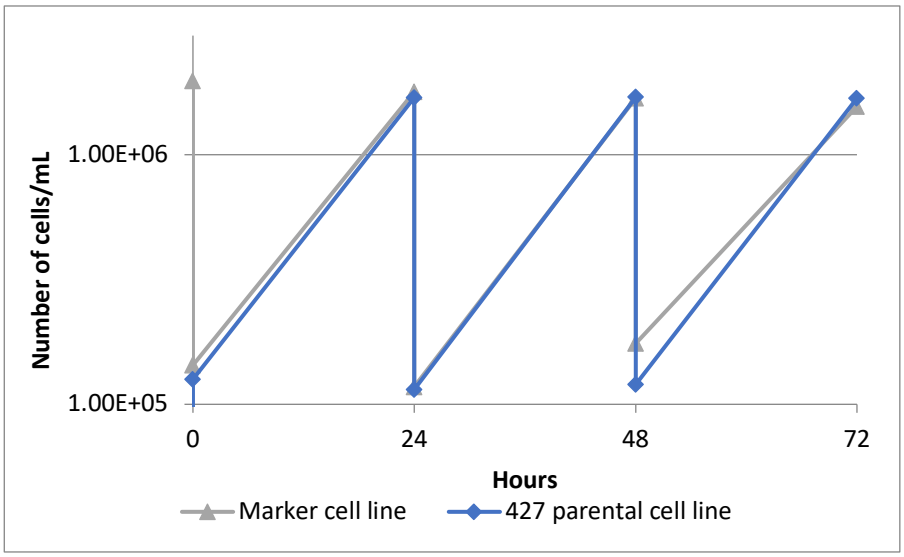

Figure 29: Growth curve of the mSc::Tb427.02.5860 marker cell line versus the 427 parental cell line.

Live cell imaging of the mSc::Tb427.02.5860 fusion protein in BSF cells confirmed that this protein indeed localised to both flagella tips throughout the cell cycle (Fig. 30). In G1 cells containing one kinetoplast and one nucleus, mSc::Tb427.02.5860 localised to the distal tip of the single flagellum (Fig. 30A); however, as the new flagellum began to grow, mSc::Tb427.02.5860 also localised to the new flagellum distal tip (Fig. 30B, inset). As the cell cycle progressed, the new flagellum continued growing and approached the anterior cell tip (Fig. 30C-D, inset). After mitosis, the new flagellum distal tip reached the anterior cell tip and emerged from the cell body as the cell entered cytokinesis (Fig. 30E-F, inset).

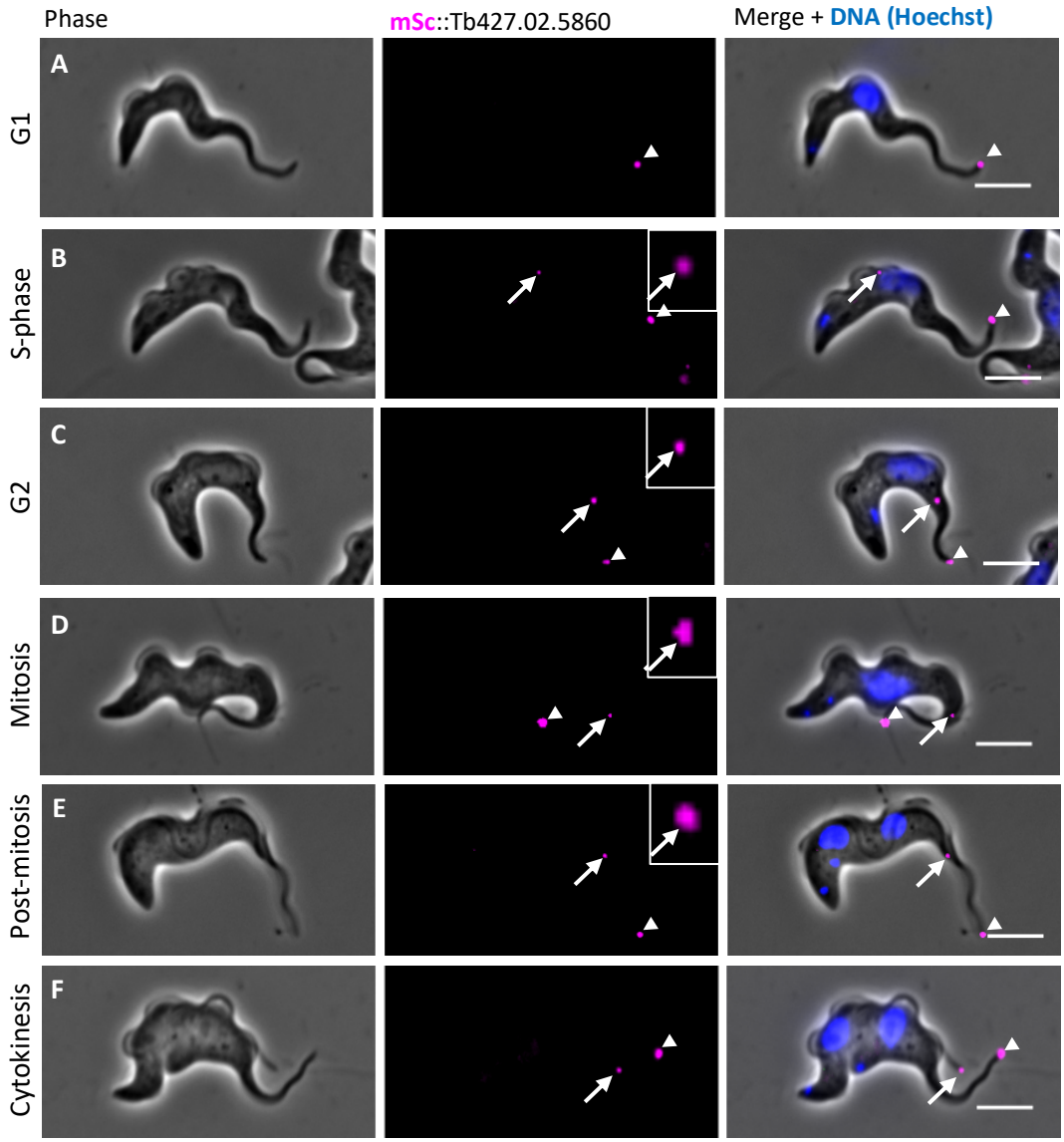

Figure 30: Cell cycle of the *T. brucei* cell line expressing a flagellum tip marker Tb427.02.5860 fused to the mScarlet fluorescence protein. A) Cell with one kinetoplast, one nucleus (1K1N) and a single flagellum (flagellum tip marker indicated with arrowhead). B) Flagellum tip marker present on the new flagellum. C-E) New flagellum distal tip has migrated past the nucleus. F) New flagellum distal tip released from the cell body during cytokinesis. Key: Old flagellum distal tip = arrowhead; new flagellum distal tip = arrow, inset box. Nuclear and Kinetoplast DNA stained with Hoechst (blue). Scale = 5 µm.

When examining the marker cell line on the microscope, it was observed that the signal intensity of the flagellum tip marker differed between the distal tip of the new and old flagellum, with the new flagellum distal tip possessing a smaller magenta foci than the old flagellum (Fig. 2B-F, arrow and arrowhead). Furthermore, the flagellum tip marker was not always visible on the new flagellum distal tip during the early stages of new flagellum growth,

suggesting that this protein may not localise to the new flagellum distal tip as soon as the new flagellum begins to grow, but may instead become visible as the tip matures as the new flagellum approaches the nucleus (Fig. 30B, inset). To investigate this quantitatively, the proportion of cells in defined cell cycle stages was examined (Fig. 31A). *T. brucei* has a defined cell cycle with the duplication of the kinetoplast and nucleus occurring at specific time-points in the cell cycle; therefore, counting the number of kinetoplasts and nuclei in a cell can indicate how the cell cycle is progressing. It was observed that over 70% of the total number of cells counted (N = 500 cells) possessed one kinetoplast and one nucleus (1K1N) (Fig. 31A), corresponding with the proportion of 1K1N cells in a population of procyclic form parasites (71.2%) (Woodward and Gull, 1990). We then determined the proportion of 1K1N, 2K1N and 2K2N cells with a visible marker signal on the new flagellum distal tip (Fig. 31B). We saw that only 9.3% of 1K1N cells possessed a visible marker signal on the new flagellum distal tip, compared to over 99% of 2K1N cells, suggesting that there may be a proportion of cells with a very short new flagellum where the flagellum tip marker is not visible yet. Furthermore, 100% of the 1K1N cells with a visible marker signal on the new flagellum (9.3%) possessed a bilobed kinetoplast, suggesting that the flagellum tip marker may become visible when the cell entered kinetoplast S-phase. According to Sherwin and Gull (1989), the new flagellum emerges from the FP during kinetoplast S-phase, when the kinetoplast is bilobed with two joined discs, indicating that the kinetoplast DNA is beginning to segregate. Perhaps the flagellum tip marker becomes visible towards the end of kinetoplast S-phase, and subsequently when the new flagellum has emerged from the flagellar pocket and grown along a portion of the cell body.

To investigate this further, defined cell positions were outlined that would allow us to track the appearance of the marker signal on the new flagellum distal tip. A trypanosome cell was split into four distinct sections (Fig. 31C):

1) Area between the kinetoplast and the nucleus.
2) Area across the nucleus.
3) Area between the anterior edge of the nucleus to the anterior cell tip.
4) The new flagellum tip is free from the cell body.

The proportion of cells possessing a visible new flagellum distal tip signal was examined relative to the defined cellular positions (Fig. 31D). 500 cells with two flagella (2F), with a visible marker signal on the new flagellum tip, were examined to determine when the marker

became visible on the new flagellum distal tip. In a small proportion of cells (14.7%), mSc::Tb427.02.5860 was clearly visible between the kinetoplast and the nucleus, however, in 31.6% and 36.2% of cells examined, mSc::Tb427.02.5860 was visible as the new flagellum was adjacent to the nucleus and between the nucleus and anterior cell tip, respectively. This suggests that mSc::Tb427.02.5860 may indeed only localise once the new flagellum distal tip has matured (Fig. 31D).

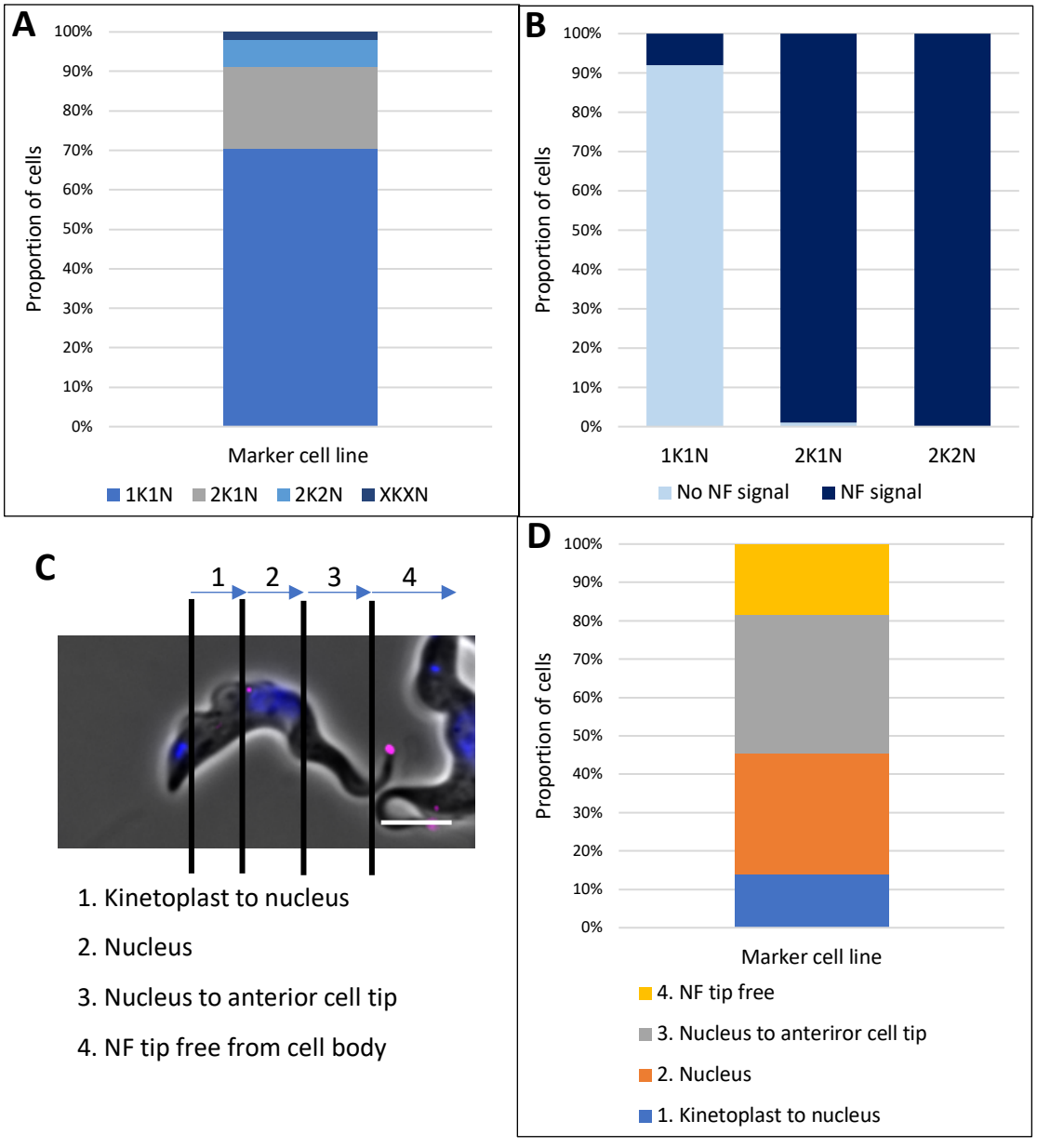

Figure 31: Marker cell line characterisation. A) Proportion of cells in defined cell cycle stages. 1K1N = one kinetoplast and one nucleus; 2K1N = two kinetoplasts and one nucleus; 2K2N = two kinetoplasts and two nuclei; XKXN = an abnormal number of kinetoplasts or nuclei such as >2K>2N, 0K3N, zoids (no nucleus) etc. N = 500 cells total. B) Proportion of 1K1N, 2K1N and 2K2N cells with a visible marker

signal on the new flagellum distal tip. N = 500 cells per stage. C) Map of defined regions of the cell. Scale = 5 μm. D) Position analysis of the new flagellum distal tip in 500 2F cells 2F.

5.3 45 putative groove proteins were identified using TrypTag

We used the TrypTag database to identify proteins present in PCF of the parasite that may potentially localise to the BSF flagellar groove. This method has an evident caveat in that we used a protein localisation database for the PCF (insect parasite) to identify proteins that localise to the groove in the BSF (mammalian parasite). However, as the groove is a structure likely associated with the developing new FAZ and new anterior cell tip, proteins localising to these areas in the PCF were selected for this screen. Proteins localising to the flagella connector were included in our screen. As this structure is associated with the distal tip of the growing new flagellum in the PCF and we wanted to determine if the FC and the groove have shared biochemistry. All FC proteins identified by TrypTag, as well as all FC proteins identified and characterised previously in the PCF (Varga *et al*., 2017) were included in this screen.

Whilst mining for putative groove proteins on TrypTag, additional criteria refined the cohort of groove candidates. These were:

1) Clear, visible signal at the distal FAZ, anterior cell tip or flagella connector.
2) An uncomplicated signal with no fluorescent localisation in multiple organelles that will obscure the visibility of the groove and flagellum tip marker.

In total, 45 putative groove candidates were identified, with 22 proteins localised to the "*Distal FAZ*," 10 proteins localised to the "*Anterior Cell Tip*" and 13 proteins localised to the "*Flagella Connector*" in PCF cells.

5.4 13 proteins localised to the BSF flagellar groove, with five distinct localisation patterns identified

Following identification of the 45 putative groove candidates, each protein was tagged with mNeonGreen in the marker cell line and examined using fluorescence microscopy. Primers used for endogenous tagging are located in **Appendix A**. To determine if a protein localised to the groove, specific criteria were developed:

1) Clear, visible elaboration of green signal (mNeonGreen tagged candidate protein) co-localising around the distal tip (mScarlet tagged marker) of the new flagellum.
2) The elaboration of green signal colocalising around the flagellum tip marker was only present in cells growing a new flagellum.
3) The elaboration of green signal colocalising around the new flagellum tip marker was not observed in PCFs on TrypTag.

The localisation screen identified 32 proteins that did not localise to the flagellar groove as the mNG signal did not fit the criteria listed above. Protein localisations of the non-groove proteins are located in **Appendix B**. I successfully generated and screened 45 proteins by fluorescence microscopy, with 13 of these proteins localising to the groove (Fig. 32-50). The 13 groove proteins were classified into five distinct categories of signal (Table 4).

Table 4: Summary of the proteins that localised to the groove in bloodstream form *T. brucei*.

Gene ID	Gene name	Published?	Localisation in BSFs	Figure
Tb427.07.3330	FAZ10	BSF – Moreira *et al*., 2017	Full length FAZ + groove	32
Tb427.01.4310	FAZ2	PCF – Sunter *et al*., 2015b	Full length FAZ + groove	33
Tb427.10.8240	CIF4	PCF – Hu *et al*., 2019	Distal FAZ + groove	35
Tb427.10.6360	FPRC	PCF – Hu *et al*., 2019	Distal FAZ + groove	36
Tb427tmp.01.3030	-	-	Groove	38
Tb427.10.13100	CIF3	BSF – Zhang *et al*., 2019	Groove	39
Tb427tmp.01.7450	TOEFAZ1/CIF1	BSF – Zhang *et al*., 2019	Groove	40
Tb427.05.3460	FAZ16	-	Groove	41
Tb427.10.890	FCP4	PCF – Varga *et al*., 2017	Groove	42
Tb427.08.7070	FAZ15	-	Comet-tail	44
Tb427.01.2710	-	PCF – Varga *et al*., 2017	Comet-tail	45
Tb427tmp.01.0400	FCP5	PCF – Varga *et al*., 2017	Complex	47
Tb427.08.4780	FLAM3	BSF – Sunter *et al*., 2015a	Complex	49

5.4.1 FAZ10 and FAZ2 localised to the full length of the old and new FAZ and to the groove.

Two proteins, Tb427.07.3330 (FAZ10) and Tb427.01.4310 (FAZ2), localised to the flagellar groove and to the full length of both the old and new FAZ in BSFs (Fig. 32-33; schematic in Fig. 34). However, in PCFs, FAZ10 localised to the intracellular domain of the FAZ (Moreira *et al*., 2017), whereas FAZ2 localised to the FAZ filament domain (Sunter *et al*., 2015a).

In G1 cells, mNG::FAZ10 localised to the full length of the FAZ of the single flagellum (Fig. 32A). During S-phase, mNG::FAZ10 localised to the full length of the FAZ of both the old and new flagellum and to the groove, seen as an elaboration at the distal end of the new flagellum (Fig. 32B-C, inset). The flagellum tip marker was not visible on the new flagellum distal tip during this cell cycle stage (Fig. 32B-C, inset). As the new flagellum elongated, mNG::FAZ10 remained localised to the FAZ and to the groove, which colocalised around the now visible new flagellum distal tip as the groove approached the anterior cell tip (Fig. 32D-E, inset). In cells with a free new flagellum distal tip, mNG::FAZ10 remained localised to the FAZ but was not localised to the groove at this stage of the cell cycle, which suggested that the groove resolved prior to cytokinesis (Fig. 32F).

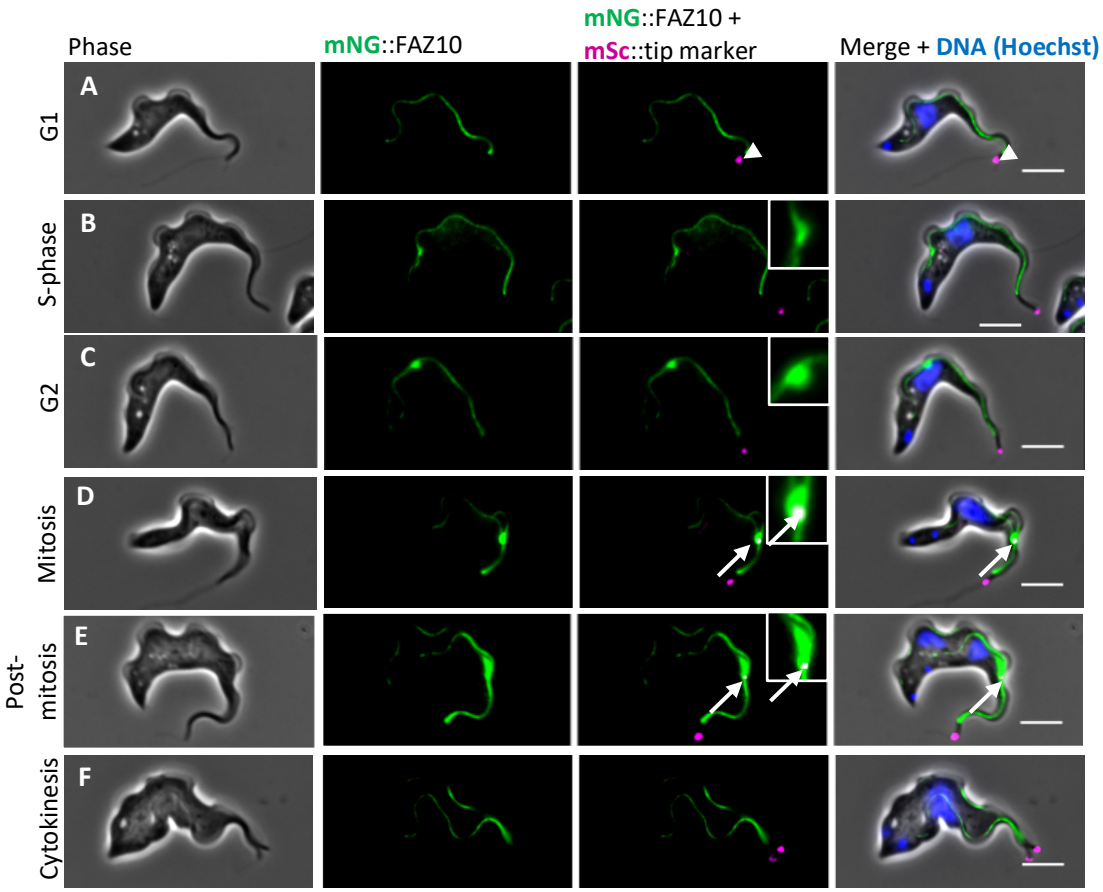

Figure 32: Cell line expressing mSc::Tb427.02.5860 and mNG::Tb427.07.3330 (FAZ10). Endogenous N-terminal tagging of FAZ10 with mNeonGreen revealed a green elaboration around the distal tip of the new flagellum in BSF cells. A-F) Presence and absence of FAZ10 through the cell cycle. Elaboration of the signal (inset box) correlating with the distal end of the new flagellum where the groove is present. Note that elaboration is not present in G1 cells (A) and when cytokinesis has initiated (F). Old flagellum distal tip indicated by white arrowhead; groove indicated by inset box; new flagellum distal tip indicated with arrow. DNA stained with Hoechst (blue). Scale = 5 µm.

In G1 cells, mNG::FAZ2 localised to the full length of the FAZ of the single flagellum (Fig. 33A); however, once the new flagellum emerged from the flagellar pocket, mNG::FAZ2 localised to the FAZ of both the old and new flagellum and to the groove, represented as an elaboration at the distal tip of the new flagellum (Fig. 33B-C, inset). Similar to mNG::FAZ10, the flagellum tip marker was not visible on the new flagellum distal tip during early new flagellum growth. As the groove migrated towards the anterior cell tip, mNG::FAZ2 remained localised to the groove and colocalised around the now visible new flagellum distal tip as the new flagellum elongated (Fig. 33D, inset). In post-mitotic cells, the flagellum tip marker on the new flagellum distal tip appeared more distal than the elaboration of green signal, suggesting that the new flagellum tip has emerged from the groove (Fig. 33E). Once cytokinesis was initiated, mNG::FAZ2 localised only to the old and new FAZ, suggesting that the groove had resolved (Fig. 33F).

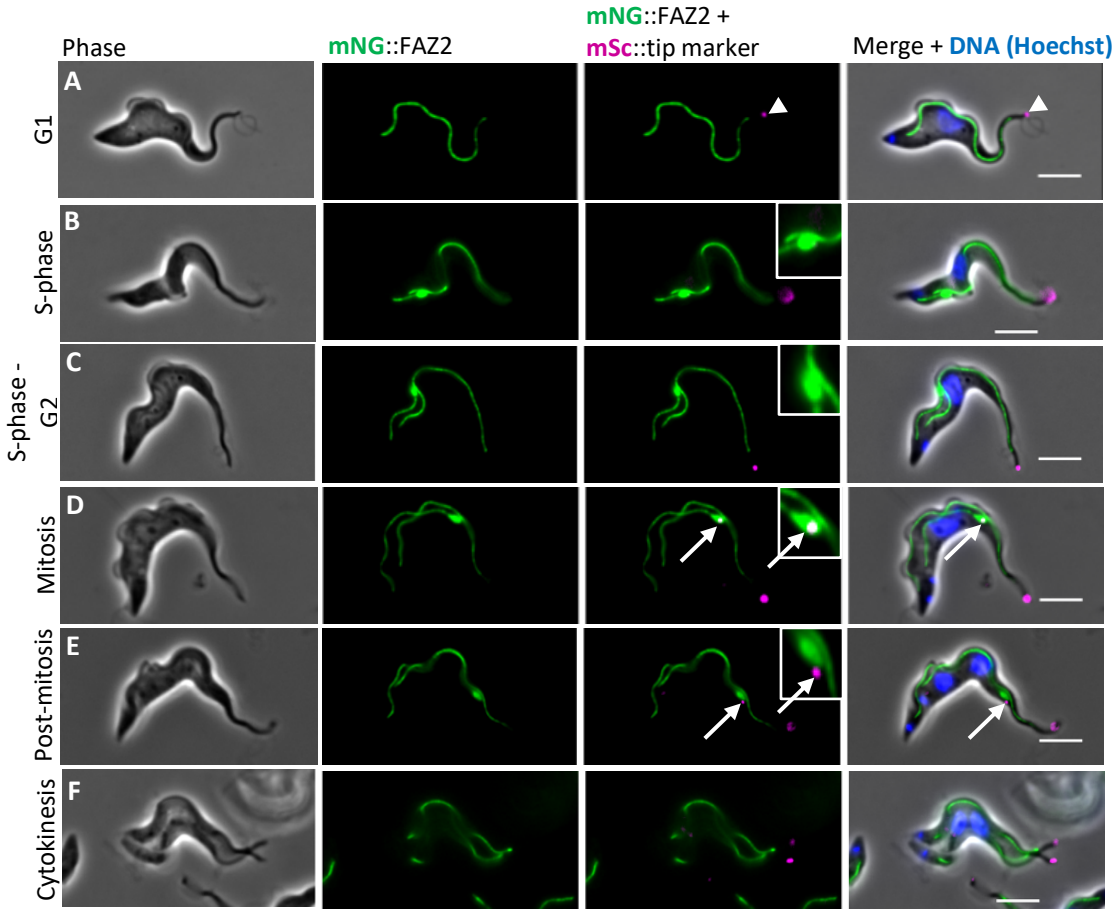

Figure 33: Cell line expressing mSc::Tb427.02.5860 and mNG::Tb427.01.4310 (FAZ2). Endogenous N-terminal tagging of FAZ2 with mNeonGreen revealed a green elaboration around the distal tip of the new flagellum in BSF cells. A-F) Presence and absence of FAZ2 through the cell cycle. Elaboration of the signal (inset box) correlating with the distal end of the new flagellum where the groove is present. Note that elaboration is not present in G1 cells (A) and when cytokinesis has initiated (F). Old flagellum

distal tip indicated by white arrowhead; groove indicated by inset box; new flagellum distal tip indicated with arrow. DNA stained with Hoechst (blue). Scale = 5 µm.

Full length FAZ + groove - FAZ10 and FAZ2

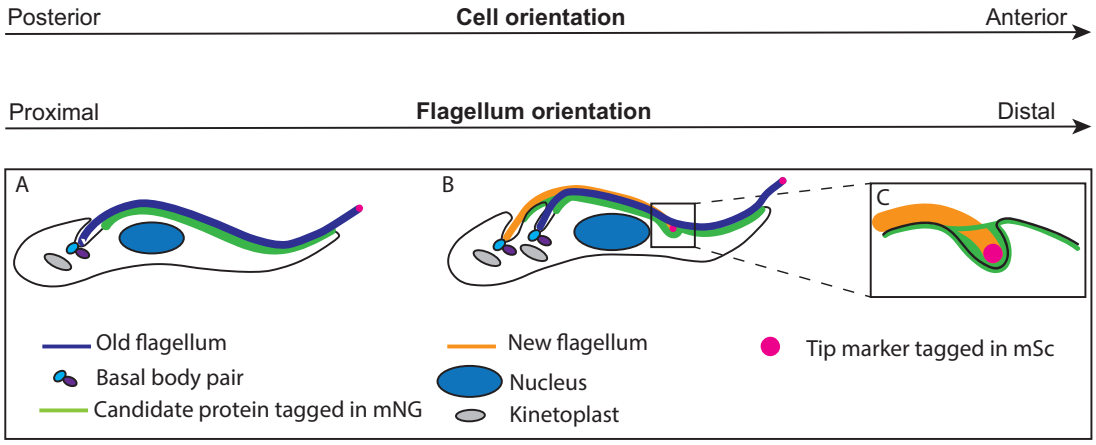

Figure 34: Schematic of the fluorescence signal of the "Full length FAZ + groove" category. A) Non-dividing G1 cell with one kinetoplast and one nucleus and a single flagellum nucleating from a single basal body pair. The candidate protein tagged in mNG localises to the full length of the FAZ of the single flagellum in non-dividing cells (green). B) Cell containing two kinetoplasts and one nucleus (2K1N). New flagellum (orange) nucleating from the new BBP at the posterior end of the cell body, with the distal tip (magenta) embedded in the groove (C).

5.4.2 FPRC and CIF4 localised to a portion of the distal FAZ of the old flagellum and to the groove.

Two proteins, Tb427.10.6360 (FPRC) and Tb427.10.8240 (CIF4), localised to the groove, with an additional foci observed along a portion of the distal end of the old FAZ (Fig. 35-36; Fig. 37 for schematic). For both cell lines, the distal FAZ foci was present throughout the cell cycle, whereas the groove foci was only present in cells growing a new flagellum. Both FPRC and CIF4 localised to the distal FAZ in the PCF (Hu *et al*., 2019).

In G1 cells, mNG::CIF4 localised to a distal portion of the FAZ of the single flagellum, appearing as a small green foci immediately proximal to the anterior cell tip (Fig. 35A, yellow arrow). Once a new flagellum began to grow, mNG::CIF4 also localised as an elaboration at the distal end of the new flagellum, representing the groove (Fig. 35B, inset). As the new flagellum elongated, the mNG::CIF4 signal became more elaborate as it colocalised around the new flagellum distal tip (Fig. 35C-D, inset). In post-mitotic cells, mNG::CIF4 remained colocalised around the new flagellum tip marker at the anterior cell tip (Fig. 35E, inset).

During cytokinesis, the new flagellum distal tip was released from the cell body and mNG::CIF4 localised to the cleavage furrow, suggesting that CIF4 plays a role in cytokinesis (Fig. 35F, inset).

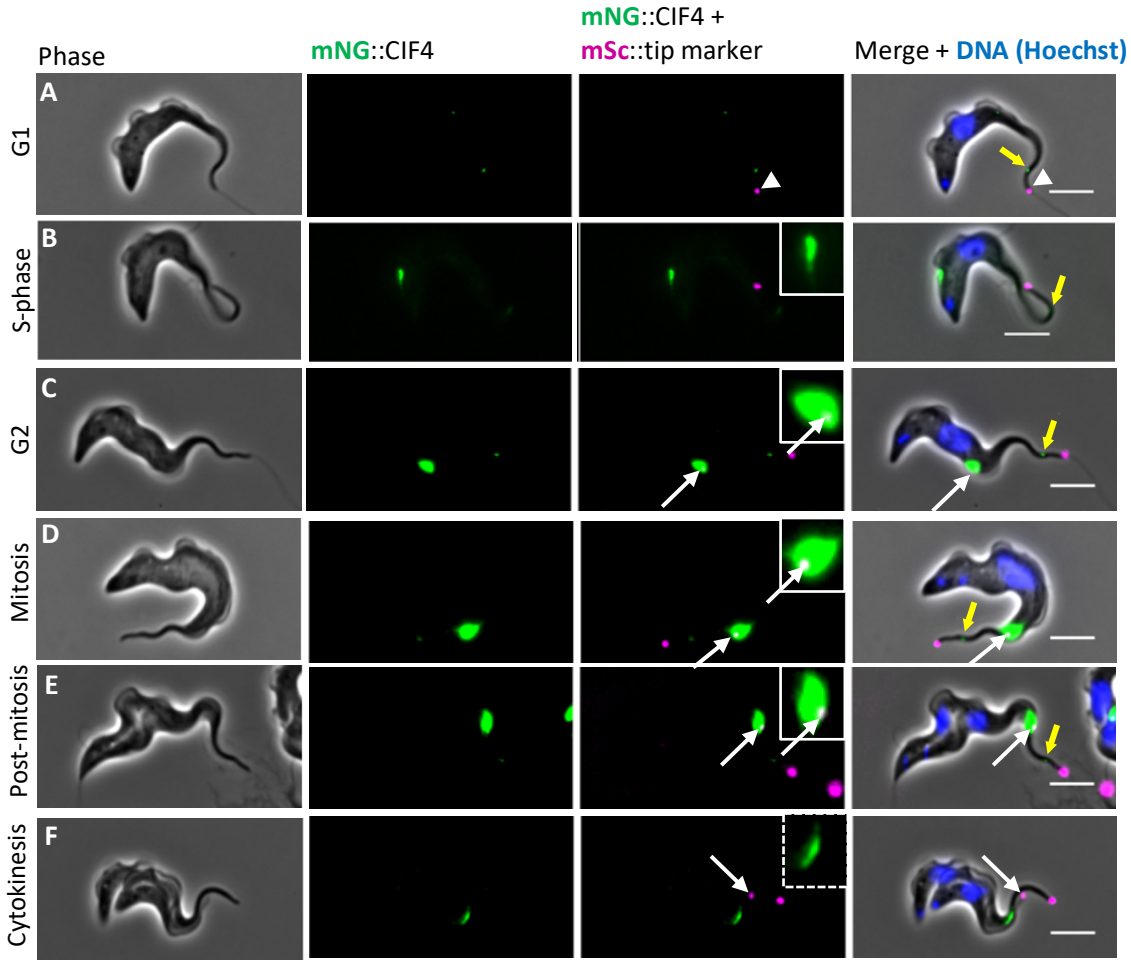

Figure 35: Cell line expressing mSc::Tb427.02.5860 and mNG::Tb427.10.8240 (CIF4). Endogenous N-terminal tagging of CIF4 with mNeonGreen revealed a green elaboration around the distal tip of the new flagellum in BSF cells. A-F) Presence and absence of CIF4 through the cell cycle. CIF4 is localised to a distinct foci at the distal FAZ (yellow arrow) through the cell cycle. Elaboration of the green signal (inset box) correlating with the distal end of the new flagellum where the groove is present. Note that elaboration is not present in G1 cells (A) and that CIF4 localises to the cleavage furrow (dashed inset box) during cytokinesis (F). Old flagellum distal tip indicated by white arrowhead; groove indicated by inset box; new flagellum distal tip indicated with arrow; distal FAZ foci indicated by yellow arrow; cleavage furrow indicated by dashed inset box. DNA stained with Hoechst (blue). Scale = 5 µm.

With regards to mNG::FPRC, it was localised to the distal portion of the FAZ of the old flagellum in G1 cells as a distinct green foci immediately proximal to the anterior cell tip (Fig. 36A, yellow arrow). Once a new flagellum began to grow, mNG::FPRC localised to the groove as an elaboration at the new flagellum distal tip (Fig. 36B-D, inset). After mitosis, mNG::FPRC

remained colocalised around the new flagellum tip marker at the anterior cell tip (Fig. 36E, inset); however, mNG::FPRC was not visible once the cell initiated a cleavage fold (Fig. 36F, inset).

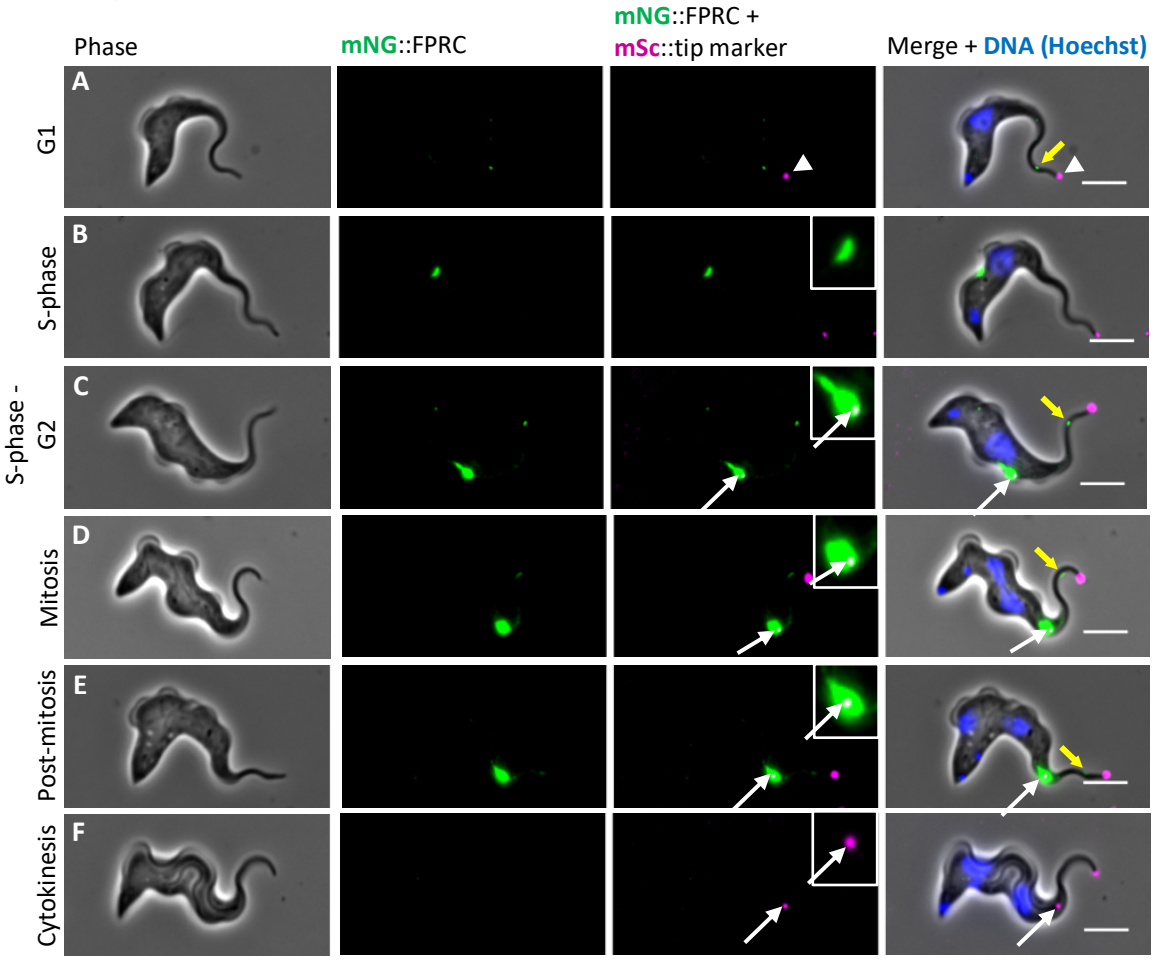

Figure 36: Cell line expressing mSc::Tb427.02.5860 and mNG::Tb427.10.6360 (FPRC). Endogenous N-terminal tagging of FPRC with mNeonGreen revealed a green elaboration around the distal tip of the new flagellum in BSF cells. A-F) Presence and absence of FPRC through the cell cycle. FPRC is localised to a distinct foci at the distal FAZ (yellow arrow) through the cell cycle. Elaboration of the green signal (inset box) correlating with the distal end of the new flagellum where the groove is present. Note that elaboration is not present in G1 cells (A) and cells undergoing cytokinesis (F). Old flagellum distal tip indicated by white arrowhead; groove indicated by inset box; new flagellum distal tip indicated with arrow; distal FAZ foci indicated by yellow arrow; cleavage furrow indicated by dashed inset box. DNA stained with Hoechst (blue). Scale = 5 µm.

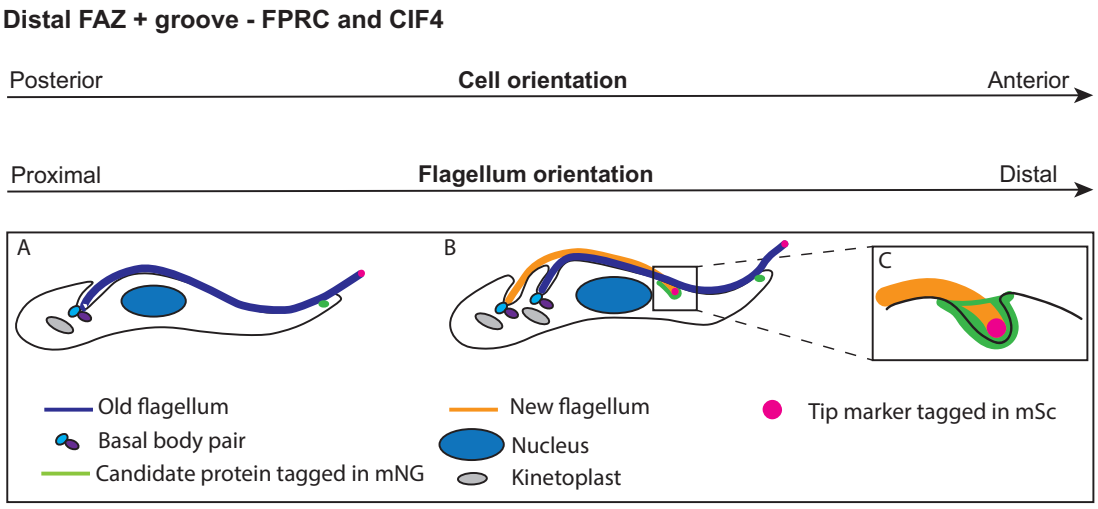

Figure 37: Schematic of the fluorescence signal of the "Distal FAZ + groove" category. A) Non-dividing G1 cell with one kinetoplast and one nucleus and a single flagellum nucleating from a single basal body pair. The candidate protein tagged in mNG localises to a portion of the distal FAZ of the single flagellum in non-dividing cells (green). B) Cell containing two kinetoplasts and one nucleus (2K1N). New flagellum (orange) nucleating from the new BBP at the posterior end of the cell body, with the distal tip (magenta) embedded in the groove (C).

5.4.3 Five proteins localised specifically to the groove.

Five proteins, Tb427tmp.01.3030, Tb427.10.13100 (CIF3), Tb427tmp.01.7450 (CIF1), Tb427.10.890 (FCP4) and Tb427.05.3460 (FAZ16), localised exclusively to the groove during new flagellum growth (Fig. 38-42; Fig. 43 for schematic). In PCFs and BSFs, both CIF1 and CIF3 localised to the new FAZ and to the cleavage furrow during cytokinesis (Zhou *et al*., 2016a; Zhang *et al*., 2019). FCP4, on the other hand, localised to the flagella connector in PCFs (Varga *et al*., 2017). FAZ16 localised to the distal FAZ in PCFs (Sunter and Gull, 2016), as does Tb427tmp.01.3030 according to TrypTag.

Endogenous tagging of Tb427tmp.01.3030 with mNeonGreen revealed an elaboration around the new flagellum distal tip in BSF cells (Fig. 38). In G1 cells with one kinetoplast and one nucleus, mNG::Tb427tmp.01.3030 was not visible (Fig. 38A); however, once the new flagellum began to grow, mNG::Tb427tmp.01.3030 localised exclusively to the groove as a small elaboration at the distal end of the new flagellum (Fig. 38B, inset). The flagellum tip marker was not visible on the new flagellum distal tip at this point (Fig. 38B, inset). In G2 and mitotic cells, mNG::Tb427tmp.01.3030 localised to the groove around the new flagellum tip marker (Fig. 38C-D, inset). mNG::Tb427tmp.01.3030 was not visible during cytokinesis,

suggesting that once the groove resolved, mNG::Tb427tmp.01.3030 was degraded or dispersed in the cell (Fig. 38E).

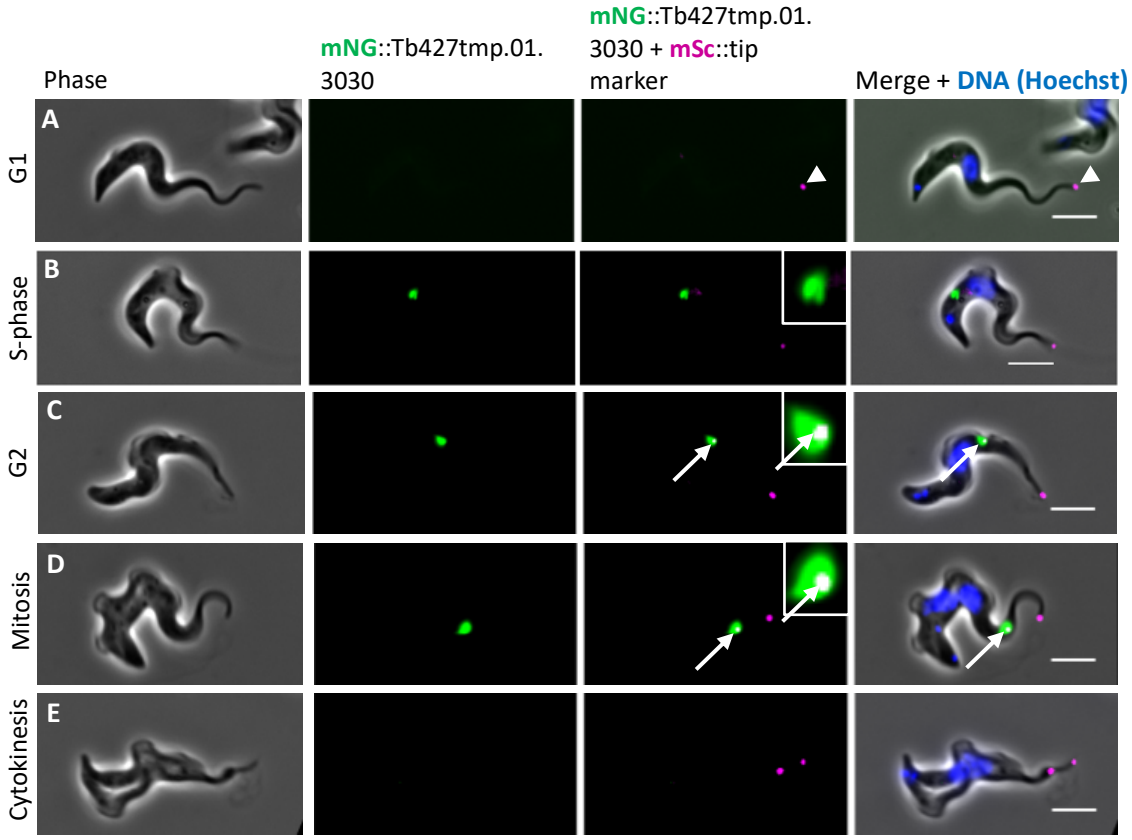

Figure 38: Cell line expressing mSc::Tb427.02.5860 and mNG::Tb427tmp.01.3030. Endogenous N-terminal tagging of Tb427tmp.01.3030 with mNeonGreen revealed a green elaboration around the distal tip of the new flagellum in BSF cells. A-E) Presence and absence of Tb427tmp.01.3030 through the cell cycle. Elaboration of the green signal (inset box) correlating with the distal end of the new flagellum where the groove is present. Note that elaboration is not present in G1 cells (A) and cells undergoing cytokinesis (E). Old flagellum distal tip indicated by white arrowhead; groove indicated by inset box; new flagellum distal tip indicated with arrow. DNA stained with Hoechst (blue). Scale = 5 µm.

mNG::CIF3 was not visible in G1 cells (Fig. 39A); however, once the new flagellum began to grow, mNG::CIF3 localised exclusively to the groove (Fig. 39B, inset). The flagellum tip marker was not visible on the new flagellum distal tip at this stage (Fig. 39B-C, inset). As the new flagellum grew, mNG::CIF3 remained localised exclusively to the groove and colocalised around the now visible the new flagellum tip marker as the groove approached the anterior cell tip (Fig. 39D, inset). In post-mitotic cells, mNG::CIF3 remained colocalised around the flagellum tip marker at the anterior cell tip, suggesting that CIF3 may be involved in cytokinesis initiation (Fig. 39E, inset) and once cytokinesis was initiated and the new

flagellum distal tip was released from the groove, mNG::CIF3 localised to the cleavage furrow, supporting an involvement in cleavage furrow ingression (Fig. 39F, inset).

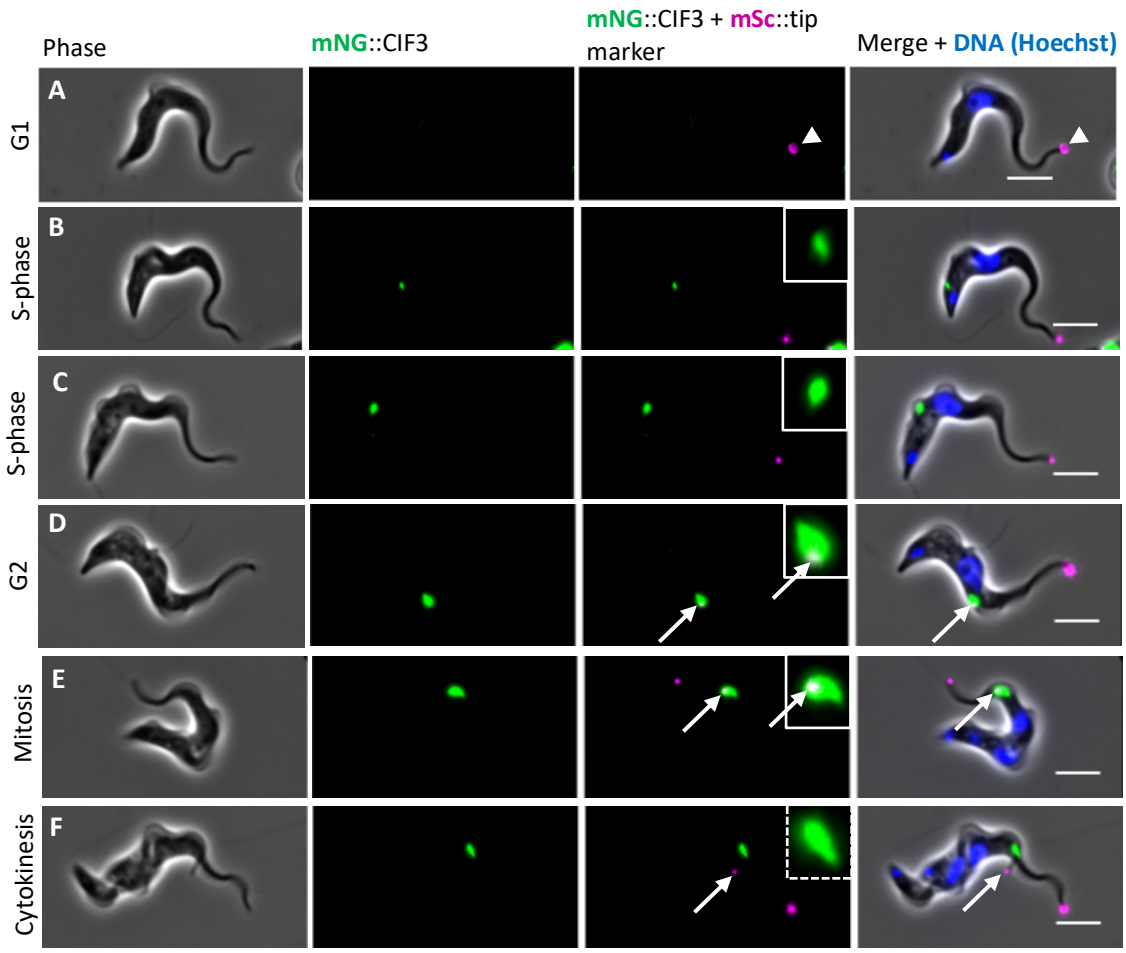

Figure 39: Cell line expressing mSc::Tb427.02.5860 and mNG::CIF3. Endogenous N-terminal tagging of CIF3 with mNeonGreen revealed a green elaboration around the distal tip of the new flagellum in bloodstream form cells. A-F) Presence and absence of CIF3 through the cell cycle. Elaboration of the green signal (inset box) correlating with the distal end of the new flagellum where the groove is present. Note that elaboration is not present in G1 cells (A). CIF3 localises to the cleavage furrow (dashed inset box) during cytokinesis (F). Old flagellum distal tip indicated by white arrowhead; groove indicated by inset box; new flagellum distal tip indicated with arrow; cleavage furrow indicated by dashed inset box. DNA stained with Hoechst (blue). Scale = 5 µm.

Similarly, CIF1::mNG was not localised in G1 cells (Fig. 40A); however, CIF1::mNG localised exclusively to the groove once the new flagellum began to grow (Fig. 40B-C, inset). CIF1::mNG remained localised to the groove and colocalised around the new flagellum tip marker as the groove approached the anterior cell tip (Fig. 40D-E, inset). In post-mitotic cells, however, CIF1::mNG remained localised at the anterior cell tip, suggesting a role in cytokinesis initiation (Fig. 40F). In cells undergoing cytokinesis, CIF1::mNG localised to the

cleavage furrow (Fig. 40G, dashed inset), supporting a role in cytokinesis furrow ingression as seen previously (Zhang *et al*., 2019).

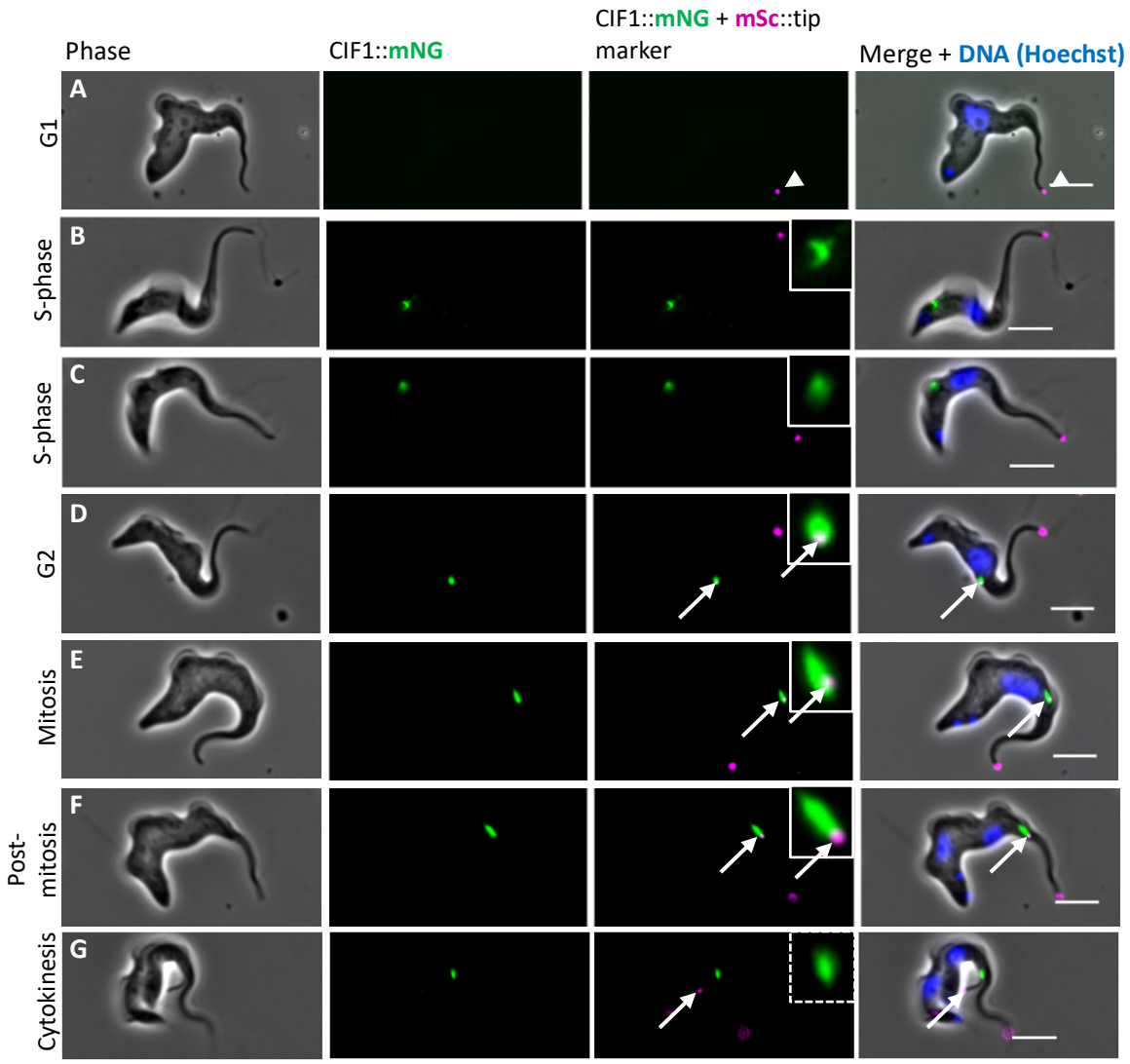

<u>Figure 40:</u> Cell line expressing mSc::Tb427.02.5860 and CIF1::mNG. Endogenous N-terminal tagging of CIF1 with mNeonGreen revealed a green elaboration around the distal tip of the new flagellum in bloodstream form cells. A-G) Presence and absence of CIF1 through the cell cycle. Elaboration of the green signal (inset box) correlating with the distal end of the new flagellum where the groove is present. Note that elaboration is not present in G1 cells (A). CIF1 localises to the cleavage furrow (dashed inset box) during cytokinesis (G). Old flagellum distal tip indicated by white arrowhead; groove indicated by inset box; new flagellum distal tip indicated with arrow; cleavage furrow indicated by dashed inset box. DNA stained with Hoechst (blue). Scale = 5 µm.

Endogenous tagging of FAZ16 with mNeonGreen revealed an elaboration around the new flagellum distal tip in BSF cells (Fig. 41). mNG::FAZ16 was not visible in G1 cells (Fig. 41A) but localised exclusively to the groove once the new flagellum began to grow (Fig. 41B-C, inset).

The flagellum tip marker was not visible on the new flagellum distal tip at this point (Fig. 41B-C, inset); however, as the cell cycle progressed, mNG::FAZ16 colocalised around the now visible new flagellum tip marker as the groove approached the anterior cell tip (Fig. 41D-F, inset). Once cytokinesis was initiated, mNG::FAZ16 was no longer visible, suggesting that once the groove resolved, mNG::FAZ16 was not longer localised (Fig. 41G, inset).

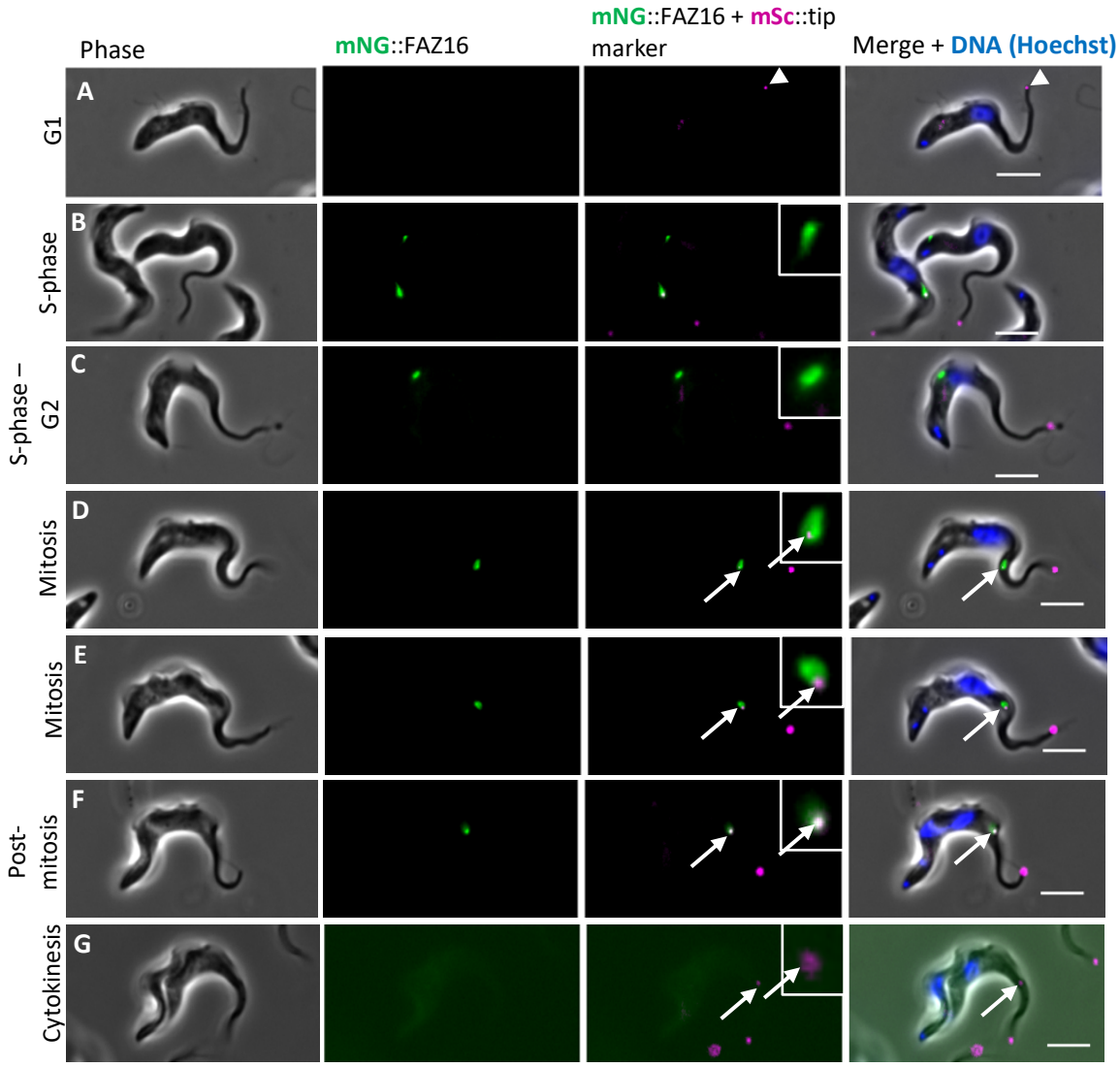

Figure 41: Cell line expressing mSc::Tb427.02.5860 and mNG::FAZ16. Endogenous N-terminal tagging of FAZ16 with mNeonGreen revealed a green elaboration around the distal tip of the new flagellum in bloodstream form cells. A-G) Presence and absence of FAZ16 through the cell cycle. Elaboration of the green signal (inset box) correlating with the distal end of the new flagellum where the groove is present. Note that elaboration is not present in G1 cells (A) and cells undergoing cytokinesis (G). Old flagellum distal tip indicated by white arrowhead; groove indicated by inset box; new flagellum distal tip indicated with arrow. DNA stained with Hoechst (blue). Scale = 5 µm.

mNG::FCP4, like the previous four proteins, was not visible in G1 cells (Fig. 42A); however, mNG::FCP4 localised specifically to the groove in cells growing a new flagellum (Fig. 42B). The flagellum tip marker was not visible on the new flagellum distal tip during early new flagellum growth (Fig. 42B-C, inset); however, after kinetoplast division, mNG::FCP4 colocalised closely around the new flagellum tip marker (Fig. 42D, inset). The expression of mNG::FCP4 suggests that FCP4 may be present in the flagellum rather than the cell body side of the groove (Fig. 42D, inset). In post-mitotic cells, the new flagellum tip marker appeared distal to mNG::FCP4, suggesting that the new flagellum tip was released from the groove at this stage (Fig. 42E, inset). In post-mitotic cells that have formed a division fold before cleavage furrow ingression, mNG::FCP4 was not visible (Fig. 42F, inset).

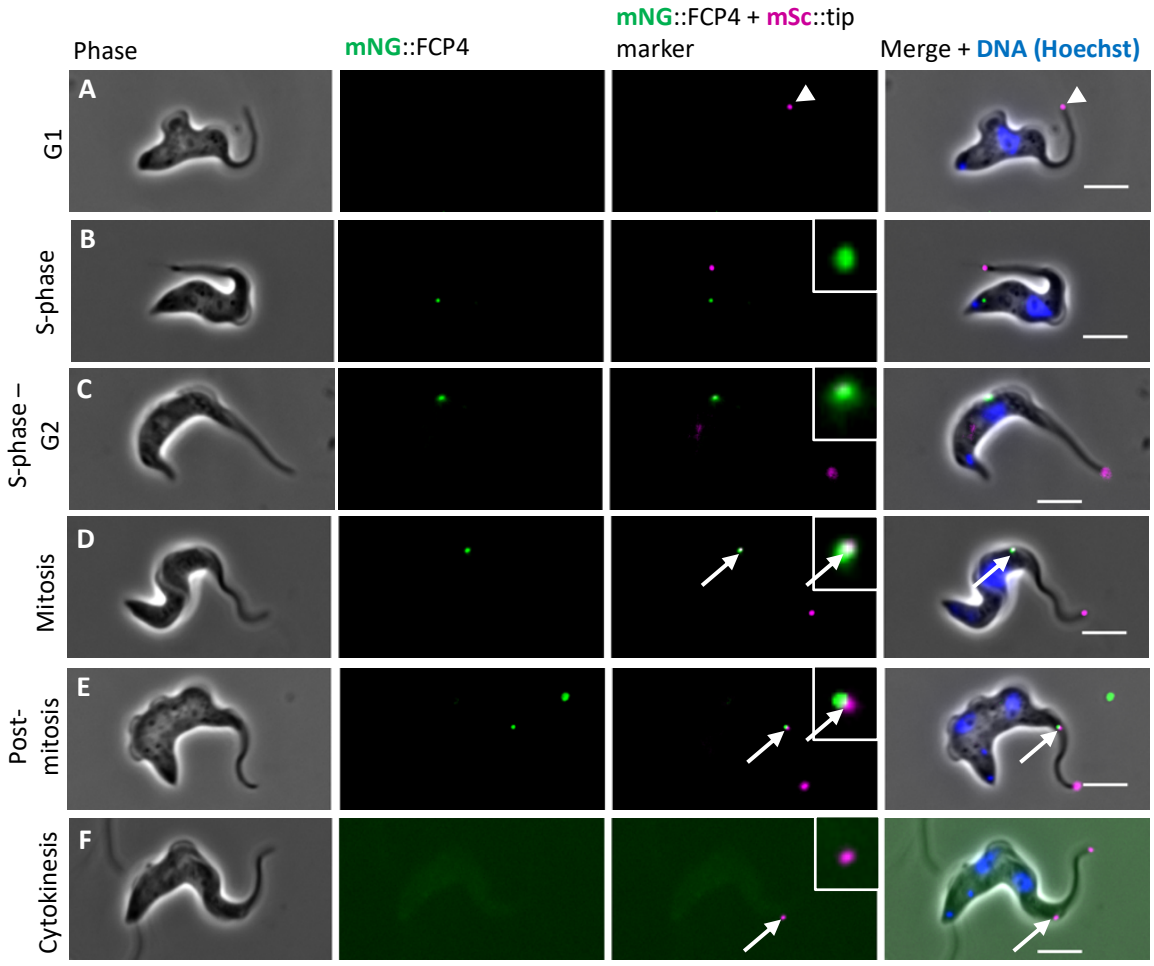

Figure 42: Cell line expressing mSc::Tb427.02.5860 and mNG::FCP4. Endogenous N-terminal tagging of FCP4 with mNeonGreen revealed a green elaboration around the distal tip of the new flagellum in bloodstream form cells. A-F) Presence and absence of FCP4 through the cell cycle. Elaboration of the green signal (inset box) correlating with the distal end of the new flagellum where the groove is present. Note that elaboration is not present in G1 cells (A) and cells undergoing cytokinesis (F). Old

flagellum distal tip indicated by white arrowhead; groove indicated by inset box; new flagellum distal tip indicated with arrow. DNA stained with Hoechst (blue). Scale = 5 µm.

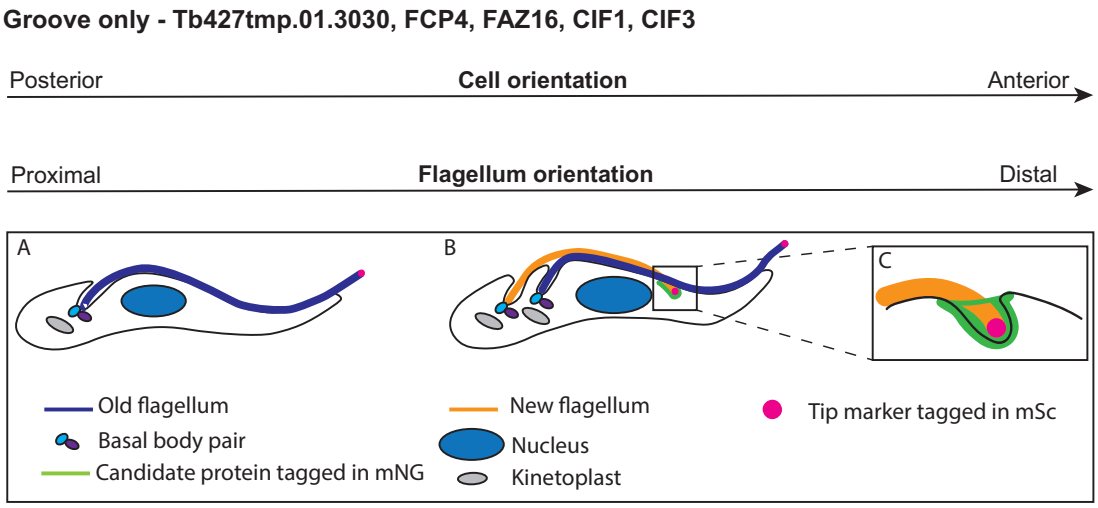

Figure 43: Schematic of fluorescence signal of the "Groove only" category comprising of tagged proteins mNG::Tb427tmp.01.3030, mNG::FCP4, mNG::FAZ16, CIF1::mNG and mNG::CIF3. A) Non-dividing G1 cell with one kinetoplast and one nucleus and a single flagellum nucleating from a single basal body pair. The candidate protein does not localise in non-dividing cells, suggesting that it is not expressed. B) Diving cell containing two kinetoplasts and one nucleus (2K1N). New flagellum (orange) nucleating from the new BBP at the posterior end of the cell body, with the distal tip (magenta) embedded in the groove (C).

5.4.4 Two proteins localised to a portion of the new FAZ and to the groove, resembling a "comet-tail".

Tb427.08.7070 (FAZ15) and Tb427.01.2710 localised to a portion of the new FAZ and to the groove, resembling a "comet-tail" during new flagellum growth (Fig. 44-45; Fig. 46 for schematic). In PCFs, FAZ15 localised to the distal FAZ (Sunter and Gull, 2016), whereas Tb427.01.2710 localised to the flagella connector according to TrypTag.

mNG::FAZ15 was not visible in G1 cells (Fig. 44A); however, after the new flagellum began to grow, mNG::FAZ15 localised to the groove (Fig. 44B, inset). As the new flagellum grew, mNG::FAZ15 colocalised around the flagellum tip marker on the new flagellum and also localised to a portion of the new FAZ immediately proximal to the groove, resembling a "comet-tail" (Fig. 44C, inset). However, as the groove migrated adjacent to the nucleus, mNG::FAZ15 was no longer localised to the new FAZ but remained localised specifically to the groove (Fig. 44D-E, inset). This may suggest that FAZ15 is involved in the initial stages of

new FAZ development. Interestingly, once the groove migrated past the nucleus, mNG::FAZ15 was no longer visible for the remaining cell cycle stages (Fig. 44F-G, inset box).

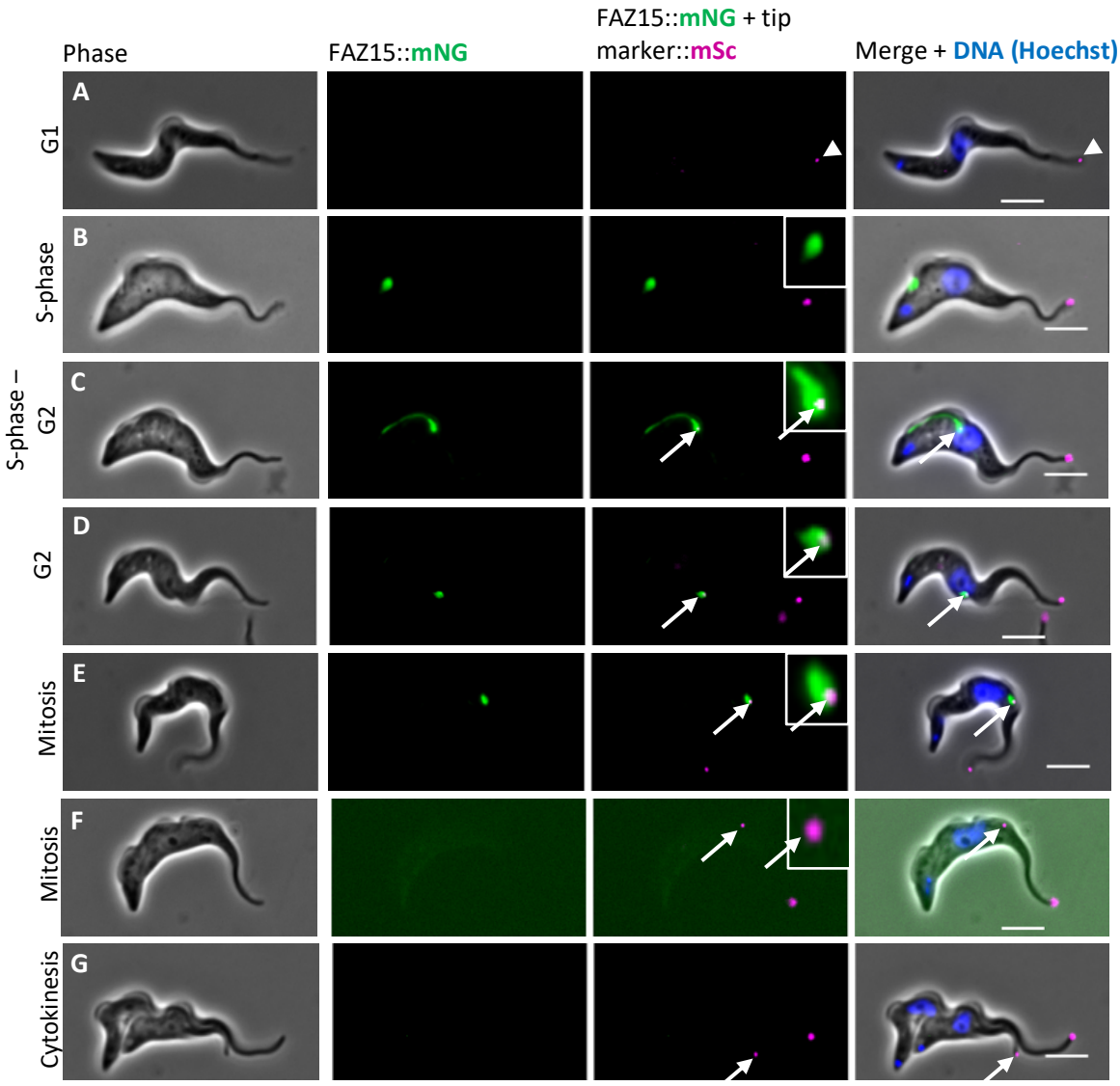

Figure 44: Cell line expressing mSc::Tb427.02.5860 and mNG::FAZ15. Endogenous N-terminal tagging of FAZ15 with mNeonGreen revealed a green elaboration around the distal tip of the new flagellum in bloodstream form cells. A-G) Presence and absence of FAZ15 through the cell cycle. Elaboration of the green signal (inset box) correlating with the distal end of the new flagellum where the groove is present. Note that elaboration is not present in G1 cells (A) and cells undergoing cytokinesis (G). Once the new flagellum passes the nucleus, FAZ15 disappears from the groove (F). During S-phase, FAZ15 also localises to a portion of the new FAZ immediately proximal to the groove (C). Old flagellum distal tip indicated by white arrowhead; groove indicated by inset box; new flagellum distal tip indicated with arrow. DNA stained with Hoechst (blue). Scale = 5 µm.

Tb427.01.2710::mNG, on the other hand, was not visible in G1 cells (Fig. 45A); however, Tb427.01.2710::mNG localised to the groove once the new flagellum began to grow (Fig.

45B, inset). As the new flagellum elongated, Tb427.01.2710::mNG remained localised to the groove around the new flagellum tip marker, but also localised to a portion of the new FAZ immediately proximal to the groove, resembling a "comet-tail" (Fig. 45C, inset). Tb427.01.2710::mNG remained localised to the groove and to the new FAZ through kinetoplast division (Fig. 45D, inset); however, in post-mitotic cells, Tb427.01.2710::mNG was no longer localised to the groove but persisted at the new FAZ (Fig. 45E, inset). Once cytokinesis was initiated, Tb427.01.2710::mNG was not visible (Fig. 45F).

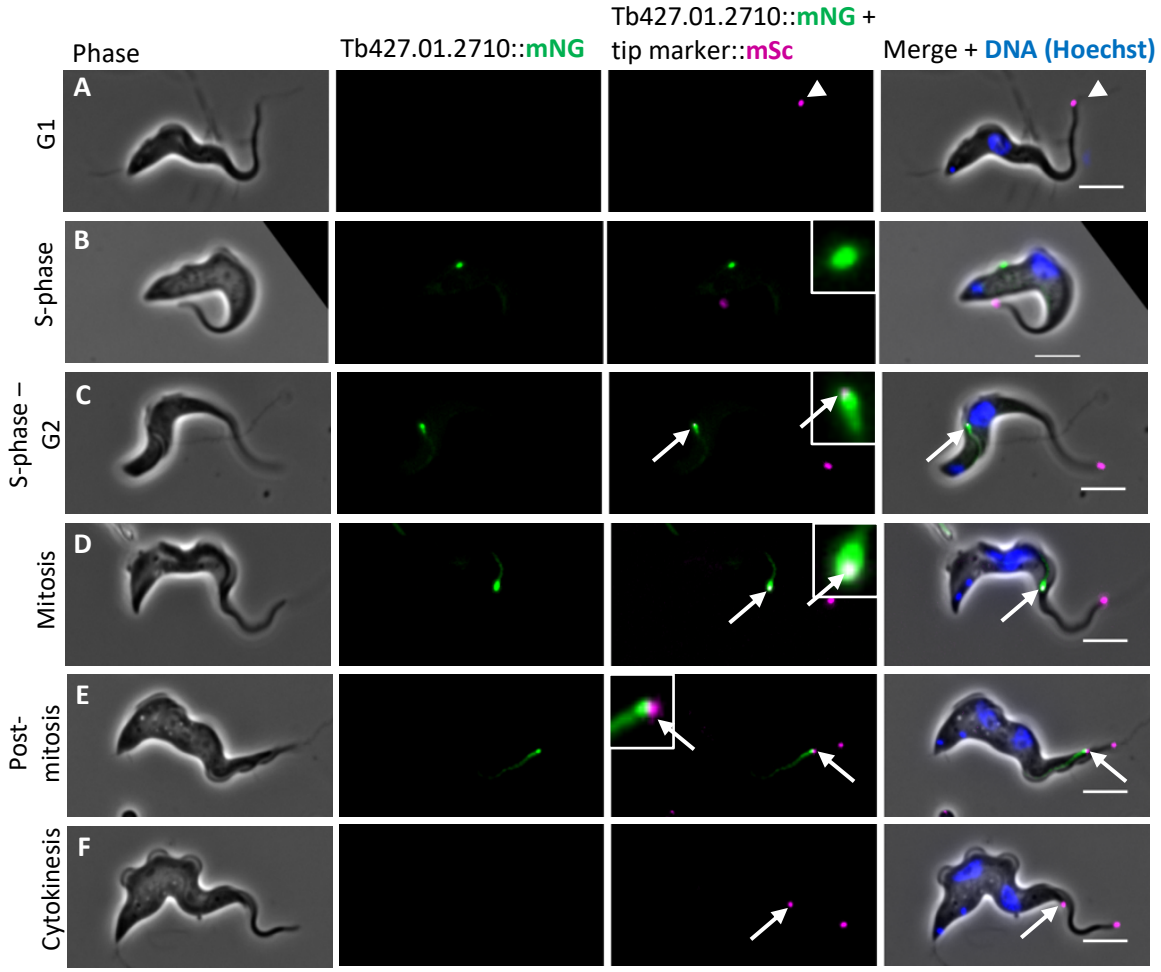

Figure 45: Cell line expressing mSc::Tb427.02.5860 and Tb427.01.2710::mNG. Endogenous C-terminal tagging of Tb427.01.2710 with mNeonGreen revealed a green elaboration around the distal tip of the new flagellum in bloodstream form cells. A-F) Presence and absence of Tb427.01.2710 through the cell cycle. Elaboration of the green signal (inset box) correlating with the distal end of the new flagellum where the groove is present. Note that elaboration is not present in G1 cells (A) and cells undergoing cytokinesis (F). During new flagellum growth, Tb427.01.2710 also localised to a portion of the new FAZ immediately proximal to the groove (C-E). Old flagellum distal tip indicated by white arrowhead; groove indicated by inset box; new flagellum distal tip indicated with arrow. DNA stained with Hoechst (blue). Scale = 5 µm.

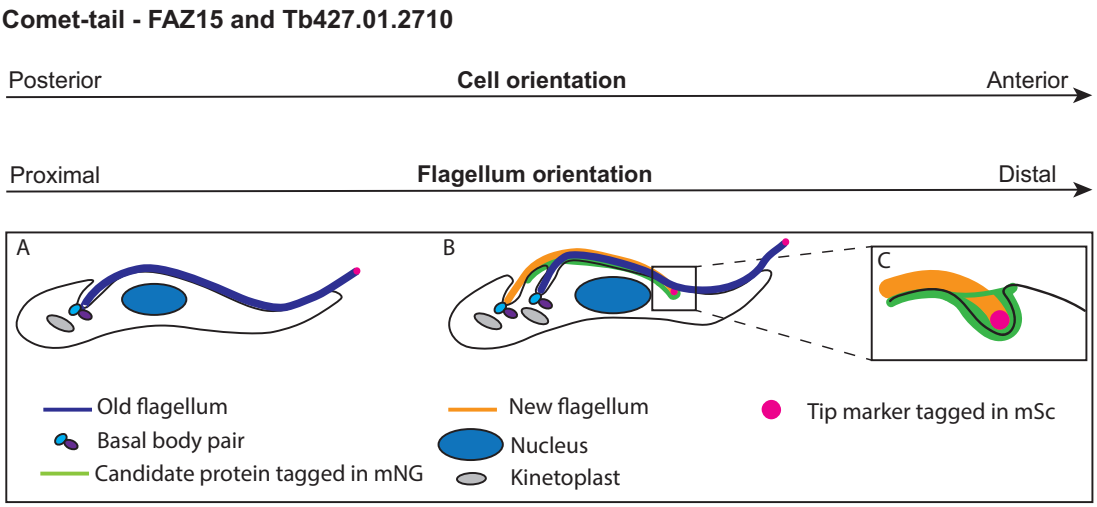

Figure 46: Schematic of fluorescence signal of the "Comet-tail" category. A) Non-dividing G1 cell with one kinetoplast and one nucleus and a single flagellum nucleating from a single basal body pair. The candidate protein tagged in mNG does not localise in non-dividing cells. B) Cell containing two kinetoplasts and one nucleus (2K1N). New flagellum (orange) nucleating from the new BBP at the posterior end of the cell body, with the distal tip (magenta) embedded in the groove (C). The candidate protein tagged in mNG also localises to a portion of the new FAZ immediately proximal to the groove (green).

5.4.5 FCP5 and FLAM3 localised to several areas in the cell and to the groove, representing a complex localisation pattern.

Two proteins, Tb427tmp.01.0400 (FCP5) and Tb427.08.4780 (FLAM3), localised to the groove and to several other areas of the cell forming a complex localisation pattern (Fig. 47-49; Fig. 48 and 50 for schematics). In PCFs, FCP5 localised to the flagella connector (Varga *et al*., 2017), whereas FLAM3 localised to the FAZ in both PCFs and BSFs (Rotureau *et al*., 2014; Sunter *et al*., 2015b; An and Li, 2018).

In G1 cells, mNG::FCP5 localised to the flagellum, basal body pair, cytoplasm and the nucleoplasm (Fig. 47A); however, in cells growing a new flagellum, mNG::FCP5 also localised to the groove (Fig. 47B, inset). At this stage, the flagellum tip marker was not visible on the new flagellum distal tip (Fig. 47B-C, inset). In mitotic cells, mNG::FCP5 localised to the groove and colocalised around the now visible new flagellum tip marker (Fig. 47D, inset). Once the cell entered cytokinesis, mNG::FCP5 was no longer localised to the groove and the new flagellum distal tip was free from the cell body (Fig. 47E, inset).

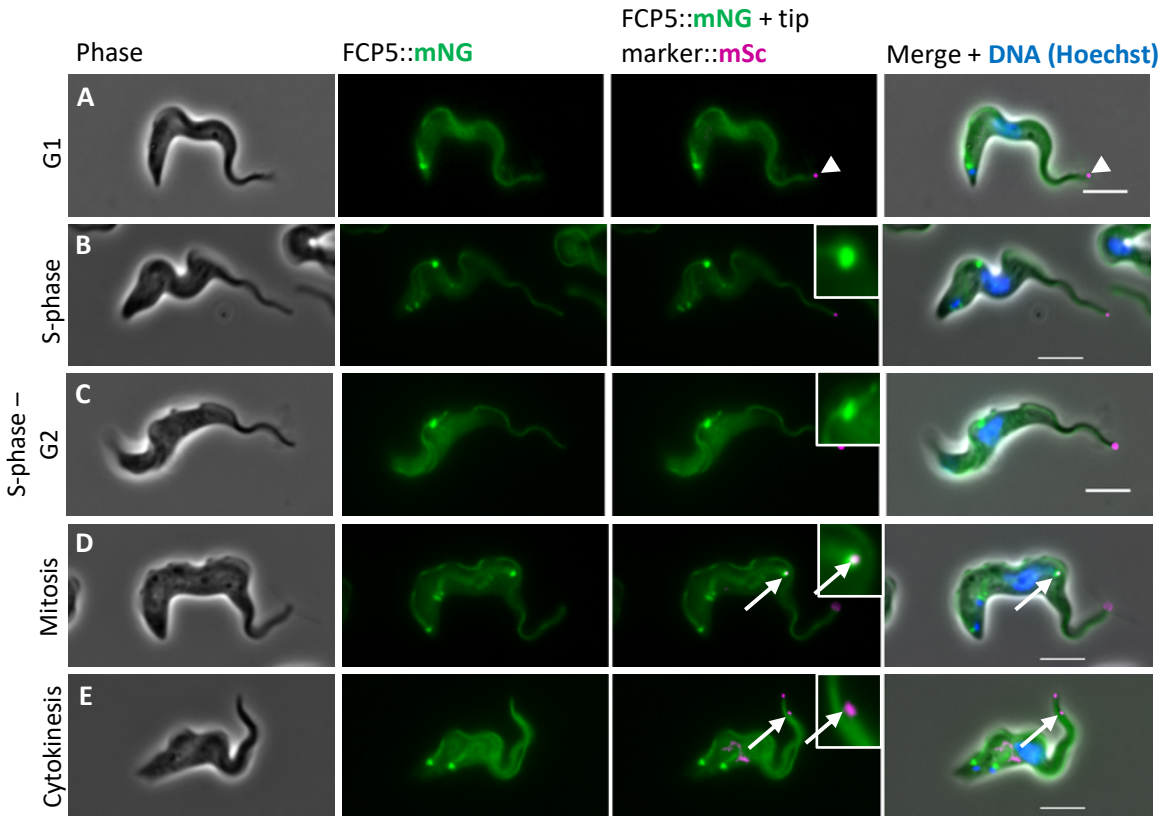

Figure 47: Cell line expressing mSc::Tb427.02.5860 and mNG::FCP5. Endogenous N-terminal tagging of FCP5 with mNeonGreen revealed a green elaboration around the distal tip of the new flagellum in bloodstream form cells. A-E) Presence and absence of FCP5 through the cell cycle. Elaboration of the green signal (inset box) correlating with the distal end of the new flagellum where the groove is present. Note that elaboration is not present in G1 cells (A) and cells undergoing cytokinesis (E). FCP5 also localises to the basal body pair, flagellum, cytoplasm and nucleoplasm through the cell cycle. Old flagellum distal tip indicated by white arrowhead; groove indicated by inset box; new flagellum distal tip indicated with arrow. DNA stained with Hoechst (blue). Scale = 5 µm.

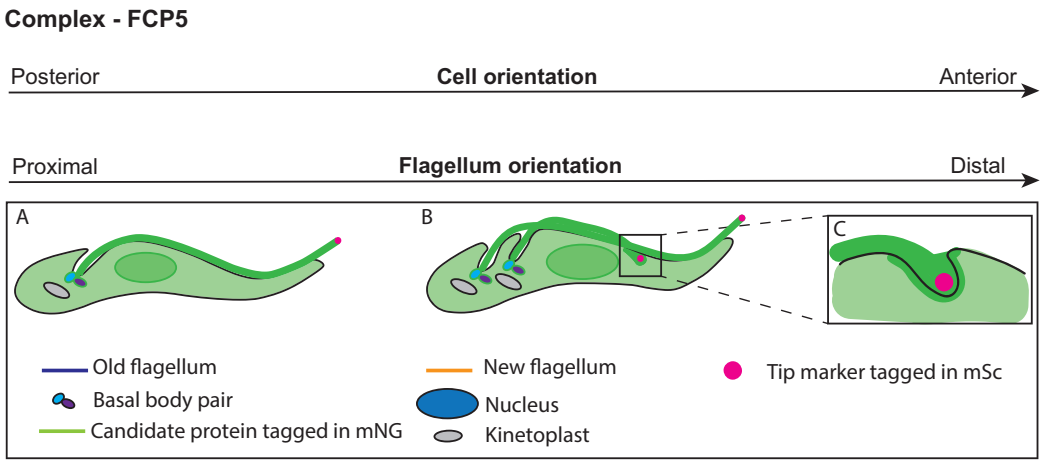

Figure 48: Schematic of fluorescence signal of the "Complex" category containing the expressed fusion protein, mNG::FCP5. A) Non-dividing G1 cell with one kinetoplast and one nucleus and a single flagellum nucleating from a single basal body pair (BBP). The tagged candidate protein localises to the

full length of the flagellum, the basal body pair, the nucleoplasm and the cytoplasm (green). B) Cell containing two kinetoplasts and one nucleus (2K1N). New flagellum (orange) nucleating from the new BBP at the posterior end of the cell body, with the distal tip (magenta) embedded in the groove (C).

In G1 cells, mNG::FLAM3, localised to the flagellum and cytoplasm (Fig. 49A), however, once a new flagellum began to grow, mNG::FLAM3 also localised as a small elaboration at the distal end of the new flagellum in the groove (Fig.49B, inset). At this stage, the flagellum tip marker was not visible on the new flagellum distal tip (Fig. 49B, inset); however, as the new flagellum grew in length, the mNG::FLAM3 groove signal colocalised around the new flagellum tip marker (Fig. 49C, inset). mNG::FLAM3 remained localised to the groove, and to the flagellum and cytoplasm, through kinetoplast and nucleus division (Fig. 49D-F, inset). In post-mitotic cells, mNG::FLAM3 was localised to the flagellum and cytoplasm but also remained localised as a small elaboration at the anterior cell tip. When cytokinesis is initiated, the new flagellum distal tip appeared free from the cell body (Fig. 49G, inset) with mNG::FLAM3 localised to the flagellum and cytoplasm only.

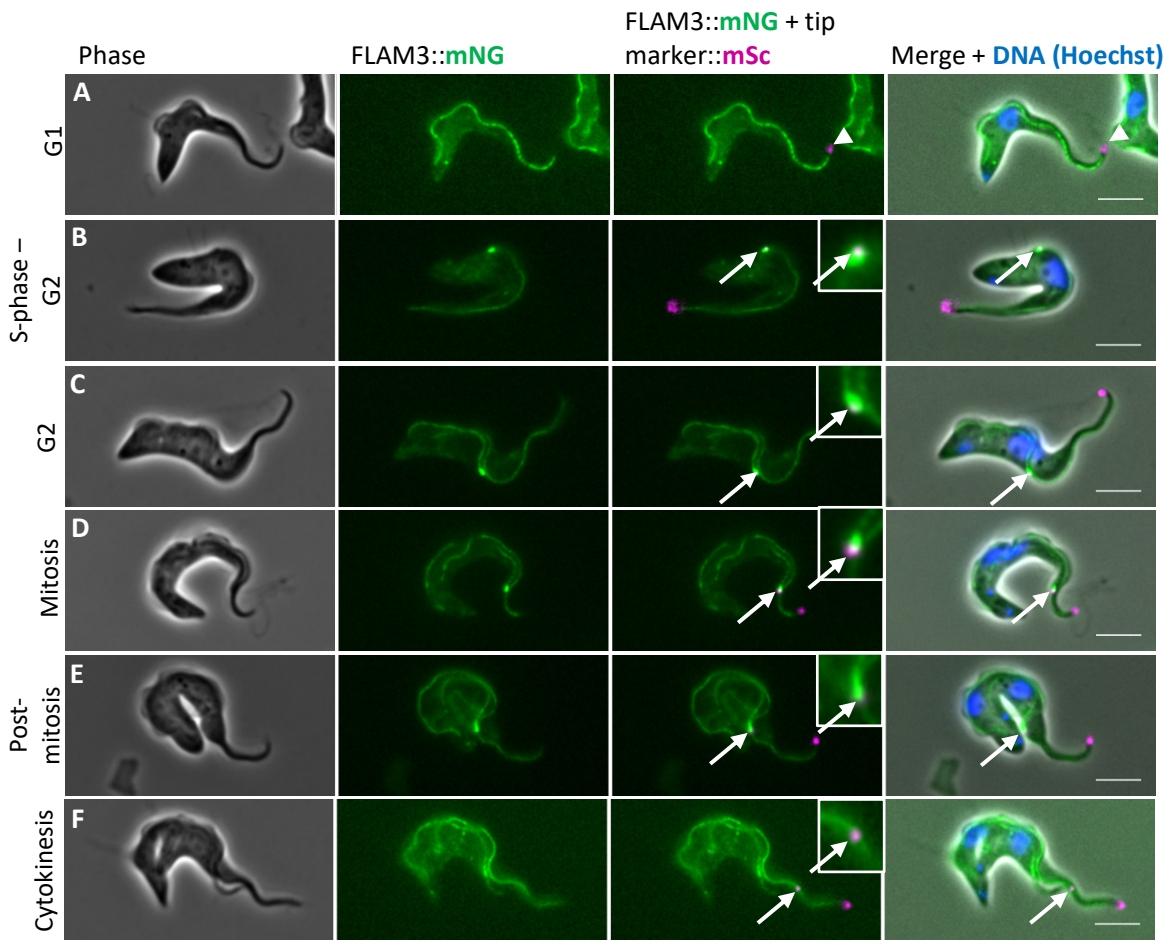

Figure 49: Cell line expressing mSc::Tb427.02.5860 and mNG::FLAM3. Endogenous N-terminal tagging of FLAM3 with mNeonGreen revealed a green elaboration around the distal tip of the new flagellum in bloodstream form cells. A-F) Presence and absence of FLAM3 through the cell cycle. Elaboration of the green signal (inset box) correlating with the distal end of the new flagellum where the groove is present. Note that elaboration is not present in G1 cells (A) and cells undergoing cytokinesis (F). FLAM3 also localises to the flagellum and cytoplasm through the cell cycle. Old flagellum distal tip indicated by white arrowhead; groove indicated by inset box; new flagellum distal tip indicated with arrow. DNA stained with Hoechst (blue). Scale = 5 µm.

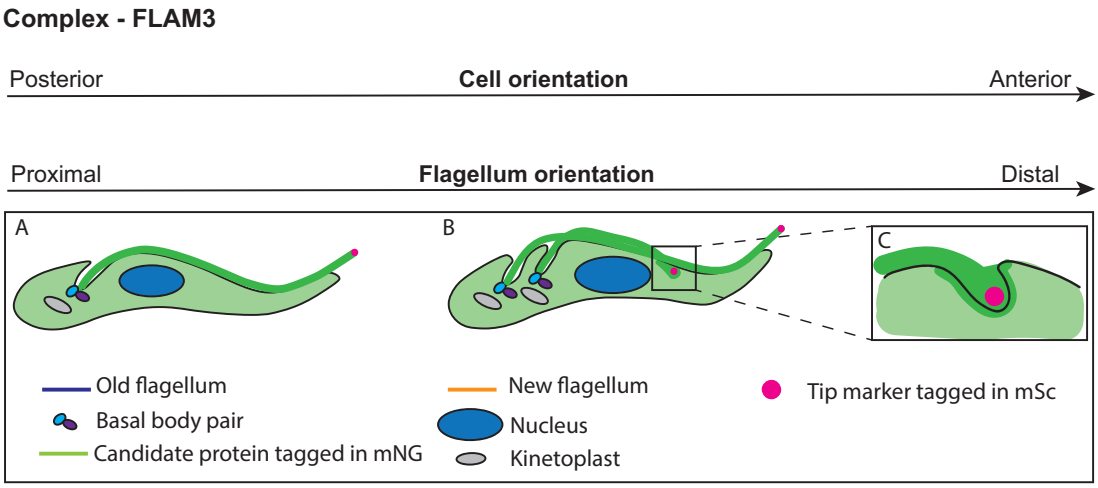

Figure 50: Schematic of fluorescence signal of the "Complex" category containing the expressed fusion protein, mNG::FLAM3. A) Non-dividing G1 cell with one kinetoplast and one nucleus and a single flagellum nucleating from a single basal body pair (BBP). The tagged candidate protein localises to the full length of the flagellum and to the cytoplasm in non-dividing cells (green). B) Diving cell during mitosis containing two kinetoplasts and one nucleus (2K1N). New flagellum (orange) nucleating from the new BBP at the posterior end of the cell body. C) Enlarged area of B showing the distal tip of the new flagellum embedded within the groove with Tb427.02.5860 expressed in magenta, surrounded by the green signal of the tagged candidate protein.

5.5 Presence and absence of the proteins as the groove resolves

The presence and absence of the groove proteins through the cell cycle was examined, paying particular attention to proteins that disappear and remain during groove resolution (Fig. 51). The cell positions defined previously (Fig. 31C) were adapted to determine the presence and absence of the mNG signal of the fluorescently tagged groove proteins in the groove. Three categories were developed based on whether a green signal (indicating the protein of interest) was visible in the groove in:

1) The area between the kinetoplast and the nucleus.

2) The area between one side of the nucleus to the other.

3) The area between the anterior edge of the nucleus to the anterior cell tip where the green signal in the groove is still present.

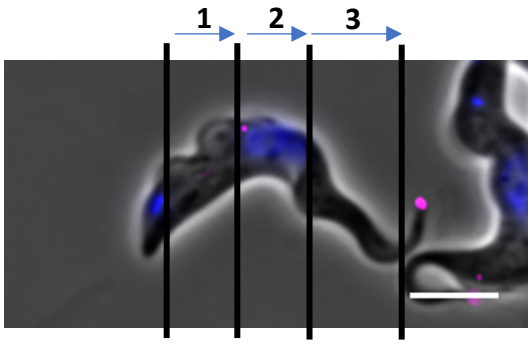

1. Kinetoplast to nucleus
2. Nucleus
3. Nucleus to anterior cell tip

Figure 51: Map of redefined positions in the cell. Scale = 5 μm.

The area between the anterior edge of the nucleus to the anterior cell tip was further defined based on whether the tagged groove protein signal was visible (3a) or not visible (3b) (Fig. 52A). For all 13 groove proteins, the mNG signal was visible from the initial formation of the groove, immediately as the new flagellum exited the flagellar pocket and embedded the distal tip in the groove (data not shown). We did not identify if certain groove proteins had a specific involvement in the initial formation of the groove as all groove proteins were present in the groove between the kinetoplast and nucleus (as seen in Fig. 52A). This data is not displayed as we decided to focus on the differences between the presence and absence of the groove proteins during groove resolution instead (Fig. 52C).

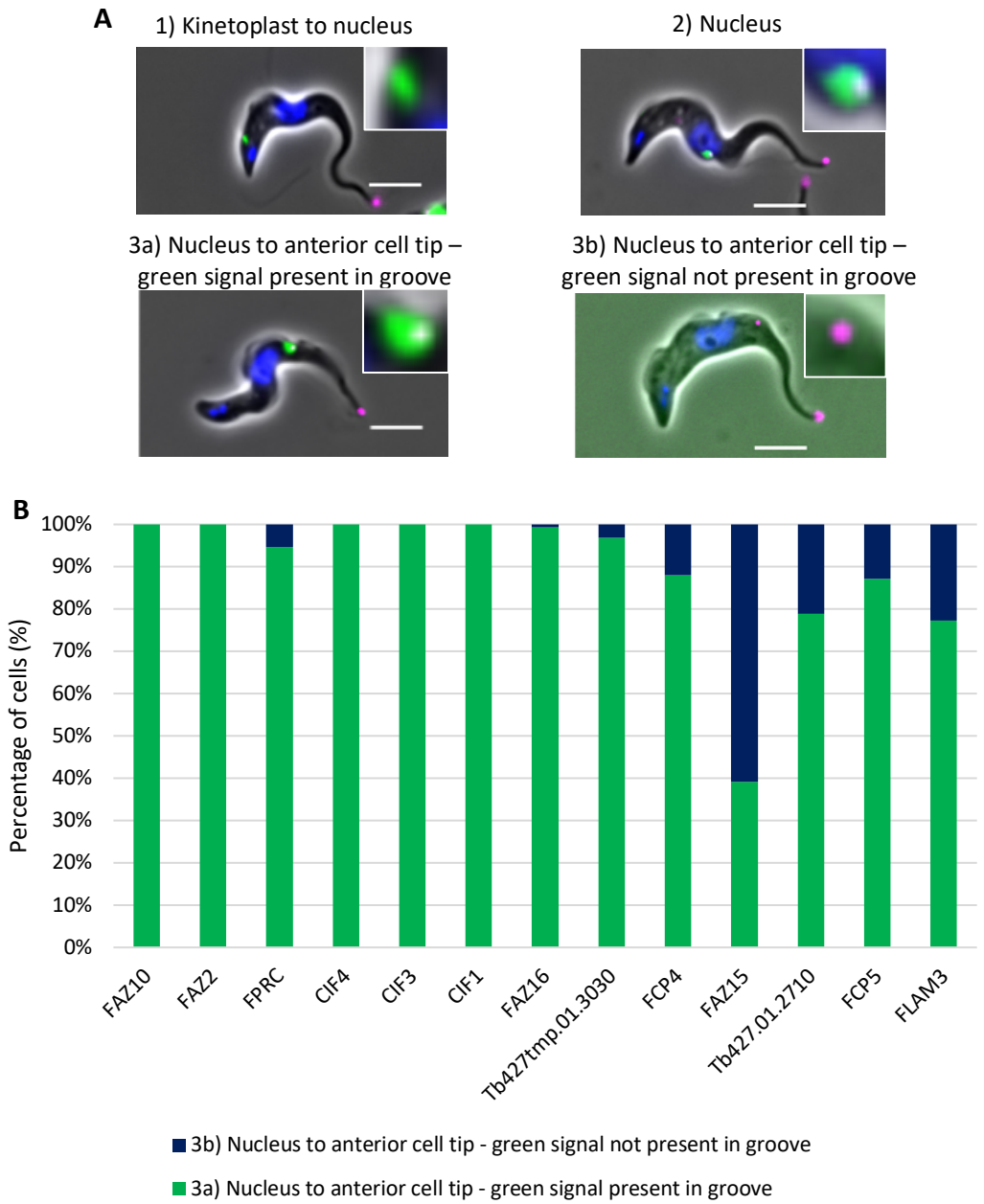

<u>Figure 52:</u> Presence and absence of the groove proteins between the nucleus and anterior cell tip. A) Example images of the defined cell positions. Scale = 5 μm. B) Presence and absence of the groove proteins between the nucleus and anterior cell tip. N = 500 2F cells where the flagellum tip marker is clearly visible on the new flagellum distal tip.

With regards to mNG::FAZ10 and mNG::FAZ2, the position analysis confirmed that both proteins were present between the nucleus and anterior cell tip in 100% of 2F cells examined for each cell line (Fig. 52B), which suggests that these two proteins remained localised at the anterior cell tip after groove resolution, potentially to support cytokinesis initiation or the development of the new anterior cell tip. This was also seen for mNG::CIF4, mNG::CIF3 and CIF1::mNG, with 100% of 2F cells examined in each cell line showing protein localisation in

the groove between the nucleus and anterior cell tip (Fig. 52B). Furthermore, these three proteins may play a role in cytokinesis due to their localisation in the cleavage furrow in cells undergoing cytokinesis (Representative images presented in Fig. 53).

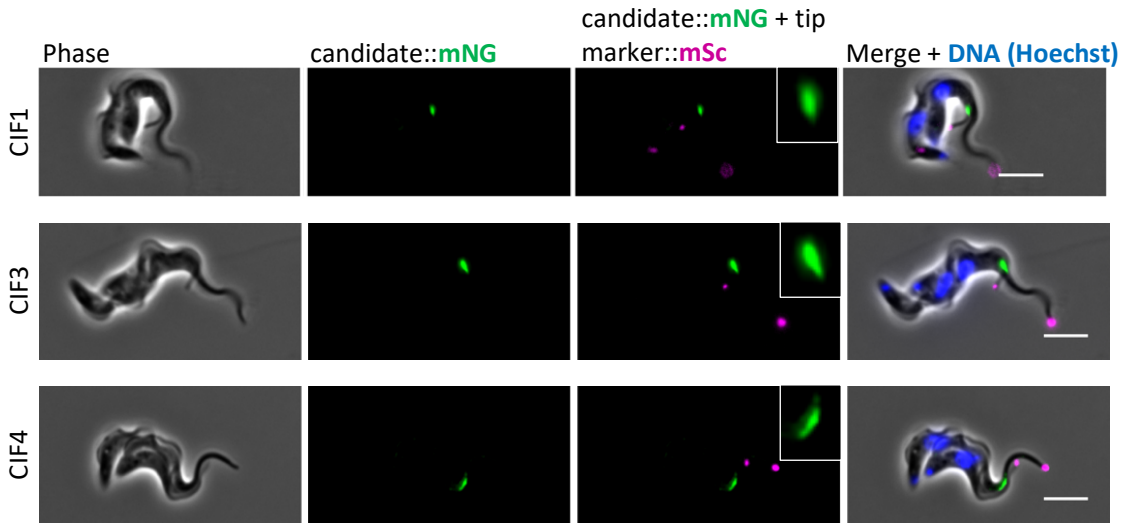

Figure 53: CIF1, CIF3 and CIF4 localised to the cleavage furrow during cytokinesis. Endogenous tagging of CIF1, CIF3 and CIF4 with mNeonGreen revealed a green foci at the site of cleavage furrow ingression (inset box). DNA stained with Hoechst (blue). Scale = 5 µm.

On the other hand, there are several proteins that are not present after the groove resolves. mNG::FPRC, mNG::FAZ16 and mNG::Tb427tmp.01.3030 appear to be present between the nucleus and anterior cell tip in the majority of 2F cells examined for each cell line; however, these proteins disappear prior to cytokinesis initiation and are not present in the cleavage furrow (Fig. 52B). This suggests that these proteins may be visible at the anterior cell tip to as the groove resolves and may play a role in the formation of the new anterior cell tip, however, the proteins disappear before cleavage furrow ingression.

mNG::FCP4, Tb427.01.2710::mNG, mNG::FCP5 and mNG::FLAM3 all possessed a proportion of 2F cells with no visible signal between the nucleus and anterior cell tip, suggesting that these four proteins may disappear as the groove revolves (Fig. 52B). Similarly, mNG::FAZ15, had the largest proportion of 2F cells (˜34%) with no visible signal between the nucleus and anterior cell tip (Fig. 25B). It is clear that mNG::FCP4, Tb427.01.2710::mNG, mNG::FLAM3, mNG::FCP5 and mNG::FAZ15 may be tested as sufficient groove-specific markers in future research, as all five proteins localised to the groove during the early stages of groove development (data not shown here) before disappearing once the groove resolved (Fig. 52B). mNG::FAZ15 is unique in that this protein was no longer visible in the groove much earlier

than the other three proteins, suggesting that this protein may even disappear from the groove before it has resolved (Fig. 52B).

5.6 Identifying protein domains using online databases.

A range of bioinformatic databases such as Pfam, SMART and NCBI were mined to determine the protein domain composition of the groove proteins. Most notably, FAZ10 is a large cytoskeletal protein containing 13 coiled-coil domains, a myosin tail domain and a chromosome segregation protein domain (Fig. 54A). FLAM3 contains no identified coiled-coil domains; however, it does contain a CLU domain (CLUstered mitochondria; Pfam: PF13236) (Fig. 54A), whereas, FAZ16 contains a LysM domain (Lysin motif; Pfam: PF01476) (Fig. 54B). FCP4, a member of the ubiquitous kinesin-15 protein family of microtubule plus-end directed motors (Boleti *et al*., 1996; Varga *et al*., 2017), contains an identified kinesin motor domain (Fig. 54A). FCP5, on the other hand, contains a serine/threonine protein kinase domain as a member of the ULK family of proteins (Varga *et al*., 2017) (Fig. 54A). FAZ15 and Tb427tmp.01.3030 did not contain any known domains according to the bioinformatics search. The majority of the 13 groove proteins possessed coiled-coil domains (Fig. 54B); however, no other domains were identified for the majority of the proteins.

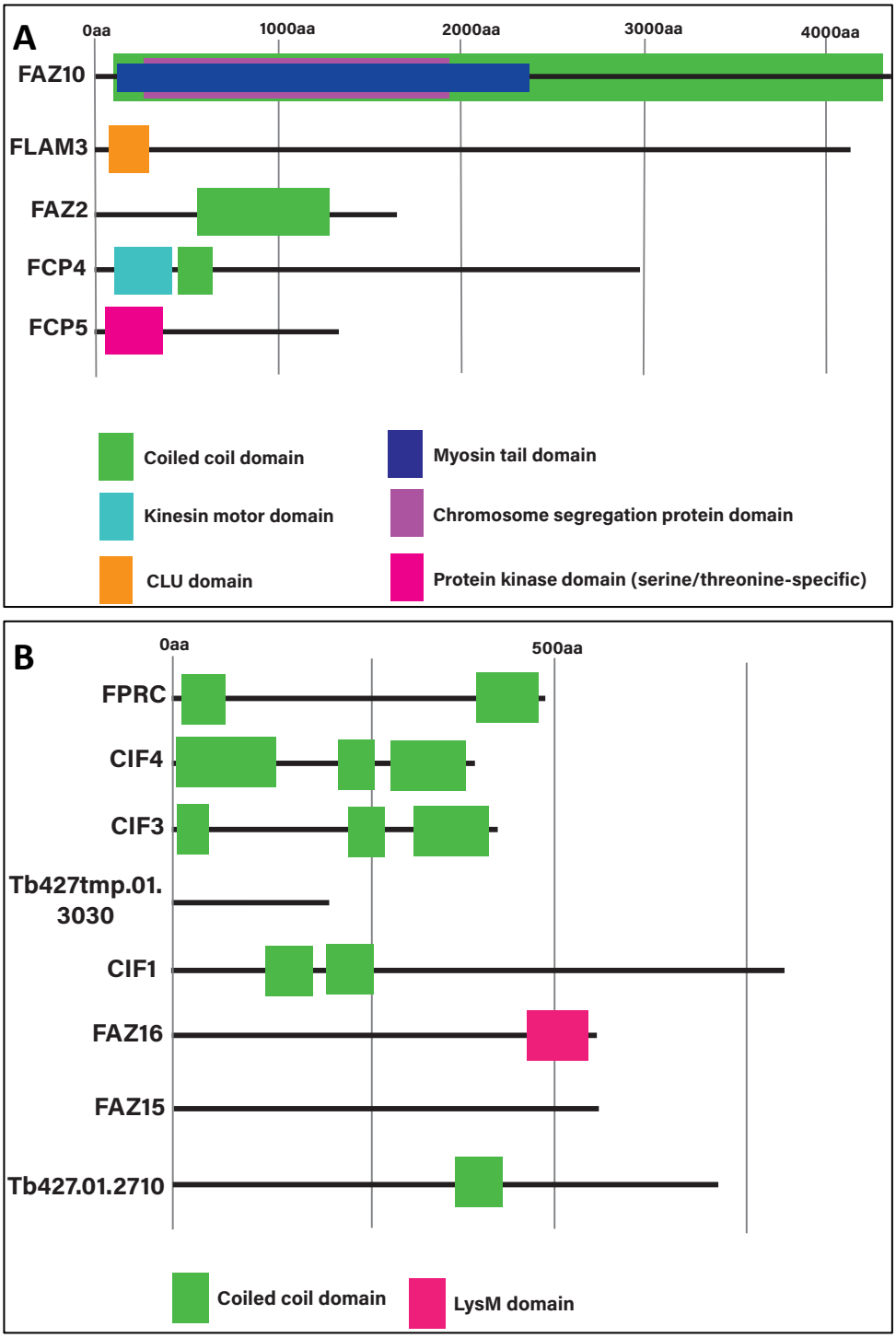

Figure 54: Domain analysis of the 13 groove proteins identified in the localisation screen. A) Large proteins from 0 to over 4000 amino acids in length. B) Smaller proteins from 0 to over 700 amino acids in length. Expected value cutoff = e^{-10}.

5.7 Some groove proteins are conserved across kinetoplastids, however, some are trypanosomatid-specific

5.7.1 Identifying orthologues of the groove proteins in other kinetoplastids via reciprocal best blast (RBB)

An online trypanosome database, https://tritrypdb.org/tritrypdb/, was mined for orthologous proteins of the 45 candidate groove proteins in selected kinetoplastid organisms. Presently, we are unsure whether the groove, or another groove-like structure, is likely to be present outside of *T. brucei*, or if proteins identified in the groove are likely to be conserved across other kinetoplastid organisms. To investigate this, specific parasitic and free-living kinetoplastid species were chosen by examining the literature surrounding kinetoplastid phylogeny and ancestry, to identify the presence of conserved proteins (Fig. 55) (Vickerman, 1994; Flegontov *et al*., 2013; Skalicky *et al*., 2017). Through this investigation, we may be able to hypothesise if groove-specific proteins have diverged and adapted to increase parasitaemia in the mammalian host. Additionally, it may highlight certain proteins, or protein complexes, that are conserved across parasitic and free-living kinetoplastid organisms which may have a role in highly conserved processes such as cytokinesis, mitosis and cell cycle progression.

As *T. brucei* is a parasitic African kinetoplastid, phylogenetic neighbours in the African *Trypanosoma* genus (*Trypanosoma vivax* and *Trypanosoma congolense)* as well as the South American parasite, *Trypanosoma cruzi,* were investigated (Fig. 55). Other parasitic kinetoplastids, such as *Leishmania major* and *Leptomonas pyrrhocoris,* were also included due to their divergence from shared phylogenetic ancestors of the *Trypanosoma* genus (Fig. 55). Additionally, organisms that are more phylogenetically distant, such as *Paratrypanosoma confusum*, the most basal trypanosomatid lineage, and *Bodo saltans*, a free-living biflagellate, were also investigated to determine which proteins are conserved among recently diverged kinetoplastids and ancestral free-living and biflagellate kinetoplastids (Fig. 55).

Orthologous proteins were initially identified using the orthologue finder tool on https://tritrypdb.org/tritrypdb/. The conservation analysis of all 45 screen candidates is summarised in **Appendix D**. Following this brief investigation, a more direct approach was

used to determine if the orthologues of the 13 groove proteins are genuine orthologues, using reciprocal best blast (RBB) (https://blast.ncbi.nlm.nih.gov/Blast.cgi?PAGE=Proteins) as this method produces more accurate results (with a cut-off value of e^{-10}).

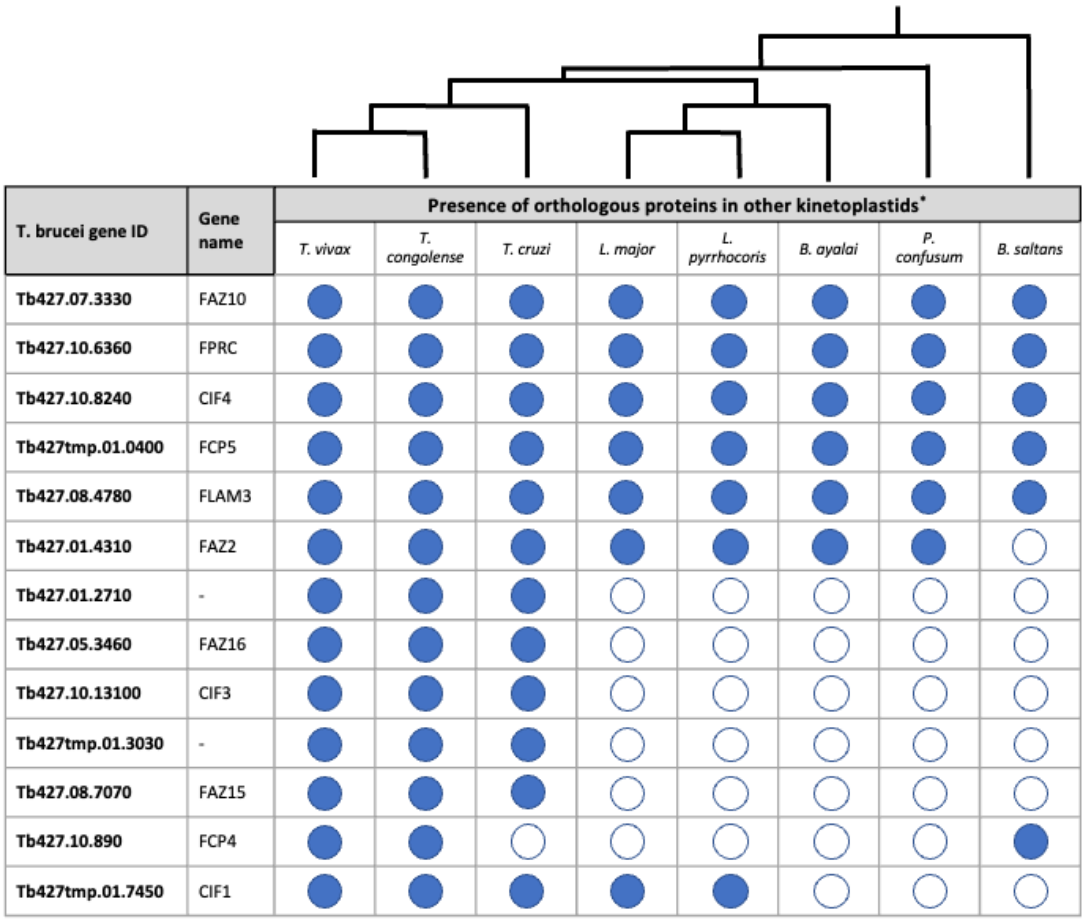

T. brucei gene ID	Gene name	Presence of orthologous proteins in other kinetoplastids*							
		T. vivax	*T. congolense*	*T. cruzi*	*L. major*	*L. pyrrhocoris*	*B. ayalai*	*P. confusum*	*B. saltans*
Tb427.07.3330	FAZ10	●	●	●	●	●	●	●	●
Tb427.10.6360	FPRC	●	●	●	●	●	●	●	●
Tb427.10.8240	CIF4	●	●	●	●	●	●	●	●
Tb427tmp.01.0400	FCP5	●	●	●	●	●	●	●	●
Tb427.08.4780	FLAM3	●	●	●	●	●	●	●	●
Tb427.01.4310	FAZ2	●	●	●	●	●	●	●	○
Tb427.01.2710	-	●	●	●	○	○	○	○	○
Tb427.05.3460	FAZ16	●	●	●	○	○	○	○	○
Tb427.10.13100	CIF3	●	●	●	○	○	○	○	○
Tb427tmp.01.3030	-	●	●	●	○	○	○	○	○
Tb427.08.7070	FAZ15	●	●	●	○	○	○	○	○
Tb427.10.890	FCP4	●	●	○	○	○	○	○	●
Tb427tmp.01.7450	CIF1	●	●	●	●	●	○	○	○

Figure 55: Protein conservation of the 13 groove proteins across selected kinetoplastids according to reciprocal best blast. Presence of orthologue indicated by a filled circle; empty circle indicates no orthologue identified. Expected-value cut-off = e^{-10}. Species (left to right): *Trypanosoma vivax; Trypanosoma congolense; Trypanosoma cruzi; Leishmania major; Leptomonas pyrrhocori; Blechomonas ayalai; Paratrypanosoma confusum; Bodo saltans.* (Phylogenetic tree adapted from Flegontov *et al*., 2013 and Skalicky *et al*., 2017).

FAZ10, FPRC, CIF4, FLAM3 and FCP5 were conserved across all kinetoplastid organisms investigated (Fig. 55), suggesting that these five proteins potentially play a general cell biology role due to their conservation pattern. FAZ2, on the other hand, is conserved across all kinetoplastids examined except for *Bodo saltans*, suggesting that FAZ2 may have evolved with the ancestral divergence from biflagellate free-living organisms to monoflagellated parasitic organisms (Flegontov *et al*., 2013; Jackson *et al*., 2016; Skalicky *et al*., 2017). CIF1 is conserved across *T. vivax*, *T. congolense*, *L. major* and *L. pyrrhocoris,* thereby potentially

acting as a cytokinesis-regulator restricted to these organisms. Five proteins (Tb427.01.2710, FAZ16, CIF3, Tb427tmp.01.3030 and FAZ15) are further restricted and are only conserved across the Trypanosomatid species, namely the African trypanosomes, *T. vivax*, *T. congolense*, and the South American trypanosome *T. cruzi* (Fig. 55). This divergence from the other kinetoplastid species may suggest that these five proteins evolved with the divergence of the *Trypanosoma* genus, coinciding with the emergence of the trypomastigote life cycle form. Interestingly, FCP4 is conserved in *T. vivax* and *T. congolense*, however, it is also conserved in *B. saltans* (Fig. 55), suggesting that FCP4 is involved in a specific structure or function conserved only in these kinetoplastids, possibly related to FCP4 being part of the ubiquitous kinesin-15 protein family of microtubule plus-end directed motors (Boleti *et al*., 1996; Varga *et al*., 2017).

5.7.2 Is the groove present in *Trypanosoma vivax* and *Trypanosoma congolense*?

In previous work, the presence of the groove in BSF *T. brucei* cells was hypothesised to be an evolutionary adaptation to enhance parasitaemia in the mammalian host (Hughes *et al*., 2013). However, it is still unknown as to whether other trypanosomatid parasites infective to mammalian hosts possess a groove or not, despite the conservation of all 13 groove proteins across the African trypanosomatids (Fig. 55). Therefore, we examined two closely related species to *T. brucei* by SBFSEM to determine if the groove was a conserved structure among these species. A *Trypanosoma congolense* IL3000 BSF (trypomastigote) strain was kindly provided by Dr Mark Carrington and Dr Paula McGregor from the University of Cambridge. Additionally, a BSF *Trypanosoma vivax* IL1392 line derived from the Y486 strain was isolated from infected mice and provided by Professor Gavin Wright and Dr Delphine Autherman from the University of York.

3D surface rendering and modelling of cells from the *T. congolense* and *T. vivax* samples were compared to a trypomastigote BSF *T. brucei* 427 parental culture strain. In *T. brucei* cells with a short new flagellum (3 µm) recently emerged from the flagellar pocket, the new flagellum distal tip was positioned in a shallow groove in the cell body plasma membrane (Fig. 56A, inset). Slices through the reconstructed area around the new flagellum distal tip showed that this groove was not deep, with the new flagellum distal tip only partially embedded in a shallow groove in the cell body plasma membrane (Fig. 56B). Furthermore, at this length, the new flagellum distal tip was positioned close to the side of the old flagellum (Fig. 56C). A

comparable model of *T. congolense* with a short new flagellum (4 µm) showed that the new flagellum distal tip was also positioned in a shallow groove in the cell body plasma membrane (Fig. 56D, inset). Slices through the reconstructed area around the new flagellum distal tip showed that, like with *T. brucei*, the new flagellum distal tip was positioned in a shallow groove in the cell body plasma membrane, and that this groove did not fully encompass the new flagellum distal tip (Fig. 56E). Like with *T. brucei*, the new flagellum distal tip was also positioned closely to the side of the old flagellum (Fig. 56F). A model of a *T. vivax* cell with a short new flagellum (4 µm), unlike *T. brucei* and *T. congolense*, showed that the new flagellum distal tip was actually tilting away from the cell body (Fig. 56G, inset). Slices through the reconstructed area around the new flagellum distal tip supported this observation, showing the most distal point of the new flagellum was not associated with the cell body plasma membrane at all (Fig. 56Hi-Hii). Like *T. brucei* and *T. congolense*, the new flagellum distal tip of *T. vivax* was touching the side of the old flagellum which is reminiscent of the flagella connector in the *T. brucei* PCF (Moreira-Leite *et al*., 2001; Briggs *et al*., 2004).

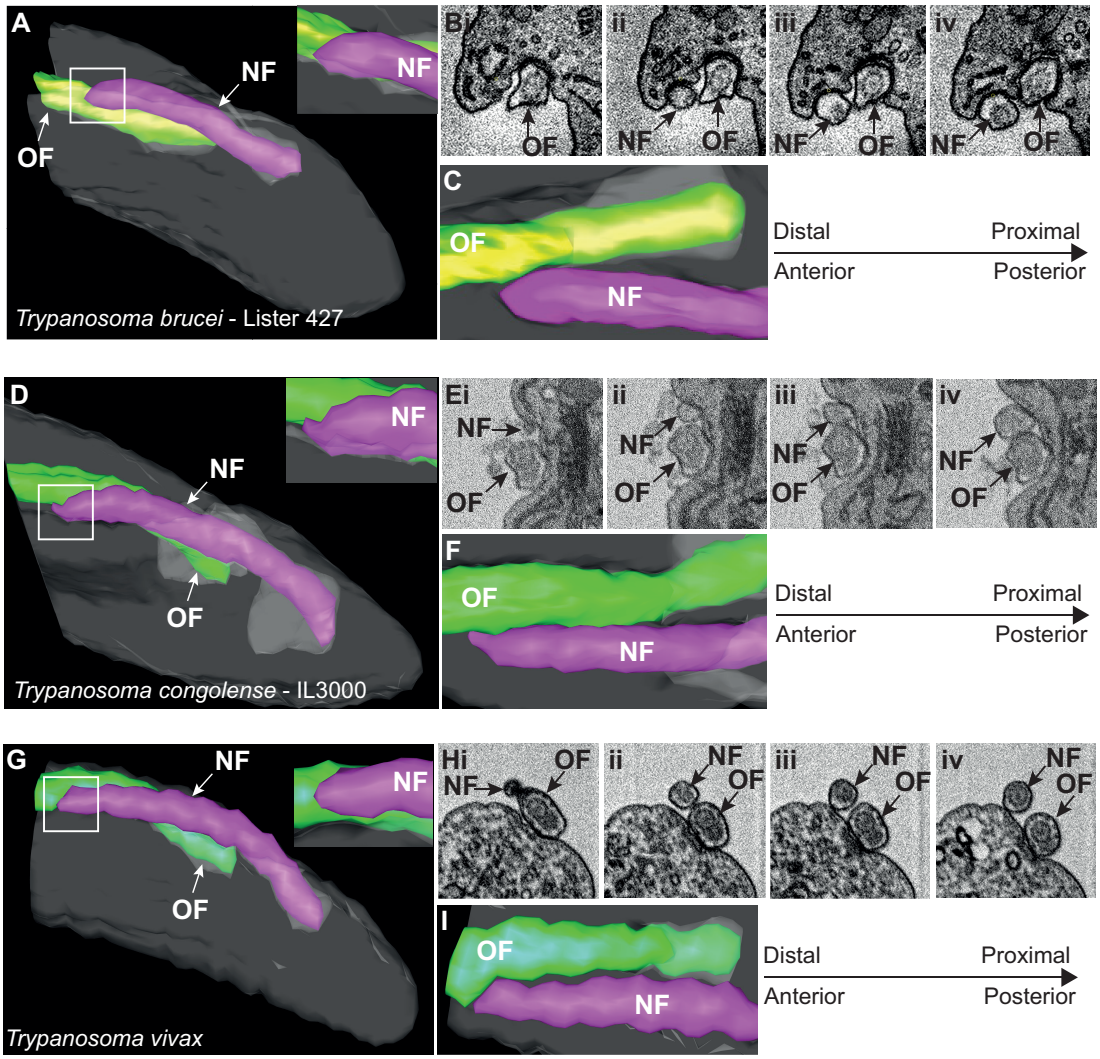

Figure 56: 3D surface rendering of representative cells with short new flagella in *T. brucei*, *T. congolense* and *T. vivax*. A) Surface rendering of a *T. brucei* cell with a short new flagellum (NF) with the distal tip positioned in a shallow indentation of the cell body plasma membrane (inset box). B) SBFSEM raw data of the reconstructed region. Distal tip of short new flagellum distal tip is not fully embedded in the cell body. C) Top view of (A). Distal tip of new flagellum positioned in close proximity to the old flagellum (OF). D) Surface rendering of a *T. congolense* cell with a short new flagellum with the distal tip positioned in a shallow indentation of the cell body plasma membrane (inset box). E) SBFSEM raw data of the reconstructed region. Distal tip of new flagellum not fully embedded in the cell body. F) Top view of (D). Distal tip of new flagellum positioned in close proximity to the old flagellum. G) Surface rendering of a *T. vivax* cell with a short new flagellum, with the distal tip tilting away from the cell body (inset box). H) SBFSEM raw data of the reconstructed region. Distal tip of short new flagellum tilts away from the cell body. I) Top view of (G). Distal tip of new flagellum touching the side of the old flagellum. N ≥ 3 models per species. Key: NF = new flagellum; OF = old flagellum.

However, in cells with a longer new flagellum, clear differences between the three species became evident (Fig. 57). In *T. brucei* cells with a longer new flagellum (14.83 µm), the new flagellum distal tip was fully embedded in a deep groove in the cell body plasma membrane (Fig. 57A, inset), representing the canonical groove structure observed by array tomography

and in previous studies (Fig. 18-19) (Hughes *et al*., 2013). Slices through the reconstructed area around the new flagellum distal tip supported this, showing that the new flagellum distal tip was fully embedded in a deep groove (Fig. 57B). Furthermore, at this length, the new flagellum distal tip was positioned further away from the side of the old flagellum, suggesting that as the new flagellum elongated, the distal tip moved further away from the old flagellum, possibly due to the insertion of microtubules between the two flagella (Fig. 57C). Contrary to *T. brucei*, the new flagellum distal tip of *T. congolense* remained positioned in a shallow groove in the cell body plasma membrane, the depth remaining unchanged when the new flagellum was short or long (Fig. 57D, inset). Slices through the reconstructed area around the new flagellum distal tip supported this, showing that the depth of the groove remained similar in cells with a short and long flagellum (Fig. 27E). Similar to *T. brucei*; however, the new flagellum was positioned further away from the side of the old flagellum at this length (Fig. 57F). *T. vivax*, on the other hand, was not comparable to *T. brucei* nor *T. congolense*, with the new flagellum distal tip of *T. vivax* still tilted away from the cell body when the new flagellum was longer (14.8 µm). Once again, slices through the reconstructed area around the new flagellum distal tip supported this, showing that the most distal point of the new flagellum was not associated with the cell body (Fig. 29Hi-Hiii); however, the distal tip of the new flagellum remained touching the old flagellum, as seen in the flagella connector in the *T. brucei* PCF (Moreira-Leite *et al*., 2001; Briggs *et al*., 2004).

Interestingly, this data has demonstrated that whilst there is protein conservation between three closely related African trypanosomatid parasites, each species displays a different association between the new flagellum distal tip, cell body and old flagellum.

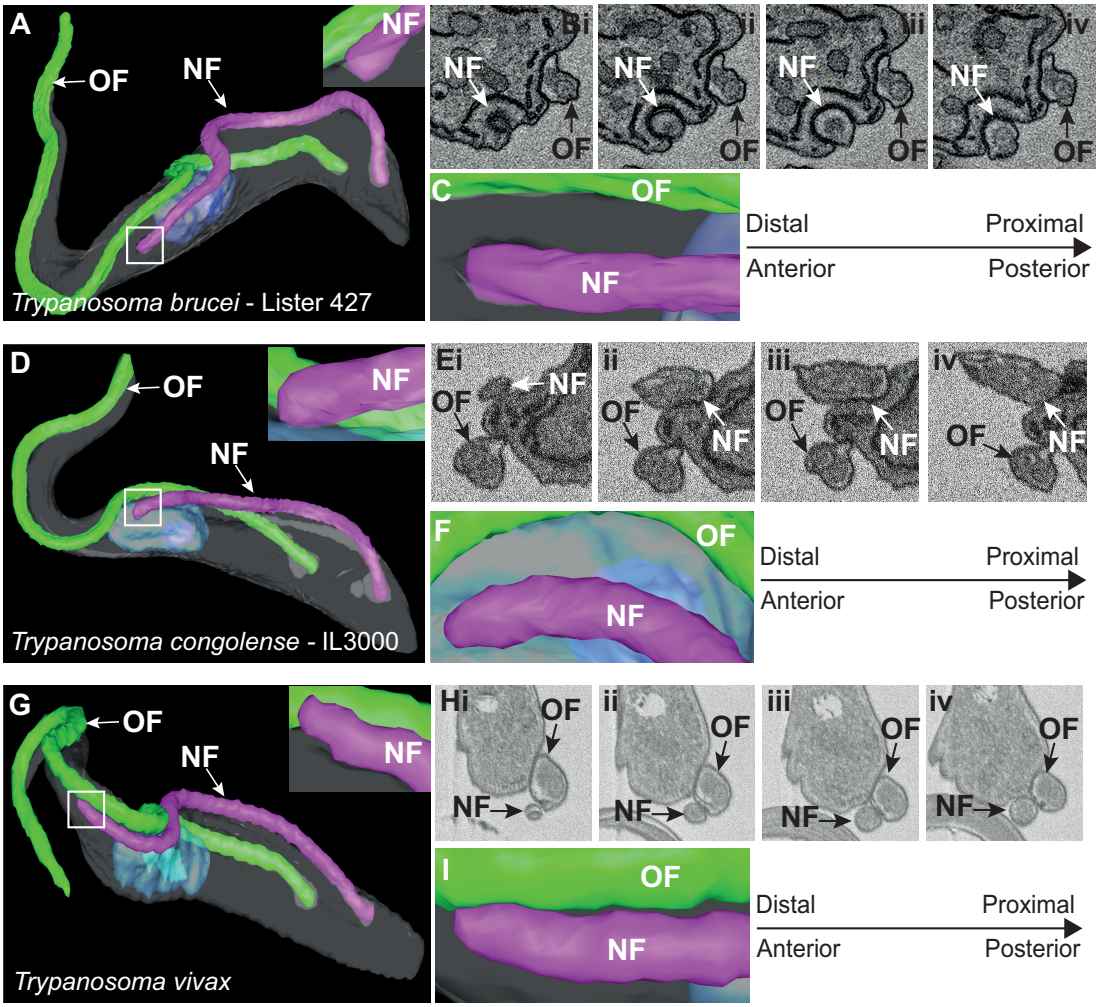

Figure 57: 3D surface rendering of representative cells with long new flagella in *T. brucei*, *T. congolense* and *T. vivax*. A) Surface rendering of a *T. brucei* cell with a long new flagellum, with the distal tip fully embedded in a deep groove in the cell body plasma membrane (inset box). B) SBFSEM raw data of the reconstructed region. Distal tip of new flagellum is fully embedded in a deep groove in the cell body. C) Top view of (A). Distal tip of new flagellum is positioned away from the old flagellum. D) Surface rendering of a *T. congolense* cell with a long new flagellum with the distal tip positioned in a shallow indentation of the cell body plasma membrane (inset box). E) SBFSEM raw data of the reconstructed region. Distal tip of new flagellum is not fully embedded in the cell body. F) Top view of (D). Distal tip of new flagellum positioned away from the old flagellum. G) Surface rendering of a *T. vivax* cell with a long new flagellum with the distal tip tilting away from the cell body plasma membrane (inset box). H) SBFSEM raw data of the reconstructed region. Distal tip of new flagellum tilting away from the cell body plasma membrane. I) Top view of (G). Distal tip of new flagellum closely associated with the old flagellum. N ≥ 3 models per species. Key: NF = new flagellum; OF = old flagellum.

6 The groove is composed of proteins involved in new flagellum tip attachment to the groove and cytokinesis initiation

6.1 Preface

To investigate the function of the 13 identified groove proteins in the BSF *T. brucei* parasite, null mutant (deletion) and inducible RNAi cell lines were generated and analysed for defects in growth rate, cell cycle progression and flagellar defects such as flagellar detachment. Each deletion cell line was generated by replacing both alleles of the gene with antibiotic resistance markers using CRISPR/Cas9-mediated gene deletion (Beneke *et al*., 2017) in the background of the flagellum tip marker cell line. Primers for CRISPR/Cas9-mediated gene deletion and confirmation are outlined in **Appendix E**. Two previously generated deletion cell lines were provided by Dr Jack Sunter to be used as positive controls for the deletion screen of the groove proteins, including a CIF4 deletion cell line and a FAZ15 deletion cell line.

I successfully generated five individual cell lines, each with a different groove gene removed from the genome of *T. brucei* (Table 5). The six remaining groove genes could not be deleted successfully, with some cell lines failing transfection in three repeat attempts and some failing PCR confirmation of the deletion. Therefore, the five successful deletion cell lines, as well as the previously generated CIF4 and FAZ15 deletion cell lines, were taken forward for further analysis.

Table 5: Summary of the CRISPR/Cas9 screen.

Gene ID	Gene name	Localisation category	Successful knockout generated
Tb427.01.4310	FAZ2	Whole FAZ + groove	No
Tb427.07.3330	FAZ10	Whole FAZ + groove	**Yes**
Tb427.10.6360	FPRC	Distal FAZ + groove	No
Tb427.10.8240	CIF4	Distal FAZ + groove	**Cell line provided**
Tb427.05.3460	FAZ16	Groove	**Yes**
Tb427.10.890	FCP4	Groove	No
Tb427.10.13100	CIF3	Groove	No
Tb427tmp.01.3030	-	Groove	**Yes**
Tb427tmp.01.7450	TOEFAZ1/CIF1	Groove	No
Tb427.01.2710	-	Comet-tail	**Yes**
Tb427.08.7070	FAZ15	Comet-tail	**Cell line provided**
Tb427.08.4780	FLAM3	Complex	No
Tb427tmp.01.0400	FCP5	Complex	**Yes**

6.2 Confirmation of the deletion of CIF4 and FAZ15 in the provided cell lines

PCR amplification was used to confirm the deletion of CIF4 and FAZ15 in the two cell lines provided by Dr Jack Sunter. Genomic DNA was extracted from the CIF4 deletion cell line to confirm the absence of the CIF4 ORF, with the same process performed to check for the absence of the FAZ15 ORF in the FAZ15 deletion cell line (Fig. 58A). We confirmed that CIF4 was successfully deleted by the absence of a DNA band when attempting to amplify the CIF4 gene in the genomic DNA of the CIF4 deletion cell line (CIF4 KO) (Fig. 58B, left of gel). The deletion of FAZ15 was also successful according to PCR amplification (Fig. 58B, right the gel).

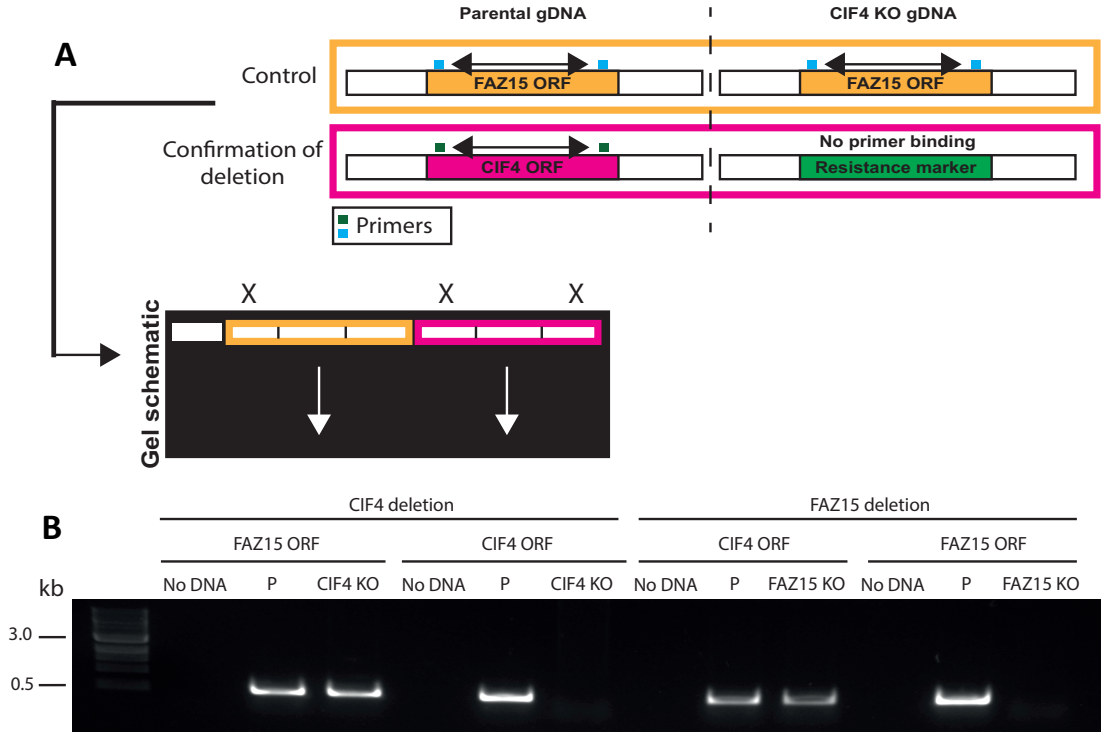

Figure 58: CIF4 and FAZ15 were successfully deleted. A) Schematic for confirming the deletion of CIF4. X denotes lanes where the reaction resulted in no DNA amplification. B) PCR confirmation of the deletion of both CIF4 (left) and FAZ15 (right). Controls for each reaction include ddH_2O (no DNA) and parental genomic DNA (P), as well as constructs that recognise another gene as a positive control.

6.3 The deletion/depletion of CIF4, Tb427.01.2710, FCP4 and Tb427tmp.01.3030 caused groove resolution defects

6.3.1 Deletion of CIF4 resulted in a cytokinesis defect and premature new flagellum tip release from the groove

6.3.1.1 Deletion of CIF4 caused a severe growth defect and a cytokinesis delay

CIF4 has been implicated in the cytokinesis initiation cascade in the PCF through RNAi studies, with the depletion of CIF4 resulting in an accumulation of multinucleic cells and a delay in cytokinesis (Hu *et al*., 2019). However, the function of CIF4 in BSFs has yet to be examined. The deletion of CIF4 caused a severe growth defect when compared to the control cell line (marker cell line expressing mSc::Tb427.02.5860) (Fig. 59). Furthermore, there was a visible increase in the number of 2K2N (arrowhead) and multinucleic cells (asterisk) in the deletion cell line compared to the control cell line (Fig. 60A-B).

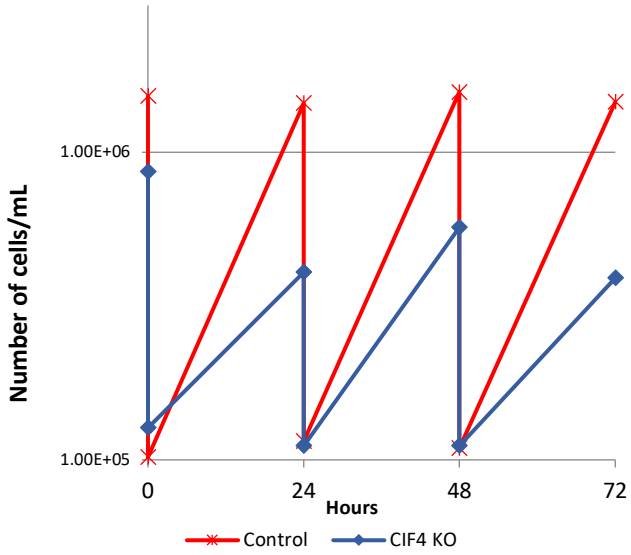

Figure 59: The deletion of CIF4 caused a growth defect. Deletion of CIF4 (blue) caused a severe growth defect.

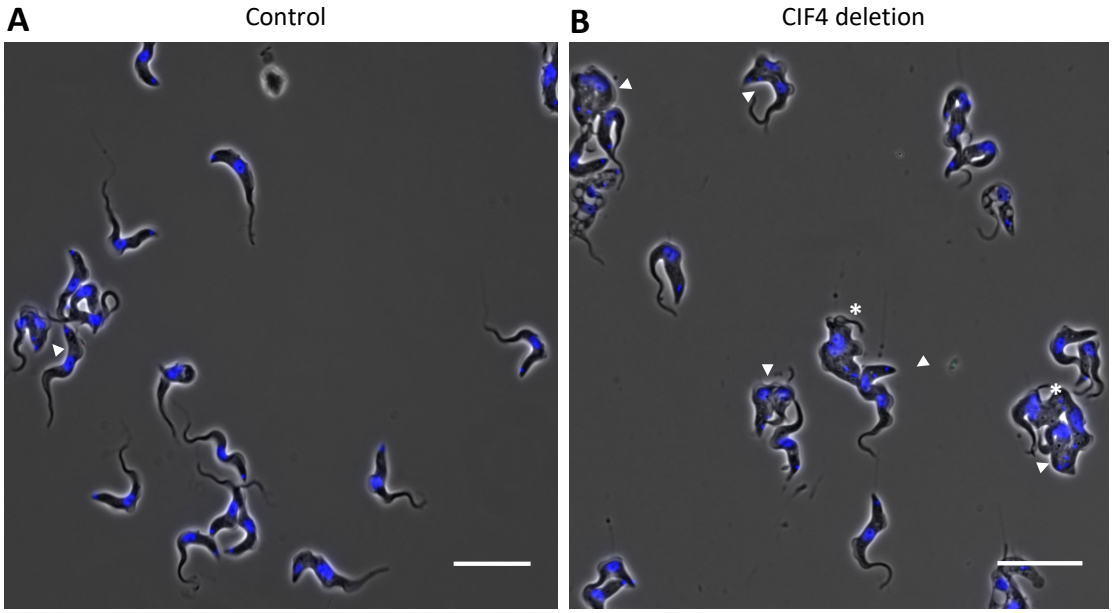

Figure 60: Deletion of CIF4 caused an accumulation of 2K2N and >2K>2N cells. A-B) Representative images of the of the control (A) and CIF4 deletion cell lines (B). Deletion of CIF4 caused increased numbers of 2K2N (arrowhead) and >2K>2N (asterisk) cells. Nuclear and Kinetoplast DNA stained with Hoechst (blue). Scale = 10 μm.

Further cell cycle analyses were performed by counting the number of kinetoplasts (K) and nuclei (N) in the cells, indicating if the deletion caused a delay to the cell cycle and at which stage. KN counts allow us to assess cell cycle defects such as an accumulation of multinucleic cells (>2K>2N) and cells with an abnormal number of kinetoplasts and nuclei ("Other") (Fig. 61).

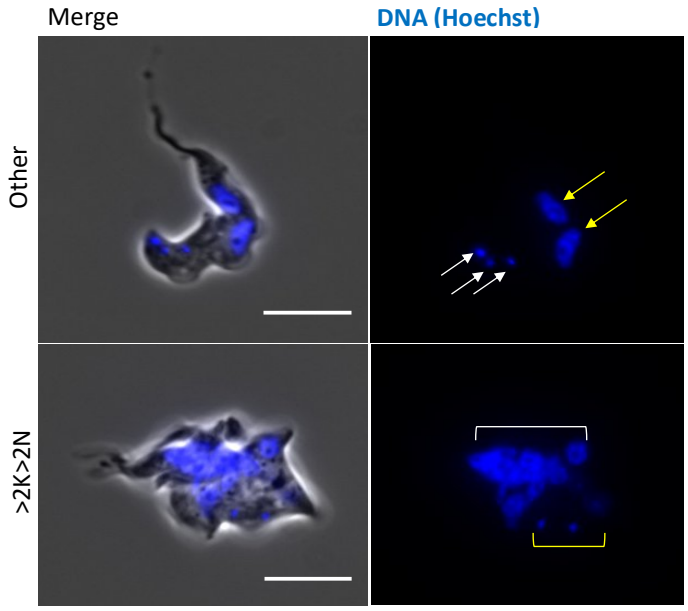

Figure 61: Example images of the "Other" and ">2K>2N" categories used for cell cycle analysis of the deletion cell lines. "Other" is a broad category consisting of cells with unusual numbers of

kinetoplasts (white arrow) and nuclei (yellow arrow), such as 0K2N, 3K2N, 3K0N, zoids (no nuclei) etc. The >2K>2N category consist of cells with multiple kinetoplasts (yellow bracket) and nuclei (white bracket) occurring in the same cell, forming an amorphous, undiscernible mass of blue (Hoechst). Scale = 5 μm.

The deletion of CIF4 caused a delay in cytokinesis, with a reduced proportion of 1K1N and 2K1N cells in the population and a stark increase in the number of multinucleic (>2K>2N) cells and zoids (cells lacking a nucleus) compared to the control cell line (Fig. 62).

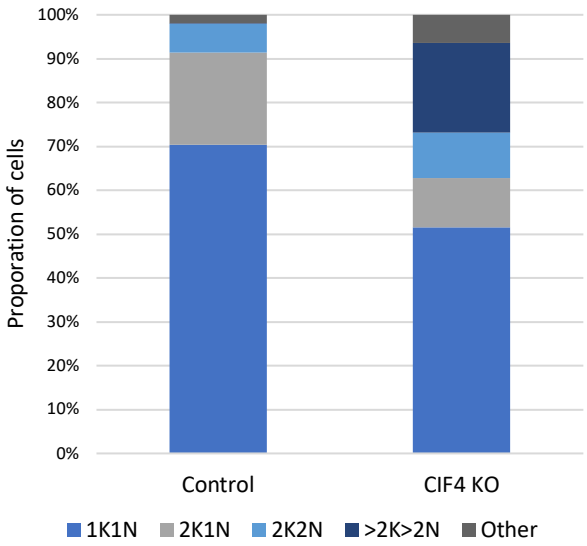

Figure 62: Deletion of CIF4 caused an accumulation of multinucleic cells. Deletion of CIF4 caused a reduction in 1K1N and 2K1N cells and an accumulation of 2K2N, >2K>2N cells. N = 500 cells per cell line. Key: K = kinetoplast; N = nucleus; >2K>2N = cells with multiple kinetoplasts and nuclei; Other = cells with an abnormal number of kinetoplasts and nuclei; KO = knockout (deletion) cell line.

6.3.1.2 Deletion of CIF4 caused premature new flagellum tip release from the groove

SEM was used to investigate the effects of the CIF4 deletion at a higher resolution. Cells with a short flagellum were comparable in appearance to the control cell line (Fig. 21B), with the new flagellum distal tip embedded in a groove (Fig. 63A). However, in dividing cells with a longer new flagellum, the distal tip was released from the groove (Fig. 63B-C). Only 3.5% of 2F cells in the CIF4 deletion cell line had a visible groove (N = 75 2F cells) (Fig. 63A, inset), compared to 77.3% of all 2F cells in the control cell line (N = 321 2F cells) (Fig. 21B-D, inset). With 94.7% of 2F cells possessing a free new flagellum distal tip, the deletion of CIF4 appeared to cause premature new flagellum tip release from the groove. The deletion also resulted in an accumulation of multiflagellated cells (>2 flagella), representing 68% of the

total population (N = 235) (Fig. 63E-F) compared to 3.5% in the control (N = 423). The division fold is able to form (Fig. 63D); however, in the multiflagellated cells, a cleavage furrow does not appear to initiate. Instead, the cells re-enter the cell cycle and nucleate a new flagellum without completing cytokinesis, leading to an accumulation of multiflagellated cells (Fig. 63E-F). Altogether, this suggests that the deletion of CIF4 caused defects in the cytokinesis initiation cascade.

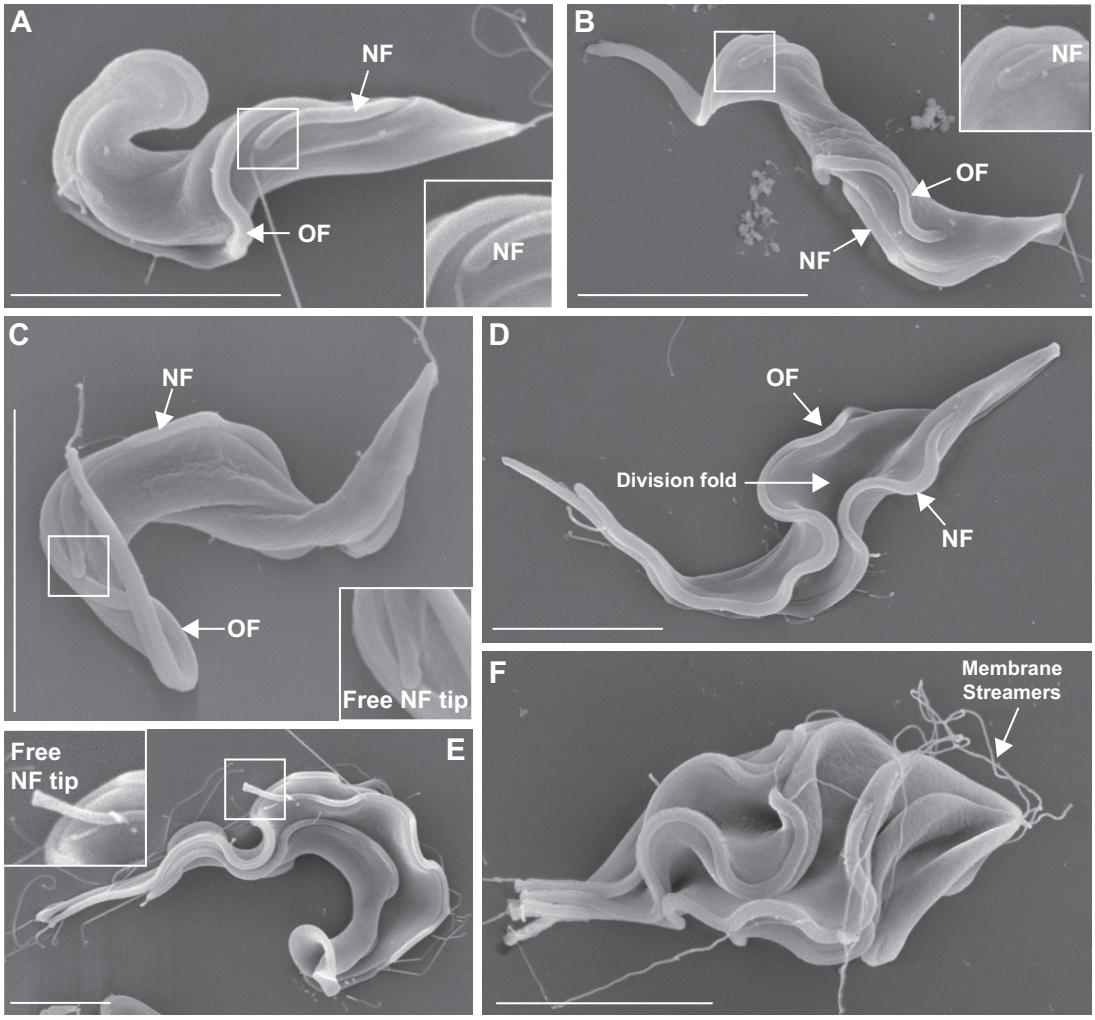

Figure 63: Deletion of CIF4 caused cytokinesis defects and premature new flagellum tip detachment. A) Distal tip of short new flagellum was embedded in a groove. B-C) New flagellum released from the groove. D) Division fold present. E-F) Multiflagellated cells, with some showing a free new flagellum tip (E). Key: NF = new flagellum; OF = old flagellum. Scale = 5μm.

To investigate quantitatively if the CIF4 deletion caused premature groove resolution and subsequently premature new flagellum tip release, we analysed the position of the new flagellum distal tip along the cell body using the flagellum tip marker as a reference (Fig. 64). Using the marker cell line as a control, we examined 500 2F cells (no multiflagellated cells)

with a visible flagellum tip marker signal on the new flagellum and categorised the cells into four distinct groups (Fig. 64):

1. Cells where the new flagellum distal tip signal was visible between the kinetoplast and the posterior edge of the nucleus.
2. Cells where the new flagellum distal tip signal was visible adjacent to the nucleus.
3. Cells where the new flagellum distal tip signal was visible between the anterior edge of the nucleus and the anterior cell tip.
4. Cells where the new flagellum distal tip signal was visible free from the cell body.

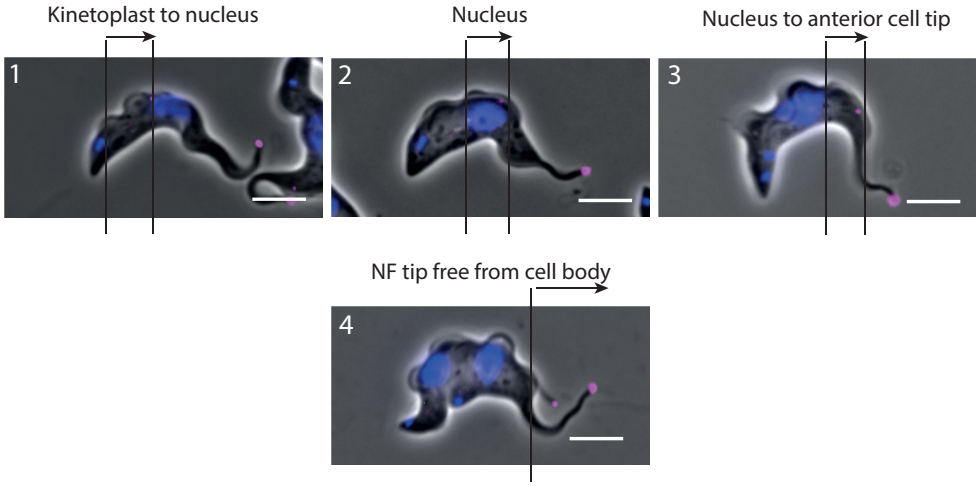

Figure 64: Example images of the defined zones used to analyse the position of the new flagellum distal tip. Scale = 5 μm.

The deletion of CIF4 caused a decrease in the number of cells with a new flagellum tip signal present between the kinetoplast and nucleus, as well as adjacent to the nucleus (Fig. 65A). Concomitant to this observation, the deletion of CIF4 caused an increase in the number of cells with a free new flagellum distal tip (Fig. 65A). The reduction in cells with an attached new flagellum tip and the subsequent accumulation of cells with a free new flagellum tip suggests that the CIF4 deletion may have caused premature new flagellum tip release from the groove. According to the SBF-SEM data outlined in Chapter 4, the new flagellum distal tip should be fully embedded in the groove during mitosis; therefore, by quantifying the proportion of 2K1N cells with a free new flagellum distal tip, we can determine if the deletion caused premature new flagellum tip release from the groove (Fig. 65B). The deletion of CIF4 caused a significant increase in the number of 2K1N cells with a free new flagellum distal tip compared to the control cell line ($p<0.0001$; Fisher's Exact Test) (Fig. 65B). Representative widefield images comparing the control and CIF4 deletion cell line show that the deletion of CIF4 resulted in the new flagellum tip marker appearing adjacent to the cell body in the 2K1N

stage when we would normally expect this signal to be directly on the cell body (indicative of the tip being embedded in the groove) as in the control cell line (Fig. 65C, arrow). We determined that this was evidence for the new flagellum tip being released from the groove.

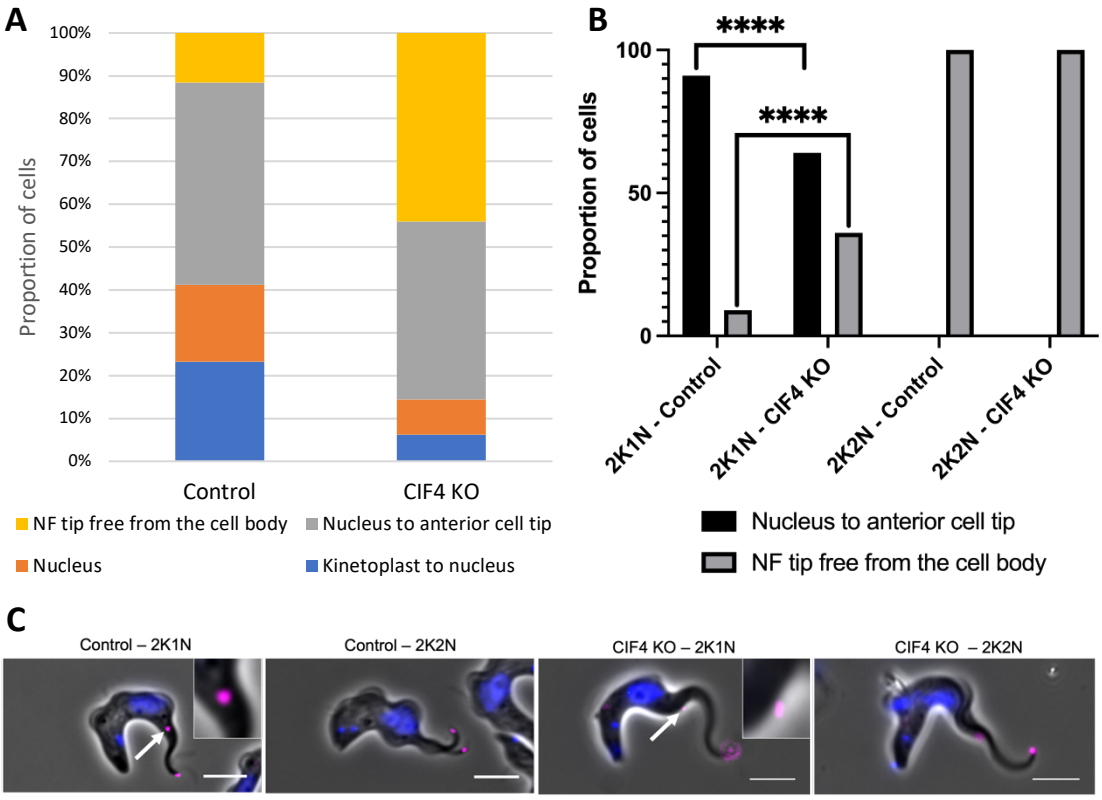

<u>Figure 65:</u> Deletion of CIF4 caused an accumulation of cells with a free new flagellum distal tip. A) Position analysis of the new flagellum tip along the cell body. Deletion of CIF4 caused an increase in cells with a free new flagellum distal tip. N = 500 2F cells per cell line. B) Position analysis of the new flagellum distal tip in 2K1N and 2K2N cells. Deletion of CIF4 caused a significant increase in 2K1N cells with a free new flagellum tip. N = 100 cells per cell type per cell line. **** = p<0.0001 by Fisher's Exact Test. C) Representative images of the 2K1N and 2K2N cells from (B), arrow indicates new flagellum tip. Key: K = kinetoplast; N = nucleus; KO = knockout (deletion) cell line.

In summary, my results show that the deletion of CIF4 results in premature release of the distal tip of the growing new flagellum from the groove and the accumulation of multiflagellated cells that are unable to complete cytokinesis.

6.3.2 Deletion of Tb427.01.2710 causes premature new flagellum distal tip release from the groove

Tb427.01.2710 is a putative flagella connector protein within the TrypTag database (http://tryptag.org); however, no functional studies have been carried out in either the PCF or BSF, leaving the function of this protein unknown. Tb427.01.2710 was successfully deleted in one of two clones tested (Clone 1) by PCR amplification (Fig. 66B). The Tb427.01.2710 deletion cell line also grew at a similar rate to the control cell line (Fig. 66C), suggesting no growth defect.

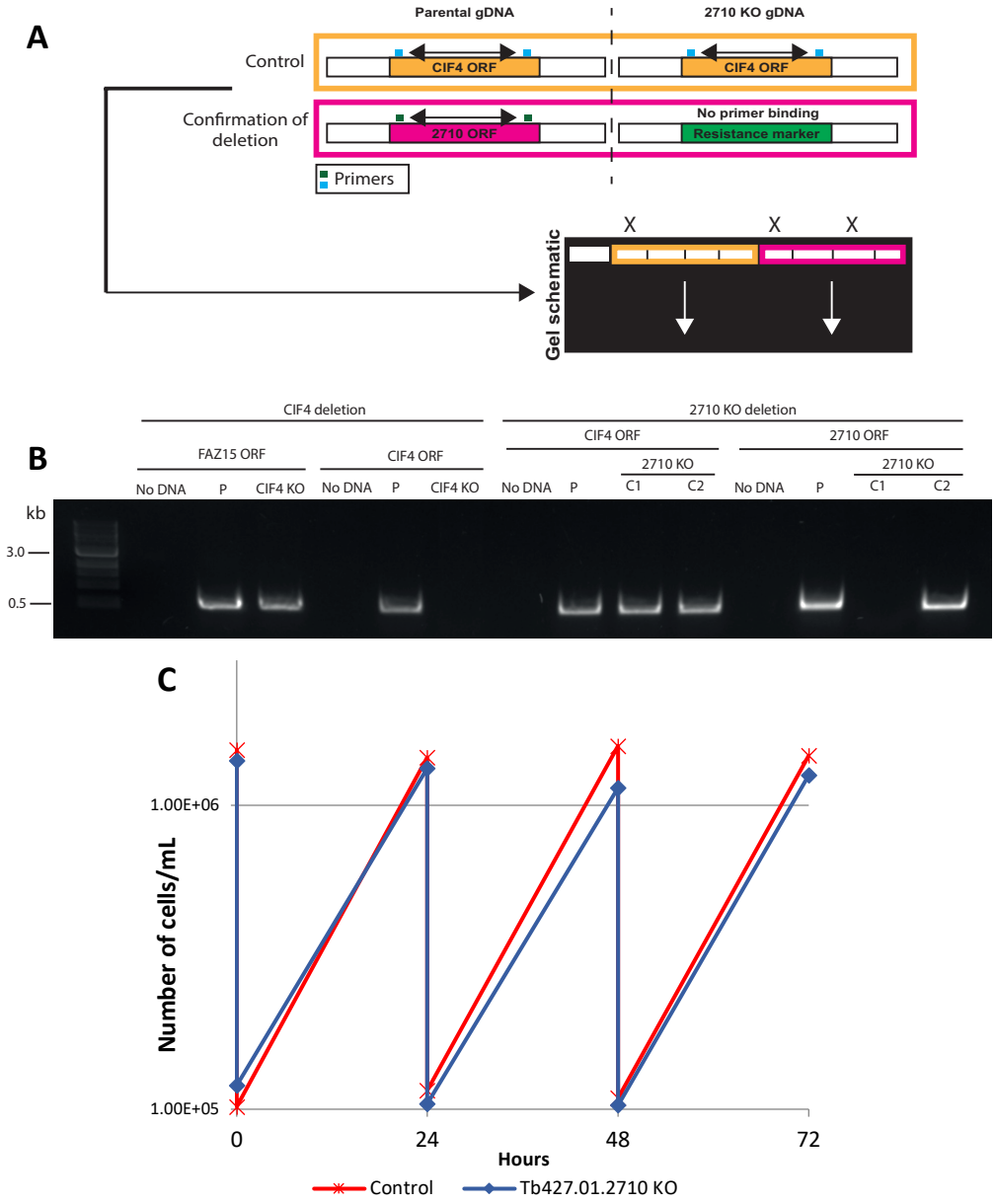

Figure 66: Deletion of Tb427.01.2710 was successful and did not cause a growth defect. A) Schematic for confirming the deletion of Tb427.01.2710. X denotes lanes where there was no DNA amplification.

B) PCR confirmation of the deletion of Tb427.01.2710 clone 1 (C1) (right of gel). Controls include ddH_2O (no DNA) and parental genomic DNA (P). We also tested for the deletion of CIF4 as a control (left of gel). C) Deletion of Tb427.01.2710 (blue) did not cause a growth defect.

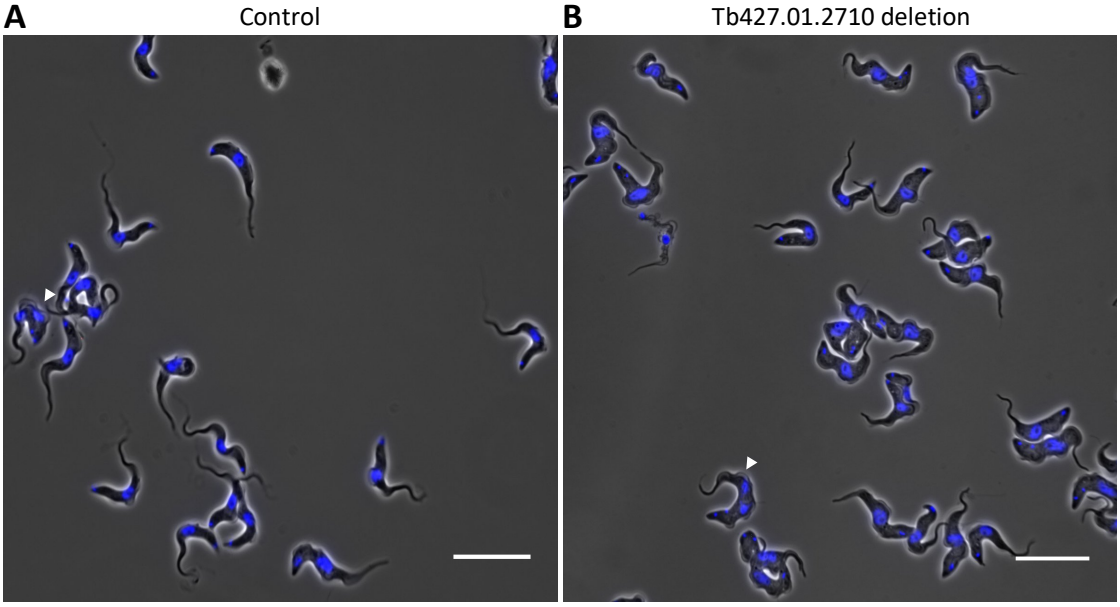

Figure 67: The Tb427.01.2710 deletion cell line was comparable to the control. Representative images of the of the control (A) and Tb427.01.2710 deletion cell lines (B). No noticeable change to the population as a result of the deletion. Key: arrowhead = 2K2N cell. Scale = 10 μm.

Using light microscopy, we saw that the Tb427.01.2710 deletion cell line was comparable in appearance to the control (Fig. 67A-B); however, cell cycle analysis showed that the deletion caused a minor decrease in the number of 1K1N cells (70% in the control; 65% in the deletion), and a slight increase in the number of 2K2N and >2K>2N (Fig. 68).

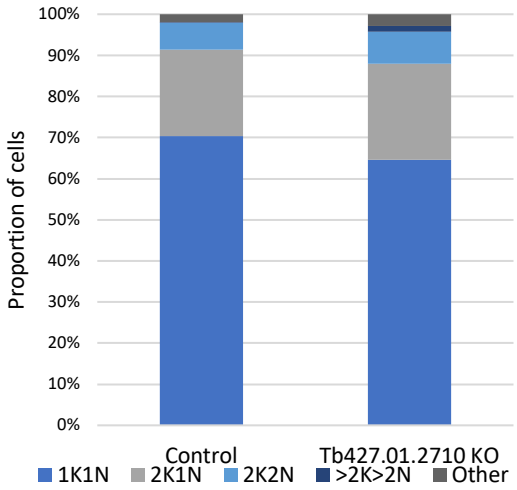

Figure 68: Deletion of Tb427.01.2710 caused a slight reduction in the number of 1K1N cells. N = 500 cells per cell line. Key: K = kinetoplast; N = nucleus; KO = knockout (deletion) cell line.

Clearly, the deletion of Tb427.01.2710 has a minimal effect on the cell cycle, however, the deletion may cause flagellar defects. Analysis of the position of the new flagellum distal tip showed that the deletion of Tb427.01.2710 caused a decrease in the number of cells with a visible new flagellum tip signal present between the kinetoplast and nucleus, and adjacent to the nucleus (Fig. 69A). This was matched by an increase in the number of cells with a free new flagellum distal tip (Fig. 69A). Furthermore, the deletion caused a significant increase in the number of 2K1N cells with a free new flagellum distal tip, from 9% in the control to over 64% in the deletion population ($p<0.0001$, Fisher's Exact Test) (Fig. 69B). Once again, the new flagellum tip signal in the 2K1N cells of the deletion cell line was positioned adjacent to the cell body, unlike in the control, suggesting that the deletion of Tb427.01.2710 caused premature new flagellum tip release from the groove (Fig. 69C, arrow).

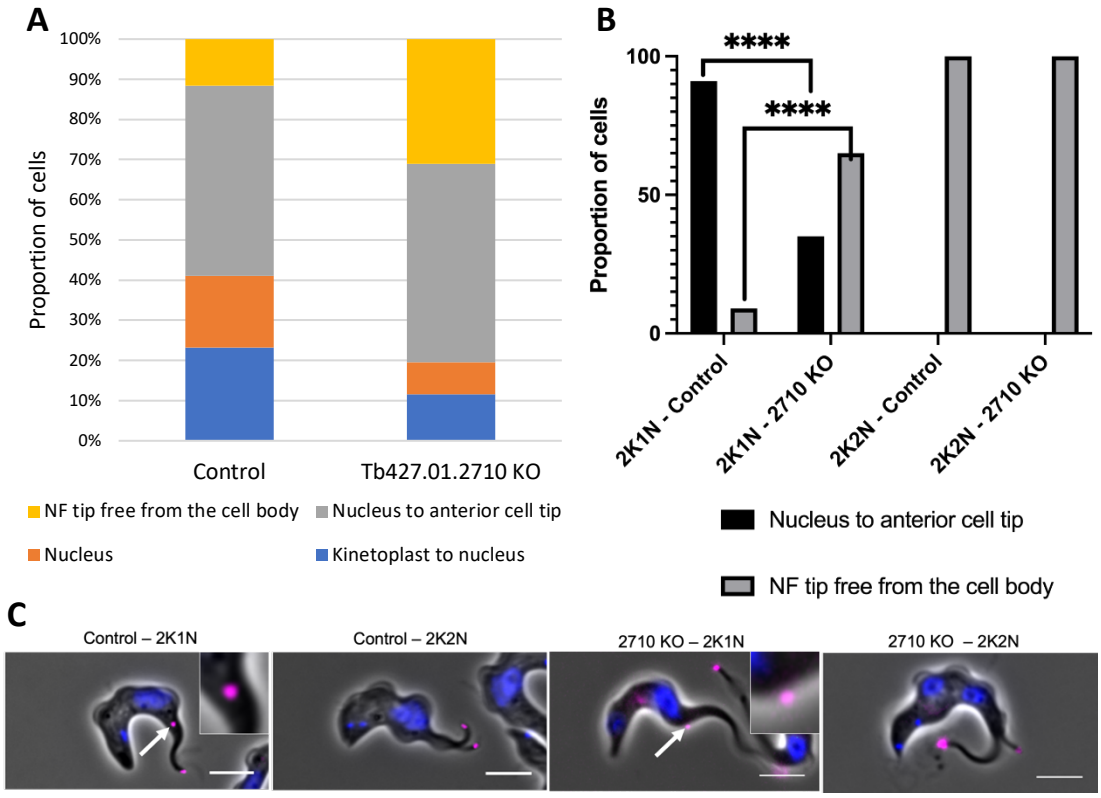

<u>Figure 69:</u> Deletion of Tb427.01.2710 caused premature new flagellum tip release from the groove. A) Position analysis of the new flagellum tip along the cell body. Deletion of Tb427.01.2710 caused an increase in cells with a free new flagellum distal tip. N = 500 2F cells per cell line. B) Position analysis of the new flagellum distal tip in 2K1N and 2K2N cells. Deletion of Tb427.01.2710 caused a significant increase in 2K1N cells with a free new flagellum tip. N = 100 cells per cell type per cell line. **** = $p<0.0001$ by Fisher's Exact Test. C) Representative images of the 2K1N and 2K2N cells from (B), arrow indicates new flagellum tip. Key: K = kinetoplast; N = nucleus; KO = knockout (deletion) cell line.

SEM analysis supported this observation, with 69.4% of 2F cells possessing a free new flagellum distal tip (N = 160) (Fig. 70B-D) compared to 22.7% in the control cell line (N = 321) (Fig. 21F-G). The deletion, however, did not appear to affect the formation of the division fold or cytokinesis (Fig. 70E-F).

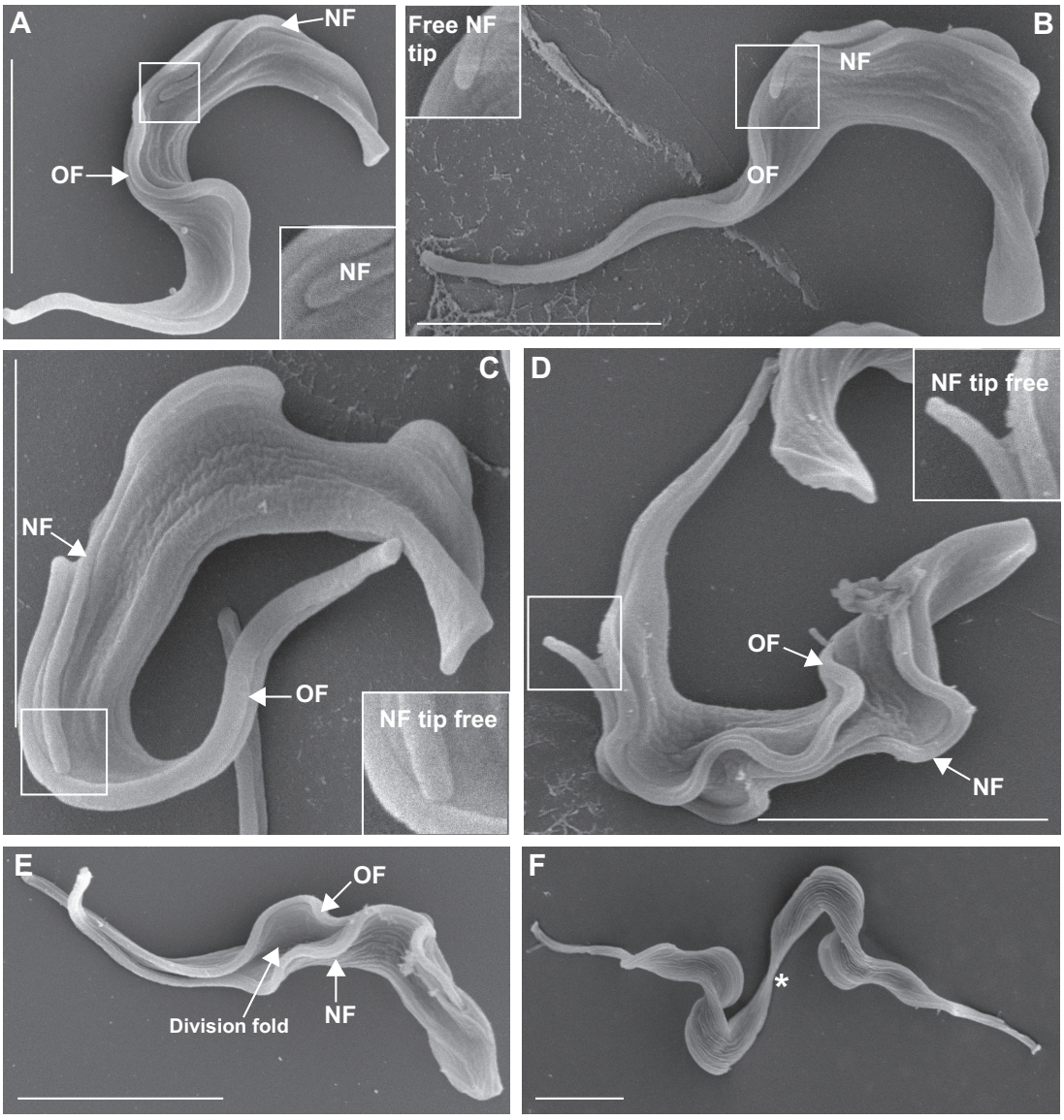

Figure 70: Deletion of Tb427.01.2710 caused premature new flagellum tip detachment. A) Distal tip of short new flagellum embedded in a shallow groove. B-D) New flagellum tip released from the groove prematurely. E) Division fold present. F) Cytokinesis occurring, with cells joined at the posterior end prior to abscission. Key: NF = new flagellum; OF = old flagellum; * = cells joined at posterior ends. Scale = 5 μm.

Therefore, it is clear that the deletion of Tb427.01.2710 resulted in premature new flagellum tip release from the groove, potentially causing a minor cell cycle delay but no growth defect.

6.3.3 Depletion of FCP4 using RNAi resulted in premature new flagellum tip release from the groove

Despite the successful deletion of five groove genes, we were unable to delete all 13 groove proteins. Six of these genes failed CRISPR/Cas9 transfection attempts three times; therefore, we used inducible RNAi cell line generation of the failed deletions for functional analyses. However, due to time constraints related to COVID-19, only one of the RNAi cell lines was analysed in detail. Flagella connector protein 4 (FCP4), a member of the ubiquitous kinesin-15 family of microtubule plus-end-directed motors is a flagella connector protein characterised in procyclic form parasites (Varga *et al*., 2017). As we hypothesise that there may be some shared biochemistry between the flagellar connector and the groove, this protein was of particular interest to us. An RNAi plasmid against FCP4 (Hairpin pDEX777 #9) was kindly provided by Dr Vladimir Varga at the Institute of Molecular Genetics, Prague.

Induction with doxycycline did not cause a growth defect, with the induced cell line growing at a similar rate to the non-induced (Fig. 71). The success of the RNAi was confirmed by the presence and absence mNG::FCP4 in the non-induced and induced populations (Fig. 72). There was a visible depletion of mNG::FCP4 at the groove foci 24 hours after induction, with only 11% of cells retaining an mNG::FCP4 signal compared to 73% in the non-induced population (Fig. 72). The depletion remained penetrant after 48 and 72 hours post-induction, with 92% of cells in each population lacking an mNG::FCP4 signal at the groove foci (Fig. 72).

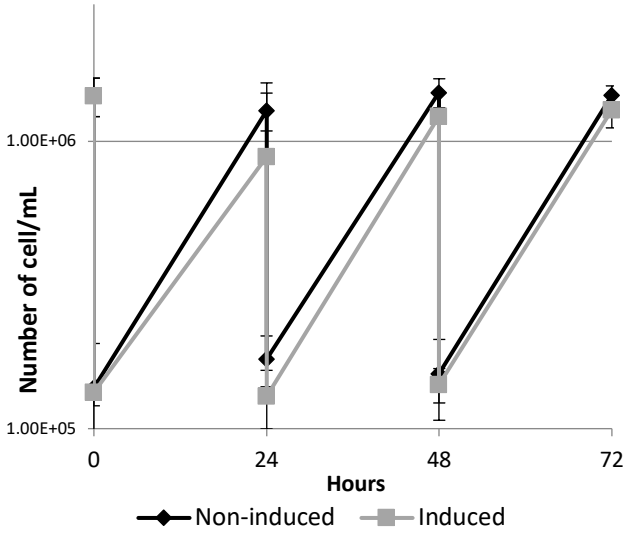

Figure 71: The depletion of FCP4 did not cause a growth defect. The FCP4 RNAi cell line was induced with doxycycline for 24, 48 and 72 hours before analysing the growth rate and cell cycle progression. Results are presented as a standard deviation of the mean ± SD (n = 3).

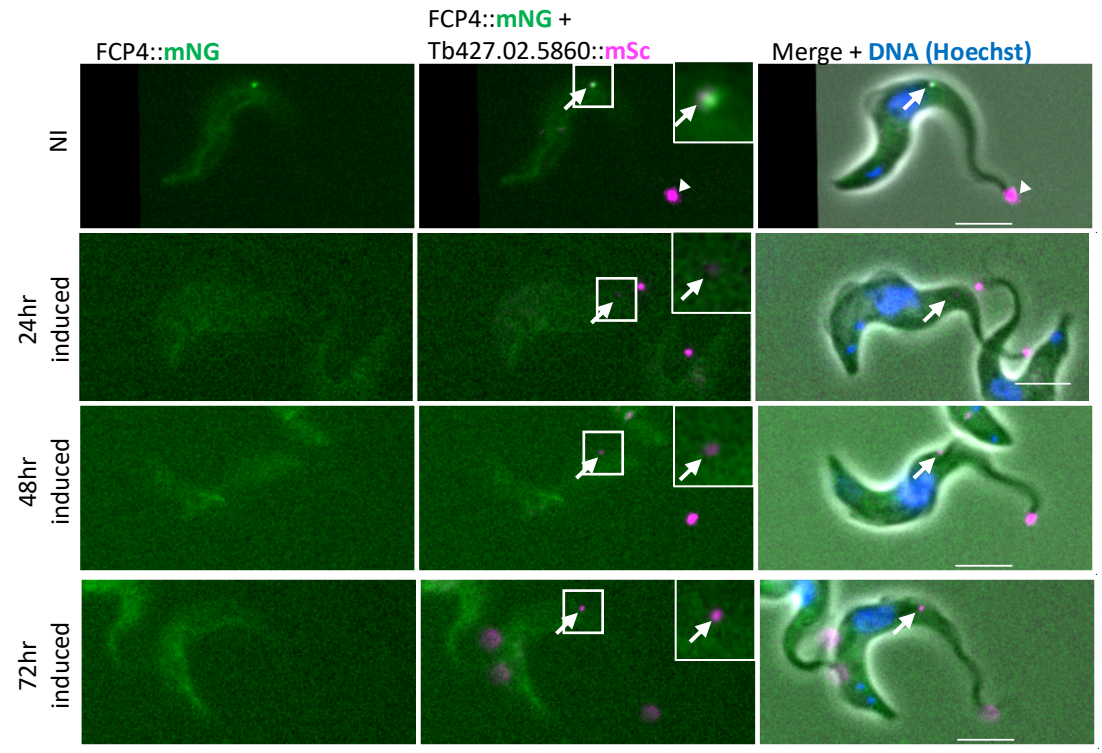

	Non-induced	24 hours induced	48 hours induced	72 hours induced
FCP4 signal present (%)	73	11	7	8
FCP4 signal absent (%)	29	89	93	92

Figure 72: Depletion of a FCP4 caused a reduction in green signal after induction, showing that the RNAi was successful and was maintained throughout 72 hours. Non-induced (NI) population shows FCP4::mNG localisation in the groove (inset box, arrow). Induced populations show that the FCP4::mNG green foci has disappeared as a result of induction with doxycycline. DNA stained with Hoechst (blue). Scale = 5 µm.

When analysing the progression of the cell cycle through KN counts, it was seen that post-induction, the FCP4 RNAi cell line showed a minor reduction in the number of 1K1N cells and a slightly increased proportion of 2K1N and 2K2N cells (Fig. 73).

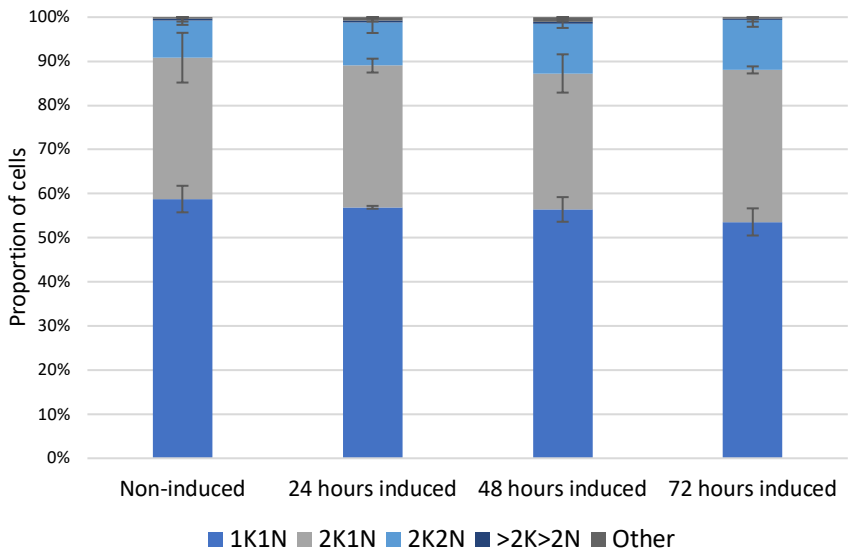

<u>Figure 73:</u> The depletion of FCP4 did not appear to affect cell cycle progression. The FCP4 RNAi cell line was induced with doxycycline for 24, 48 and 72 hours before analysing the cell cycle progression. Results are presented as a standard deviation of the mean ± SD (n = 3). N = 500 cells per time-point. Key: K = kinetoplast; N = nucleus.

As FCP4 localises to the flagella connector in the PCF (Varga *et al.*, 2017), and to the groove in the BSF, we hypothesised that FCP4 may play a role in new flagellum tip attachment to the groove. In order to determine if the depletion of FCP4 caused any flagellar defects, the position of the new flagellum tip signal along the cell body was analysed (Fig. 74). It was evident that the depletion of FCP4 caused a reduction in the number of cells with a new flagellum tip signal present between the kinetoplast and nucleus, and adjacent to the nucleus, particularly 72 hours post-induction (Fig. 74). Furthermore, there was an increase in the number of cells with a free new flagellum tip, with ˜9% of cells in the non-induced population having a free new flagellum distal tip; however, 72 hours after induction, this number increased to ˜30% of cells (Fig. 74).

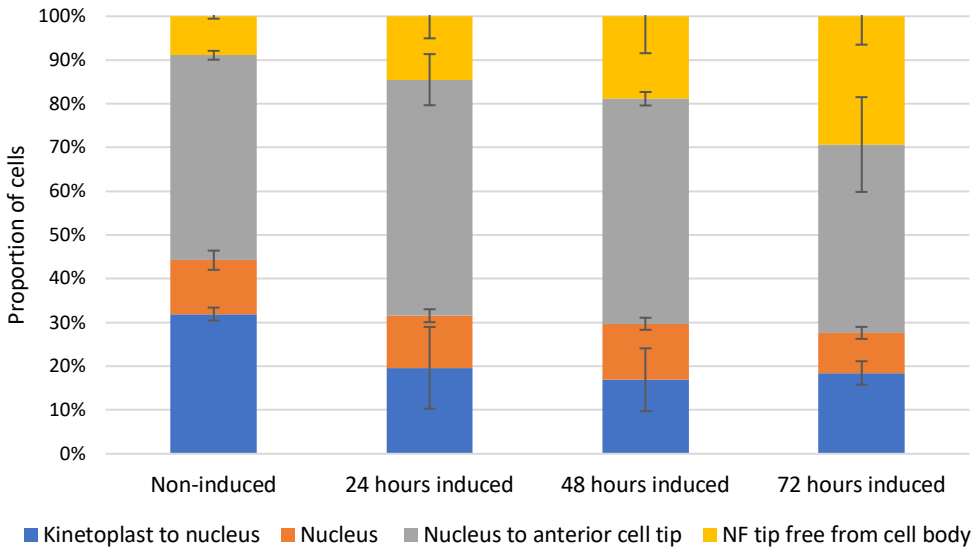

<u>Figure 74:</u> The depletion of FCP4 cause an accumulation of cells with a free new flagellum distal tip. Analysis of the position of the new flagellum distal tip along the cell body in the non-induced and induced FCP4 RNAi cell lines. After induction with doxycycline, there is a progressive accumulation of cells with a free new flagellum distal tip. Results are presented as a standard deviation of the mean ± SD (n = 3). N = 500 cells per time-point.

In order to determine if this increase resulted from a cytokinesis defect or premature new flagellum tip release from the groove, we quantified the number of 2K1N cells with a free new flagellum distal tip (Fig. 75A). We saw that the depletion of FCP4 caused an increase (60%) in the number of 2K1N cells with a free new flagellum distal tip, compared to ˜3% of 2K1N cells in the non-induced population (Fig. 75A-B). Furthermore, like with CIF4 and Tb427.01.2710, the new flagellum tip signal in 2K1N cells was adjacent to the cell body, unlike in the control. This confirmed that the depletion of FCP4 indeed caused premature new flagellum tip release from the groove.

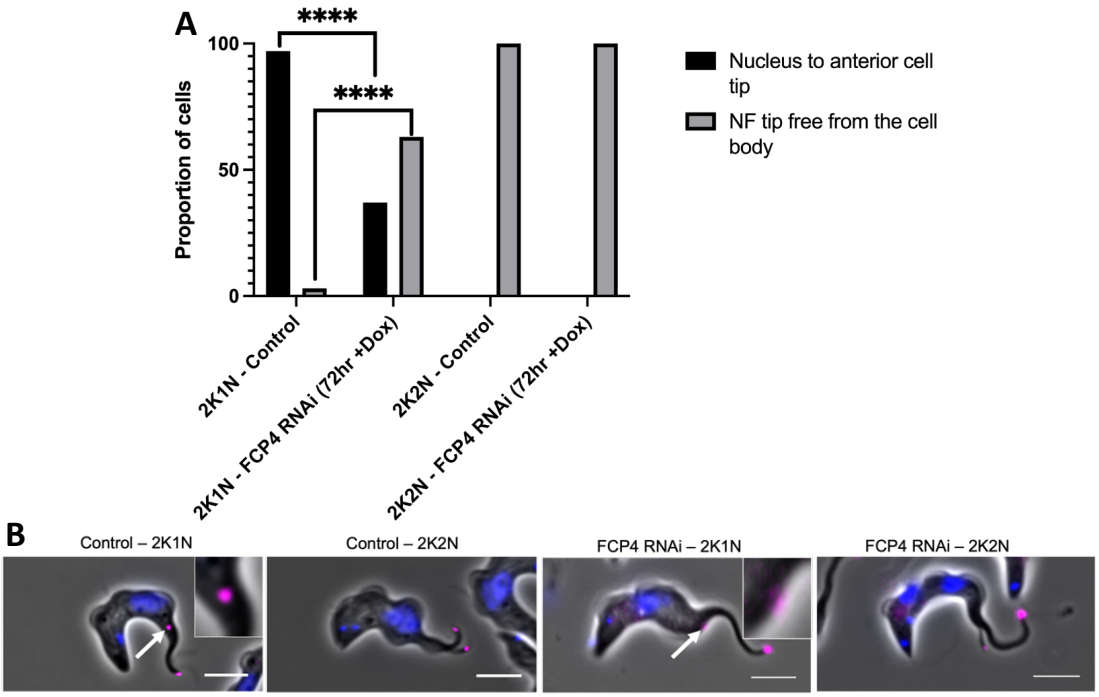

Figure 75: Depletion of FCP4 caused premature new flagellum tip release from the groove. A) Position analysis of the new flagellum distal tip in 2K1N and 2K2N cells. Depletion of FCP4 caused an increase in the number of 2K1N cells with a free new flagellum tip compared to the control (non-induced). N = 100 cells per cell type in both cell lines. **** = $p<0.0001$ by Fisher's Exact Test. B) Representative images of the 2K1N and 2K2N cells from (A), arrow indicates new flagellum tip. Key: K = kinetoplast; N = nucleus; +Dox = induced with doxycycline.

This observation was supported by SEM, with 64.4% of 2F cells (N = 161) having a free new flagellum distal tip 72 hours post-induction compared to 22.7% in the non-induced cell line (N = 271) (Fig. 76C-D). Despite this, 35.6% of 2F cells in the FCP4 RNAi cell line still possessed a groove (Fig. 76A-B), suggesting that the depletion of FCP4 did not halt groove formation but rather caused premature new flagellum tip release from the groove during mitosis. Furthermore, the depletion of FCP4 did not affect the formation of the division fold or cytokinesis (Fig. 76D-E).

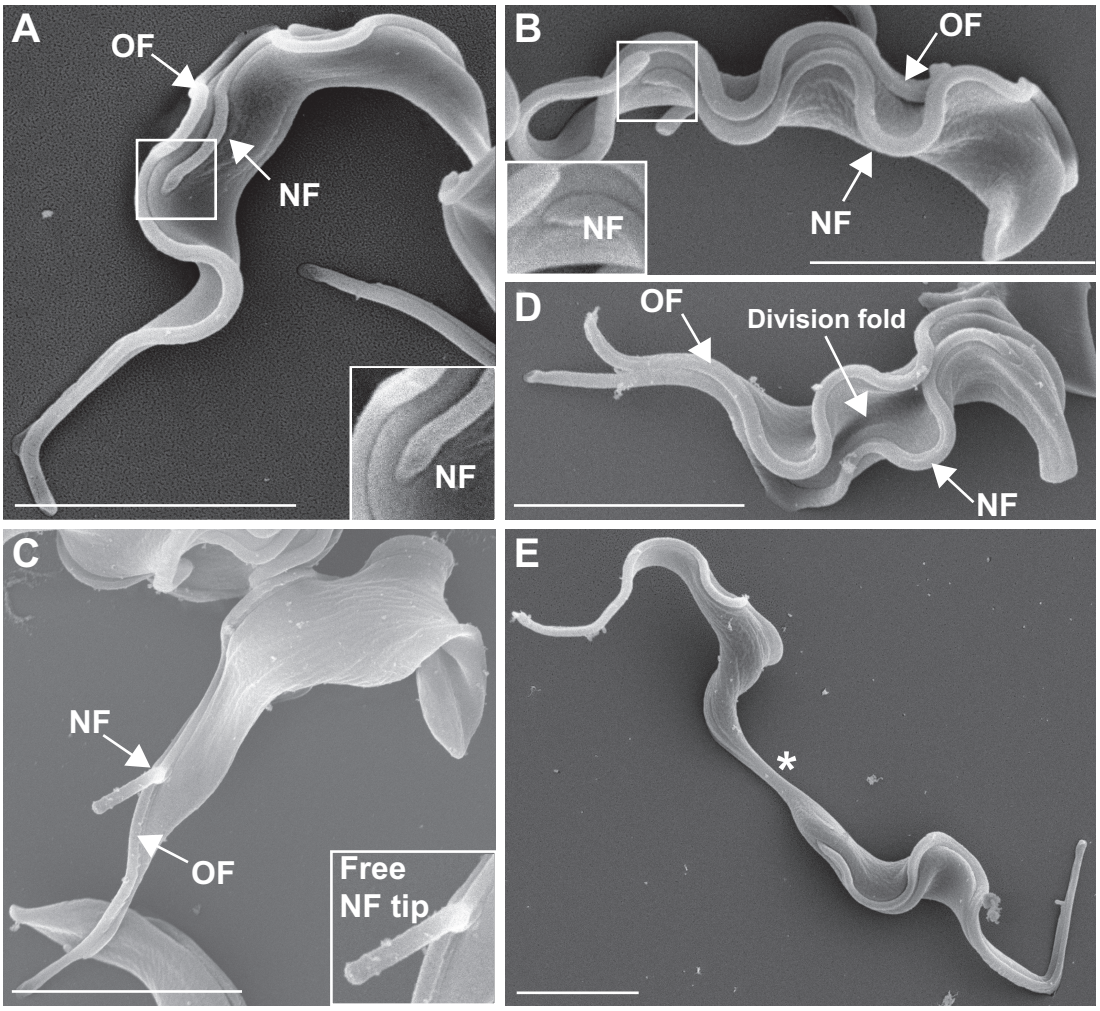

Figure 76: Depletion of FCP4 caused premature new flagellum tip detachment. A-B) Distal tip of new flagellum embedded in a groove. C) New flagellum tip released from the groove prematurely. D) Division fold present. E) Cytokinesis occurring with cells joined at the posterior end prior to abscission. Key: NF = new flagellum; OF = old flagellum; * = cells joined at posterior ends. Scale = 5 μm.

In summary, the depletion of FCP4 using RNAi resulted in the premature release of the new flagellum distal tip from the groove.

6.3.4 Deletion of Tb427tmp.01.3030 caused delayed new flagellum tip release from the groove

Tb427tmp.01.3030 is a putative distal FAZ protein identified through the TrypTag database (http://tryptag.org); however, no functional studies have been carried out in either PCFs or BSFs. Tb427tmp.01.3030 was successfully deleted according to PCR amplification (Fig. 77B). The deletion of Tb427tmp.01.3030, however, did not cause a growth defect, with the deletion cell line growing at a similar rate to the control cell line (Fig. 77C).

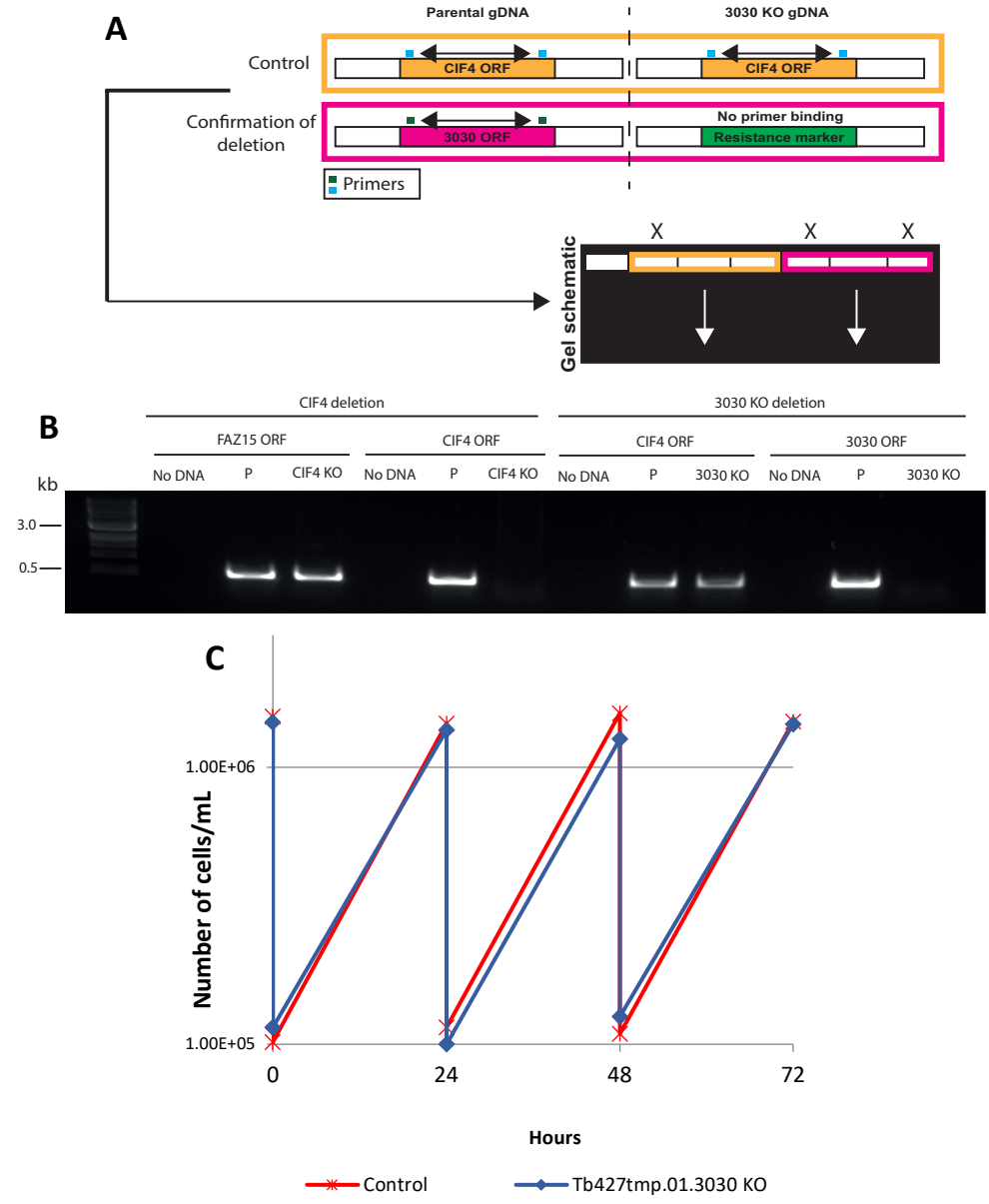

Figure 77: Deletion of Tb427tmp.01.3030 was successful and did not cause a growth defect. A) Schematic for confirming the deletion of Tb427tmp.01.3030. X denotes lanes where there was no DNA amplification. B) PCR confirmation of the deletion of Tb427tmp.01.3030. Controls include ddH_2O

(no DNA) and parental genomic DNA (P). We also tested for the deletion of CIF4 as a control (left of gel). C) Deletion of Tb427tmp.01.3030 did not cause a growth defect.

Furthermore, the deletion of Tb427tmp.01.3030 appeared comparable with the control cell line by widefield examination (Fig. 78A-B). However, analysis of the cell cycle confirmed that the deletion did result in a slight decrease in the number of 1K1N cells and an increase in the number of 2K2N and >2K>2N cells (Fig. 78C), suggesting that the deletion may have caused a minor delay to the progression of the cell cycle.

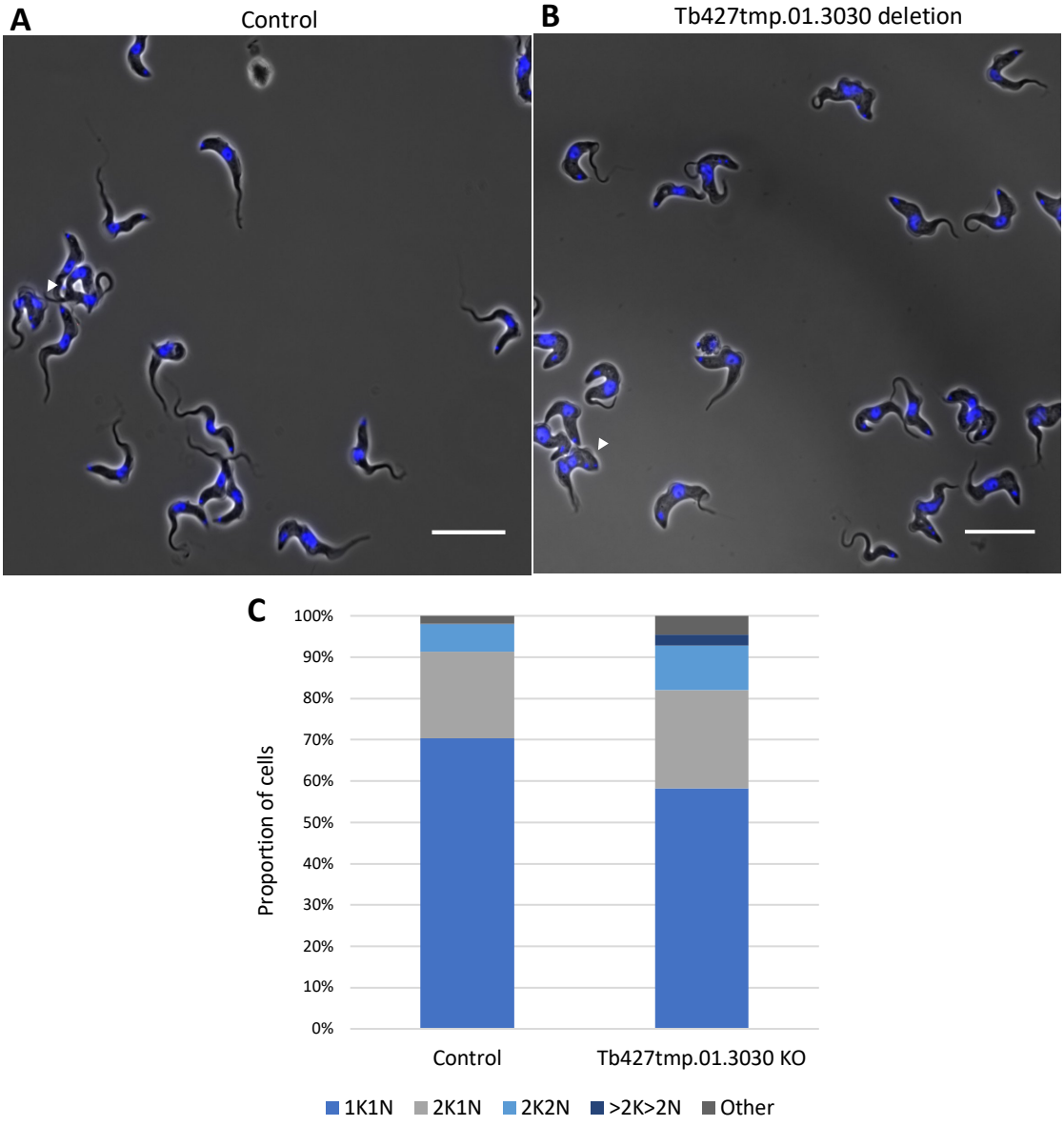

Figure 78: Deletion of Tb427tmp.01.3030 caused a minor delay to the cell cycle. A-B) Representative images of the of the control (A) and Tb427tmp.01.3030 deletion cell line (B). Scale = 10 μm. C) Cell cycle analysis showing that the deletion of Tb427tmp.01.3030 caused a slight reduction in the number of 1K1N cells and an increase in 2K2N and >2K>2N cells. N = 500 cells per cell line. Key: K = kinetoplast; N = nucleus; KO = knockout (deletion) cell line

When analysing the position of the new flagellum tip signal along the cell body, we saw that the deletion of Tb427tmp.01.3030 caused a decrease in the number of cells with a new flagellum tip signal present between the kinetoplast and nucleus, and adjected to the nucleus (Fig. 79A). Furthermore, an increased proportion of cells with a new flagellum tip signal present between the anterior edge of the nucleus and anterior cell tip was observed, as well as the number of cells with a free new flagellum tip (Fig. 79A).

When quantifying the number of 2K1N cells with a free new flagellum tip, we saw that only 2% of 2K1N cells in the Tb427tmp.01.3030 deletion cell line had a free new flagellum tip compared to 9% for the control ($p<0.01$, Fisher's Exact Test) (Fig. 79B). Additionally, the number of 2K2N cells with a free new flagellum distal tip in the deletion cell line decreased to 85% compared to 100% of 2K2N cells in the control cell line ($p<0.0001$, Fisher's Exact Test) (Fig. 79B). In the deletion cell line, the new flagellum tip signal remained positioned over the cell body in the 2K2N cells, suggesting that there may be a delay in releasing the new flagellum tip from the groove as we would expect to see a free new flagellum tip in the 2K2N stage, as seen in the control (Fig. 79C, arrow).

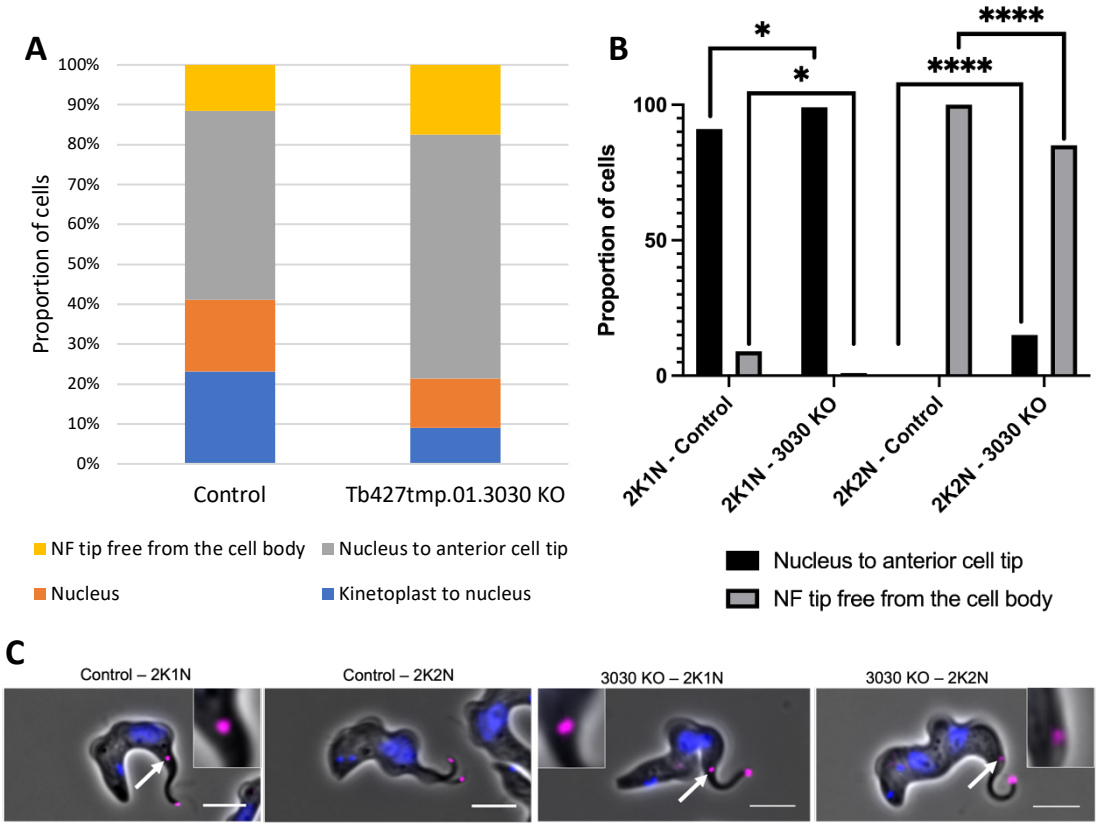

Figure 79: Deletion of Tb427tmp.01.3030 caused a delay in new flagellum tip release from the groove. A) Position analysis of the new flagellum distal tip along the cell body. Deletion of Tb427tmp.01.3030 caused an increase in the number of cells with a free new flagellum distal tip. N =

500 2F cells per cell line. B) Position analysis of the new flagellum distal tip in 2K1N and 2K2N cells. Deletion of Tb427tmp.01.3030 caused a significant increase in the number of 2K1N and 2K2N cells with an attached new flagellum distal tip. N = 100 cells per cell type in both cell lines. * = p=0.016; **** = p<0.0001 by Fisher's Exact Test. C) Representative images of the 2K1N and 2K2N cells from (A), arrow indicates new flagellum tip. Key: K = kinetoplast; N = nucleus; KO = knockout (deletion) cell line.

This was supported by SEM, with the deletion of Tb427tmp.01.3030 causing an increased proportion of 2F cells possessing a groove (86% of 2F cells; N = 122) (Fig. 80A-C) compared to the control cell line (77.3% of 2F cells; N = 321) (Fig. 21B-D). In the deletion cell line, the groove was still present later than expected (Fig. 80C) compared to the control (Fig. 21E). However, the deletion of Tb427tmp.01.3030 did not affect the formation of the division fold or cytokinesis (Fig. 80D-E).

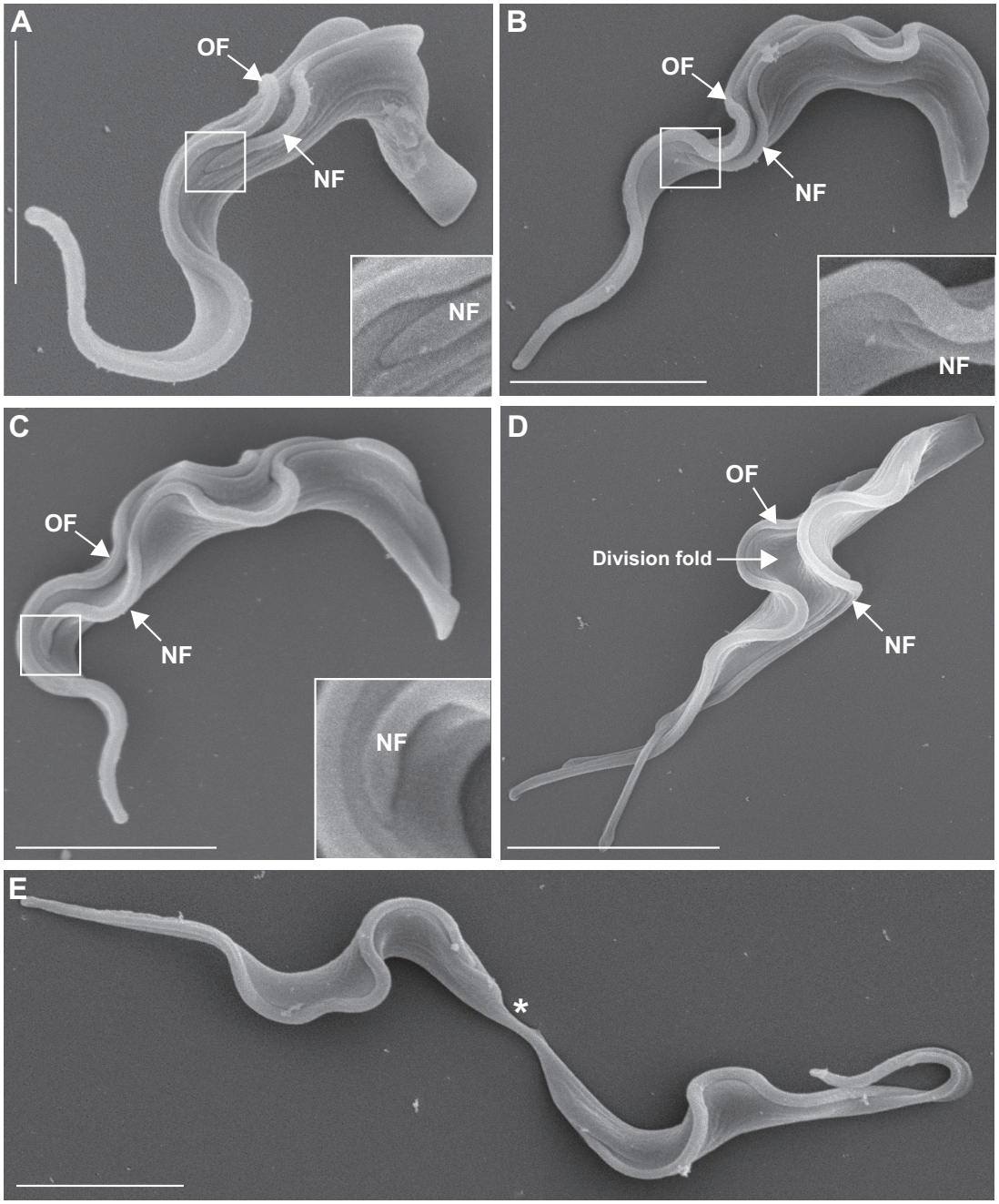

<u>Figure 80:</u> Deletion of Tb427tmp.01.3030 caused delayed new flagellum tip release from the groove. A-C) Distal tip of new flagellum embedded in the groove. D) Division fold present. E) Cytokinesis occurring with cells joined at the posterior end prior to abscission. Key: NF = new flagellum; OF = old flagellum; * = cytokinetic bridge. Scale = 5 μm.

In summary, the deletion of Tb427tmp.01.3030 resulted in the delayed release of the new flagellum distal tip from the groove.

6.4 The deletion of FAZ15, FAZ16, FAZ10 and FCP5 caused either a cytokinesis defect or a minor delay to the cell cycle

6.4.1 Deletion of FAZ15 caused a cytokinesis defect due to an accumulation of pre-cytokinetic cells and delayed new flagellum tip release

Previously, FAZ15 was identified as an interactor of TbPLK and a component of the FAZ in the PCF (McAllaster *et al*., 2015; Sunter and Gull, 2016). However, the function and localisation of FAZ15 in BSFs has yet to be examined. The deletion of FAZ15 caused a severe growth defect when compared to the control cell line (Fig. 81). According to widefield microscopy, there was also a visible increase in the number of 2K2N (arrowhead) cells in the population compared to the control cell line (Fig. 82A-B), suggesting a resulting cytokinesis defect due to a build-up of pre-cytokinetic cells.

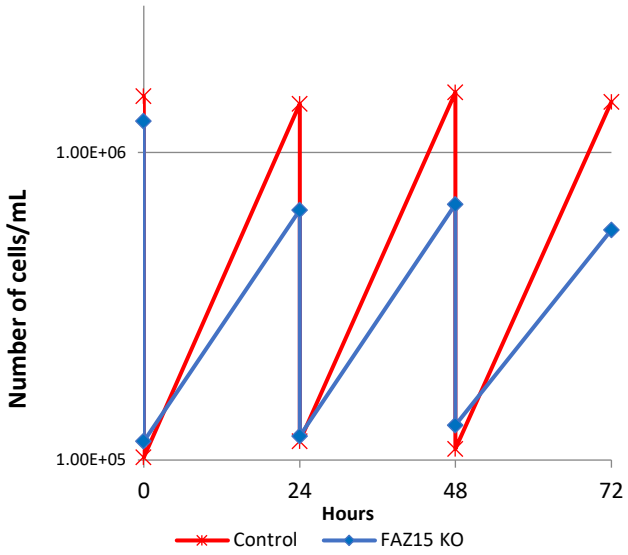

Figure 81: Deletion of FAZ15 resulted in a severe growth defect.

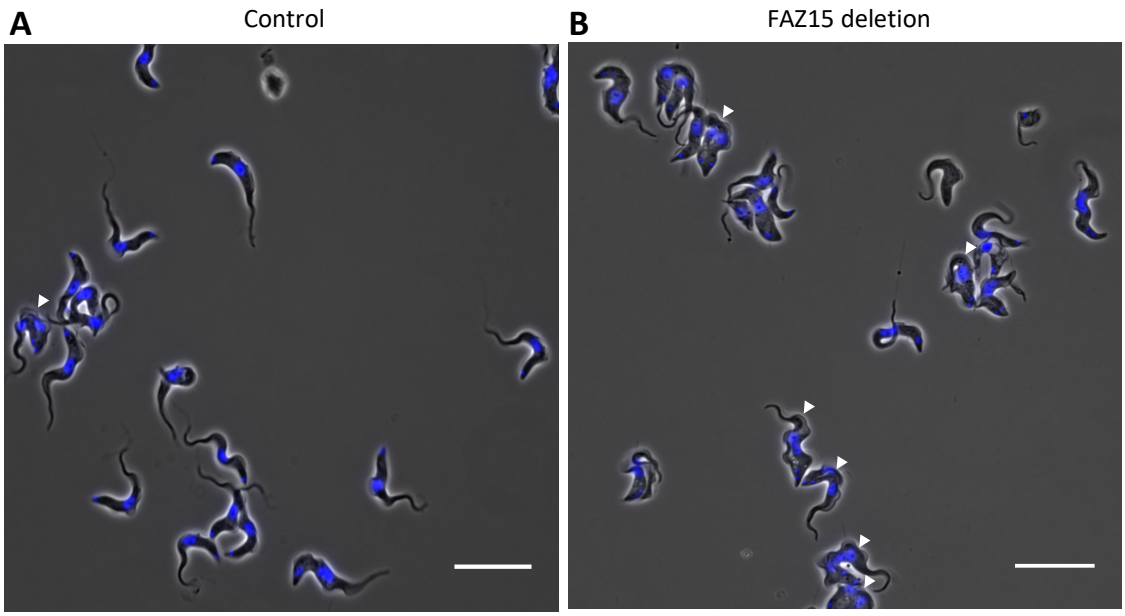

Figure 82: Deletion of FAZ15 resulted in an accumulation of 2K2N cells. Representative images of the of the control (A) and FAZ15 deletion (B) cell lines. Deletion of FAZ15 caused an increase in 2K2N cells (arrowhead). Scale = 10 μm.

Furthermore, cell cycle analysis confirmed that the FAZ15 deletion caused a reduction in the number of 1K1N and 2K1N cells and a prominent increase in the number of >2K>2N and zoid cells (Fig. 83), suggesting that the FAZ15 deletion caused a cell cycle delay through the accumulation of pre-cytokinetic (2K2N) and >2K>2N cells.

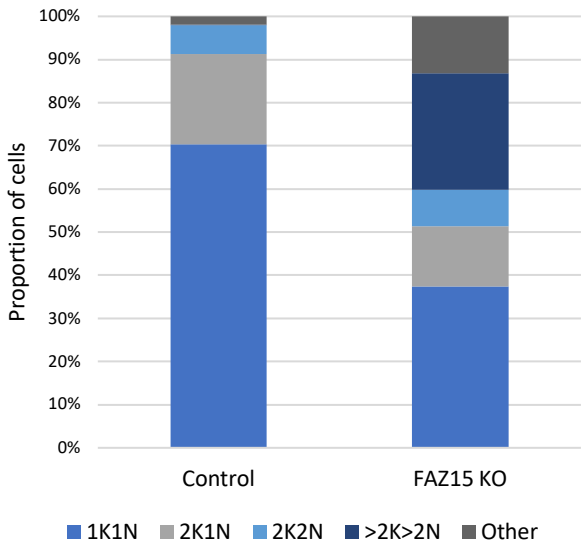

Figure 83: Deletion of FAZ15 caused an increase in >2K>2N and zoid cells. Deletion of FAZ15 caused a reduction in 1K1N and 2K1N cells and an accumulation of >2K>2N and cells in the "Other" category. N = 500 cells per cell line. Key: K = kinetoplast; N = nucleus; KO = knockout (deletion) cell line.

SEM analysis confirmed that in the deletion cell line, 50.4% of the total number of cells counted (N = 258) have multiple flagella (Fig. 84D-F), compared to 3.5% (N = 423) in the control. The FAZ15 deletion did not affect the formation of the division fold (Fig. 84C), suggesting that the deletion disrupted the ingression of a cleavage furrow instead. Furthermore, the FAZ15 deletion may impair the abscission of the membrane connecting the posterior ends during cytokinesis (Fig. 84D-F, asterisk). It is evident that the deletion of FAZ15 affects cytokinesis initiation in the BSF, resulting in an accumulation of multiflagellated cells. Only 9.3% of all 2F cells examined (N = 128) had a visible groove (Fig. 84A), with the remaining 90.7% of 2F cells identified as pre-cytokinetic 2F cells with the new flagellum free from the cell (as seen in Fig. 84B-C).

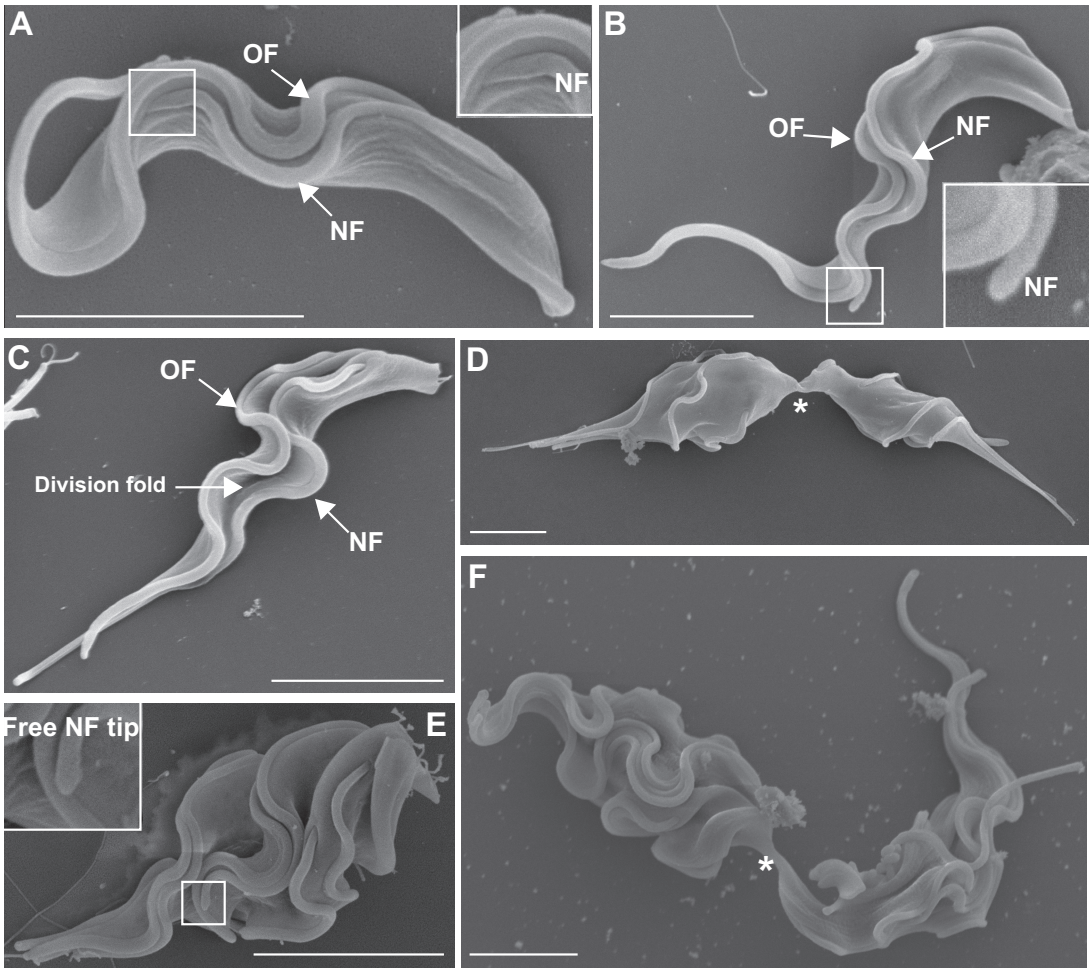

Figure 84: Deletion of FAZ15 caused an accumulation of multiflagellated cells. A) Distal tip of the new flagellum embedded in the groove. B) Distal tip of the new flagellum released from the groove. C) Division fold present. D-F) Multiflagellated cells, some still joined at the posterior end. Key: NF = new flagellum; OF = old flagellum; * = cytokinetic bridge. Scale = 5 μm.

Through position analysis of the new flagellum tip signal, we saw that the deletion of FAZ15 caused a decrease in the number of cells with a new flagellum tip signal present between the kinetoplast and nucleus (Fig. 85A) and an increase in the number of cells with a free new flagellum distal tip (Fig. 85A). However, when quantifying the number of 2K1N cells with a free new flagellum distal tip, it was clear that the FAZ15 deletion did not cause premature new flagellum tip release from the groove, as the number of 2K1N cells with a free new flagellum distal tip was comparable with the control cell line (Fig. 85B). Instead, the increased number of cells with a free new flagellum tip (Fig. 85A) was due to an accumulation of 2K2N cells, not premature new flagellum tip release. Interestingly, there was a significant decrease ($p<0.05$, Fisher's Exact Test) in the number of 2K2N cells with a free new flagellum distal tip in the deletion cell line (Fig. 85B-C), suggesting that the deletion of FAZ15 may delay the release of the new flagellum tip from the groove, like with the Tb427tmp.01.3030 deletion.

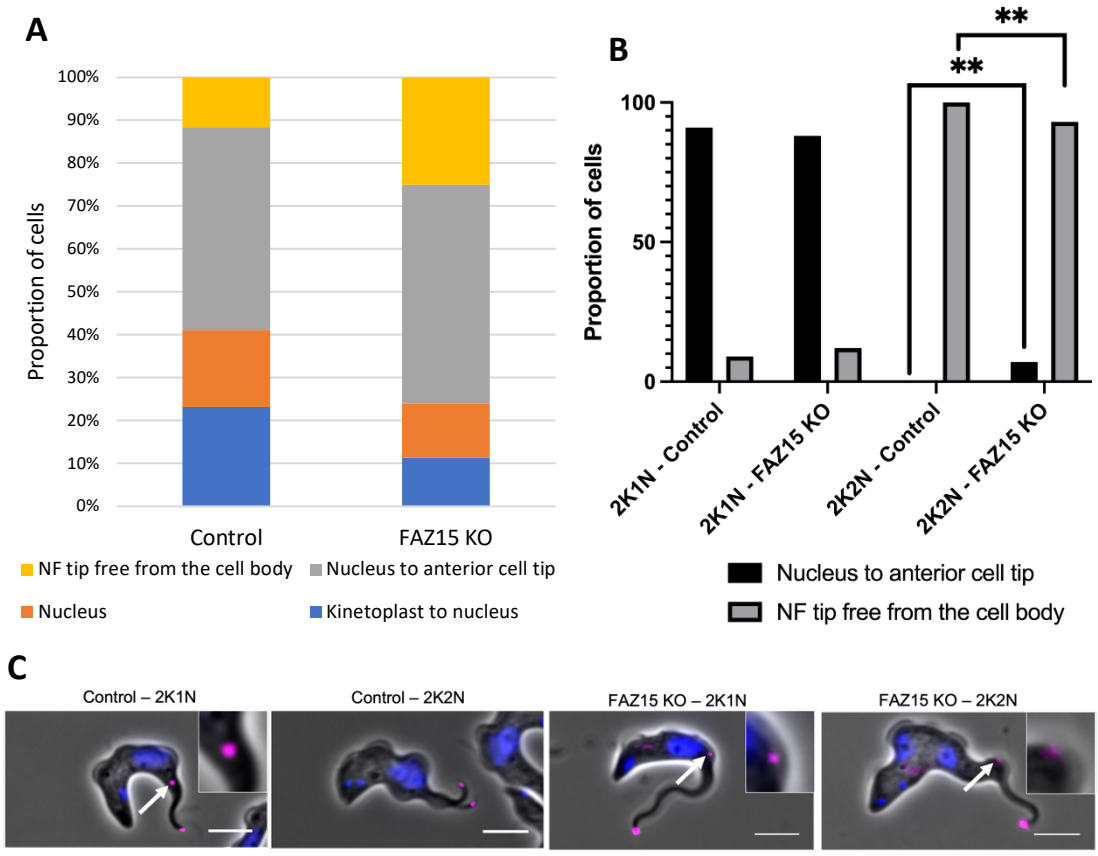

Figure 85: Deletion of FAZ15 caused an increase in pre-cytokinetic cells and delayed new flagellum tip release. A) Position analysis of the new flagellum distal tip along the cell body. Deletion of FAZ15 caused an increase in the number of cells with a free new flagellum distal tip. N = 500 2F cells per cell line. B) Position analysis of the new flagellum distal tip in 2K1N and 2K2N cells. Deletion of FAZ15 caused a significant increase in the number of 2K1N and 2K2N cells with an attached new flagellum distal tip. N = 100 cells per cell type in both cell lines. ** = $p<0.05$ by Fisher's Exact Test. C)

Representative images of the 2K1N and 2K2N cells from (B), arrow indicates new flagellum tip. Key: K = kinetoplast; N = nucleus; KO = knockout (deletion) cell line.

It is clear that the deletion of FAZ15 resulted in an accumulation of pre-cytokinetic 2F and >2K>2N cells, thereby delaying the cell cycle. Furthermore, the deletion of FAZ15 appears to cause delayed new flagellum tip release from the groove.

6.4.2 Deletion of FAZ16 caused a cytokinesis delay through the accumulation of >2K>2N and pre-cytokinetic 2F cells

FAZ16, like FAZ15, was identified as an interactor TbPLK and a component of the FAZ in the PCF (McAllaster *et al*., 2015; Sunter and Gull, 2016). However, the function and localisation of FAZ16 in BSFs has yet to be examined. The deletion of FAZ16 was confirmed by PCR amplification, with one out of three clones tested (clone 2) successfully deleted from the genome (Fig. 86B). CIF4 was used as a positive control for the PCR confirmation of FAZ16 according to the schematic outlined (A) and clone 2 was used for further analysis due to the success of the FAZ16 deletion.

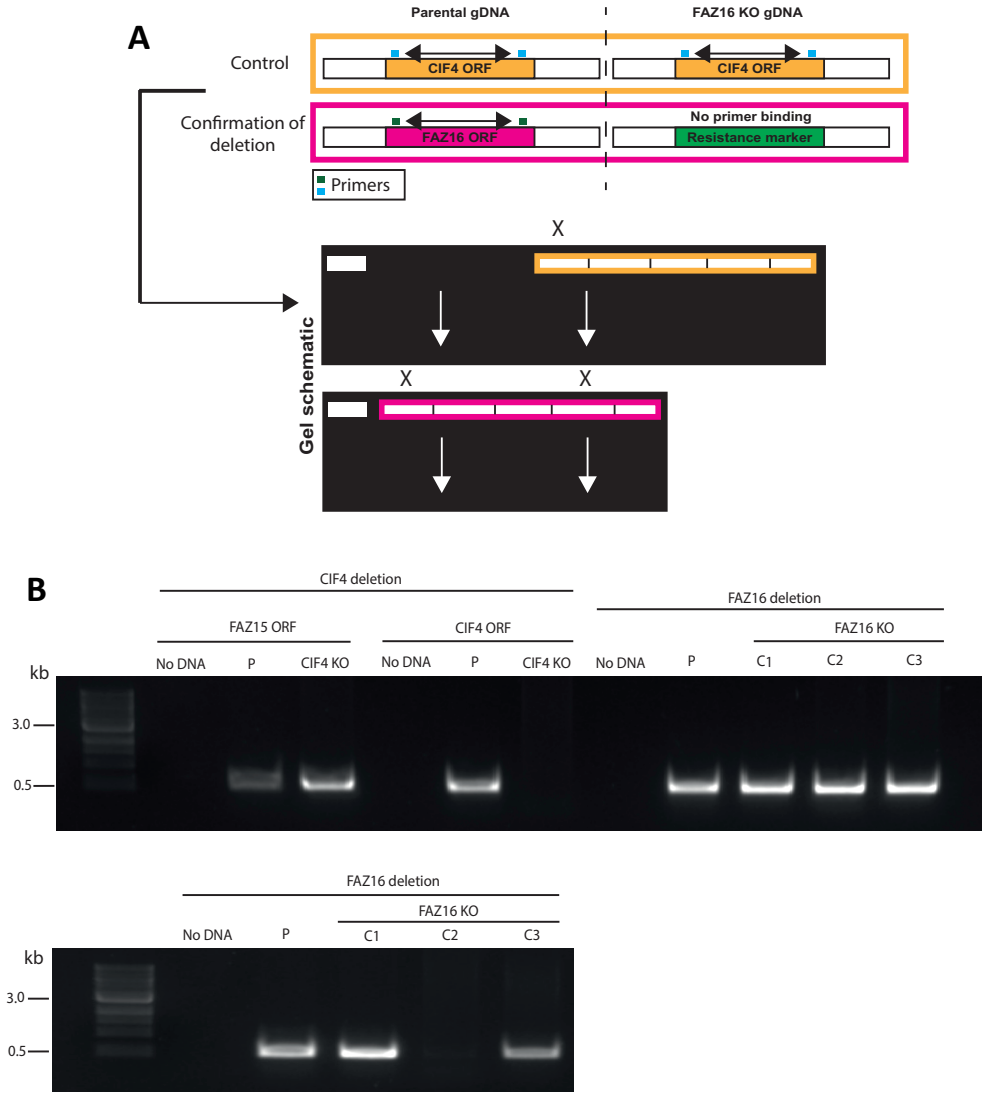

Figure 86: FAZ16 was successfully deleted. A) Schematic for confirming the deletion of FAZ16. X denotes lanes where there was no DNA amplification. B) PCR confirmation of the deletion of FAZ16 clone 2 (C2) (bottom gel). Controls include ddH_2O (no DNA) and parental genomic DNA (P). We also tested for the deletion of CIF4 as a control (left of gel).

The deletion of FAZ16 caused a severe growth defect compared to the control cell line (Fig. 87A). When examined by widefield microscopy, it was seen that the FAZ16 deletion caused an increase in 2K2N (arrowhead) and multinucleic cells (>2K>2N) (asterisk) compared to the control cell line (Fig. 87B-C).

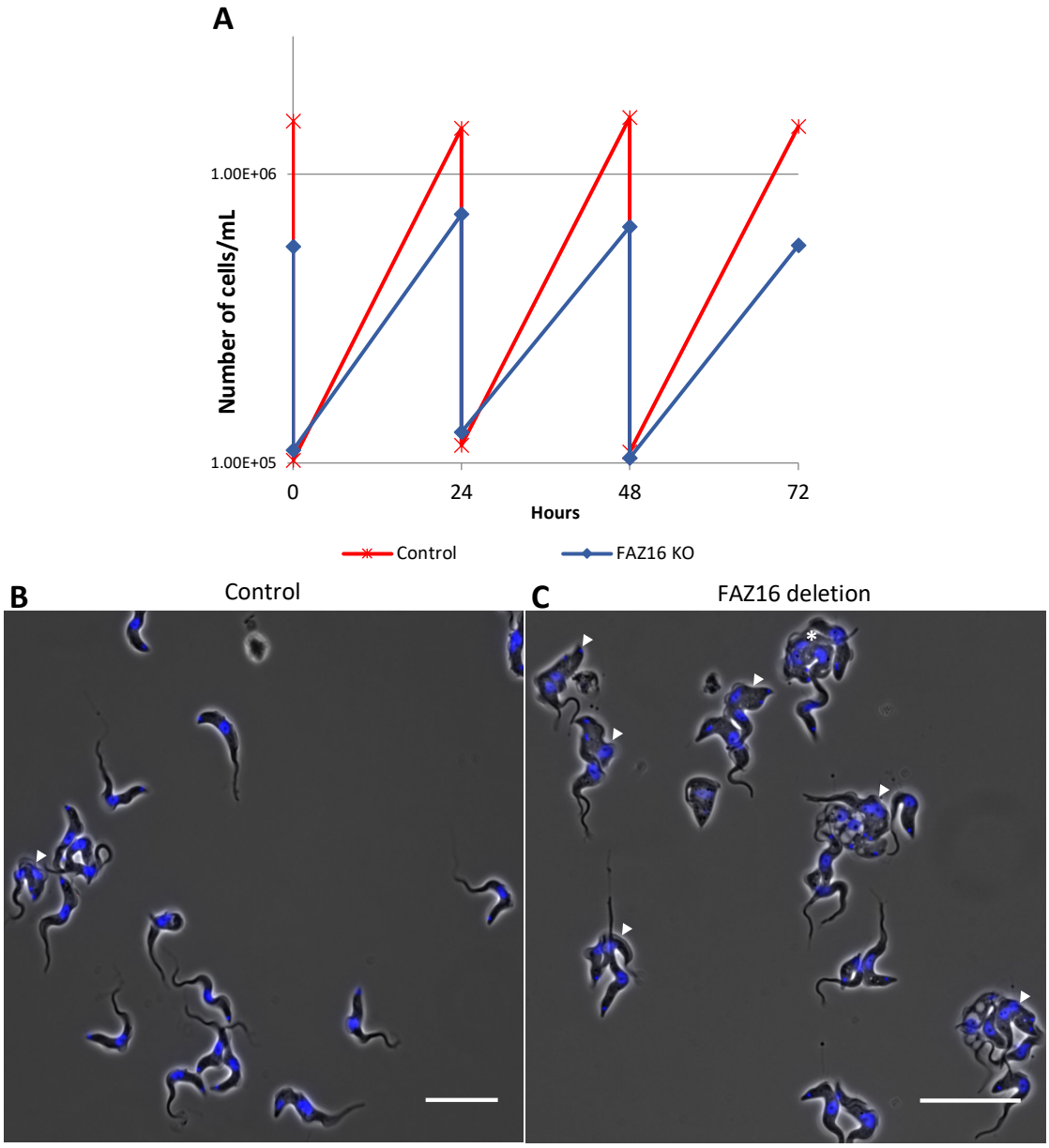

<u>Figure 87:</u> Deletion of FAZ16 caused growth defect and an accumulation of 2K2N cells. A) Deletion of FAZ16 (blue) caused a growth defect. B) Representative images of the of the control (B) and FAZ15 deletion (C) cell lines. The deletion of FAZ16 caused an increased number of 2K2N (arrowhead) and >2K>2N cells (asterisk). Scale = 10 μm.

To quantify the accumulation of abnormal cells, we analysed the progression of the cell cycle and saw that the deletion of FAZ16 caused an increased number of >2K>2N cells from <1%

in the control cell line to ˜27% in the FAZ16 deletion cell line (Fig. 88). This, paired with a decrease in the number of 1K1N and 2K1N cells, suggests that the deletion of FAZ16 caused a delay in cytokinesis through a build-up of 2K2N and multinucleic cells (Fig. 88).

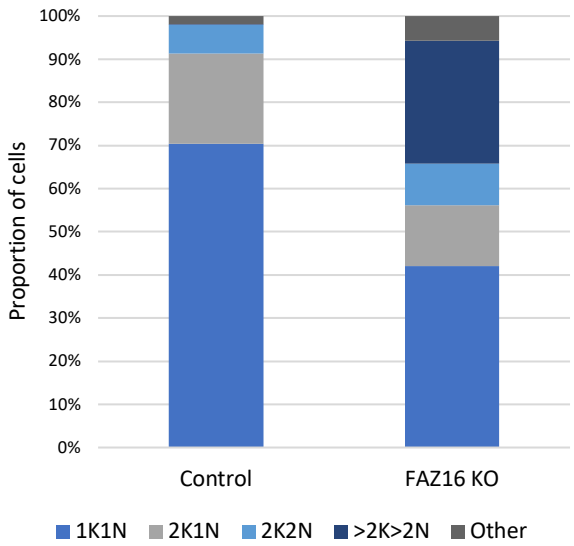

Figure 88: Deletion of FAZ16 caused an accumulation of multinucleic cells. Deletion of FAZ16 caused a reduced number of 1K1N and 2K1N cells and an accumulation >2K>2N cells. N = 500 cells per cell line. Key: K = kinetoplast; N = nucleus; KO = knockout (deletion) cell line.

Furthermore, analysis of the position of the new flagellum tip signal along the cell body showed that the deletion of FAZ16 caused a decrease in the number of cells with a new flagellum tip signal between the kinetoplast and nucleus, and an increase in the number of cells with a free new flagellum distal tip (Fig. 89A). However, the increase in cells with a free new flagellum tip was not due to premature new flagellum tip release from the groove as the number of 2K1N cells with a free new flagellum tip was comparable to the control (Fig. 89B-C). Therefore, the deletion of FAZ16 did indeed cause an increase in cells with two free flagella tips but this was attributed to a build-up of pre-cytokinetic cells rather than an increased proportion 2K1N cells with a free new flagellum tip.

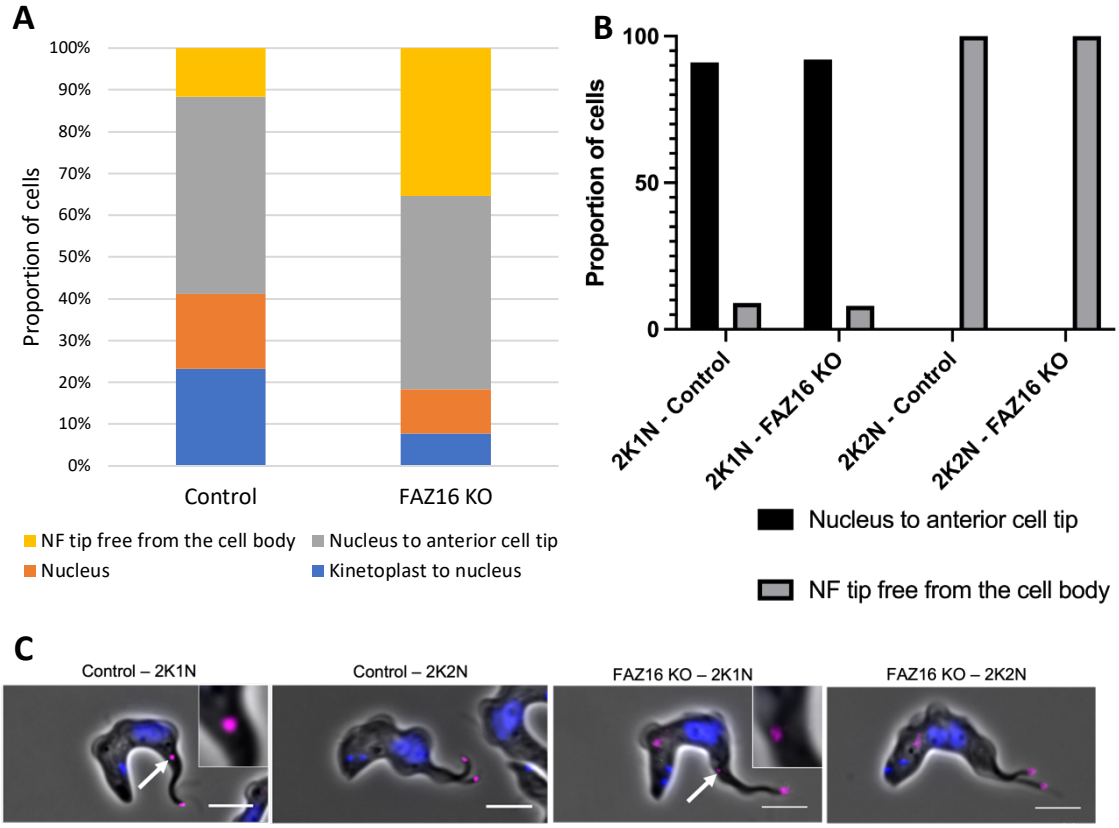

<u>Figure 89:</u> Deletion of FAZ16 caused an increase in pre-cytokinetic 2F cells. A) Position analysis of the new flagellum distal tip along the cell body. Deletion of FAZ16 caused an increased number of cells with a free new flagellum distal tip. N = 500 2F cells per cell line. B) Position analysis of the new flagellum distal tip in 2K1N and 2K2N cells. N = 100 cells per cell type in both cell lines. C) Representative images of the 2K1N and 2K2N cells from (B), arrow indicates new flagellum tip. Key: K = kinetoplast; N = nucleus; KO = knockout (deletion) cell line.

This was supported through SEM analysis, with the new flagellum of 77.3% of 2F cells embedded in the groove, (N = 108), which is comparable to the control cell line (77.3% 2F cells, N = 321) (Fig. 90A-C). Furthermore, the FAZ16 deletion did not affect the formation of the division fold (Fig. 90); however, there was an increase in multiflagellated cells (47.7%; N = 151) (Fig. 90F) compared to the control (3.5%; N = 423).

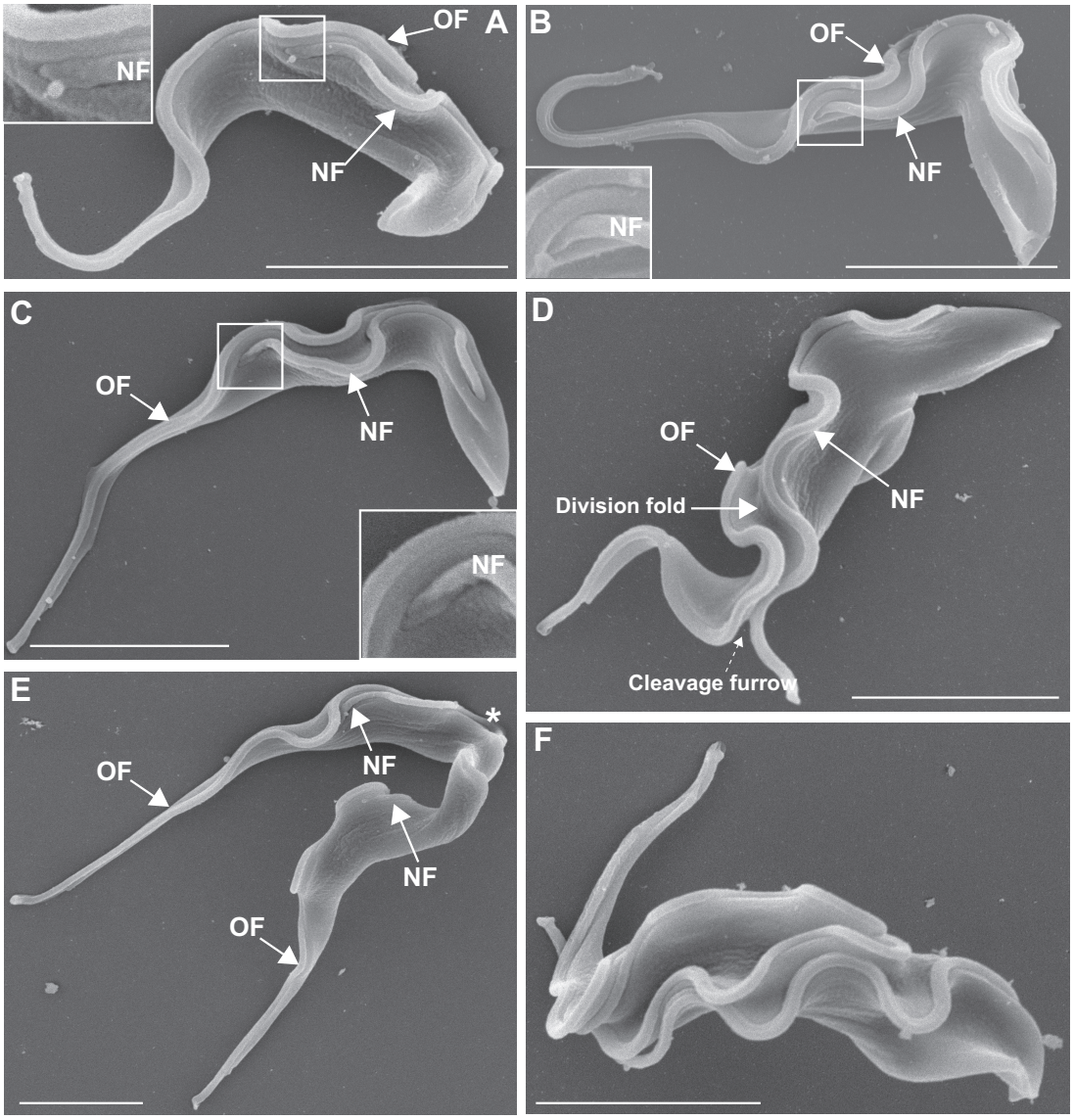

Figure 90: Deletion of FAZ16 caused an accumulation of multiflagellated cells. A-C) Distal tip of the new flagellum embedded in the groove. D) Distal tip of the new flagellum released from the groove and presence of the division fold and cleavage furrow. E-F) Multiflagellated cells, some still joined at the posterior end (E). Key: NF = new flagellum; OF = old flagellum; * = cytokinetic bridge. Scale = 5 μm.

Therefore, it is clear that the deletion of FAZ16 led to an accumulation of pre-cytokinetic 2F and multiflagellated cells, resulting in a cytokinesis defect and cell cycle delay.

6.4.3 Deletion of FAZ10 caused a minor delay to the cell cycle and new flagellum detachment from the cell body

FAZ10 localises to the intracellular domain of the FAZ in BSFs, with the depletion of FAZ10 resulting in delays to the cell cycle and flagellar detachment as a result of FAZ instability (Moreira *et al*., 2017). The deletion of FAZ10 was confirmed in one of three clones (clone 2) tested using PCR amplification (Fig. 91B). Furthermore, the FAZ10 deletion cell line grew at a slightly slower rate than the control cell line, potentially indicating a minor cell cycle delay (Fig. 91C).

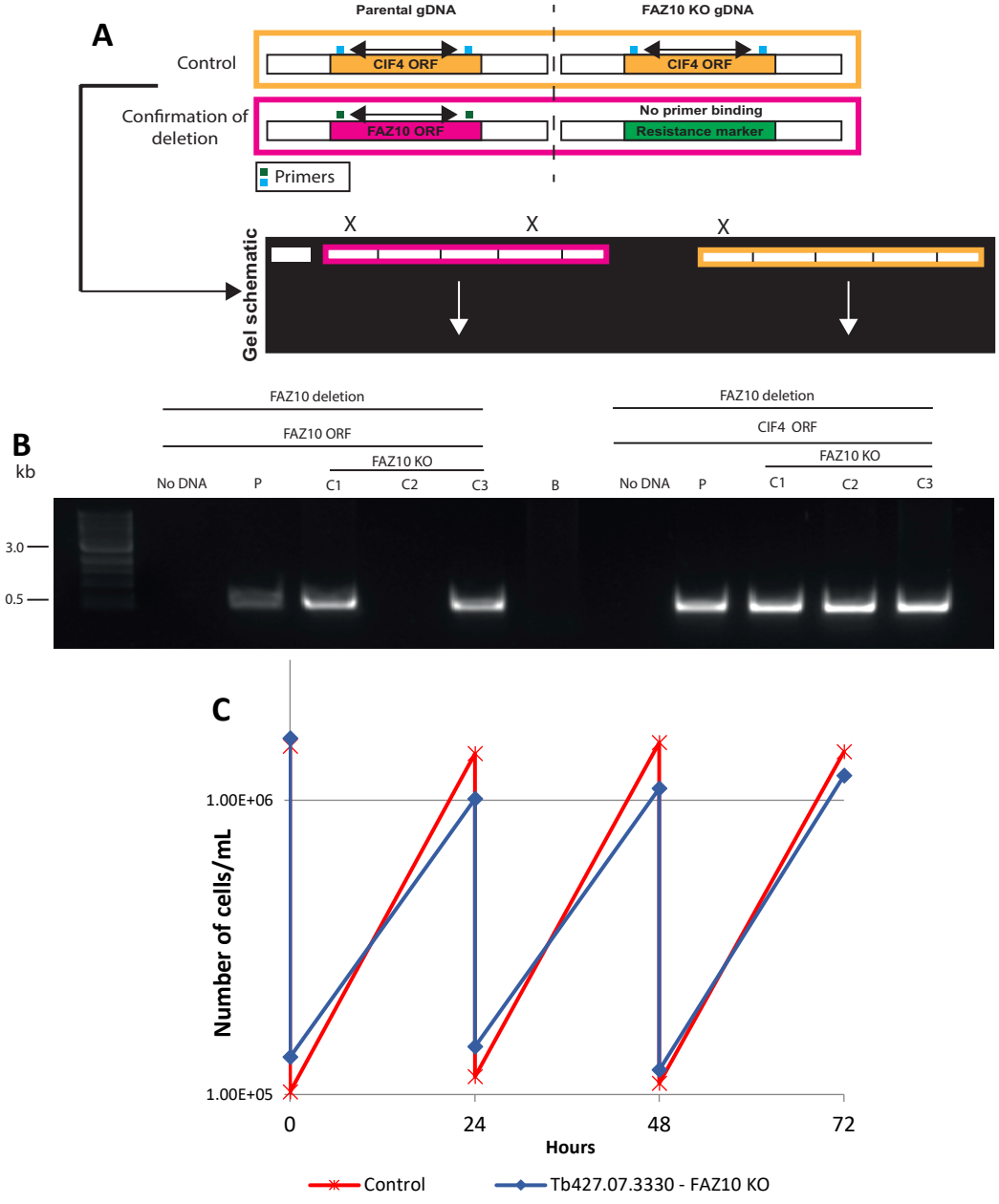

Figure 91: Deletion of FAZ10 was successful and caused a slight delay in the growth rate. A) Schematic for confirming the deletion of FAZ10. B) PCR confirmation of the deletion of FAZ10 clone 2

(left of gel). Controls include ddH_2O (no DNA) and parental genomic DNA (P) as well as constructs that recognise another gene (CIF4) as the positive control. C) Deletion of FAZ10 (blue) caused a slight growth defect.

Using widefield microscopy, it was observed that there was an increased number of 2K2N (arrowhead) cells in the FAZ10 deletion cell line compared to the control (Fig. 92A-B). Additionally, there was a visible increase in the number of free flagella on the slide compared to the control cell line (Fig. 92A-B, yellow arrows). Furthermore, the deletion of FAZ10 resulted in a reduction in 1K1N cells and an increase in 2K2N and >2K>2N cells (Fig. 92C). This suggested that the FAZ10 deletion caused a delay to the progression of the cell cycle through an accumulation of 2K2N and >2K>2N cells prior to cytokinesis.

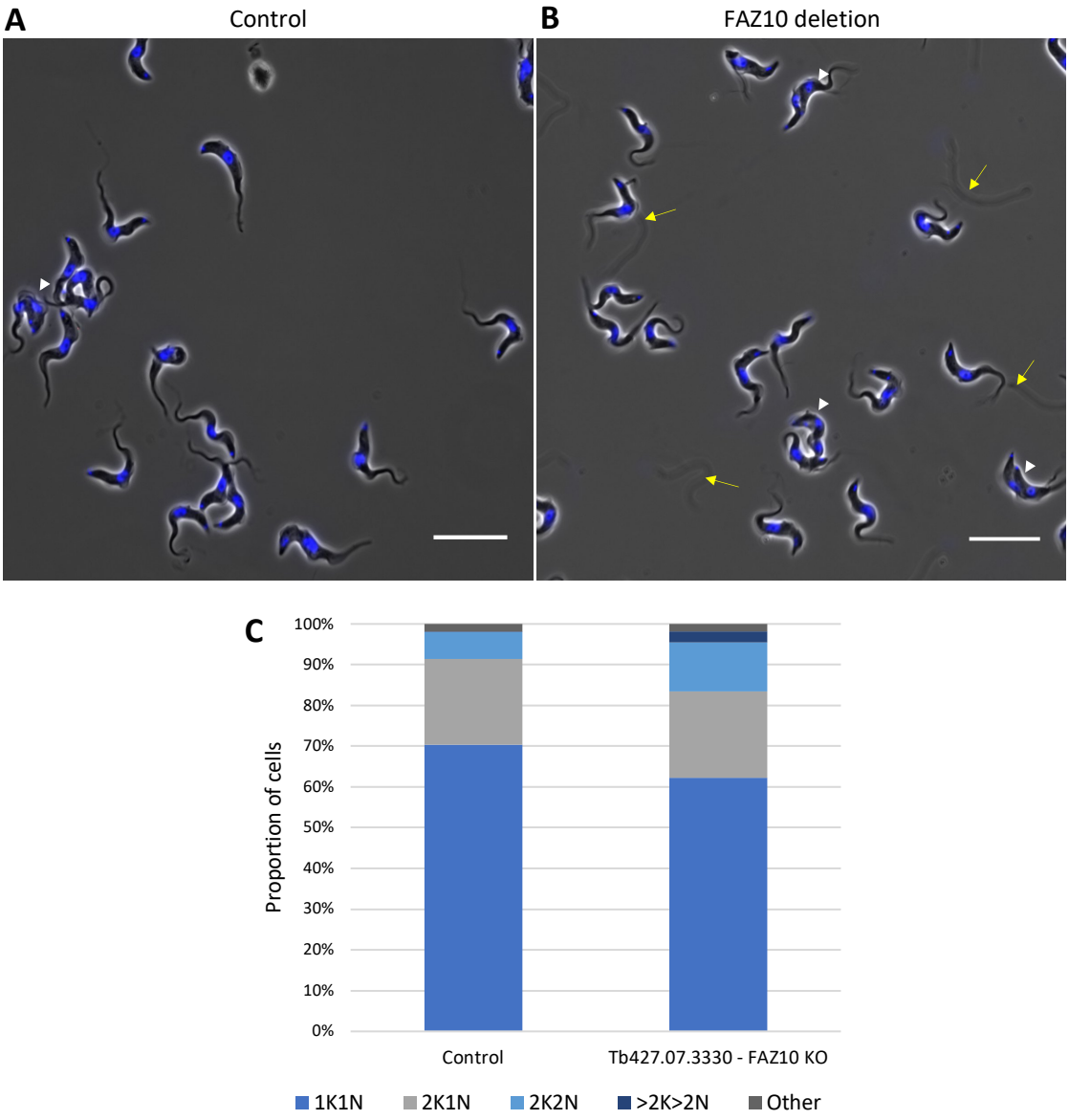

Figure 92: Deletion of FAZ10 caused an accumulation of 2K2N cells and free flagella. A-B) Representative images of the of the control (A) and FAZ10 deletion (B) cell lines. Deletion of FAZ10

caused an accumulation of 2K2N cells (arrowhead) and free flagella (yellow arrow). Scale = 10 μm. C) Deletion of FAZ10 caused a reduced number of 1K1N cells and an increased number of 2K2N and >2K>2N cells. N = 500 cells per cell line. Key: K = kinetoplast; N = nucleus; KO = knockout (deletion) cell line.

When examining the position of the new flagellum tip signal, it was clear that the FAZ10 deletion caused a decrease proportion of cells with a new flagellum tip signal between the kinetoplast and nucleus, and adjacent to the nucleus (Fig. 93A). This was matched with an increase in cells with a new flagellum distal tip signal between the anterior edge of the nucleus and anterior cell tip, as well as cells with a free new flagellum tip (Fig. 93A). This difference, however, is not attributed to premature new flagellum tip release from the groove, as the FAZ10 deletion cell line had a comparable proportion of 2K1N cells with a free new flagellum tip to the control (Fig. 93B). There was actually a significant decrease ($p<0.001$, Fisher's Exact Test) in the number of 2K2N cells with a free new flagellum tip in the FAZ10 deletion cell line (Fig. 93B-C, arrow), suggesting that the deletion may delay new flagellum tip release from the groove.

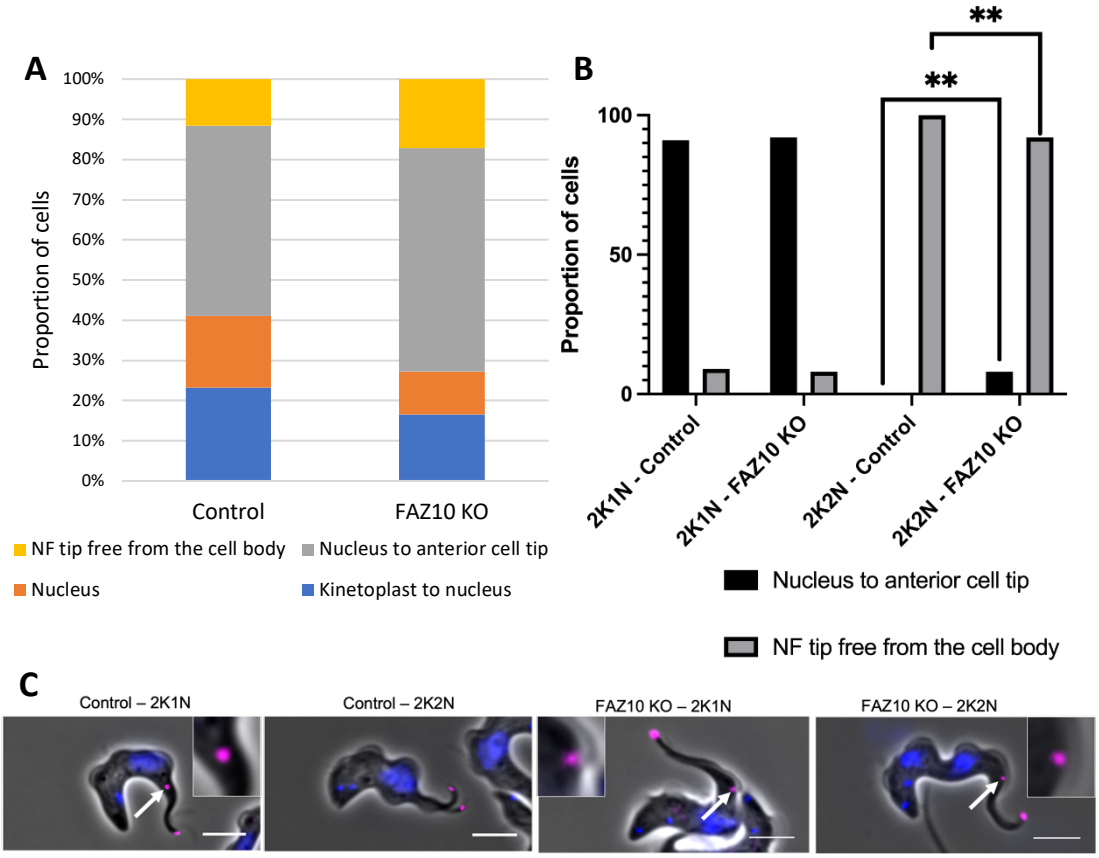

Figure 93: Deletion of FAZ10 caused an accumulation of cells with an attached new flagellum tip. A) Position analysis of the new flagellum distal tip along the cell body. Deletion of FAZ10 caused an accumulation in cells with a new flagellum tip signal visible between the anterior edge of the nucleus

and anterior cell tip, as well as an increase in cells with a free new flagellum tip. B) Position analysis of the new flagellum tip in 2K1N and 2K2N cells. Deletion of FAZ10 caused an increase in 2K2N cells with an attached new flagellum tip. N = 100 cells per cell type in both cell lines. ** = p=0.0065 by Fisher's Exact Test. C) Representative images of the 2K1N and 2K2N cells from (B), arrow indicates new flagellum tip. Key: K = kinetoplast; N = nucleus; KO = knockout (deletion) cell line.

SEM analysis showed that the FAZ10 deletion caused an accumulation of cells with 2-4 flagella each joined by their posterior ends (6.8%, N = 88) (Fig. 94D, asterisk) compared to the control cell line (2.1%, N = 423), suggesting that the deletion of FAZ10 may affect the abscission of the posterior ends during cytokinesis. The majority of 2F cells had a groove (74.4%; N = 74) (Fig. 94A-B); however, 6.7% of all 2F cells had a fully detached new flagellum, except for at the flagellar pocket (Fig. 94E-F). This suggests that the FAZ10 deletion may compromise the integrity of the FAZ, leading to flagellum detachment from the cell body. This was seen previously during FAZ10 depletion in BSF (Moreira *et al*., 2017) and supports the observation of free flagella stuck via widefield microscopy (Fig. 92B, yellow arrows). Potentially the centrifugation process prior to widefield microscopy caused these cells with a partially detached new flagellum to lose their flagellum entirely, resulting in free flagella stuck to the microscope slide (Fig. 92B, yellow arrows).

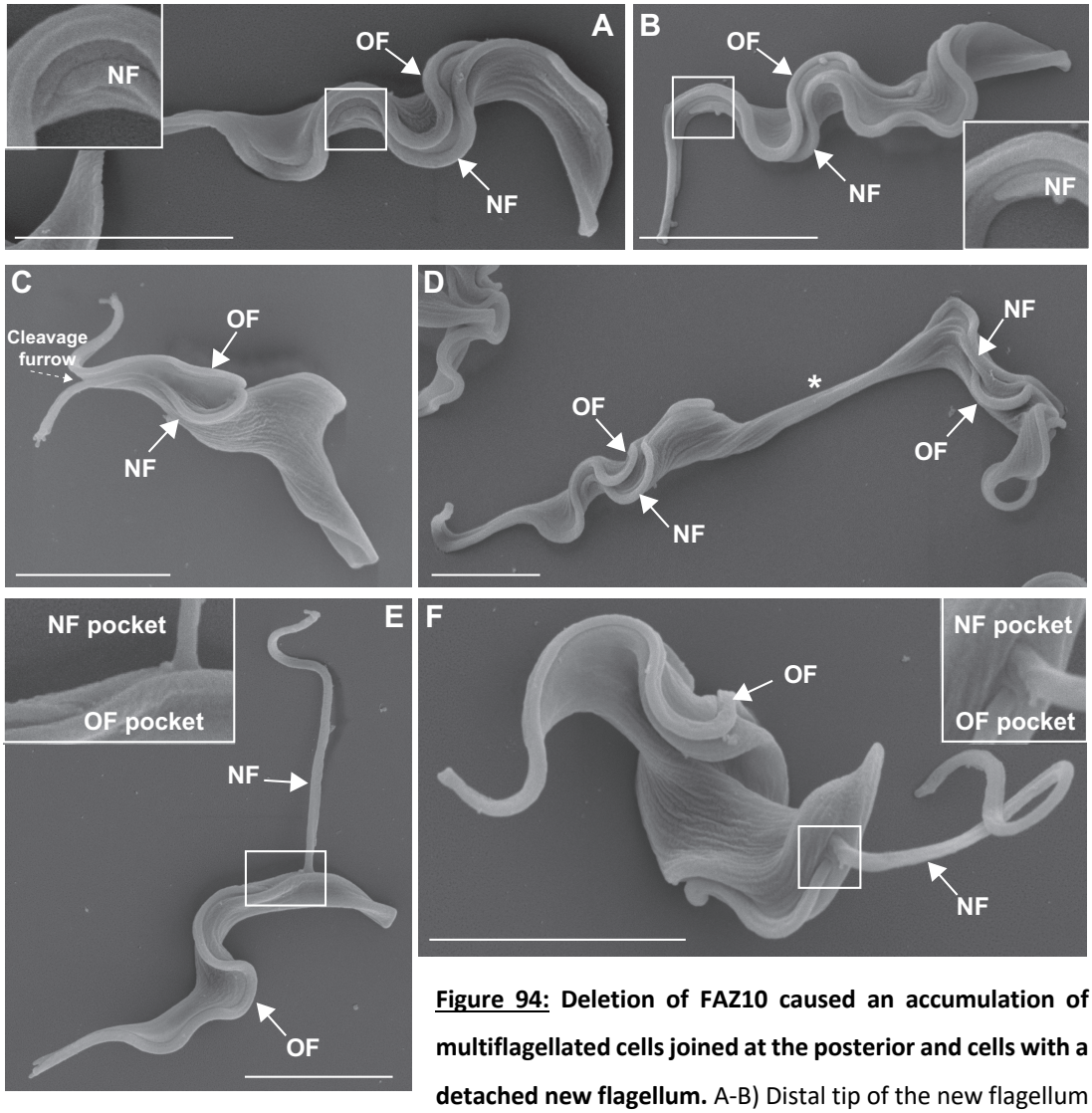

<u>Figure 94:</u> Deletion of FAZ10 caused an accumulation of multiflagellated cells joined at the posterior and cells with a detached new flagellum. A-B) Distal tip of the new flagellum embedded in the groove. C) Division fold present. D) Multiflagellated cells joined by their posterior ends by a cytokinetic bridge (asterisk). E-F) New flagellum is detached from the cell body. Key: NF = new flagellum; OF = old flagellum; * = cytokinetic bridge. Scale = 5 μm.

To summarise, the deletion of FAZ10 resulted in an accumulation of 2K2N and >2K>2N cells, causing a delay in the progression of the cell cycle. Furthermore, the FAZ10 deletion may affect the integrity of the FAZ, particularly the new FAZ, with an increased number of detached new flagella in both the SEM and widefield microscopy images.

6.4.4 Deletion of FCP5 caused a minor delay to the cell cycle but did not impact the groove

FCP5 (Tb427tmp.01.0400), a member of the ubiquitous Unc-51-like kinase (ULK4) family of proteins, is a protein that localised to the flagella connector in the PCF (Varga *et al*., 2017). The function and localisation of FCP5 has yet to be determined in the BSF. The deletion of FCP5 clone 3 (C3) was confirmed by PCR amplification (Fig. 95B).

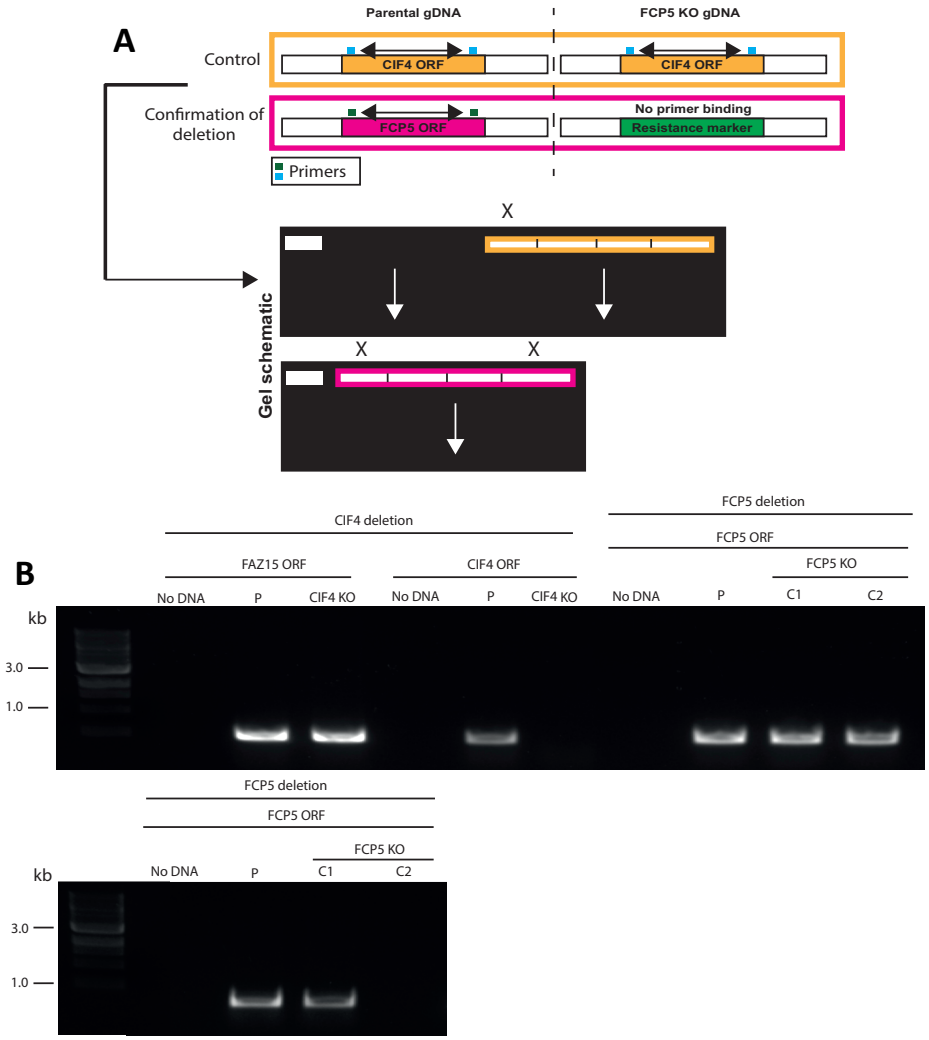

Figure 95: Deletion of FCP5 clone 2 was successful. A) Schematic for confirming the deletion of FCP5. B) PCR confirmation of the deletion of FCP5 clone 2 (C3). Controls include ddH_2O (no DNA) and parental genomic DNA (P). We also tested for the deletion of CIF4 as a control (left of gel).

It was observed that the deletion of FCP5 resulted in a slightly slower growth rate than the control cell line (Fig. 96A) and initial light microscopy examination showed that the deletion may have slightly increased the proportion of 2K2N cells compared to the control cell line (Fig. 96B-C).

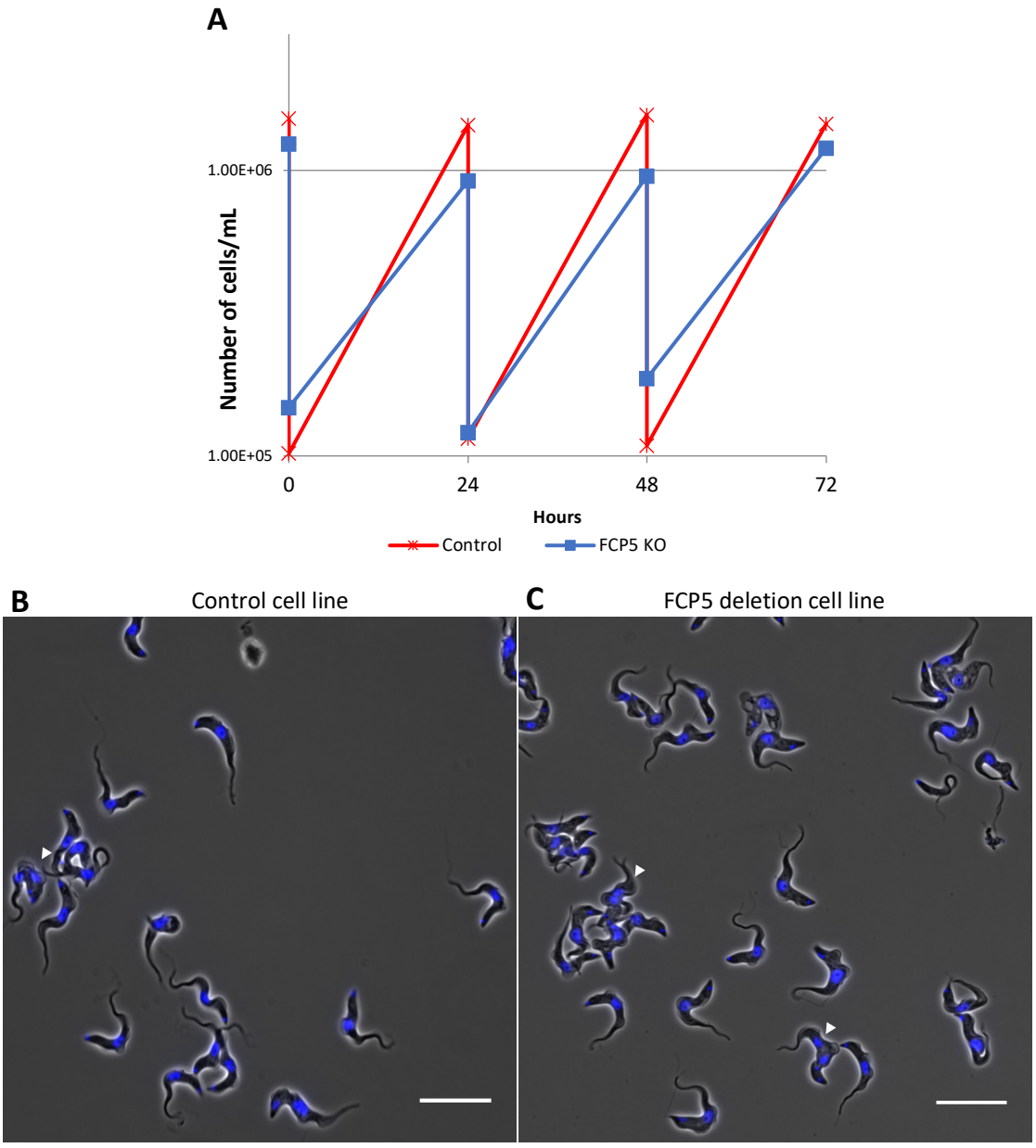

Figure 96: Deletion of FCP5 caused a growth defect. A) Deletion of FCP5 (blue) caused a slight growth defect. B-C) Representative images of the of the control (B) and FCP5 deletion (C) cell lines. Deletion of FCP5 caused an increased number of 2K2N (arrowhead) cells. Scale = 10 μm.

When analysing the cell cycle, we saw that the deletion of FCP5 caused a reduction in 1K1N and 2K1N cells and an increase in 2K2N and >2K>2N cells in the population (Fig. 97). This suggested that the deletion of FCP5 may cause a delay to the progression of the cell cycle, resulting in a slower growth rate compared to the control.

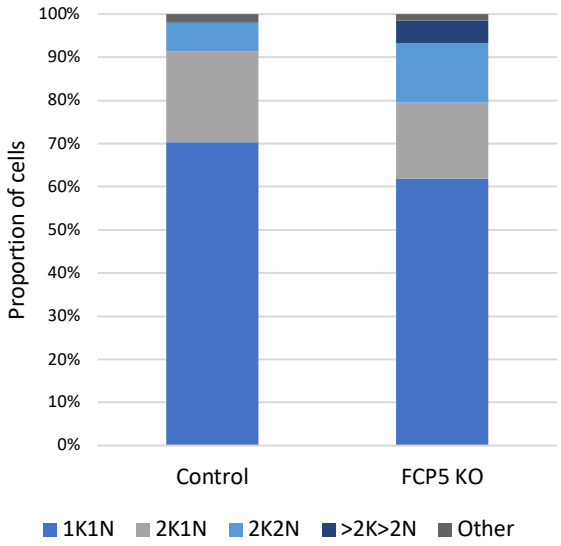

Figure 97: Deletion of FCP5 caused an accumulation of 2K2N and >2K>2N cells. Deletion of FCP5 caused a reduced number of 1K1N and 2K1N cells and an accumulation of 2K2N and >2K>2N cells. N = 500 cells per cell line. Key: K = kinetoplast; N = nucleus; KO = knockout (deletion) cell line.

Furthermore, we saw that the FCP5 deletion caused a slight reduction in the proportion of cells with a new flagellum tip signal present between the kinetoplast and nucleus, and adjacent to the nucleus (Fig. 98A). This was matched by an increase in cells with a new flagellum tip signal visible between the anterior edge of the nucleus and anterior cell tip, and cells with a free new flagellum tip (Fig. 98A). It was also seen that there was no significant difference in the number of 2K1N cells with a free new flagellum tip in the FCP5 deletion cell line compared to the control (Fig. 98B-C, arrow), suggesting that the deletion of FCP5 did not result in premature new flagellum tip release from the groove. This further suggests that there may be a minor delay to the cell cycle, most likely before cytokinesis due to the increased proportion of 2K2N and >2K>2N cells.

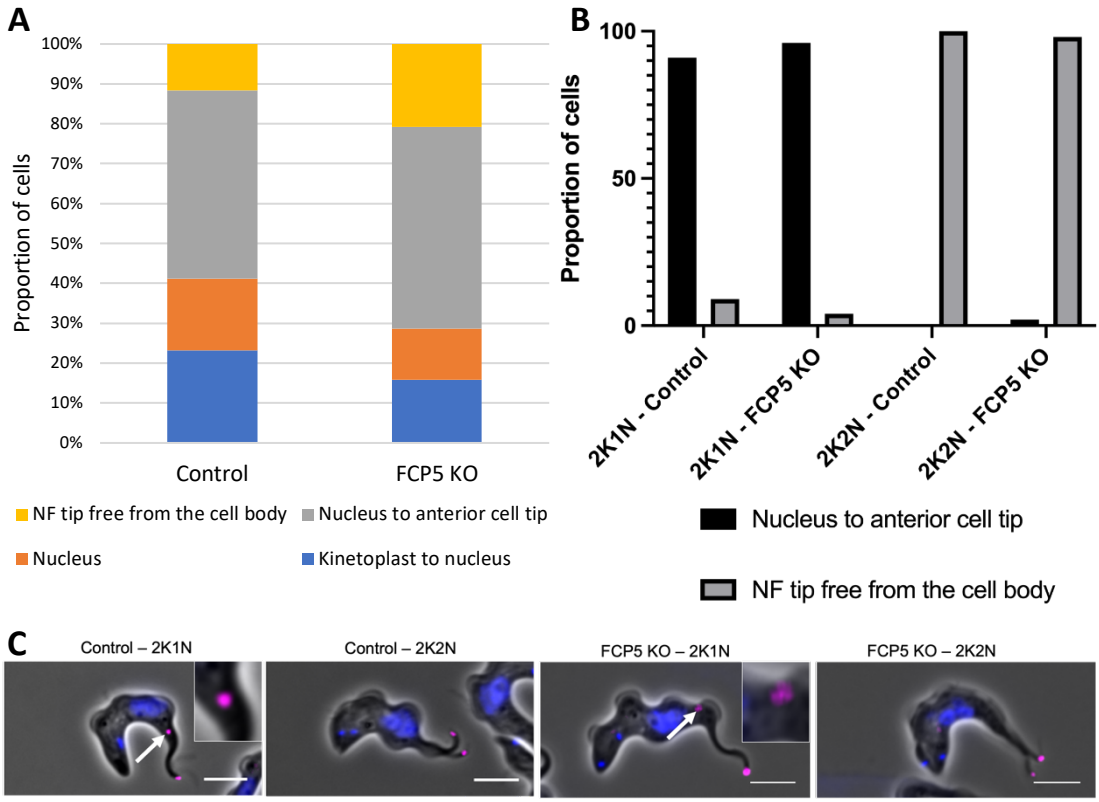

<u>Figure 98:</u> Deletion of FCP5 caused an accumulation of pre-cytokinetic cells. A) Position analysis of the new flagellum along the cell body. Deletion of FCP5 caused an accumulation in cells with a free new flagellum distal tip. N = 500 2F cells per cell line. B) Position analysis of the new flagellum distal tip in 2K1N and 2K2N cells. N = 100 cells with two flagella tip signals. N = 100 cells per cell type in both cell lines. C) Representative images of the 2K1N and 2K2N cells from (B), arrow indicates new flagellum tip. Key: K = kinetoplast; N = nucleus; KO = knockout (deletion) cell line.

The deletion of FCP5 did not appear to cause premature new flagellum tip release from the groove according to SEM, with a groove present in 71.4% of 2F cells (N = 53) like in the control (77.3% of 2F cells; N = 321) (Fig. 99A-B). However, the number of 2F cells with a free new flagellum distal tip increased slightly from 22.7% in the control cell line (N = 321 2F cells) to 28.6% (N = 49 2F cells) in the FCP5 deletion cell line (Fig. 99C-D). There was also a small proportion of multiflagellated cells in the FCP5 deletion population (7.5%; N = 53) (Fig. 99F). Altogether, this suggests that the deletion of FCP5 caused an accumulation of pre-cytokinetic 2F and >2K>2N cells, resulting in a slight delay to the cell cycle.

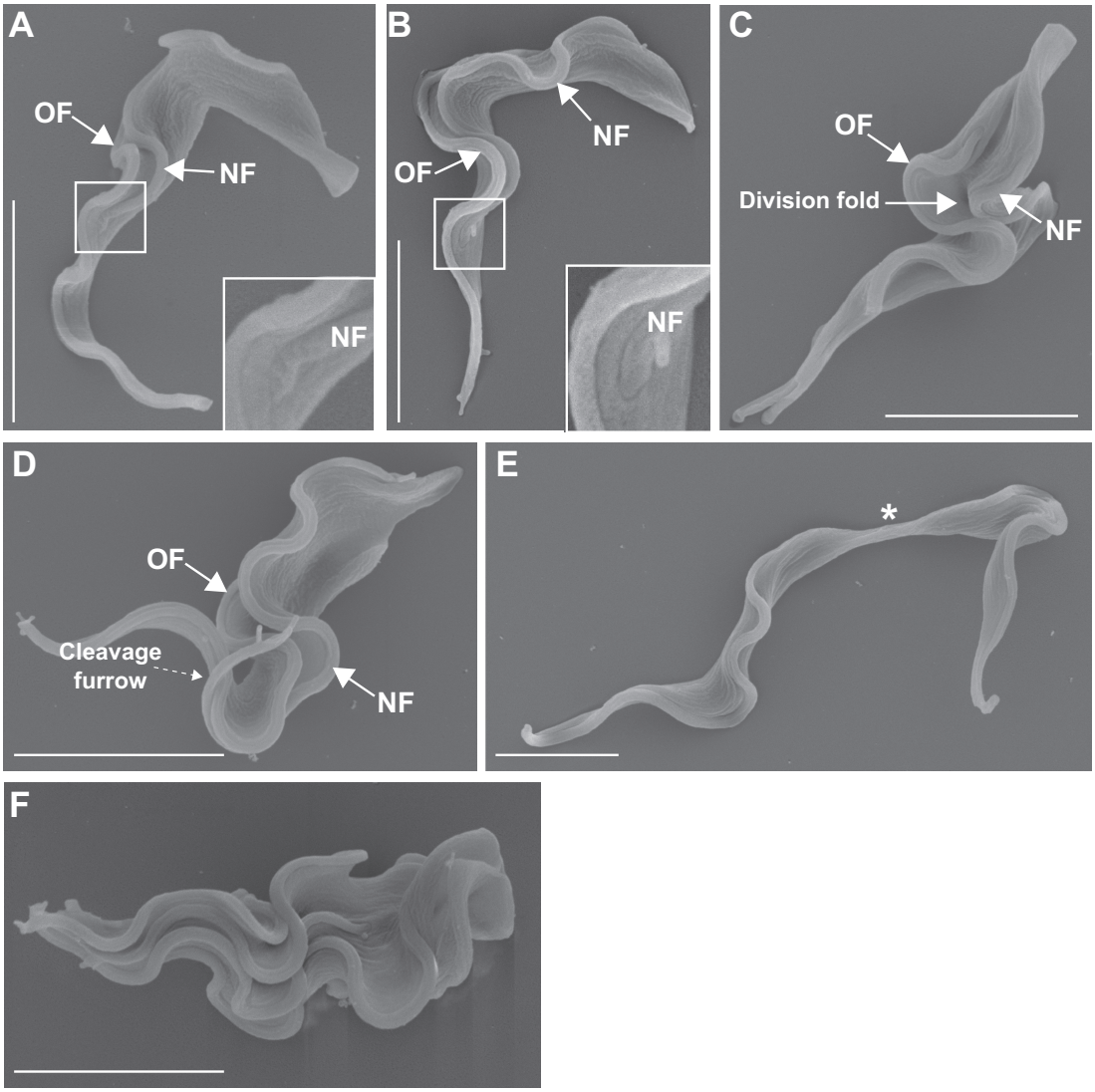

Figure 99: Deletion of FCP5 caused a minor accumulation of multiflagellated cells but no other observable defects. A-B) Distal tip of the new flagellum embedded in the groove. C-D) Division fold and cleavage furrow present. E) Cytokinesis occurring. F) Multiflagellated cell. Key: NF = new flagellum; OF = old flagellum; * = cytokinetic bridge. Scale = 5 μm.

7 Discussion

7.1 Preface

The aim of this PhD project was to identify the protein components of the bloodstream form flagellar groove, and to determine when the groove resolves. To achieve this aim, we endogenously tagged a cohort of putative flagellar groove proteins identified on the TrypTag database and used high resolution microscopy to investigate key cell cycle events surrounding groove resolution. I identified 13 proteins that localise to the BSF flagellar groove, with five distinct fluorescent patterns observed: 1) Full length FAZ and groove; 2) Distal FAZ and groove; 3) Groove only; 4) "Comet-tail"; 5) Complex.

Five genes were successfully deleted from the *T. brucei* BSF genome (Table 5). Two previously generated cell lines, with CIF4 and FAZ15 deleted respectively, were provided as positive controls for the PCR confirmation of the deletion of the other generated cell lines. The functional analysis of the groove proteins revealed three proteins involved in new flagellum tip attachment in the groove: CIF4, Tb427.01.2710 and FCP4, with their deletion/depletion resulting in premature new flagellum tip release from the groove. In contrast to this, the deletion of two proteins, Tb427tmp.01.3030 and FAZ15, appeared to cause delayed new flagellum tip release from the groove. Altogether, this suggests that the tethering of the new flagellum distal tip in the groove involves a complex arrangement of several proteins from the flagellum side and cell body side of the junction.

Furthermore, three proteins (CIF4, FAZ15 and FAZ16) appear to be involved in cytokinesis initiation, with the deletion of these proteins resulting in an accumulation of multiflagellated and multinucleic cells and a cell cycle delay and severe growth defect. The deletion of two further proteins, FAZ10 and FCP5, caused a delay in the growth rate and progression of the cell cycle, however, these proteins did not appear to be involved in new flagellum tip attachment in the groove. These results have provided a knowledge base of the composition and function of the groove.

7.2 Groove resolves as the new flagellum length exceeds the old flagellum length

The groove resolves to release the new flagellum distal tip in order to enter cytokinesis and complete the cell cycle. The exact timing of groove resolution was previously unknown (Hughes *et al*., 2013); however, using 3D reconstructions of several SBFSEM datasets, we have determined that groove resolution correlates with new flagellum length. We saw that as the new flagellum grew, there was a point at which the new flagellum length surpassed the old flagellum length, with this crossover occurring post-mitosis and correlating with groove resolution. In the reconstructed 2K2N cells in which the groove had resolved, the average length of the new flagellum (28.7 µm) was longer than average length of the old flagellum (25.0 µm). Interestingly, this differs slightly to the concept of FC resolution in the PCF, as the FC reaches a "stop-point" at approximately 0.6 of the length of the old flagellum; however, once the FC has halted its migration (Davidge *et al*., 2006), the new flagellum continues to elongate until it reaches approximately 80% the length of the old flagellum (Calvo-Álvarez *et al*., 2021). During this time, the cleavage furrow starts to ingress before the FC resolves and releases the new flagellum distal tip (Moreira-Leite *et al*., 2001; Briggs *et al*., 2004). The elongation of the new flagellum continues in the daughter cell inheriting that flagellum, until it reaches its maximum length which is equivalent to the flagellum of the daughter cell that inherited the old flagellum (Farr and Gull, 2009; Calvo-Álvarez *et al*., 2021), highlighting a clear morphogenetic difference between the PCF and BSF. However, it is clear that the FC "stop-point" is reached post-mitosis (Davidge *et al*., 2006), supporting a similarity between the growth of the new flagellum in the BSF and PCF.

Conversely, in our study we determined that in the BSF, the groove resolved when the new flagellum reached ˜1.16 the length of the old flagellum, suggesting that the length of the new flagellum may trigger groove resolution. Potentially, the fact that the FP associated with the new flagellum is positioned more posterior in BSFs than is seen in PCFs allows this extension to occur (Wheeler *et al*., 2013). Furthermore, the new flagellum does not appear to elongate once the groove has resolved, reaching its maximum length (averaging 27.5 µm) post-mitosis. Recently, it has been seen that FLAM8, a flagellum maturation marker, reaches its maximum expression at the distal tip of the new flagellum post-mitosis, suggesting that the new flagellum fully matures at this stage of the cell cycle (Calvo-Álvarez *et al*., 2021). This halt in new flagellum growth is reminiscent of the grow-and-lock model in PCFs (Bertiaux *et al*., 2018); however, the new flagellum does not continue to elongate in the daughter cell

inheriting that flagellum and may actually shorten during cytokinesis. The putative locking of new flagellum growth in the BSF post-mitosis may be advantageous by limiting protein turnover in the flagellum and energy expenditure when the cell is about to enter cytokinesis in the highly hazardous environment of the mammalian bloodstream.

The formation of the new anterior cell tip is required to complete cytokinesis; however, the mechanism for remodelling this area of the cell is still unknown. According to our SBFSEM data (Chapter 4) and previous literature (Hughes *et al*., 2017), we propose that the groove resolves prior to the formation of the anterior cell tip and is potentially the trigger for anterior cell tip remodelling. With this in mind, we have proposed three distinct models of groove resolution and anterior cell tip formation. The “Release” model depicts that as the groove approaches the anterior end of the cell, the new flagellum reaches its maximum length and is released from the groove. The groove resolves and the new anterior cell tip is formed from the point at which the new flagellum was released from the groove (Fig. 100) (Hughes *et al*., 2017). Experimental evidence shows that the detachment point of the new flagellum was ˜1 µm behind the detachment point of the old flagellum at the anterior cell tip and it has been hypothesised that this may be the point at which the groove resolves, and the new anterior cell tip is likely to form (Hughes *et al*., 2017).

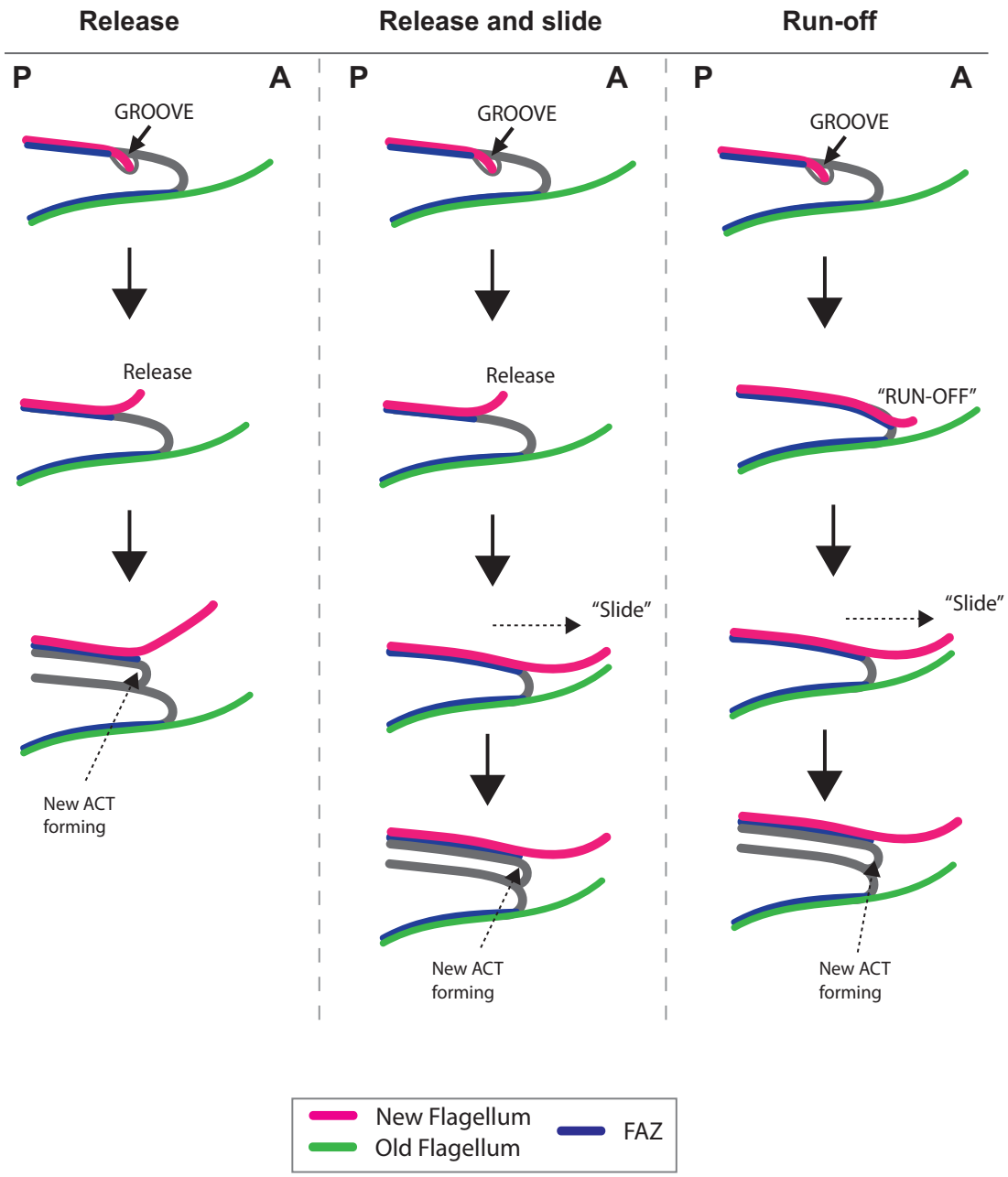

Figure 100: Proposed models for groove resolution and new anterior cell tip formation. The three models depicted are the **"**Release", "Release-and-slide" and "Run-off". Key: P = posterior; A = anterior; ACT = anterior cell tip.

The "Release-and-slide" model, on the other hand, depicts that once the new flagellum distal tip is released from the groove, the new flagellum slides along the outside of the cell body until the new flagellum tip overhangs the cell body. Furthermore, the new anterior cell tip is formed adjacent to the old anterior cell tip (Fig. 100). Potentially, the ability of the new flagellum to slide along the outside of the cell body is due to dynamic remodelling of other cytoskeletal components, such as the sliding of the subpellicular microtubules (Abeywickrema *et al*., 2019) or the proximal addition of FAZ proteins in a conveyor-belt

fashion resulting in the flagellum/FAZ complex sliding along the cell body (Sunter *et al*., 2015b). Finally, the "Run-off model" depicts that the new flagellum is released when the groove effectively "runs-off" the anterior cell tip, with the new anterior cell tip formed adjacent to the old anterior cell tip (Fig. 100).

The next thing to consider is how groove resolution and the remodelling of the subpellicular microtubule array are associated in each proposed model. In the "Release" model, if the site of groove resolution is indeed the site at which the new anterior cell tip is formed, then perhaps this occurs through plasma membrane in-folding in the residual gap in the microtubule array, where the groove was positioned prior to resolution (Fig. 101A-B). Perhaps, as predicted with the division fold (Campbell and De Graffenried, 2020), the microtubules at the site of groove resolution draw inwards to generate a membrane fold between the two nascent anterior cell tips (Fig. 101C-D). This may facilitate microtubule remodelling through depolymerisation/polymerisation at the new and old anterior cell tip through the extension of extant microtubules or the insertion of new microtubules into the array (Sherwin *et al*., 1987; Sherwin and Gull, 1989; Woodward and Gull, 1990). Furthermore, as with the division fold, it is likely that there is invasion and cross-link breakage between existing microtubules (Campbell and De Graffenried, 2020).

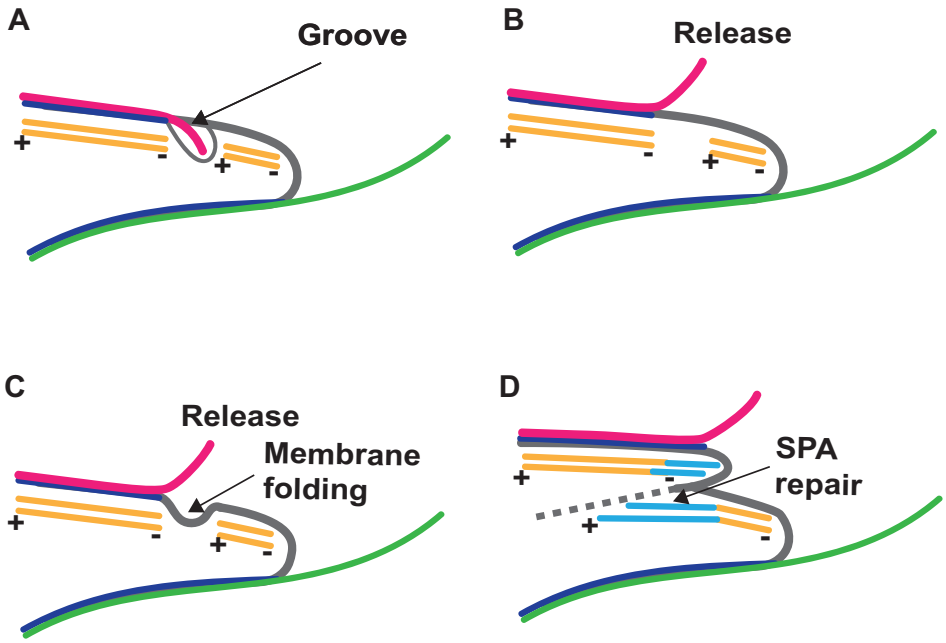

Figure 101: Subpellicular microtubule array repair in the "Release" model. A) The groove migrates to the anterior cell tip, bounded by subpellicular microtubules (SPA) on either side. B) The new flagellum tip is released from the groove, leaving a gap in the subpellicular microtubule array. C)

Membrane infolding in the post-groove gap. D) Nascent anterior cell tips defined by the remodelling of the subpellicular microtubules and membrane infolding. Key: + = plus-end of microtubules; - = minus-end of microtubules.

However, in the "Release-and-slide" model, as the new flagellum distal tip emerges from the groove, this gap may need to be repaired to maintain the highly ordered crosslinked microtubule array (Fig. 102A-B). The groove is bounded by subpellicular microtubules and considering the polarity of the subpellicular microtubule array (Robinson *et al*., 1995), it has been predicted that the proximal face of the groove is likely adjacent to the minus-ends of the subpellicular microtubules, whereas the distal face of the groove is likely adjacent to the plus-ends of the microtubules anterior to the groove (Fig. 102A) (Hughes *et al*., 2013). When the groove resolves and releases the distal tip of the new flagellum, the microtubule array may recover through the addition of tubulin dimers to the extant microtubules at the anterior cell tip or through the nucleation of new microtubules from the side of the extant microtubules (Sherwin and Gull, 1989; Sinclair and De Graffenried, 2019). The formation of the new anterior cell tip adjacent to the old anterior cell tip may involve the sorting and bundling of microtubules, as is seen at the posterior end of the cell during cleavage furrow ingression and the formation of two nascent posterior ends (Sinclair and De Graffenried, 2019).

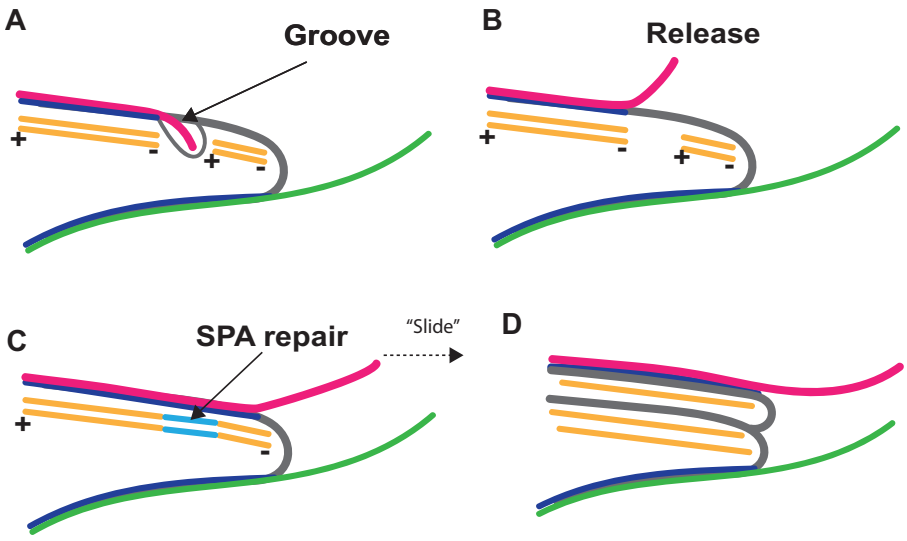

<u>Figure 102:</u> Subpellicular microtubule array repair in the "Release-and-slide" model. A) The groove migrates to the anterior cell tip, bounded by subpellicular microtubules on either side. B) The new flagellum tip is released from the groove, leaving a gap in the subpellicular microtubule array. C) Repair of the subpellicular microtubule array through tubulin dimer addition or insertion of new microtubules. D) Nascent anterior cell tips adjacent to each other defined by the remodelling of the subpellicular microtubules and membrane segregation.

Finally, in the "Run-off" model, when the groove resolves at the anterior cell tip (Fig. 103A-B), the subpellicular microtubules continue elongating through the addition of tubulin dimers posterior to the groove whereas the microtubules anterior to the groove may be depolymerised and broken down as the groove moves (Fig. 103C-D) (Sherwin and Gull, 1989; Robinson *et al*., 1995).

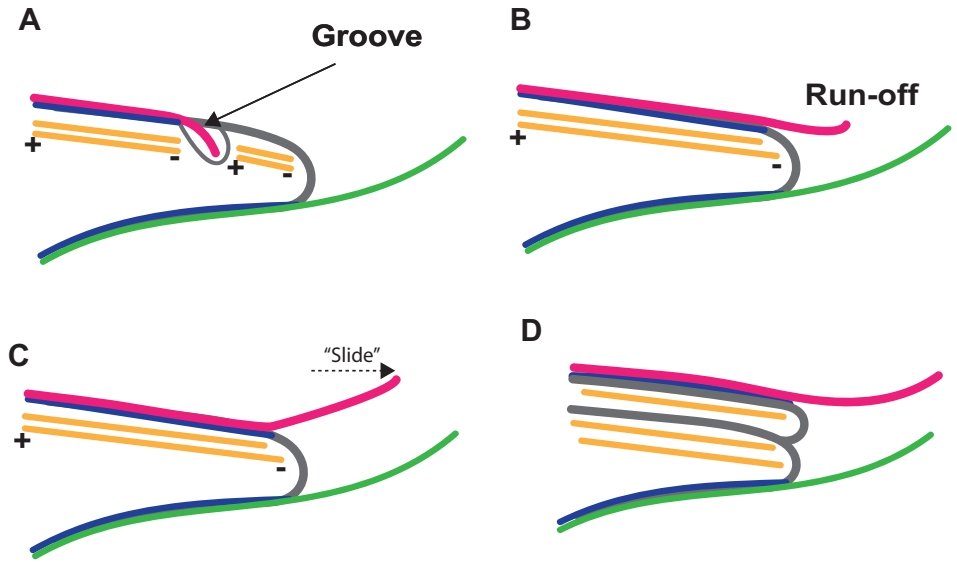

Figure 103: Subpellicular microtubule array repair in the "Run-off" model. A) The groove migrates to the anterior cell tip, bounded by subpellicular microtubules on either side. B-C) The groove "runs-off" the anterior cell tip, releasing the new flagellum tip before sliding along the outside of the cell body. The subpellicular microtubules continue elongating posterior to the groove to repair the gap left as the groove migrates. D) Nascent anterior cell tips adjacent to each other defined by the remodelling of the subpellicular microtubules and membrane segregation.

It is clear that further work on the remodelling of the anterior cell tip after groove resolution is necessary to understand the dynamics of the microtubules surrounding the groove and anterior cell tip, as well as how the proposed models are affected in mutant cell lines where cytokinesis is delayed, or premature new flagellum tip release occurs. Using 3D reconstruction to model the anterior region of cells during and after groove resolution is required to further understand the mechanics of the remodelling of this area of the cell prior to cytokinesis.

7.3 FCP4 and Tb427.01.2710 tether the new flagellum distal tip to the groove junction

Two proteins, FCP4 and Tb427.01.2710 are involved in new flagellum distal tip attachment to the groove junction, with their deletion and depletion resulting in premature new flagellum tip release from the groove. FCP4, a member if the ubiquitous kinesin-15 family of microtubule plus-end-directed motors is responsible for linking the plus ends of the extending new flagellum axoneme microtubules to the flagella connector (FC) membrane junction in PCFs (Varga *et al*., 2017). In our study, FCP4 localises specifically to the flagellar groove as a distinct foci around the new flagellum tip marker, suggesting that FCP4 is localised to the flagellum side of the groove cell junction. Furthermore, through bioinformatics, we have confirmed the presence of a conserved kinesin motor domain in the BSF which was previously identified in the PCF (Varga *et al*., 2017). This domain is responsible for ATP binding and hydrolysis (Sack *et al*., 1997), suggesting that FCP4 is capable of active motility (Varga *et al*., 2017). The depletion of FCP4 in our study resulted in premature new flagellum tip release from the groove, with this phenotype also seen when we deleted the putative FC protein Tb427.01.2710. As FCP4 links the axonemal microtubules to the FC in the PCF (Varga *et al*., 2017), this function may be conserved in the BSF, with FCP4 potentially linking the axonemal microtubules of the new flagellum to the groove junction during new flagellum growth. To confirm this, we would need to test the microtubule binding activity of FCP4 and is something to consider for future work. Using high-resolution Immunogold-EM would help to identify where exactly FCP4 and Tb427.01.2710 localise in the groove, as has been done previously for the FC with great success (Varga *et al*., 2017).

7.4 The groove is an elaboration of the FAZ

The groove has been described as an elaboration of the FAZ due to the presence of an electron-dense network of filaments underlying the cytoplasmic face of the groove, with filaments radiating across the cell body plasma membrane through the flagellar membrane (Hughes *et al*., 2013). Previously, it has been confirmed that FAZ10 localises to the groove through DOT-1 antibody localisation supporting the hypothesis that the groove may be an elaboration of the FAZ; however, as FAZ1 is absent from the groove itself, these filament extensions do not represent a canonical FAZ filament (Hughes *et al*., 2013).

In our study, we have identified several known FAZ proteins that localise to the flagellar groove in the BSF, supporting the hypothesis that the transmembrane filament extensions present in the groove may represent an elaboration of the FAZ. These proteins include FLAM3, FAZ2, FAZ10, FAZ15 and FAZ16 (Rotureau *et al*., 2014; Sunter *et al*., 2015a; Sunter and Gull, 2016; Moreira *et al*., 2017; An and Li, 2018). These proteins were chosen for our screen due to their localisation to the distal FAZ and full length FAZ on TrypTag (http://tryptag.org). In both PCFs and BSFs, FLAM3 has been seen to localise to the flagellum filament of the FAZ and to the FC (Rotureau *et al*., 2014; Sunter *et al*., 2015a; An and Li, 2018); however, FAZ2 localises to the cell body FAZ filament in PCFs (Sunter *et al*., 2015a). FAZ10, on the other hand, localises to the intermembrane staples in the intraflagellar zone of the FAZ in PCFs and BSFs (Moreira *et al*., 2017). It is clear that the groove contains essential FAZ proteins involved in the structure and stability of the transmembrane junction from both the flagellum membrane and cell body membrane sides of the junction (Sunter *et al*., 2015b).

FLAM3 contains an N-terminal CLU (CLUstered mitochondrion) domain, with the mammalian orthologue, CLUH, linked to cytoskeletal remodelling (Gao *et al*., 2014), raising the possibility of the CLU-domain aiding in the cytoskeletal activity of FLAM3 in the FAZ of *T. brucei*. Furthermore, FAZ10 and FAZ2 both contain coiled-coil domains, suggesting their involvement in FAZ stability (Sunter *et al*., 2015a; Moreira *et al*., 2017). As FLAM3 and FAZ10 are highly conserved across all kinetoplastids examined by RBB, it is possible that these proteins may have initially evolved to function in FAZ stability and were subsequently co-opted to maintain the stability of the groove junction in BSFs. However, FAZ2 is well conserved across all kinetoplastids, except *Bodo saltans*, suggesting that FAZ2 may have evolved with the ancestral divergence from biflagellate free-living organisms to monoflagellated parasitic organisms (Flegontov *et al*., 2013; Jackson *et al*., 2016; Skalicky *et al*., 2017).

Two trypanosomatid-specific proteins, FAZ15 and FAZ16, were identified as interactors of TbPLK at the tip of the new FAZ in PCFs (McAllaster *et al*., 2015); however, their localisation and function in BSFs has yet to be explored. The deletion of both proteins in our study caused a cytokinesis defect, suggesting a role in cytokinesis initiation; however, with a lack of identified protein domains in FAZ15, it is difficult to predict how this might occur. We identified the presence of a C-terminal LysM domain in FAZ16 which was intriguing as LysM domains are mostly associated with chitinase domains in a variety of algae and nematodes

(Ponting *et al*., 1999; Spaink, 2004). Potentially, the FAZ16 LysM domain may be involved in signal transduction, as LysM domain receptors in various plant species (*Lotus japonicus* and *Medicago truncatula*) are involved in the recognition of lipochitin oligosaccharide signal molecules secreted by symbiotic and pathogenic bacteria (Spaink, 2004). Perhaps, the cytokinesis defect due to the FAZ15 and FAZ16 deletions may merely be due to the instability of the new FAZ, as it has been seen that the absence of certain integral FAZ components does indeed disrupt cytokinesis, such as FLAM3, FAZ1, FAZ10 and FAZ2 (Sunter *et al*., 2015a; Sunter and Gull, 2016; Moreira *et al*., 2017).

Despite the presence of several FAZ proteins in the groove, the filament extensions in the groove junction are decidedly more complex than the canonical FAZ filament in that these extensions have to undergo dynamic change to facilitate the release of the new flagellum distal tip during groove resolution. The mechanism for this release is still unknown, however, it is clear that this has to occur in order for the groove to resolve. Further investigation using Immuno-EM and immunoprecipitation are needed to identify the precise localisation and interaction of these proteins in order to fully understand how the groove resolves and releases the new flagellum distal tip.

7.5 The full embedding of the new flagellum distal tip in a groove appears to be unique to *T. brucei*

In previous work, the presence of the groove in bloodstream form *T. brucei* cells was hypothesised to be an evolutionary adaptation to enhance parasitaemia in the mammalian host (Hughes *et al*., 2013). However, it is still unknown as to whether other trypanosomatid parasites that infect mammalian hosts possess a groove or not, despite all 13 identified groove proteins being conserved in the African Trypanosomatids, *T. vivax* and *T. congolense*. Therefore, we examined two closely related trypanosomatid species to *T. brucei* by SBFSEM to determine if the groove was a conserved structure.

3D surface rendering and modelling of trypomastigote cells from the *T. congolense* and *T. vivax* BSF were compared to a *T. brucei* 427 parental culture strain to determine if these species possess a groove or not. We determined that the culture adapted IL3000 *T. congolense* strain did not possess a canonical groove where the distal tip of the new flagellum is fully embedded in the cell body plasma membrane. However, we observed that the distal

tip of the new flagellum in *T. congolense* is positioned in a shallow indentation in the cell body plasma membrane. This observation is reminiscent of the so-called "groove in the plasma membrane" seen in *Peranema trichophorum* (Roth, 1959). According to Roth (1959), the ridges of the pellicle underlying the plasma membrane are adapted to form a groove in which the trailing flagellum lies. Furthermore, tubular elements extending across the membrane and penetrating the outer zone of the flagellum were observed in the free-living phagotrophic Euglenozoa, *Peranema trichophorum* (Roth, 1959), raising an interesting question as to the presence of filamentous extensions connecting the distal tip of the new flagellum to the plasma membrane in this shallow indentation in *T. congolense*. The flagella in *Hydra attenuate* are also positioned within a groove in the pellicle (Wood, 1959), as are the shorter flagella in the trophozoite form of the fish-infective ectoparasite and kinetoplastid, *Ichtyobodo salmonis* (Isaksen *et al*., 2011), suggesting that the presence of plasma membrane indentations in which flagella are positioned may be a more common occurrence that thought. Furthermore, perhaps the depth of the groove seen in *T. brucei* BSFs is unusual and has been specifically adapted in this particular strain of kinetoplastid parasite. With the technological development of SBFSEM, identifying the presence of groove-like structures or adaptations in a variety of organisms is possible, allowing us to further define the criteria for a flagellar groove.

The 3D reconstruction of *T. vivax* cells isolated from the bloodstream of infected mice poses interesting trypanosomatid-related biological questions. We saw that the distal tip of the growing new flagellum was not associated with the cell body plasma membrane in the same way as *T. brucei*, or even *T. congolense*. Instead, the new flagellum distal tip is tilted away from the cell body as the new flagellum grows, with no evidence of plasma membrane invagination associated with the new flagellum distal tip (Fig. 104). However, the new flagellum distal tip is in close proximity to the lateral surface of the old flagellum, reminiscent of the *T. brucei* FC (Fig. 104), suggesting the possibility that the BSF form of *T. vivax* has repurposed this PCF-specific transmembrane junction for new flagellum growth. Interestingly, *T. vivax* possesses orthologous proteins of all the FC proteins included in our screen according to TritrypDB (https://tritrypdb.org/tritrypdb/app) (**Appendix D**), supporting the hypothesis that the BSF of *T. vivax* appears to utilise a FC. The resolution of SBFSEM is limited, therefore, higher resolution thin-section TEM or electron tomography is needed to investigate this hypothesis in more detail.

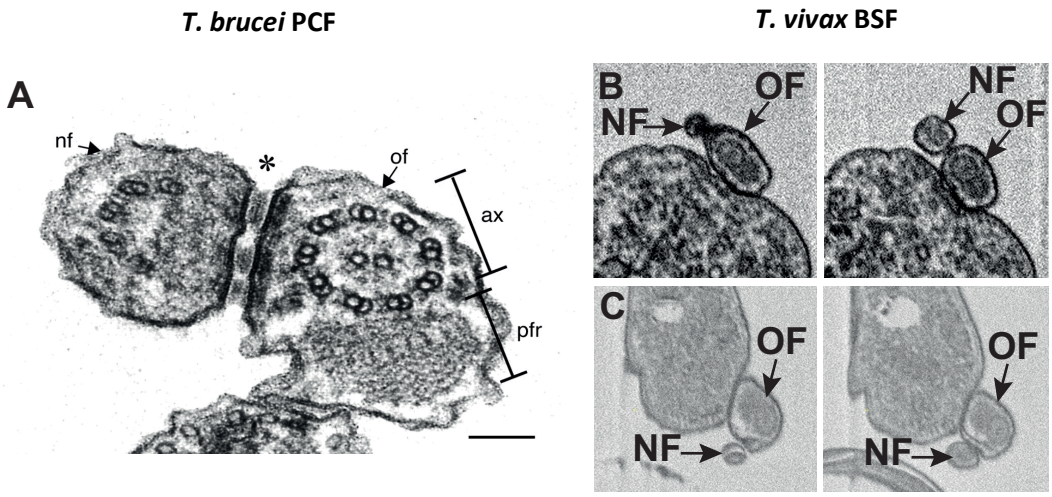

Figure 104: The *T. brucei* FC versus the *T. vivax* BSF new flagellum distal tip. A) Transverse section through the FC in the PCF of *T. brucei* showing the FC joining two flagella external to the cell body (Reproduced with copyright permission from The Company of Biologists, taken from Briggs *et al*., 2004). B-C) Transverse sections through the flagella of two individual *T. vivax* BSF cells, with a short (B) and a longer new flagellum (C). The new flagellum appears to be physically touching the old flagellum external to the cell body. Key: OF = old flagellum; NF = new flagellum; Ax = axoneme; PFR = paraflagellar rod.

Despite the close phylogenetic relationship between the three trypanosomatids, all three display species-specific adaptations regarding the distal tip of the new flagellum during new flagellum growth, possibly as a result of tissue tropism-specific adaptations, which can have a direct impact on the parasite life cycle through promoting persistence in the host (Pereira *et al*., 2019). As *T. brucei*, *T. vivax* and *T. congolense* alternate between the insect vector and the mammalian host, distinct adaptations are evident in the chosen ecological niche of each parasite species. In the insect vector, the tsetse fly, *T. brucei* PCFs migrate towards the salivary glands, whereas, *T. congolense* PCFs colonise the proboscis (Pereira *et al*., 2019). *T. vivax*, on the other hand does not have a PCF stage and instead colonises the fly mouthparts as soon as the fly takes an infected bloodmeal (Pereira *et al*., 2019). The lack of a PCF stage during the lifecycle of *T. vivax* poses an interesting biological question as to why a *T. brucei* PCF-specific structure, the FC, may have been repurposed in the BSF of *T. vivax*.

Furthermore, it was hypothesised that the groove was specifically adapted to reduce the exposure of parasite proteins present in an external structure, like the FC, from being

exposed to the mammalian immune system (Hughes *et al*., 2013). This raises the question as to the biological advantage of having a FC in the BSF of *T. vivax* when these parasites operate both extracellularly and intravascularly (Pereira *et al*., 2019). In the BSF trypomastigote, a discrete FC structure might enhance the exposure to the mammalian antibodies when the FC is resolved at the end of the cell cycle by leaving an exposed face on the FC when the two cells split (Davidge *et al*., 2006; Hughes *et al*., 2013). Perhaps, the presence of a FC in the BSF of *T. vivax* may be due to the parasite being capable of intravascular invasion as well as extracellular and extravascular replication (Pereira *et al*., 2019). However, the reasons as to why certain parasite life cycle forms choose specific tissues or environments is poorly understood but are more than likely multifactorial and need to be investigated further in the future (Pereira *et al*., 2019).

7.6 Concluding remarks and future perspectives

The discovery of groove proteins in the bloodstream form of *T. brucei* was initiated by analysing the PCF localisation database, TrypTag (http://tryptag.org). Since these two lifecycle forms are biologically and morphogenetically different (Wheeler *et al*., 2013), this creates the potential for missing BSF-specific proteins during our initial candidate search. As the flagellar groove is a structure specific to the BSF (Hughes *et al*., 2013; this work), there may be key proteins involved in the structure and function of the groove absent from our screen. Furthermore, proteins like FCP5 have distinctly different localisation pattern between the PCF and BSF (Varga *et al*., 2017; this work), suggesting that there may be proteins present in the PCF that did not fall into our search criteria of "Distal FAZ", "Anterior cell tip" or "flagella connector" as they localised elsewhere in the PCF, however, in the BSF these protein may localise to the flagellar groove. This raises the possibility of there being potential groove proteins yet to be discovered. Future research should focus on identifying further groove proteins using techniques such as immunoprecipitation to give further insight into the complexity of the groove in the BSF of *T. brucei*.

We identified 13 proteins that localise to the flagellar groove (Chapter 5) and together with the results from the deletion screen and previous literature, we have proposed a map of putative groove protein localisation (Fig. 105). The model of the groove is compared to a model of the FC (adapted from Varga *et al*., 2017) to highlight similarities and difference between these two transmembrane junctions in *T. brucei*.

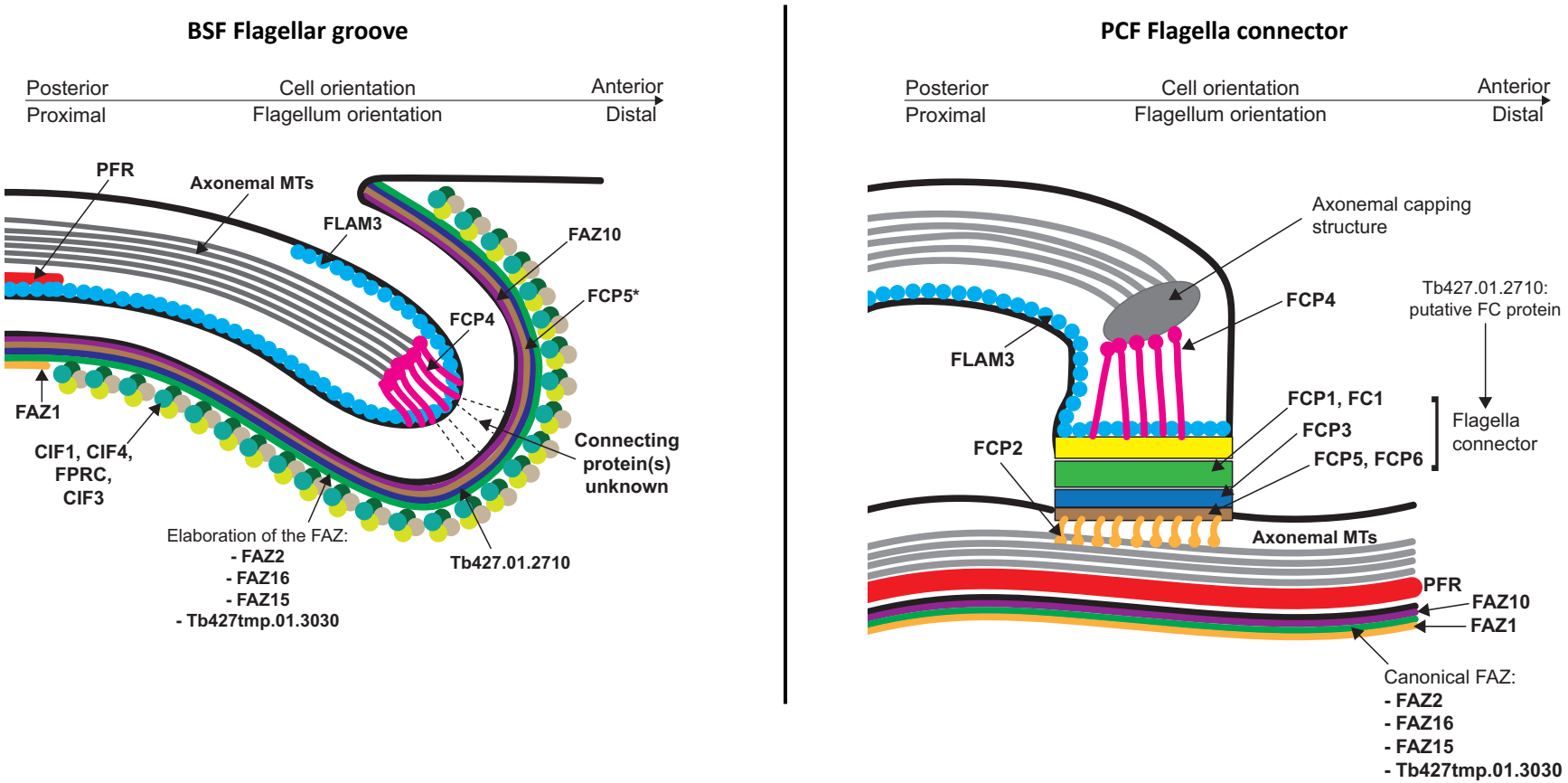

<u>Figure 105:</u> Comparative models of the composition of the groove in the BSF and flagella connector in the PCF of *T. brucei*. Key: * = FCP5 localises also to the cytoplasm, nucleoplasm and basal body pair (FC schematic adapted from Varga *et al.*, 2017).

In summary, on the flagellum side of the groove junction, FLAM3 is hypothesised to localise to the flagellum filament extensions of the elaboration of the FAZ predicted to be present in the groove (Rotureau *et al*., 2014; Sunter *et al*., 2015a; An and Li, 2018) (Fig. 105). FCP4 is hypothesised to localise to the flagellum side of the groove, potentially involved in axonemal microtubule binding activity as seen in the FC in PCFs (Varga *et al*., 2017) (Fig. 105). FAZ1 does not localise to the groove (Hughes et al., 2013); however, it is hypothesised that FAZ10, FAZ2, FAZ16, FAZ15 and Tb427tmp.01.3030 localise to the cell body side of the groove according to their localisation pattern in our screen (Chapter 5), highlighting the presence of an elaboration of the FAZ present in the groove (Fig. 105). CIF1, CIF3, CIF4 and FPRC may form a complex on the cell body side of the groove, as they do at the new FAZ in the PCF (Kurasawa *et al*., 2018; Zhang *et al*., 2019) (Fig. 105). FCP5, on the other hand, appears to localise to the cell body side of the groove (Chapter 5), contrary to its localisation in zones 4-5 in the FC (Varga *et al*., 2017) (Fig. 105). In the BSF, FCP5 also localises to elsewhere in the cell (Chapter 5), suggesting that FCP5 has been repurposed for a more general cell biology role than seen in the PCF. Another putative FC protein, Tb427.01.2710, is predicted to be localised to the cell body side of the groove; however, the precise localisation of Tb427.01.2710 remains unknown in the FC as well (Fig. 105).

All 13 groove proteins are conserved in the BSF of *T. vivax* and *T. congolense*, however, both of these species lack the canonical groove seen in *T. brucei*. This raises an interesting question as to where do these groove proteins localise in the other trypanosomatids? Using endogenous tagging, it may be possible to examine the localisation of the groove proteins in the BSF culture form of *T. congolense*, which may help to further understand the difference in the association between the cell body and the new flagellum distal tip in these three species.

The groove is a key structure during new flagellum growth in the bloodstream form of *T. brucei*. Contributing to previous research on the groove, we have investigated the protein composition of this complex transmembrane structure and revealed functional groups involved in cytokinesis initiation and new flagellum distal tip attachment to the groove. Furthermore, we have determined that the groove resolves as the new flagellum surpasses the old flagellum in length, and that this event occurs post-mitosis and prior to cytokinesis. Further understanding of the groove may provide information on possible weaknesses in the

trypanosome's life cycle that could be examined for exploitation in the future with novel targets for vaccine research and disease control schemes.

8 References

Abedin, M., & King, N. (2010). Diverse evolutionary paths to cell adhesion. *Trends in cell biology*, *20*(12), 734–742. https://doi.org/10.1016/j.tcb.2010.08.002

Abeywickrema, M., Vachova, H., Farr, H., Mohr, T., Wheeler, R. J., Lai, D. H., Vaughan, S., Gull, K., Sunter, J. D., & Varga, V. (2019). Non-equivalence in old- and new-flagellum daughter cells of a proliferative division in Trypanosoma brucei. *Molecular Microbiology*, *112*(3), 1024–1040. https://doi.org/10.1111/mmi.14345

Aksoy, S., Attardo, G., Berriman, M., Christoffels, A., Lehane, M., Masiga, D., & Toure, Y. (2014). Human African Trypanosomiasis Research Gets a Boost: Unraveling the Tsetse Genome. *PLoS Neglected Tropical Diseases*, *8*(4), 6–8. https://doi.org/10.1371/journal.pntd.0002624

An, T., & Li, Z. (2018). An orphan kinesin controls trypanosome morphology transitions by targeting FLAM3 to the flagellum. *PLoS Pathogens*, *14*(5), 1–24. https://doi.org/10.1371/journal.ppat.1007101

Autheman, D., Crosnier, C., Clare, S., Goulding, D. A., Brandt, C., Harcourt, K., Tolley, C., Galaway, F., Khushu, M., Ong, H., Romero-Ramirez, A., Duffy, C. W., Jackson, A. P., & Wright, G. J. (2021). An invariant Trypanosoma vivax vaccine antigen induces protective immunity. *Nature*, *595*(7865), 96–100. https://doi.org/10.1038/s41586-021-03597-x

Bastin, P., Sherwin, T., & Gull, K. (1998). Paraflagellar rod is vital for trypanosome motility. *Nature*, *391*(6667), 548. https://doi.org/10.1038/35300

Bastin, P., MacRae, T. H., Francis, S. B., Matthews, K. R., & Gull, K. (1999). Flagellar Morphogenesis: Protein Targeting and Assembly in the Paraflagellar Rod of Trypanosomes. *Molecular and Cellular Biology*, *19*(12), 8191–8200. https://doi.org/10.1128/mcb.19.12.8191

Bastin, P., Pullen, T. J., Moreira-Leite, F. F., & Gull, K. (2000). Inside and outside of the trypanosome flagellum: A multifunctional organelle. *Microbes and Infection*, *2*(15), 1865–1874. https://doi.org/10.1016/S1286-4579(00)01344-7

Beattie, P., & Gull, K. (1997). Cytoskeletal architecture and components involved in the attachment of Trypanosoma congolense epimastigotes. *Parasitology*, *115 (Pt 1)*, 47–55. https://doi.org/10.1017/s0031182097001042

Beneke, T., Madden, R., Makin, L., Valli, J., Sunter, J., & Gluenz, E. (2017). A CRISPR Cas9 high-throughput genome editing toolkit for kinetoplastids. Royal Society Open Science, *4*(5), 1–16. https://doi.org/10.1098/rsos.170095

Bennett V. (1985). The membrane skeleton of human erythrocytes and its implications for more complex cells. *Annual review of biochemistry*, *54*, 273–304. https://doi.org/10.1146/annurev.bi.54.070185.001421

Bertiaux, E., Morga, B., Blisnick, T., Rotureau, B., & Bastin, P. (2018). A Grow-and-Lock Model for the Control of Flagellum Length in Trypanosomes. *Current Biology*, *28*(23), 3802-3814.e3. https://doi.org/10.1016/j.cub.2018.10.031

Boleti, H., Karsenti, E., & Vernos, I. (1996). Xklp2, a novel Xenopus centrosomal kinesin-like protein required for centrosome separation during mitosis. *Cell*, *84*(1), 49. https://doi.org/10.1016/s0092-8674(00)80992-7

Bonhivers, M., Nowacki, S., Landrein, N., & Robinson, D. R. (2008). Biogenesis of the trypanosome endo-exocytotic organelle is cytoskeleton mediated. *PLoS biology*, *6*(5), e105. https://doi.org/10.1371/journal.pbio.0060105

Branche, C., Kohl, L., Toutirais, G., Buisson, J., Cosson, J., & Bastin, P. (2006). Conserved and specific functions of axoneme components in trypanosome motility. *Journal of cell science*, *119*(Pt 16), 3443–3455. https://doi.org/10.1242/jcs.03078

Briggs, L. J., McKean, P. G., Baines, A., Moreira-Leite, F., Davidge, J., Vaughan, S., & Gull, K. (2004). The flagella connector of Trypanosoma brucei: An unusual mobile transmembrane junction. *Journal of Cell Science*, *117*(9), 1641–1651. https://doi.org/10.1242/jcs.00995

Brooker, B. E. (1971). The fine structure of Crithidia fasciculata with special reference to the organelles involved in the ingestion and digestion of protein. *Zeitschrift Für Zellforschung Und Mikroskopische Anatomie*, *116*(4), 532–563. https://doi.org/10.1007/BF00335057

Broussard, J. A., Yang, R., Huang, C., Nathamgari, S., Beese, A. M., Godsel, L. M., Hegazy, M. H., Lee, S., Zhou, F., Sniadecki, N. J., Green, K. J., & Espinosa, H. D. (2017). The desmoplakin-intermediate filament linkage regulates cell mechanics. *Molecular biology of the cell*, *28*(23), 3156–3164. https://doi.org/10.1091/mbc.E16-07-0520

Buckley, C. D., Tan, J., Anderson, K. L., Hanein, D., Volkmann, N., Weis, W. I., Nelson, W. J., & Dunn, A. R. (2014). Cell adhesion. The minimal cadherin-catenin complex binds to actin filaments under force. *Science (New York, N.Y.)*, *346*(6209), 1254211. https://doi.org/10.1126/science.1254211

Burki, F., Roger, A. J., Brown, M. W., & Simpson, A. G. B. (2020). The New Tree of Eukaryotes. *Trends in Ecology and Evolution*, *35*(1), 43–55. https://doi.org/10.1016/j.tree.2019.08.008

Calvo-Álvarez, E., Bonnefoy, S., Salles, A., Benson, F. E., McKean, P. G., Bastin, P., & Rotureau, B. (2021). Redistribution of FLAgellar Member 8 during the trypanosome life cycle: Consequences for cell fate prediction. *Cellular Microbiology*, *23*(9), 1–17. https://doi.org/10.1111/cmi.13347

Campbell, P. C., & De Graffenried, C. L. (2020). Alternate histories of cytokinesis: Lessons from the trypanosomatids. *Molecular Biology of the Cell*, *31*(24), 2631–2639. https://doi.org/10.1091/mbc.E19-12-0696

Cross, F., & Umen, J. (2015). The Chlamydomonas cell cycle. *The Plant Journal*, *82*(3), 370-392. doi: 10.1111/tpj.12795

Davidge, J. A., Chambers, E., Dickinson, H. A., Towers, K., Ginger, M. L., McKean, P. G., & Gull, K. (2006). Trypanosome IFT mutants provide insight into the motor location for mobility of the flagella connector and flagellar membrane formation. *Journal of Cell Science*, *119*(19), 3935–3943. https://doi.org/10.1242/jcs.03203

Dean, S., Sunter, J., Wheeler, R. J., Hodkinson, I., Gluenz, E., & Gull, K. (2015). A toolkit enabling efficient, scalable and reproducible gene tagging in trypanosomatids. *Open Biology*, *5*(1). https://doi.org/10.1098/rsob.140197

Dean, S., Sunter, J., & Wheeler, R. (2017). TrypTag.org: A Trypanosome Genome-wide Protein Localisation Resource. *Trends In Parasitology*, *33*(2), 80-82. doi: 10.1016/j.pt.2016.10.009

De Graffenried, C. L., Anrather, D., Rauendorf, F. Von, & Warren, G. (2013). Polo-like kinase phosphorylation of bilobe-resident TbCentrin2 facilitates flagellar inheritance in Trypanosoma brucei. *Molecular Biology of the Cell*, *24*(12), 1947–1963. https://doi.org/10.1091/mbc.E12-12-0911

DeGrasse, J. A., DuBois, K. N., Devos, D., Siegel, T. N., Sali, A., Field, M. C., Rout, M. P., & Chait, B. T. (2009). Evidence for a shared nuclear pore complex architecture that is conserved from the last common eukaryotic ancestor. *Molecular & cellular proteomics : MCP*, *8*(9), 2119–2130. https://doi.org/10.1074/mcp.M900038-MCP200

Souza, W., Rossi, M., Kitajima, E., Santos, R., & Roitman, I. (1976). An electron-microscopic study of Herpetomonas sp. (Leptomonas pessoai). *Canadian Journal Of Microbiology*, *22*(2), 197-203. doi: 10.1139/m76-027

Fanning, A. S., Van Itallie, C. M., & Anderson, J. M. (2012). Zonula occludens-1 and -2 regulate apical cell structure and the zonula adherens cytoskeleton in polarized epithelia. *Molecular biology of the cell*, *23*(4), 577–590. https://doi.org/10.1091/mbc.E11-09-0791

Farr, H., & Gull, K. (2009). Functional studies of an evolutionarily conserved, cytochrome b5 domain protein reveal a specific role in axonemal organisation and the general phenomenon of post-division axonemal growth in trypanosomes. *Cell Motility And The Cytoskeleton*, *66*(1), 24-35. doi: 10.1002/cm.20322

Field, M. C., & Carrington, M. (2009). The trypanosome flagellar pocket. *Nature reviews. Microbiology*, *7*(11), 775–786. https://doi.org/10.1038/nrmicro2221

Flegontov, P., Votýpka, J., Skalický, T., Logacheva, M. D., Penin, A. A., Tanifuji, G., Onodera, N. T., Kondrashov, A. S., Volf, P., Archibald, J. M., & Lukeš, J. (2013). Paratrypanosoma is a novel early-branching trypanosomatid. *Current Biology*, *23*(18), 1787–1793. https://doi.org/10.1016/j.cub.2013.07.045

Foth, B. J., Goedecke, M. C., & Soldati, D. (2006). New insights into myosin evolution and classification. *Proceedings of the National Academy of Sciences of the United States of America*, *103*(10), 3681–3686. https://doi.org/10.1073/pnas.0506307103

Gadelha, C., Rothery, S., Morphew, M., McIntosh, J. R., Severs, N. J., & Gull, K. (2009). Membrane domains and flagellar pocket boundaries are influenced by the cytoskeleton in African trypanosomes. *Proceedings of the National Academy of Sciences of the United States of America*, *106*(41), 17425–17430. https://doi.org/10.1073/pnas.0909289106

Gao, J., Schatton, D., Martinelli, P., Hansen, H., Pla-Martin, D., Barth, E., Becker, C., Altmueller, J., Frommolt, P., Sardiello, M., & Rugarli, E. I. (2014). CLUH regulates mitochondrial biogenesis by binding

mRNAs of nuclear-encoded mitochondrial proteins. *The Journal of cell biology*, *207*(2), 213–223. https://doi.org/10.1083/jcb.201403129

Garcia, M. A., Nelson, W. J., & Chavez, N. (2018). Cell-Cell Junctions Organize Structural and Signalling Networks. *Cold Spring Harbor perspectives in biology*, *10*(4), a029181. https://doi.org/10.1101/cshperspect.a029181

García-Salcedo, J. A., Pérez-Morga, D., Gijón, P., Dilbeck, V., Pays, E., & Nolan, D. P. (2004). A differential role for actin during the life cycle of *Trypanosoma brucei*. *EMBO Journal*, *23*(4), 780–789. https://doi.org/10.1038/sj.emboj.7600094

Garrod, D., & Chidgey, M. (2008). Desmosome structure, composition and function. *Biochimica et biophysica acta*, *1778*(3), 572–587. https://doi.org/10.1016/j.bbamem.2007.07.014

Gluenz, E., Höög, J. L., Smith, A. E., Dawe, H. R., Shaw, M. K., & Gull, K. (2010). Beyond 9+0: noncanonical axoneme structures characterize sensory cilia from protists to humans. *FASEB journal : official publication of the Federation of American Societies for Experimental Biology*, *24*(9), 3117–3121. https://doi.org/10.1096/fj.09-151381

Gluenz, E., Povelones, M. L., Englund, P. T., & Gull, K. (2011). The Kinetoplast Duplication Cycle in *Trypanosoma brucei* Is Orchestrated by Cytoskeleton-Mediated Cell Morphogenesis . *Molecular and Cellular Biology*, *31*(5), 1012–1021. https://doi.org/10.1128/mcb.01176-10

Gluenz, E., Wheeler, R. J., Hughes, L., & Vaughan, S. (2015). Scanning and three-dimensional electron microscopy methods for the study of *Trypanosoma brucei* and *Leishmania mexicana* flagella. *Methods in Cell Biology*, *127*(Figure 1), 509–542. https://doi.org/10.1016/bs.mcb.2014.12.011

Griffiths, S., Portman, N., Taylor, P. R., Gordon, S., Ginger, M. L., & Gull, K. (2007). RNA interference mutant induction in vivo demonstrates the essential nature of trypanosome flagellar function during mammalian infection. *Eukaryotic Cell*, *6*(7), 1248–1250. https://doi.org/10.1128/EC.00110-07

Gull K. (1999). The cytoskeleton of trypanosomatid parasites. *Annual review of microbiology*, *53*, 629–655. https://doi.org/10.1146/annurev.micro.53.1.629

Hamill, L. C., Kaare, M. T., Welburn, S. C., & Picozzi, K. (2013). Domestic pigs as potential reservoirs of human and animal trypanosomiasis in Northern Tanzania. *Parasites and Vectors*, *6*(1), 1–7. https://doi.org/10.1186/1756-3305-6-322

Hammarton, T. C. (2007). Cell cycle regulation in Trypanosoma brucei. *Molecular and Biochemical Parasitology*, *153*(1), 1–8. https://doi.org/10.1016/j.molbiopara.2007.01.017

Hammarton, T. C. (2019). Who Needs a Contractile Actomyosin Ring? The Plethora of Alternative Ways to Divide a Protozoan Parasite. *Frontiers in Cellular and Infection Microbiology*, *9*, 1–30. https://doi.org/10.3389/fcimb.2019.00397

Han, X., Huang, L. J., Feng, D., Jiang, W., Miu, W., & Li, N. (2019). Plasmodesmata-related structural and functional proteins: The long sought-after secrets of a cytoplasmic channel in plant cell walls. *International Journal of Molecular Sciences*, *20*(12). https://doi.org/10.3390/ijms20122946

Hartwell, L. H., Culotti, J., & Reid, B. (1970). Genetic control of the cell-division cycle in yeast. I. Detection of mutants. *Proceedings of the National Academy of Sciences of the United States of America*, *66*(2), 352–359. https://doi.org/10.1073/pnas.66.2.352

Hayes, P., Varga, V., Olego-Fernandez, S., Sunter, J., Ginger, M. L., & Gull, K. (2014). Modulation of a cytoskeletal calpain-like protein induces major transitions in trypanosome morphology. *Journal of Cell Biology*, *206*(3), 377–384. https://doi.org/10.1083/jcb.201312067

Hemphill, A., & Ross, C. A. (1995). Flagellum-mediated adhesion of Trypanosoma congolense to bovine aorta endothelial cells. *Parasitology Research*, *81*(5), 412–420. https://doi.org/10.1007/BF00931503

Hilenski, L., & Walne, P. (2004). ULTRASTRUCTURE OF THE FLAGELLA OF THE COLORLESS PHAGOTROPH PERANEMA TRICHOPHORUM (EUGLENOPHYCEAE).II. FLAGELLAR ROOTS1. *Journal Of Phycology*, *21*(1), 125-134. doi: 10.1111/j.0022-3646.1985.00125

Hilton, N. A., Sladewski, T. E., Perry, J. A., Pataki, Z., Sinclair-Davis, A. N., Muniz, R. S., Tran, H. L., Wurster, J. I., Seo, J., & de Graffenried, C. L. (2018). Identification of TOEFAZ1-interacting proteins reveals key regulators of Trypanosoma brucei cytokinesis. *Molecular Microbiology*, *109*(3), 306–326. https://doi.org/10.1111/mmi.13986

Hogan, J. C., Jr, & Patton, C. L. (1976). Variation in intramembrane components of Trypanosoma brucei from intact and x-irradiated rats: a freeze-cleave study. *The Journal of protozoology*, *23*(2), 205–215. https://doi.org/10.1111/j.1550-7408.1976.tb03757.x

Höög, J. L., Bouchet-Marquis, C., McIntosh, J. R., Hoenger, A., & Gull, K. (2012). Cryo-electron tomography and 3-D analysis of the intact flagellum in Trypanosoma brucei. *Journal of Structural Biology*, *178*(2), 189–198. https://doi.org/10.1016/j.jsb.2012.01.009

Höög, J. L., Lacomble, S., Bouchet-Marquis, C., Briggs, L., Park, K., Hoenger, A., & Gull, K. (2016). 3D Architecture of the Trypanosoma brucei Flagella Connector, a Mobile Transmembrane Junction. *PLoS Neglected Tropical Diseases*, *10*(1), 1–17. https://doi.org/10.1371/journal.pntd.0004312

Hu, H., An, T., Kurasawa, Y., Zhou, Q., & Li, Z. (2019). The trypanosome-specific proteins FPRC and CIF4 regulate cytokinesis initiation by recruiting CIF1 to the cytokinesis initiation site. *Journal of Biological Chemistry*, *294*(45), 16672–16683. https://doi.org/10.1074/jbc.RA119.010538

Hughes, L., Towers, K., Starborg, T., Gull, K., & Vaughan, S. (2013). A cell-body groove housing the new flagellum tip suggests an adaptation of cellular morphogenesis for parasitism in the bloodstream form of Trypanosoma brucei. *Journal of Cell Science*, *126*(24), 5748–5757. https://doi.org/10.1242/jcs.139139

Hughes, L., Borrett, S., Towers, K., Starborg, T., & Vaughan, S. (2017). Patterns of organelle ontogeny through a cell cycle revealed by whole-cell reconstructions using 3D electron microscopy. *Journal of Cell Science*, *130*(3), 637–647. https://doi.org/10.1242/jcs.198887

Ikeda, K. N., & De Graffenried, C. L. (2012). Polo-like kinase is necessary for flagellum inheritance in Trypanosoma brucei. *Journal of Cell Science*, *125*(13), 3173–3184. https://doi.org/10.1242/jcs.101162

Jackson, A., Otto, T., Aslett, M., Armstrong, S., Bringaud, F., Schlacht, A., Hartley, C., Sanders, M., Wastling, J., Dacks, J., Acosta-Serrano, A., Field, M., Ginger, M. and Berriman, M. (2016). Kinetoplastid Phylogenomics Reveals the Evolutionary Innovations Associated with the Origins of Parasitism. *Current Biology*. The Authors, 26(2), pp. 161–172.

Khan, S., & Scholey, J. M. (2018). Assembly, Functions and Evolution of Archaella, Flagella and Cilia. *Current Biology*, *28*(6), R278–R292. https://doi.org/10.1016/j.cub.2018.01.085

Kohl, L., Sherwin, T., & Gull, K. (1999). Assembly of the Paraflagellar Rod and the Flagellum Attachment Zone Complex During the Trypanosoma brucei Cell Cycle. *The Journal Of Eukaryotic Microbiology*, *46*(2), 105-109. doi: 10.1111/j.1550-7408.1999.tb04592.x

Kohl, L., Robinson, D., & Bastin, P. (2003). Novel roles for the flagellum in cell morphogenesis and cytokinesis of trypanosomes. *EMBO Journal*, *22*(20), 5336–5346. https://doi.org/10.1093/emboj/cdg518

Krupnova, T., Sasabe, M., Ghebreghiorghis, L., Gruber, C. W., Hamada, T., Dehmel, V., Strompen, G., Stierhof, Y. D., Lukowitz, W., Kemmerling, B., Machida, Y., Hashimoto, T., Mayer, U., & Jürgens, G. (2009). Microtubule-associated kinase-like protein RUNKEL needed [corrected] for cell plate expansion in Arabidopsis cytokinesis. *Current biology : CB*, *19*(6), 518–523. https://doi.org/10.1016/j.cub.2009.02.021

Kumar, P., & Wang, C. C. (2006). Dissociation of cytokinesis initiation from mitotic control in a eukaryote. *Eukaryotic cell*, *5*(1), 92–102. https://doi.org/10.1128/EC.5.1.92-102.2006

Kurasawa, Y., Hu, H., Zhou, Q., & Li, Z. (2018). The trypanosome-specific protein CIF3 cooperates with the CIF1 protein to promote cytokinesis in *Trypanosoma brucei*. *The Journal of biological chemistry*, *293*(26), 10275–10286. https://doi.org/10.1074/jbc.RA118.003113

Lacomble, S., Vaughan, S., Gadelha, C., Morphew, M. K., Shaw, M. K., McIntosh, J. R., & Gull, K. (2009). Three-dimensional cellular architecture of the flagellar pocket and associated cytoskeleton in trypanosomes revealed by electron microscope tomography. *Journal of Cell Science*, *122*(8), 1081–1090. https://doi.org/10.1242/jcs.045740

Lacomble, S., Vaughan, S., Gadelha, C., Morphew, M. K., Shaw, M. K., McIntosh, J. R., & Gull, K. (2010). Basal body movements orchestrate membrane organelle division and cell morphogenesis in Trypanosoma brucei. *Journal of Cell Science*, *123*(17), 2884–2891. https://doi.org/10.1242/jcs.074161

LaCount, D. J., Barrett, B., & Donelson, J. E. (2002). Trypanosoma brucei FLA1 is required for flagellum attachment and cytokinesis. *The Journal of biological chemistry*, *277*(20), 17580–17588. https://doi.org/10.1074/jbc.M200873200

Langousis, G., & Hill, K. L. (2014). Motility and more: the flagellum of Trypanosoma brucei. *Nature reviews. Microbiology*, *12*(7), 505–518. https://doi.org/10.1038/nrmicro3274

Li, J., Lykotrafitis, G., Dao, M., & Suresh, S. (2007). Cytoskeletal dynamics of human erythrocyte. *Proceedings of the National Academy of Sciences of the United States of America*, *104*(12), 4937–4942. https://doi.org/10.1073/pnas.0700257104

Liu, M., Guan, Z., Shen, Q., Lalor, P., Fitzgerald, U., O'Brien, T., Dockery, P., & Shen, S. (2016). Ulk4 Is Essential for Ciliogenesis and CSF Flow. *The Journal of neuroscience : the official journal of the Society for Neuroscience*, *36*(29), 7589–7600. https://doi.org/10.1523/JNEUROSCI.0621-16.2016

Livanos, P., & Müller, S. (2019). Division Plane Establishment and Cytokinesis. *Annual review of plant biology*, *70*, 239–267. https://doi.org/10.1146/annurev-arplant-050718-100444

Maric, D., Epting, C. L., & Engman, D. M. (2010). Composition and sensory function of the trypanosome flagellar membrane. *Current opinion in microbiology*, *13*(4), 466–472. https://doi.org/10.1016/j.mib.2010.06.001

McAllaster, M. R., Ikeda, K. N., Lozano-Núñez, A., Anrather, D., Unterwurzacher, V., Gossenreiter, T., Perry, J. A., Crickley, R., Mercadante, C. J., Vaughan, S., & De Graffenried, C. L. (2015). Proteomic identification of novel cytoskeletal proteins associated with TbPLK, an essential regulator of cell morphogenesis in Trypanosoma brucei. *Molecular Biology of the Cell*, *26*(17), 3013–3029. https://doi.org/10.1091/mbc.E15-04-0219

Moreira, B. P., Fonseca, C. K., Hammarton, T. C., & Baqui, M. M. (2017). Giant FAZ10 is required for flagellum attachment zone stabilization and furrow positioning in *Trypanosoma brucei*. *Journal of cell science*, *130*(6), 1179–1193. https://doi.org/10.1242/jcs.194308

Moreira-Leite, F. F., Sherwin, T., Kohl, L., & Gull, K. (2001). A trypanosome structure involved in transmitting cytoplasmic information during cell division. *Science (New York, N.Y.)*, *294*(5542), 610–612. https://doi.org/10.1126/science.1063775

Nekrasova, O. E., Amargo, E. V., Smith, W. O., Chen, J., Kreitzer, G. E., & Green, K. J. (2011). Desmosomal cadherins utilize distinct kinesins for assembly into desmosomes. *Journal of Cell Biology*, *195*(7), 1185–1203. https://doi.org/10.1083/jcb.201106057

Nozaki, T., Haynes, P. A., & Cross, G. A. M. (1996). Characterization of the Trypanosoma brucei homologue of a Trypanosoma cruzi flagellum-adhesion glycoprotein. In *Molecular and Biochemical Parasitology* (Vol. 82, Issue 2, pp. 245–255). https://doi.org/10.1016/0166-6851(96)02741-7

Odronitz, F., & Kollmar, M. (2007). Drawing the tree of eukaryotic life based on the analysis of 2,269 manually annotated myosins from 328 species. *Genome Biology*, *8*(9), 1–23. https://doi.org/10.1186/gb-2007-8-9-r196

Oh, S. A., Johnson, A., Smertenko, A., Rahman, D., Park, S. K., Hussey, P. J., & Twell, D. (2005). A divergent cellular role for the FUSED kinase family in the plant-specific cytokinetic phragmoplast. *Current biology : CB*, *15*(23), 2107–2111. https://doi.org/10.1016/j.cub.2005.10.044

Ovcinnikov, N. M., Delektorskij, V. V., & Kosmacheva, S. A. (1974). Ultrastructural characteristics of Trichomonas vaginalis. An electron microscopical study. *The British Journal of Venereal Diseases*, *50*(1), 22–39. https://doi.org/10.1136/sti.50.1.22

Pereira, S. S., Trindade, S., De Niz, M., & Figueiredo, L. M. (2019). Tissue tropism in parasitic diseases. *Open Biology*, *9*(5). https://doi.org/10.1098/rsob.190036

Ploubidou, A., Robinson, D. R., Docherty, R. C., Ogbadoyi, E. O., & Gull, K. (1999). Evidence for novel cell cycle checkpoints in trypanosomes: kinetoplast segregation and cytokinesis in the absence of mitosis. *Journal of cell science*, *112 (Pt 24)*, 4641–4650.

Ponting, C. P., Aravind, L., Schultz, J., Bork, P., & Koonin, E. V. (1999). Eukaryotic signalling domain homologues in archaea and bacteria. Ancient ancestry and horizontal gene transfer. *Journal of Molecular Biology*, *289*(4), 729–745. https://doi.org/10.1006/jmbi.1999.2827

Richards, T. A., & Cavalier-Smith, T. (2005). Myosin domain evolution and the primary divergence of eukaryotes. *Nature*, *436*(7054), 1113–1118. https://doi.org/10.1038/nature03949

Robinson, D. R., Sherwin, T., Ploubidou, A., Byard, E. H., & Gull, K. (1995). Microtubule polarity and dynamics in the control of organelle positioning, segregation, and cytokinesis in the trypanosome cell cycle. *The Journal of cell biology*, *128*(6), 1163–1172. https://doi.org/10.1083/jcb.128.6.1163

Roth, L. (1959). An Electron-Microscope Study of the Cytology of the Protozoan Peranema trichophorum*. *The Journal Of Protozoology*, *6*(2), 107-116. doi: 10.1111/j.1550-7408.1959.tb03935

Rotureau, B., Subota, I., & Bastin, P. (2011). Molecular bases of cytoskeleton plasticity during the Trypanosoma brucei parasite cycle. *Cellular Microbiology*, *13*(5), 705–716. https://doi.org/10.1111/j.1462-5822.2010.01566.x

Rotureau, B., Blisnick, T., Subota, I., Julkowska, D., Cayet, N., Perrot, S., & Bastin, P. (2014). Flagellar adhesion in Trypanosoma brucei relies on interactions between different skeletal structures in the flagellum and cell body. *Journal of Cell Science*, *127*(1), 204–215. https://doi.org/10.1242/jcs.136424

Portman, N., & Gull, K. (2010). The paraflagellar rod of kinetoplastid parasites: from structure to components and function. *International journal for parasitology*, *40*(2), 135–148. https://doi.org/10.1016/j.ijpara.2009.10.005

Sack, S., Müller, J., Marx, A., Thormählen, M., Mandelkow, E. M., Brady, S. T., & Mandelkow, E. (1997). X-ray structure of motor and neck domains from rat brain kinesin. *Biochemistry*, *36*(51), 16155–16165. https://doi.org/10.1021/bi9722498

Schofield, C. J., & Kabayo, J. P. (2008). Trypanosomiasis vector control in Africa and Latin America. *Parasites and Vectors*, *1*(1), 1–7. https://doi.org/10.1186/1756-3305-1-24

Schroeder, T. E. (1972). The contractile ring: II. determining its brief existence, volumetric changes, and vital role in cleaving arbacia eggs. *Journal of Cell Biology*, *53*(2), 419–434. https://doi.org/10.1083/jcb.53.2.419

Sebé-Pedrós, A., Grau-Bové, X., Richards, T. A., & Ruiz-Trillo, I. (2014). Evolution and classification of myosins, a paneukaryotic whole-genome approach. *Genome Biology and Evolution*, *6*(2), 290–305. https://doi.org/10.1093/gbe/evu013

Shapiro, L., & Weis, W. I. (2009). Structure and biochemistry of cadherins and catenins. *Cold Spring Harbor perspectives in biology*, *1*(3), a003053. https://doi.org/10.1101/cshperspect.a003053

Shen, L., Black, E. D., Witkowski, E. D., Lencer, W. I., Guerriero, V., Schneeberger, E. E., & Turner, J. R. (2006). Myosin light chain phosphorylation regulates barrier function by remodeling tight junction structure. *Journal of Cell Science*, *119*(10), 2095–2106. https://doi.org/10.1242/jcs.02915

Sherwin, T., Schneider, A., Sasse, R., Seebeck, T., & Gull, K. (1987). Distinct localization and cell cycle dependence of COOH terminally tyrosinolated alpha-tubulin in the microtubules of Trypanosoma brucei brucei. *The Journal of cell biology*, *104*(3), 439–446. https://doi.org/10.1083/jcb.104.3.439

Sherwin, T. and Gull, K. (1989). The Cell Division Cycle of *Trypanosoma brucei brucei*: Timing of Event Markers and Cytoskeletal Modulations. *Philosophical Transactions of the Royal Society B: Biological Sciences*, 323(1218), pp. 573-588.

Sinclair-Davis, A. N., McAllaster, M. R., & De Graffenried, C. L. (2017). A functional analysis of TOEFAZ1 uncovers protein domains essential for cytokinesis in Trypanosoma brucei. *Journal of Cell Science*, *130*(22), 3918–3932. https://doi.org/10.1242/jcs.207209

Skalický, T., Dobáková, E., Wheeler, R. J., Tesařová, M., Flegontov, P., Jirsová, D., Votýpka, J., Yurchenko, V., Ayala, F. J., & Lukeš, J. (2017). Extensive flagellar remodeling during the complex life cycle of Paratrypanosoma, an early-branching trypanosomatid. *Proceedings of the National Academy of Sciences of the United States of America*, *114*(44), 11757–11762. https://doi.org/10.1073/pnas.1712311114

Sonneborn, T. M. (1964). the Determinants and Evolution of Life. the Differentiation of Cells. *Proceedings of the National Academy of Sciences of the United States Of*, *51*(1961), 915–929. https://doi.org/10.1073/pnas.51.5.915

Spaink, H. P. (2004). Specific recognition of bacteria by plant LysM domain receptor kinases. *Trends in Microbiology*, *12*(5), 201–204. https://doi.org/10.1016/j.tim.2004.03.001

Sun, S. Y., Wang, C., Yuan, Y. A., & He, C. Y. (2013). An intracellular membrane junction consisting of flagellum adhesion glycoproteins links flagellum biogenesis to cell morphogenesis in Trypanosoma brucei. *Journal of Cell Science*, *126*(2), 520–531. https://doi.org/10.1242/jcs.113621

Sunter, J. D., Varga, V., Dean, S., & Gull, K. (2015a). A dynamic coordination of flagellum and cytoplasmic cytoskeleton assembly specifies cell morphogenesis in trypanosomes. *Journal of cell science*, *128*(8), 1580–1594. https://doi.org/10.1242/jcs.166447

Sunter, J. D., Benz, C., Andre, J., Whipple, S., McKean, P. G., Gull, K., Ginger, M. L., & Lukeš, J. (2015b). Modulation of flagellum attachment zone protein FLAM3 and regulation of the cell shape in Trypanosoma brucei life cycle transitions. *Journal of cell science*, *128*(16), 3117–3130. https://doi.org/10.1242/jcs.171645

Sunter, J. D., & Gull, K. (2016). The Flagellum Attachment Zone: 'The Cellular Ruler' of Trypanosome Morphology. *Trends in parasitology*, *32*(4), 309–324. https://doi.org/10.1016/j.pt.2015.12.010

Takeichi M. (2014). Dynamic contacts: rearranging adherens junctions to drive epithelial remodelling. *Nature reviews. Molecular cell biology*, *15*(6), 397–410. https://doi.org/10.1038/nrm3802

Tetley, L., & Vickerman, K. (1985). Differentiation in Trypanosoma brucei: host-parasite cell junctions and their persistence during acquisition of the variable antigen coat. *Journal of cell science*, *74*, 1–19.

Umeda, K., Matsui, T., Nakayama, M., Furuse, K., Sasaki, H., Furuse, M., & Tsukita, S. (2004). Establishment and characterization of cultured epithelial cells lacking expression of ZO-1. *The Journal of biological chemistry*, *279*(43), 44785–44794. https://doi.org/10.1074/jbc.M406563200

Van Itallie, C. M., Fanning, A. S., Bridges, A., & Anderson, J. M. (2009). ZO-1 stabilizes the tight junction solute barrier through coupling to the perijunctional cytoskeleton. *Molecular biology of the cell*, *20*(17), 3930–3940. https://doi.org/10.1091/mbc.e09-04-0320

Van Itallie, C. M., & Anderson, J. M. (2014). Architecture of tight junctions and principles of molecular composition. *Seminars in cell & developmental biology*, *36*, 157–165. https://doi.org/10.1016/j.semcdb.2014.08.011

Varga, V., Moreira-Leite, F., Portman, N., & Gull, K. (2017). Protein diversity in discrete structures at the distal tip of the trypanosome flagellum. *Proceedings of the National Academy of Sciences of the United States of America*, *114*(32), E6546–E6555. https://doi.org/10.1073/pnas.1703553114

Vaughan, S., & Gull, K. (2008). The structural mechanics of cell division in Trypanosoma brucei. *Biochemical Society transactions*, *36*(Pt 3), 421–424. https://doi.org/10.1042/BST0360421

Vaughan, S., Kohl, L., Ngai, I., Wheeler, R., & Gull, K. (2008). A Repetitive Protein Essential for the Flagellum Attachment Zone Filament Structure and Function in Trypanosoma brucei. *Protist*, *159*(1), 127-136. http://doi: 10.1016/j.protis.2007.08.005

Vaughan S. (2010). Assembly of the flagellum and its role in cell morphogenesis in Trypanosoma brucei. *Current opinion in microbiology*, *13*(4), 453–458. https://doi.org/10.1016/j.mib.2010.05.006

Vickerman, K. (1962). The mechanism of cyclical development in trypanosomes of the Trypanosoma brucei sub-group: an hypothesis based on ultrastructural observations. *Transactions of the Royal Society of Tropical Medicine and Hygiene*, *56*, 487–495. https://doi.org/10.1016/0035-9203(62)90072-x

Vickerman, K. (1969). On the surface coat and flagellar adhesion in trypanosomes. *Journal of Cell Science*, *5*(1), 163–193. https://doi.org/10.1242/jcs.5.1.163

Vickerman K. (1973). The mode of attachment of Trypanosoma vivax in the proboscis of the tsetse fly Glossina fuscipes: an ultrastructural study of the epimastigote stage of the trypanosome. *The Journal of protozoology*, *20*(3), 394–404. https://doi.org/10.1111/j.1550-7408.1973.tb00909.x

Vickerman K. (1985). Developmental cycles and biology of pathogenic trypanosomes. *British medical bulletin*, *41*(2), 105–114. https://doi.org/10.1093/oxfordjournals.bmb.a072036

Vickerman K. (1994). The evolutionary expansion of the trypanosomatid flagellates. *International journal for parasitology*, *24*(8), 1317–1331. https://doi.org/10.1016/0020-7519(94)90198-8

Vincensini, L., Blisnick, T., & Bastin, P. (2011). 1001 Model Organisms To Study Cilia and Flagella. *Biology of the Cell*, *103*(3), 109–130. https://doi.org/10.1042/bc20100104

Waters, A. M., & Beales, P. L. (2011). Ciliopathies: an expanding disease spectrum. *Pediatric nephrology (Berlin, Germany)*, *26*(7), 1039–1056. https://doi.org/10.1007/s00467-010-1731-7

Wilson, C. W., Nguyen, C. T., Chen, M. H., Yang, J. H., Gacayan, R., Huang, J., Chen, J. N., & Chuang, P. T. (2009). Fused has evolved divergent roles in vertebrate Hedgehog signalling and motile ciliogenesis. *Nature*, *459*(7243), 98–102. https://doi.org/10.1038/nature07883

Wood, R. L. (1959). Intercellular attachment in the epithelium of Hydra as revealed by electron microscopy. *The Journal of Biophysical and Biochemical Cytology*, *6*, 343–352. https://doi.org/10.1083/jcb.6.3.343

Woodward, R., & Gull, K. (1990). Timing of nuclear and kinetoplast DNA replication and early morphological events in the cell cycle of Trypanosoma brucei. *Journal of cell science*, *95 (Pt 1)*, 49–57.

World Health Organization. (2021). *Human African trypanosomiasis*. Available at: https://www.who.int/trypanosomiasis_african/en/ [Accessed 20 Sept. 2021].

Wheeler, R. J., Scheumann, N., Wickstead, B., Gull, K., & Vaughan, S. (2013). Cytokinesis in Trypanosoma brucei differs between bloodstream and tsetse trypomastigote forms: implications for microtubule-based morphogenesis and mutant analysis. *Molecular microbiology*, *90*(6), 1339–1355. https://doi.org/10.1111/mmi.12436

Wheeler, R. J., Gull, K., & Sunter, J. D. (2019). Coordination of the Cell Cycle in Trypanosomes. *Annual review of microbiology*, *73*, 133–154. https://doi.org/10.1146/annurev-micro-020518-115617

Zhang, R., Zhang, C., Zhao, Q., & Li, D. (2013). Spectrin: structure, function and disease. *Science China. Life sciences*, *56*(12), 1076–1085. https://doi.org/10.1007/s11427-013-4575-0

Zhang, X., Li, S. J., Li, Z., He, C. Y., Hide, G., Lai, D. H., & Lun, Z. R. (2019). Cell cycle and cleavage events during in vitro cultivation of bloodstream forms of Trypanosoma lewisi, a zoonotic pathogen. *Cell cycle (Georgetown, Tex.)*, *18*(5), 552–567. https://doi.org/10.1080/15384101.2019.1577651

Zhou, Q., Liu, B., Sun, Y., & He, C. Y. (2011). A coiled-coil- and C2-domain-containing protein is required for FAZ assembly and cell morphology in Trypanosoma brucei. *Journal of Cell Science*, *124*(22), 3848–3858. https://doi.org/10.1242/jcs.087676

Zhou, Q., Hu, H., He, C. Y., & Li, Z. (2015). Assembly and maintenance of the flagellum attachment zone filament in Trypanosoma brucei. *Journal of Cell Science*, *128*(13), 2361–2372. https://doi.org/10.1242/jcs.168377

Zhou, Q., Gu, J., Lun, Z. R., Ayala, F. J., & Li, Z. (2016a). Two distinct cytokinesis pathways drive trypanosome cell division initiation from opposite cell ends. *Proceedings of the National Academy of Sciences of the United States of America*, *113*(12), 3287–3292. https://doi.org/10.1073/pnas.1601596113

Zhou, Q., Hu, H., & Li, Z. (2016b). An EF-hand-containing protein in Trypanosoma brucei regulates cytokinesis initiation by maintaining the stability of the cytokinesis initiation factor CIF1. *Journal of Biological Chemistry*, *291*(28), 14395–14409. https://doi.org/10.1074/jbc.M116.726133

Zhou, Q., An, T., Pham, K., Hu, H., & Li, Z. (2018). The CIF1 protein is a master orchestrator of trypanosome cytokinesis that recruits several cytokinesis regulators to the cytokinesis initiation site. *The Journal of biological chemistry*, *293*(42), 16177–16192. https://doi.org/10.1074/jbc.RA118.004888

Zihni, C., Mills, C., Matter, K., & Balda, M. S. (2016). Tight junctions: From simple barriers to multifunctional molecular gates. *Nature Reviews Molecular Cell Biology*, *17*(9), 564–580. https://doi.org/10.1038/nrm.2016.80

9 Appendix A: Tagging primers and relevant information regarding the gene of interest

Gene ID	Gene Name	Localisation on TrypTag	Terminal tagged	MW (kDa)	Isoelectric point (pI)	Transcript length (bp)	Protein length (aa)	Upstream Forward primer	Downstream Reverse primer	5' sgRNA (guide) primer
Tb427.01.2260	SMP1-2	Anterior cell tip, flagellar pocket, pellicular membrane, flagellar membrane	C	14.03	9.2	390	129	GACAGGCGCCGCAGGGGATCTGGCAGGAAAggttctggtagtggttccgg	CTCTACTCTCATTCTCATTCTCATTTACCTccaatttgagagacctgtgc	gaaattaatacgactcactataggCAAACACAAAGCACACAAAGgttttagagctagaaatagc
Tb427.01.2710	-	Flagella connector, cytoplasm	C	76.09	8.96	2148	715	CCTTCTGTAGATCCAACAAAAGAAAAAAATggttctggtagtggttccgg	GGAGGTAGGAAGGATGCGGTAACTGCTGCGccaatttgagagacctgtgc	gaaattaatacgactcactataggTGAGGATCGGAATAGTTGCGgttttagagctagaaatagc
Tb427.01.4310	FAZ2	FAZ	N	183.87	9.52	4917	1638	Cell line provided by the Dunn School, Oxford University.		
Tb427.03.1020	FAZ13	Distal FAZ, anterior cell tip	N	54.34	5.14	1482	493	Cell line provided by the Dunn School, Oxford University.		
Tb427.03.4710	FAZ23	FAZ	C	59.53	6.89	1635	544	GACAAGAGCATTTCGTCAGTTGGCGAGCCGgtataatgcagacctgctgc	GGGTTCACACTCCGAGAGGGTGTGTTGCATactacccgatcctgatccag	gaaattaatacgactcactataggCGCTGAAAGCAGTGTCAACGgttttagagctagaaatagc
Tb427.03.4960	FCP2	Flagella connector	C	182.36	6.12	4785	1594	TGCCGATGCTGCGGCAATGCTCAACTTGTGggttctggtagtggttccgg	GTGTCACGTCCTTGAAAAGGGGGAGTTCCGccaatttgagagacctgtgc	gaaattaatacgactcactataggCTAGCGTACATTACCGTCTGgttttagagctagaaatagc
Tb427.04.2060	FAZ8	FAZ	C	66.83	5.04	1761	586	GAACAATCGGCGAGGTTGCCTTCTGCTCCGggttctggtagtggttccgg	ATTCCACCCCTCCCCCCGTTTTTGGCACCGccaatttgagagacctgtgc	gaaattaatacgactcactataggCCCGTCACTCAAAACACCATgttttagagctagaaatagc
Tb427.04.3740	FAZ1	FAZ	N	192.56	4.32	5079	1692	Cell line provided by the Dunn School, Oxford University.		
Tb427.04.5340	FAZ11	Anterior cell tip, FAZ	N	95.03	7.8	2508	835	Cell line provided by the Dunn School, Oxford University.		
Tb427.05.3460	FAZ16	Distal FAZ (cell cycle dependent), cleavage furrow	N	57.53	4.5	1614	537	TTCTCTTTCTGCCACCACTTTTTTTTTCCAgtataatgcagacctgctgc	CCTGTCGATCTGGCACGATACGCTATTCATactaccgatcctgatccag	gaaattaatacgactcactataggGCGAACGCACTTGCGATAAAgttttagagctagaaatagc
Tb427.07.3330	FAZ10	FAZ, anterior cell tip	N	502.95	4.27	13429	4334	Cell line provided by the Dunn School, Oxford University.		

Tb427.07.5240	FAZ21	Distal FAZ, anterior cell tip	N	53.44	9.04	1473	490	Cell line provided by the Dunn School, Oxford University.		
Tb427.08.960	FCP1	Flagella connector	C	237.53	5.28	6585	2194	GTTTCTCTCTCATGTGATTCGTCGCACAACggttctggtagtggttccgg	TTCGTATCTTATCCATTCATAATCCATCCCcaatttgagagacctgtgc	gaaattaatacgactcactataggCAATGGATGCCACTCTGTTGgttttagagctagaaatagc
Tb427.08.4780	FLAM3	FAZ, reticulated cytoplasm	N	468.18	5.22	12456	4151	CTTTGTTTTTAGATAATAGAAAGAAAAAAAgtataatgcagacctgctgc	GCGCTGTTCATTTTGATTGCGCCGTCTCATactaccgatcctgatccag	gaaattaatacgactcactataggACCAAAGTACCGGGAGGTTCgttttagagctagaaatagc
Tb427.08.5350	-	Distal FAZ, anterior cell tip	C	19.01	8.97	513	170	AAGCAACACCGCTGGTATGCGCACGGGGGCggttctggtagtggttccgg	GCCACGTCTGGCTCGCCGTTGGGTAAACCGccaatttgagagacctgtgc	gaaattaatacgactcactataggTAACCGACTTTAAGCAGCCGgttttagagctagaaatagc
Tb427.08.6830	'Putative kinesin'	Anterior cell tip, reticulated cytoplasm	N	198.62	7.42	5460	1819	TAGTGGGGCGAGCAATTTTTGCACCTTCCTgtataatgcagacctgctgc	GTCGTCAGTCGTATTAGCTCCACGTCGCATactaccgatcctgatccag	gaaattaatacgactcactataggGACTAGCAGCAATAGTGACGgttttagagctagaaatagc
Tb427.08.7070	FAZ15	Distal FAZ (cell cycle dependent)	N	35.46	7.05	951	316	Cell line provided by the Dunn School, Oxford University.		
Tb427.08.7540	FCP3	Flagella connector	C	118.64	5.65	3327	1108	GTGGGTACAGCGCCCACACTCTCCCTTGCGgtataatgcagacctgctgc	GAGTTCTGCAGTCCCATTGGTGTCCAGCATactaccgatcctgatccag	gaaattaatacgactcactataggTTACGTTTACCTCACGCGCAgttttagagctagaaatagc
Tb427.10.840	FAZ6	Distal FAZ, anterior cell tip	C	195.62	6.06	5160	1719	AATCTGATTACTGATCCTCATGAGAGGTCGggttctggtagtggttccgg	CCTTTTCATTTATTTGTTTATTTTCTTCCTccaatttgagagacctgtgc	gaaattaatacgactcactataggTGTATCATTTTATGTACAAAgttttagagctagaaatagc
Tb427.10.890	FCP4	Flagella connector	N	324.1	5.25	8867	2888	TTACGGTGTAGGTGTGCAATTAATTTTTCGgtataatgcagacctgctgc	AACCACCTGTACACATGGTTTGTGCAACATactaccgatcctgatccag	gaaattaatacgactcactataggCATAGAAGCTTCGCTACGGCgttttagagctagaaatagc
Tb427.10.2610	DUF1935	Anterior cell tip, FAZ, cytoplasm	N	53.35	4.61	2795	484	Cell line provided by the Dunn School, Oxford University.		
Tb427.10.5870	FAZ25	FAZ, anterior cell tip	N	49.49	9.82	1371	456	ATATATATATATATATCGTTTCGTATTTAAgtataatgcagacctgctgc	GCTTGAGGAGCTCGTGTCTTGAAAAATCATactacccgatcctgatccag	gaaattaatacgactcactataggCCATAACATCGTACCTGTAGgttttagagctagaaatagc
Tb427.10.6360	FPRC	Distal FAZ, cytoplasm	N	55.48	4.79	1464	487	Cell line provided by the Dunn School, Oxford University.		

Tb427.10.7210	FAZ17	FAZ, anterior cell tip	C	26.26	9.45	687	228	TCGAATGATATGGATGATTCTGATGAAGGAggttctggtagtggttccgg	CAATGAAGACCACAACTGGGATTAGCACCAccaatttgagagacctgtgc	gaaattaatacgactcactataggTGTGGTGCTAATCCCAGTTGgttttagagctagaaatagc
Tb427.10.8240	CIF4	Distal FAZ, anterior cell tip	N	42.85	6.06	1125	374	Cell line provided by the Dunn School, Oxford University.		
Tb427.10.9380	'SEP domain containing protein'	Anterior cell tip, cytoplasm, flagellum	N	60.03	6.12	1644	547	ATACGGAAGATAAGGTTGCTTTTGCATCCCgtataatgcagacctgctgc	AAACTTCTGTAAGGGCGCATCCACTGGCATactacccgatcctgatccag	gaaattaatacgactcactataggCGGCTACCCACCTATGAGATgttttagagctagaaatagc
Tb427.10.9720	REAP-1	Distal FAZ	N	64.35	11.26	1176	591	Cell line provided by the Dunn School, Oxford University.		
Tb427.10.11650	-	Distal FAZ, FAZ, hook complex	N	17.39	4.07	486	161	ACCAGCGGGTCATACAAACGGACGCTCATTgtataatgcagacctgctgc	TTGTCTTACTTTCGAGTCTCCACAACCCATactacccgatcctgatccag	gaaattaatacgactcactataggTCATACACAAAGAAAGGGAGgttttagagctagaaatagc
Tb427.10.13100	CIF3	Distal FAZ (cell cycle dependent)	N	50.99	5.72	1317	438	Cell line provided by the Dunn School, Oxford University.		
Tb427.10.15390	FAZ7	Anterior cell tip, cytoplasm	C	123.46	9.46	3288	1095	TTCGCTAATCCGCACTCTTCACGGCCACGCggttctggtagtggttccgg	CCCCTTCTCATTGTGTCCTTTCCTCATTTTccaatttgagagacctgtgc	gaaattaatacgactcactataggAAGGTACTAACCCTACTGCGgttttagagctagaaatagc
Tb427.10.12360	-	Flagella connector, cytoplasm, nuclear lumen	N	18.6	9.76	513	170	TTATTTTCCAGGAACACCTTCCGCCTTCCTgtataatgcagacctgctgc	GTTTCCGGATTTTGCTTTTGTTGCTTTCATactaccgatcctgatccag	gaaattaatacgactcactataggCCAACGGAGATGTGTGAAGGgttttagagctagaaatagc
Tb427.10.12470	-	Distal FAZ, anterior cell tip	C	58.36	6.10	1584	527	AGGGCAACGCGAAGGCGCGCAGGGACACCAgtataatgcagacctgctgc	CGCTGCCGAATCAAGCTCCGGTAAACTCATactaccgatcctgatccag	gaaattaatacgactcactataggTGTTTGCTTGTCCCCCCTCCgttttagagctagaaatagc
Tb427tmp.01.0200	'Putative Katanin p60 ATPase-containing subunitA'	Anterior and posterior cell tip, cytoplasm	N	62.44	9.7	1665	554	TTCTTAACTTCNCAATTTTTGCTATTTACTgtataatgcagacctgctgc	ATTCACCAGCACGTCATTAGATGTGCTCATactaccgatcctgatccag	gaaattaatacgactcactataggGCTAACCCTCAAAGTGTAGAgttttagagctagaaatagc
Tb427tmp.01.0400	FCP5	Flagella connector, cytoplasm	N	137.82	6.96	3762	1253	TTTTTAGTCGGTTGTGTTGTCTTTCTCAGCgtataatgcagacctgctgc	AATTTCGTCGTAAATATGATAATTGTTCATactaccgatcctgatccag	gaaattaatacgactcactataggTTCAGGGGGAGAAAGGAGAAgttttagagctagaaatagc

Tb427tmp.01.1050	FAZ20	Anterior cell tip	C	85.48	10.03	2292	763	TTGCAAGGAGGCGAACAGCCTGAGGGGACGggttctggtagtggttccgg	TCGTCCCTATCTCCCCCTTTCCTTCCTCCAccaatttgagagacctgtgc	gaaattaatacgactcactataggAGAAGGTGGGGAATAAAGAAgttttagagctagaaatagc
Tb427tmp.01.1680	'Putative polyubiquitin'	Flagella connector, cytoplasm, nuclear lumen, endocytic	N	76.7	6.64	2058	685	TTTATTATGCACCTTTAACACAAAAAACCGgtataatgcagacctgctgc	ACCGGTAAGAGTTTTCACGAAGATCTGCATactaccgatcctgatccag	gaaattaatacgactcactataggCTCTTAATTGTTAGCGGACAgttttagagctagaaatagc
Tb427tmp.01.3030	-	Distal FAZ (cell cycle dependent)	N	23.02	5.08	639	212	Cell line provided by the Dunn School, Oxford University.		
Tb427tmp.01.7450	CIF1/TOEFAZ1	FAZ (cell cycle dependent), cleavage furrow	N	85.48	10.03	2376	791	GGTCGTAGGACGACAGTTTCTTCCAAATCGggttctggtagtggttccgg	GTGTGAAATATATATATATATATAACTTccaattgagagacctgtgc	gaaattaatacgactcactataggAGTAACTTCCTTTGCACGCCgtttttagagctagaaatagc
Tb427tmp.02.0190	FAZ12	Anterior cell tip, cortical cytoskeleton	N	121.1	6.89	3246	1081	Cell line provided by the Dunn School, Oxford University.		
Tb427tmp.02.1000	-	Flagella connector	N	91.94	4.64	2553	850	GTAGTTTACACTTTAGGTTACTTCTGTCAGgtataatgcagacctgctgc	GTCACCCGACGAATCCAAACCACCAAACATactaccgatcctgatccag	gaaattaatacgactcactataggAAGTTGAGGAGGTGTAGCCGgttttagagctagaaatagc
Tb427tmp.02.0890	-	FAZ, anterior cell tip	C	34.96	10.29	939	312	CGTTCAAGCCGCGCCAACGGCTATACATATggttctggtagtggttccgg	TCAGCACTTCACAATAAAAACAAGGAACCAccaatttgagagacctgtgc	gaaattaatacgactcactataggCCACCACCAATGAGAATAGTgttttagagctagaaatagc
Tb427tmp.02.2050	FCP6	Flagella connector (identified by Varga et al., 2017)	N	123.4	7.57	3342	1113	GAAATATACTAGGTATTGAGAAGTCATCCAgtataatgcagacctgctgc	AAGGTGACCTACAACAGAATTAGATGGCATactacccgatcctgatccag	gaaattaatacgactcactataggTCAAGTTTAAACACGGACCTgttttagagctagaaatagc
Tb427tmp.47.0015	FC1	Flagella connector	C	128.12	8.37	3471	1156	TCCTGGTATCCATTATACTTCACTGATGAAggttctggtagtggttccgg	AGGAAAAAGGAAAAGAAAAATCTGCGTCCAccaatttgagagacctgtgc	gaaattaatacgactcactataggTTGGTGTGATTGTTGCCGCTgttttagagctagaaatagc
Tb427tmp.50.0007	Dynein light chain LC8 (DYNLL1)	Flagella connector, axoneme, basal body, pro-basal body, anterior cell tip, nucleus	N	10.43	6.79	273	90	ATTTTTGTTTTCCCTTATCTTTCTTTTCCTgtataatgcagacctgctgc	CTTAATAATAGCTTTCCGATCAGTAGACATactaccgatcctgatccag	gaaattaatacgactcactataggCGAAGACAGAAAGGACTATAgttttagagctagaaatagc
Tb427tmp.211.0160	FAZ31	Distal FAZ, FAZ, cytoplasm	C	70.75	6.99	1929	642	Cell line provided by the Dunn School, Oxford University.		

10 Appendix B: Localisation of the 45 candidate proteins

Gene ID	Name	Procyclic form localisation	Bloodstream form localisation	Procyclic form (TrypTag)	Bloodstream form
Tb427.01.4310	FAZ2	FAZ, distal FAZ	FAZ, groove		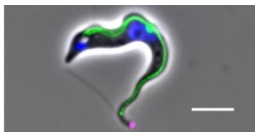
Tb427.03.1020	FAZ13	Distal FAZ, anterior cell tip	Distal FAZ, anterior cell tip, cytoplasm	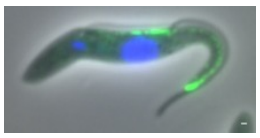	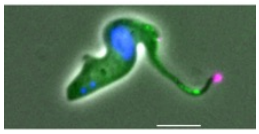
Tb427.04.3740	FAZ1	FAZ, cytoplasm	FAZ	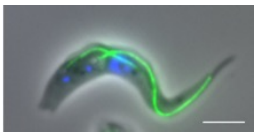	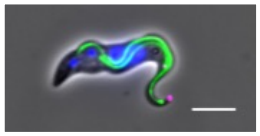
Tb427.05.3460	FAZ16	Distal FAZ (cell cycle dependent), cytoplasm	Groove	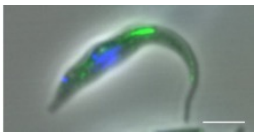	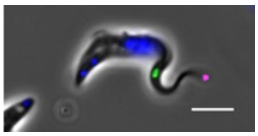
Tb427.07.3330	FAZ10	Distal FAZ, anterior cell tip	Distal FAZ, groove	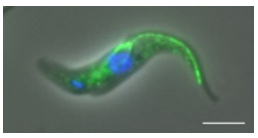	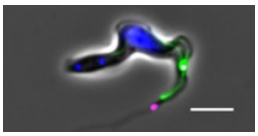
Tb427.07.5240	FAZ21	Distal FAZ, anterior cell tip	Anterior cell tip, cytoplasm	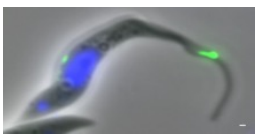	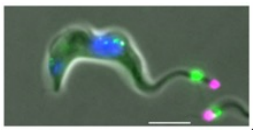
Tb427.08.7070	FAZ15	Distal FAZ, anterior cell tip, cytoplasm	Distal FAZ (cell cycle dependent), groove	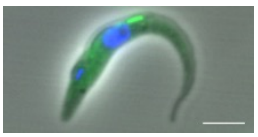	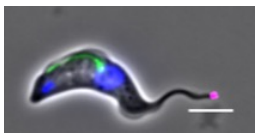
Tb427.10.8240	CIF4	Distal FAZ, anterior cell tip	Distal FAZ, groove	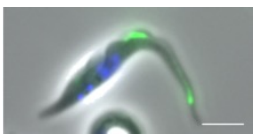	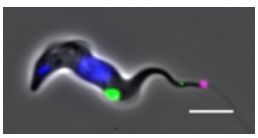
Tb427.10.6360	FPRC	Distal FAZ, cytoplasm	Distal FAZ, groove	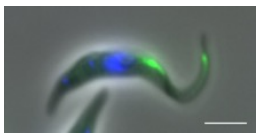	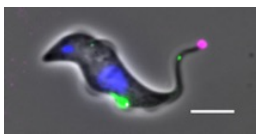
Tb427.10.840	FAZ6	Distal FAZ, anterior cell tip	Distal FAZ, anterior cell tip, cytoplasm	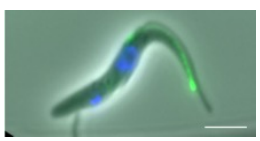	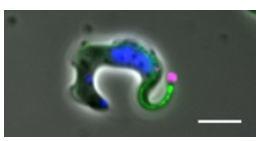
Tb427.10.9720	REAP-1	Distal FAZ	Distal FAZ, anterior cell tip, cytoplasm	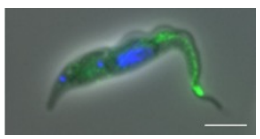	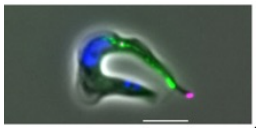

Gene ID	Name	Procyclic form localisation	Bloodstream form localisation	Procyclic form (TrypTag)	Bloodstream form
Tb427.10.11650		Distal FAZ and entire FAZ, hook complex	Cytoplasm, endoplasmic reticulum	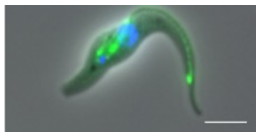	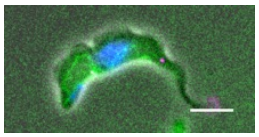
Tb427.10.13100	CIF3	Distal FAZ (cell cycle dependent), cleavage furrow	Groove	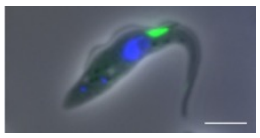	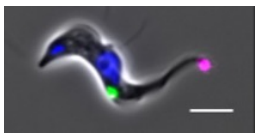
Tb427tmp.02.0190	FAZ12	Distal FAZ, anterior cell tip, cytoplasm	Distal FAZ, anterior cell tip, cytoplasm	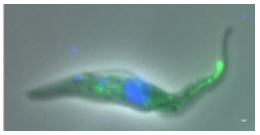	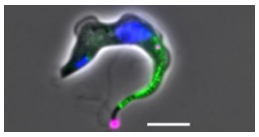
Tb427tmp.01.3030		Distal FAZ (cell cycle dependent)	Groove	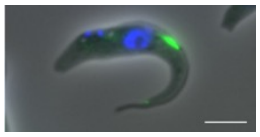	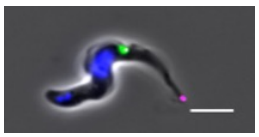
Tb427.01.2260	SMP1-2	Anterior cell tip, flagellar membrane, pellicular membrane, flagellar pocket	Flagellar membrane, pellicular membrane	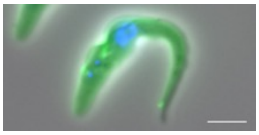	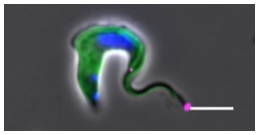
Tb427.04.5340	FAZ11	Anterior cell tip, FAZ	Anterior cell tip, FAZ	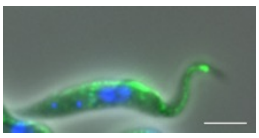	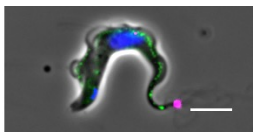
Tb427.08.6830	Kinesin	Anterior cell tip, reticulated cytoplasm	Anterior cell tip, cytoplasm	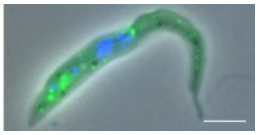	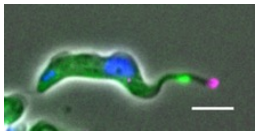
Tb427.08.8180		Anterior cell tip, FAZ, cytoplasm	Anterior cell tip, FAZ, cytoplasm	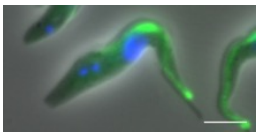	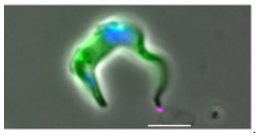
Tb427.10.2610	DUF1935	FAZ, anterior cell tip, cytoplasm	Anterior cell tip, cytoplasm	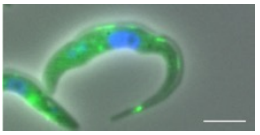	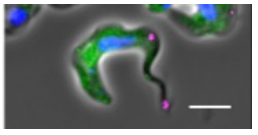
Tb427.10.15390	FAZ7	Anterior cell tip, cytoplasm	Cytoplasm	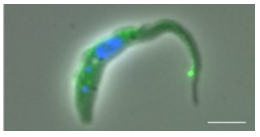	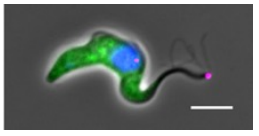
Tb427tmp.01.0200	Katanin	Anterior and posterior cell tip, cytoplasm	Cytoplasm	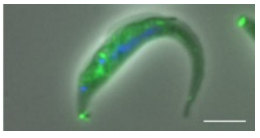	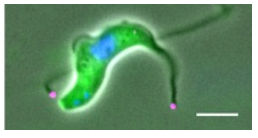

Gene ID	Name	Procyclic form localisation	Bloodstream form localisation	Procyclic form (TrypTag)	Bloodstream form
Tb427tmp.01.1050	FAZ20	Anterior cell tip	Anterior cell tip, cytoplasm	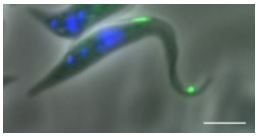	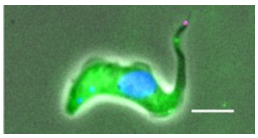
Tb427tmp.01.7450	CIF1/ TOEFAZ1	FAZ, cell cycle dependent, anterior cell tip, New FAZ tip, cleavage furrow	Groove	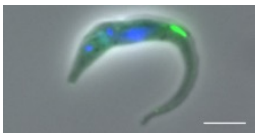	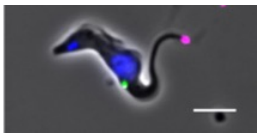
Tb427.01.2710		Flagella connector, cytoplasm	Groove, distal FAZ (cell cycle dependent)	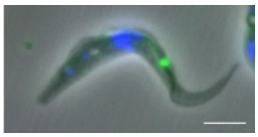	
Tb427.03.4960	FCP2/ TbKinX1	Flagella connector, cytoplasm	Cytoplasm		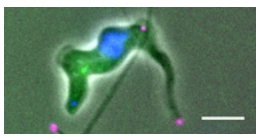
Tb427.08.960	FCP1	Flagella connector, cytoplasm		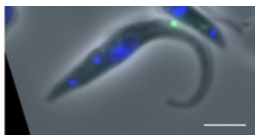	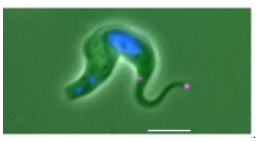
Tb427.08.7540	FCP3	Flagella connector, cytoplasm	Cytoplasm	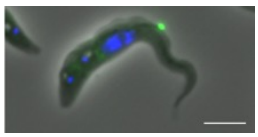	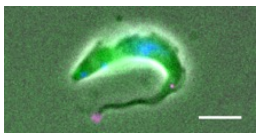
Tb427.10.890	FCP4/ TbKin15	Flagella connector	Groove		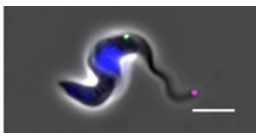
Tb427.10.9380		Flagella connector, cytoplasm	Cytoplasm, FAZ	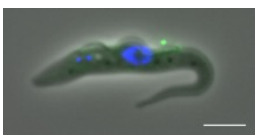	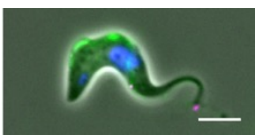
Tb427.10.12360		Flagella connector, cytoplasm, cleavage furrow	Cytoplasm	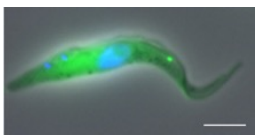	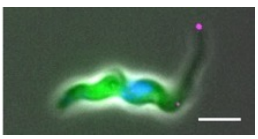
Tb427tmp.02.1000		Flagella connector, endocytic	Cytoplasm	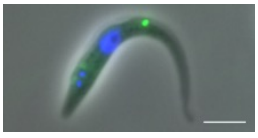	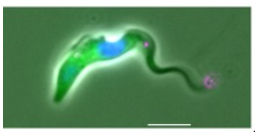
Tb427tmp.01.0400	FCP5/ TbULK4	Flagella connector, cytoplasm	Groove, cytoplasm, flagellar membrane	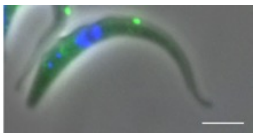	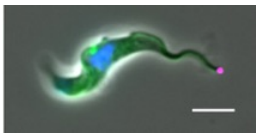

Gene ID	Name	Procyclic form localisation	Bloodstream form localisation	Procyclic form (TrypTag)	Bloodstream form
Tb427tmp.01.1680	Polyubiquitin	Flagella connector, cytoplasm, endocytic	Cytoplasm	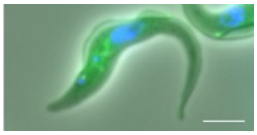	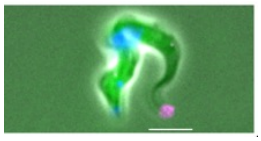
Tb427tmp.50.0007	Dynein light chain LC8 (DYNLL1)	Flagella connector, axoneme, basal body, anterior cell tip	Cytoplasm	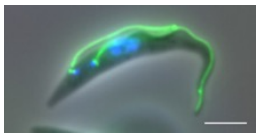	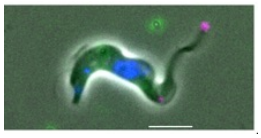
Tb427tmp.47.0015	FC1	Axoneme, cytoplasm, proximal cell tip	Cytoplasm	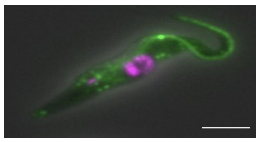	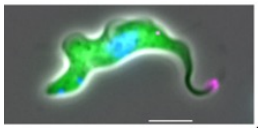
Tb427tmp.02.2050	FCP6/ TbULK	Flagella connector	Cytoplasm	No image on TrypTag.org	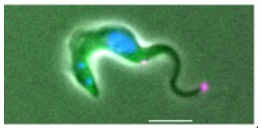
Tb427.03.4710	FAZ23	FAZ	Cytoplasm	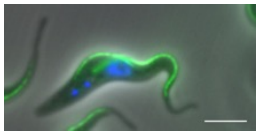	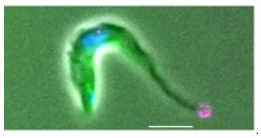
Tb427.04.2060	FAZ8	FAZ	FAZ	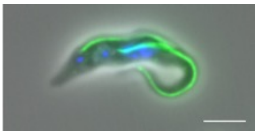	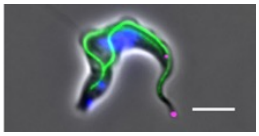
Tb427.08.4780	FLAM3	FAZ, cytoplasm	Groove, cytoplasm	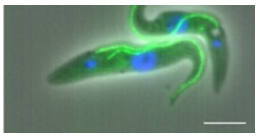	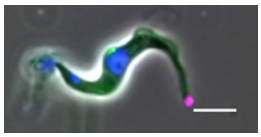
Tb427.08.5350		Distal FAZ, anterior cell tip, cortical cytoskeleton	Cytoplasm	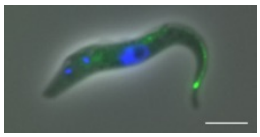	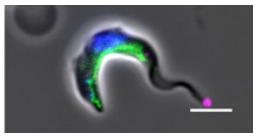
Tb427.10.5870	FAZ25	FAZ, anterior cell tip		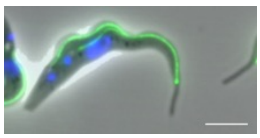	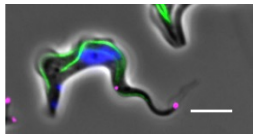
Tb427.10.7210	FAZ17	FAZ, anterior cell tip	Cytoplasm	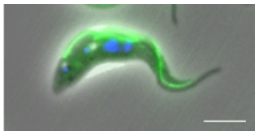	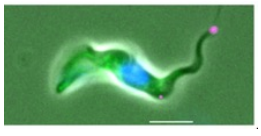
Tb427.10.12470		FAZ, anterior cell tip			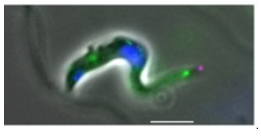

Gene ID	Name	Procyclic form localisation	Bloodstream form localisation	Procyclic form (TrypTag)	Bloodstream form
Tb427tmp.02.0890		Distal FAZ, anterior cell tip		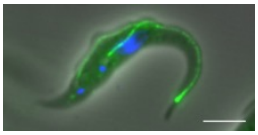	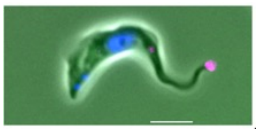

11 Appendix C: Non-groove proteins

Gene ID	Representative 2K1N cell	Localisation in the BSF
Tb427.04.3740 – FAZ1	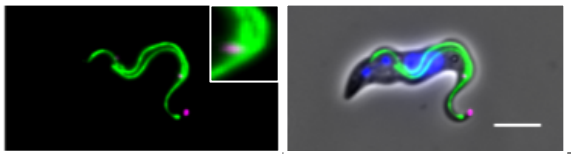	Full length FAZ
Tb427.03.1020 – FAZ13	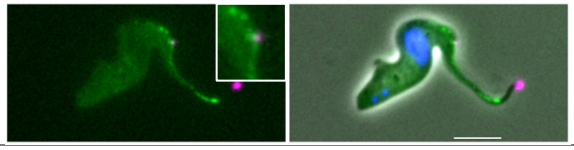	Distal FAZ, anterior cell tip, cytoplasm
Tb427.07.5240 – FAZ21	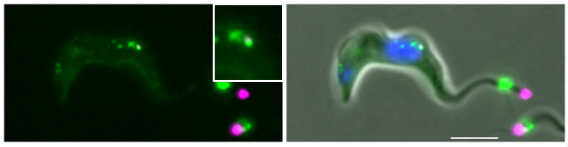	Anterior cell tip, cytoplasm
Tb427.10.840 – FAZ6	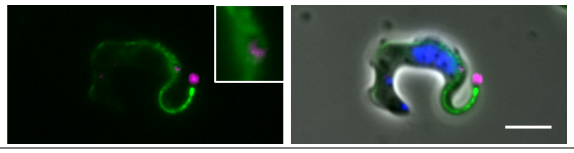	Distal FAZ, anterior cell tip, cytoplasm
Tb427.10.9720 – REAP1	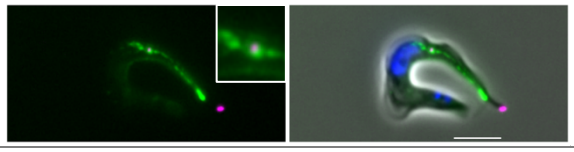	Distal FAZ, anterior cell tip, cytoplasm
Tb427.10.11650	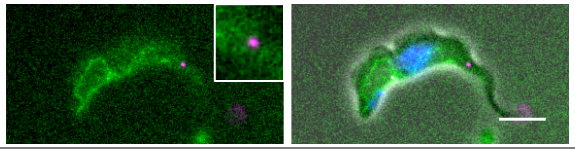	Cytoplasm, endoplasmic reticulum
Tb427tmp.02.0190 – FAZ12		Distal FAZ, anterior cell tip, cytoplasm
Tb427.01.2260 – SMP1-2	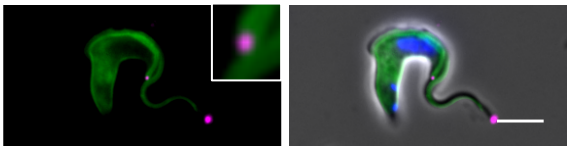	Flagellar membrane, pellicular membrane
Tb427.04.5340 – FAZ11	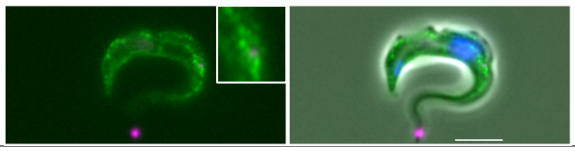	Anterior cell tip, FAZ
Tb427.08.6830	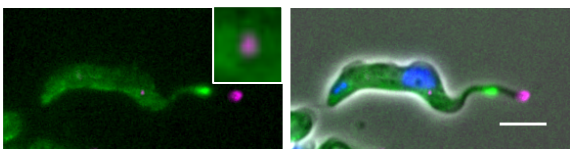	Anterior cell tip, cytoplasm

Tb427.09.8180	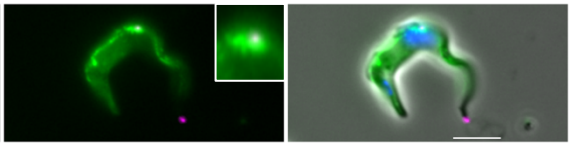	Anterior cell tip, FAZ, cytoplasm
Tb427.10.2160 – DUF1935	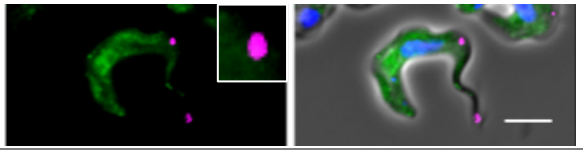	Anterior cell tip, cytoplasm
Tb427.10.15390 – FAZ7	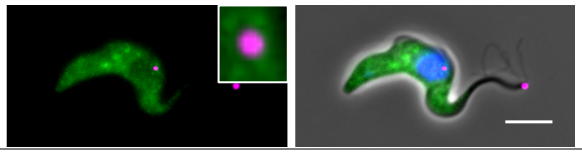	Cytoplasm
Tb427tmp.01.0200 - Katanin	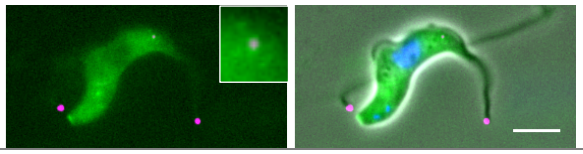	Cytoplasm
Tb427tmp.01.1050 – FAZ20	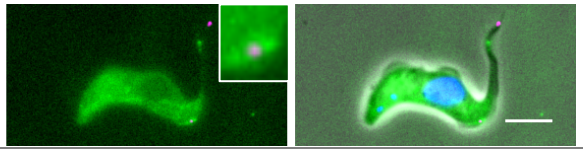	Anterior cell tip, cytoplasm
Tb427.03.4960 – FCP2	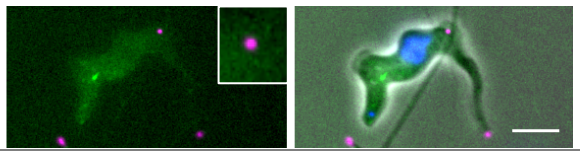	Cytoplasm
Tb427.08.960 – FCP1	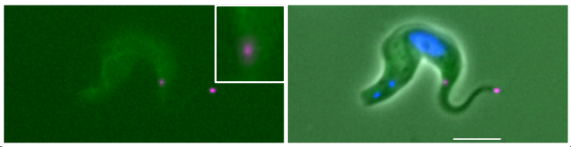	Cytoplasm, ER
Tb427.08.7540 – FCP3	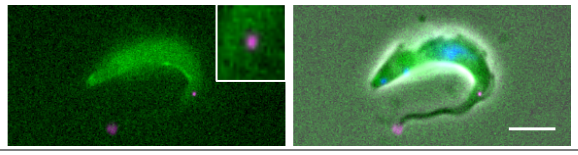	Cytoplasm
Tb427.10.9380	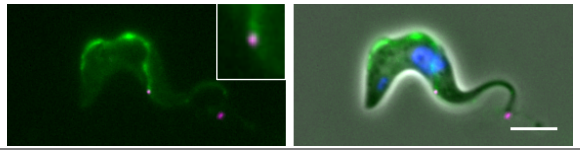	Cytoplasm, FAZ
Tb427.10.12360	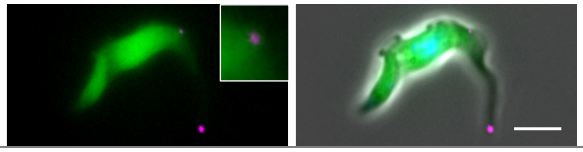	Cytoplasm
Tb427tmp.02.1000	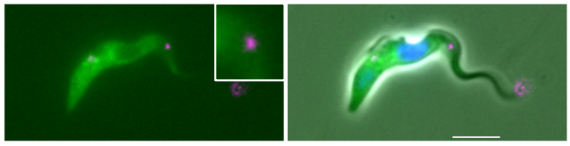	Cytoplasm
Tb427tmp.01.1680	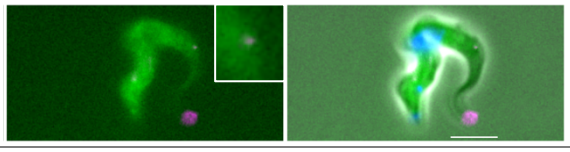	Cytoplasm

Tb427tmp.50.0007	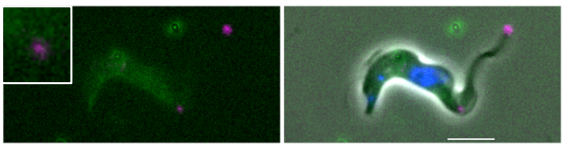	Cytoplasm
Tb427tmp.47.0015 – FC1	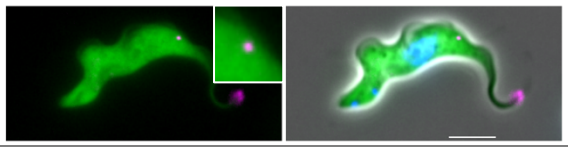	Cytoplasm
Tb427tmp.02.2050 – FCP6	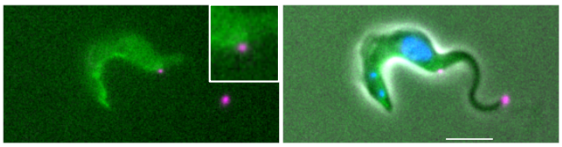	Cytoplasm
Tb427.03.4710 – FAZ23	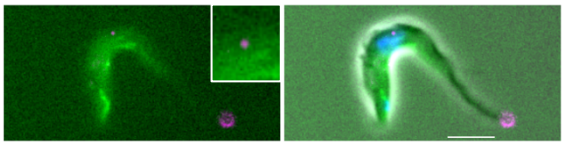	Cytoplasm
Tb427.04.2060 – FAZ8	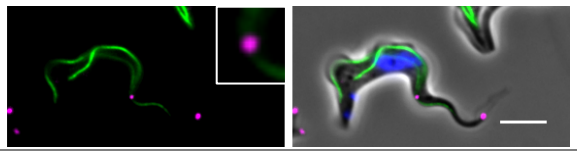	FAZ
Tb427.08.5350	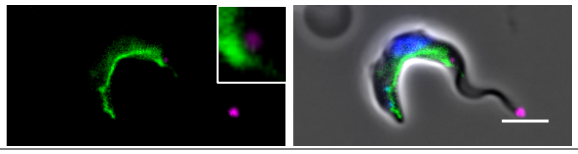	Cytoplasm
Tb427.10.7210 – FAZ17	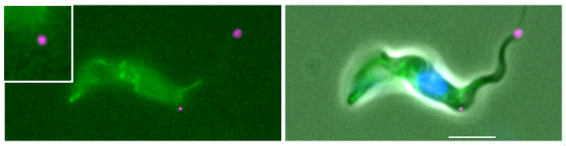	Cytoplasm
Tb427.10.12470	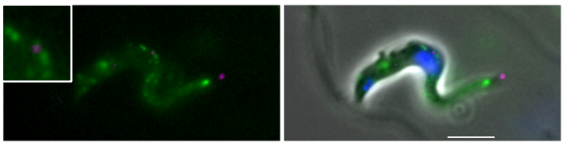	Cytoplasm, anterior cell tip
Tb427tmp.02.0890	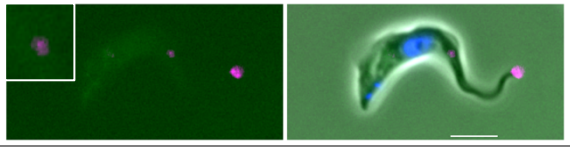	Cytoplasm
Tb427.10.5870 – FAZ25	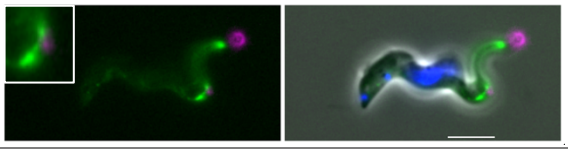	Cytoplasm, anterior cell tip

12 Appendix D: Conservation of the candidate groove proteins

Table 1: Protein conservation across selected kinetoplastids according to https://tritrypdb.org/tritrypdb/. Presence of orthologue indicated by a filled circle; empty circle indicates no orthologue identified. Proteins clustered according to notable conservation patterns.

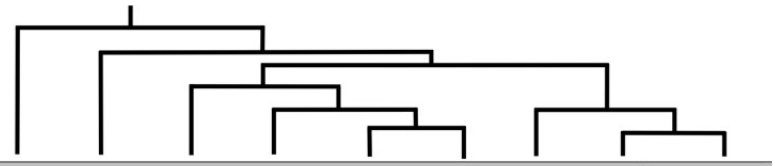

T. brucei gene ID	Gene name	Presence of orthologous proteins in other kinetoplastids*								
		B. saltans	*P. confusum*	*T. cruzi*	*T. vivax*	*T. congolense*	*T. brucei*	*B. ayalai*	*L. pyrrhocoris*	*L. major*
Tb427.03.4960	FCP2	●	●	●	●	●	●	●	●	●
Tb427.04.3740	FAZ1	●	●	●	●	●	●	●	●	●
Tb427.07.3330	FAZ10	●	●	●	●	●	●	●	●	●
Tb427.08.4780	FLAM3	●	●	●	●	●	●	●	●	●
Tb427.08.960	FCP1	●	●	●	●	●	●	●	●	●
Tb427.10.6360	FPRC	●	●	●	●	●	●	●	●	●
Tb427.10.8240	CIF4	●	●	●	●	●	●	●	●	●
Tb427.10.15390	FAZ7	●	●	●	●	●	●	●	●	●
Tb427tmp.01.0200	-	●	●	●	●	●	●	●	●	●
Tb427tmp.01.1050	FAZ20	●	●	●	●	●	●	●	●	●
Tb427tmp.02.1000	-	●	●	●	●	●	●	●	●	●
Tb427tmp.01.0400	FCP5	●	●	●	●	●	●	●	●	●
Tb427tmp.01.1680	-	●	●	●	●	●	●	●	●	●
Tb427tmp.50.0007	DYNLL1	●	●	●	●	●	●	●	●	●
Tb427tmp.02.2050	FCP6	●	●	●	●	●	●	●	●	●
Tb427.01.2260	SMP1-2	○	●	●	●	●	●	●	●	●
Tb427.01.4310	FAZ2	○	●	●	●	●	●	●	●	●
Tb427.04.2060	FAZ8	○	●	●	●	●	●	●	●	●
Tb427.04.5340	FAZ11	○	●	●	●	●	●	●	●	●
Tb427.08.6830	-	○	●	●	●	●	●	●	●	●
Tb427.10.2610	-	○	●	●	●	●	●	●	●	●
Tb427.10.12470	-	○	●	●	●	●	●	●	●	●
Tb427.01.2710	-	○	○	●	●	●	●	○	○	○
Tb427.03.1020	FAZ13	○	○	●	●	●	●	○	○	○
Tb427.03.4710	FAZ23	○	○	●	●	●	●	○	○	○
Tb427.05.3460	FAZ16	○	○	●	●	●	●	○	○	○
Tb427.10.5870	FAZ25	○	○	●	●	●	●	○	○	○
Tb427.10.13100	CIF3	○	○	●	●	●	●	○	○	○
Tb427tmp.01.3030	-	○	○	●	●	●	●	○	○	○
Tb427tmp.211.0160	-	○	○	●	●	●	●	○	○	○
Tb427tmp.02.0890	-	○	○	●	●	●	●	○	○	○

Tb427.07.5240	FAZ21	○	○	○	●	●	●	○	○	○
Tb427.08.5350	-	○	○	○	●	●	●	○	○	○
Tb427.08.7070	FAZ15	○	○	○	●	●	●	○	○	○
Tb427.08.7540	FCP3	○	○	○	●	●	●	○	○	○
Tb427.10.890	FCP4	●	○	○	●	●	●	○	○	○
Tb427.10.7210	FAZ17	○	○	●	●	○	●	○	○	○
Tb427.10.840	FAZ6	●	○	●	●	●	●	●	●	●
Tb427.10.9380	-	●	○	●	●	●	●	●	●	●
Tb427.10.9720	REAP-1	○	○	●	○	●	●	○	○	○
Tb427.10.11650	-	●	●	●	○	●	●	●	●	●
Tb427.10.12360	-	●	●	●	●	●	●	○	○	○
Tb427tmp.02.0190	FAZ12	○	○	●	●	●	●	●	●	●
Tb427tmp.01.7450	CIF1	○	○	○	●	●	●	○	●	●
Tb427tmp.47.0015	FC1	●	○	○	●	●	●	●	●	●

* **- Species identification:** *Trypanosoma viviax (T. vivax); Trypanosoma congolense (T. congolense); Trypanosoma cruzi (T. cruzi); Leishmania major (L. major); Blechomonas ayalai (B. ayalai); Leptomonas pyrrhocoris (L. pyrrhocoris); Bodo saltans (B. saltans); Paratrypanosoma confusum (P. confusum).*

13 Appendix E: Primers for CRISPR/Cas9 and deletion confirmation

Table 1: CRISPR/Cas9 primers.

Gene ID	Gene Name	Upstream forward primer*	Downstream reverse primer**	5' sgRNA primer***	3' sgRNA primer***
Tb427.01.2710	-	ACCCATTTTTCACCTC CAGAGAGTGTGAAA	ACATTAGACGTCATTC ATCGACTGTAACCT	AGTACCTGGTCCCAA AACCC	CGGTATCTCATACACT ACCT
Tb427.01.4310	FAZ2	AAAAAAGGAAGGAAC CGAACACAGCGGCCG	ACATAAGAAAAAGCC ATATCTAATTCTCCT	ACAGTCGTTGACAAA CCCCA	GGGAGGAGACGACA AATAAA
Tb427.05.3460	FAZ16	TTCTCTTTCTGCCACC ACTTTTTTTTTCC	TCTCTGGAATCGGCAT TCAGTTATCTCTAA	GCGAACGCACTTGCG ATAAA	ACCCGTCGAAGAACT GCTAA
Tb427.07.3330	FAZ10	GGAAGGGGGAGAGT AGCAAAGTGTCAACC A	ACATTAGACGTCATTC ATCGACTGTAACCT	AGTACCTGGTCCCAA AACCC	CGGTATCTCATACACT ACCT
Tb427.08.4780	FLAM3	CTTTGTTTTTAGATAA TAGAAAGAAAAAAA	GCCACCTCCTATTCAC TAGACCTAAAACCT	ACCAAAGTACCGGGA GGTTC	GACCGCCATTGTTGTA TGAG
Tb427.08.7070	FAZ15	ATAACTCTCCCTCCCC TCCCCCCCTCCCCA	CAATGGTATCTTTGCA AAAGCGAGCTTCTA	GGTAGATATCTCCGT GGGAT	ACCGTCTATGAAGAC CAGAA
Tb427.10.890	FCP4	TTACGGTGTAGGTGT GCAATTAATTTTTCG	ATTCTGCTTTGTTTTGT CGCGAACCGCAAC	CATAGAAGCTTCGCTA CGGC	ACCCGTCGAAGAACT GCTAA
Tb427.10.6360	FPRC	TGACATCCCATCTCTT CCCTCTTCCCTTCC	TCCCTCTTAAACTATC TCAGCTATACCCTC	TTTCCCCCCTTCATTAA CAA	CGCACACGAACGCGA CGACA
Tb427.10.8240	CIF4	TTTAAAAAGGGAAAG TATTGTTAACCTACG	GTTTGCCACACTTCAC GCGCGGGATGACCC	AATACATAGAGGTGA GCCAC	TGTGATGTTGTAGGG TACGC
Tb427.10.13100	CIF3	TTTTAAAAAAAAAAGT ACCGTTGACGGAGA	AGGGGCGCTGAAAAT GTTCTC	GCACTAGGGTTTCAG TCTTG	TGATGGCAATGTGAC GTCAT
Tb427tmp.01.0400	FCP5	TTTTTAGTCGGTTGTG TTGTCTTTCTCAGC	GCACTATGTGCTGCCA GATACACTCGCCCT	TTCAGGGGGAGAAAG GAGAA	CGAGAGGATGATTGG TAGTG
Tb427tmp.01.3030	-	TCTCCTTTCAGTATAG CCCCGTGTTTTCCC	CACAGGCTCCTCTACA AGTT	GTGGAACCCCCACGC AAGCGTTCTGCGCAG	GGAGGTGGTGGTGG GAAAAG
Tb427tmp.01.7450	CIF1	TCATATATTGATAGGG AGGGATTTCTAAGT	GTGTGAAATATATATA TATATATATAACTT	TGACGCGAGAAAGGA GCTTC	AGTAACTTCCTTTGCA CGCC

* Upstream forward primers flanked by a standard primer binding site (20 nucleotide sequence) at the 3' end. For example, the FAZ15 upstream forward primer was designed as follows: ATAACTCTCCCTCCCCTCCCCCCCTCCCCAgtataatgcagacctgctgc.

** Downstream forward primers flanked by a standard primer binding site (20 nucleotide sequence) at the 5' end. For example, the FAZ15 downstream forward primer was designed as follows: CAATGGTATCTTTGCAAAAGCGAGCTTCTAccggaaccactaccagaacc.

*** Both the 5' sgRNA and 3' sgRNA primers flanked on either side by standard primer binding sites encoding the T7 RNAP promoter (gaaattaatacgactcactatagg) and the Cas-9-backbone-start sequence (gttttagagctagaaatagc). For example, the FAZ15 5' sgRNA and 3' sgRNA primers were designed as follows: gaaattaatacgactcactataggGGTAGATATCTCCGTGGGATgttttagagctagaaatagc and gaaattaatacgactcactataggACCGTCTATGAAGACCAGAAgttttagagctagaaatagc respectively.

Table 2: Deletion confirmation primers.

Gene ID	Gene Name	Upstream forward primer*	Downstream reverse primer**
Tb427.01.2710	-	AACCTCTTAAGCAGTAGTAGCC	CCCCAACCCTGCACCAAAT
Tb427.01.4310	FAZ2	AACTGGAGCGAGCTGAGTTGG	TGCTGTAACCCGCAGTCCC
Tb427.05.3460	FAZ16	AAGTTGAGCCCCCAGAATCTAG	GCTTCTTCAACAGTGGCTGCT
Tb427.07.3330	FAZ10	ATCGACGAAGGCCGTCAAC	ACCTTCTCTCTGACACACTCC
Tb427.08.4780	FLAM3	TGAGGAAGAGATGTTGCAGCG	CACCACCAGCTGCACTCTTC
Tb427.08.7070	FAZ15	AACAGGTGTACAGGCGCTAC	AGTTCACACTCTGCGACCG
Tb427.10.890	FCP4	TCCTCGAAGACATGCTGAGG	AGTTTGTGACACTGAACGCC

Tb427.10.6360	FPRC	GCAGGCTAACCTAGATGTACTG	ATATGTCACATGGGAGAGCGC
Tb427.10.8240	CIF4	GCTTAAGAAAGAAACGCGAGATC	GTGTTTCATTTTGCTTTGAGCG
Tb427.10.13100	CIF3	AGGAAGTGGGAAGTATGCAAC	CCTCGTACCGCCTGTGCATC
Tb427tmp.01.0400	FCP5	AAACCAGATGCAACAAGCCC	CAGCAGCATAGCGTGACGAC
Tb427tmp.01.3030	-	GACCGATTCCGACAAAACACG	CTACGAAGTGCACAACGGC
Tb427tmp.01.7450	CIF1	CCAGTAACCAATCCATCGGCT	GCGACTGCTGCTCTCATTACTG